Medical School
Biotechnology and Drug Development Research Laboratory
Curtin Health Innovation Research Institute

Bile acid-based bio micro/nanotechnologies; biocompatibility studies

Božica Kovacevic

0000-0002-9359-7840

This thesis is presented for the Degree of
Doctor of Philosophy of
Curtin University

May 2024

Declaration

To the best of my knowledge and belief, this thesis contains no materials previously published by any other person except where due acknowledgment has been made.

This thesis contains no materials which have been accepted for the reward of any other degree or diploma in any university.

Signature: *Bozica Kovacevic*

Date: 25.05.2024.

Acknowledgement

Firstly, I acknowledge all my supervisors, Dr Hani Al-Salami, and Dr Armin Mooranian for encouraging me to work independently throughout my doctoral studies.

I wish to thank the technical, support, and administrative staff at Curtin Medical School and Curtin Health Innovation Research Institute for their continuous training, support, and guidance.

Finally, I am especially thankful to my family for their support throughout my studies. Without their support and understanding, my studies would not have been possible.

Bozica Kovacevic

May 2024

Abstract

A wide range of biocompatible hydrogels is a common biomaterial for micro and nano-encapsulation, injectable gels, and bioprinted scaffolds. All of these can be used for drug and cell delivery. Developing safe, biocompatible biomaterial with permeation enhancers can be valuable to many therapies, allowing for prolonged, focal drug delivery.

Bile acids are surfactants with unique chemical structures with rigid steroid core that gives them a curved shape. On the convex side, they are hydrophobic, and on the concave, they are hydrophilic. Based on this, bile acid can self-assemble into micelles and react with the surrounding environment. Bile acids are permeation enhancers. They promote paracellular and transcellular drug absorption by widening tight junctions between cells and transporting liposoluble drugs through membranes in the form of micelles. BAs increase membrane permeability through micelles and cell swelling in low concentrations. Bile acids associate with membrane phospholipids at concentrations above critical micellar concentration, causing a membranolytic effect directly proportional to BA's enhancer effect.

Bile acids have beneficial effects on biomaterials, like lowering matrix erosion, reducing swelling and increasing mechanical strength. This is crucial as it provides durability and lowers the degradation of biomaterials in common biological conditions. Bile acids have antioxidant and anti-inflammatory effects on cells encapsulated within biomaterials. Bile acid can activate several important membrane and nuclear receptors, leading to immunomodulatory effects, lowered fibrosis, and lowered pro-inflammatory response. Bile acids can reduce ER stress in some cells, but these effects are versatile and concentration-dependent, and proper formulation is crucial to obtain these positive effects. Designing and developing biocompatible hydrogel with incorporated bile acid is a major aim of this thesis.

Different types of hydrogels have been developed using a wide range of polymers, including sodium alginate, Poloxamer 407, polysaccharides, chitosan, polytetrafluoroethylene and others. Bile acids were incorporated within the polymer matrix, and resulting hydrogels were

tested for their rheological properties and biocompatibility on five different cell lines. The best-performing formulation in terms of rheology and biological impact on cells was smart thermoresponsive cyclodextrin-based nanogels with deoxycholic acid, which can be potential drug delivery vehicles for inner ear drug delivery.

List of Publications

This thesis encompasses 10 publications that are central to the research hypothesis:

Published/in press:

1. **Kovacevic B**, Jones M, Ionescu C, Walker D, Wagle S, Chester J, Foster T, Brown D, Mikov M, Mooranian A, Al-Salami H. The emerging role of bile acids as critical components in nanotechnology and bioengineering: Pharmacology, formulation optimizers and hydrogel-biomaterial applications. Biomaterials. 2022;283:121459.

2. **Kovacevic B**, Ionescu CM, Jones M, Wagle SR, Lewkowicz M, Đanić M, Mikov M, Mooranian A, Al-Salami H. The Effect of Deoxycholic Acid on Chitosan-Enabled Matrices for Tissue Scaffolding and Injectable Nanogels. Gels. 2022;8(6):358.

3. **Kovacevic B,** Ionescu CM, Wagle SR, Jones M, Lewkowicz M, Wong EYM, Đanić M, Mikov M, Mooranian A, Al-Salami H. Impact of Novel Teflon-DCA Nanogel Matrix on Cellular Bioactivity. Journal of Pharmaceutical Sciences. 2023;112(3):700-7.

4. **Kovacevic B,** Ionescu CM, Jones M, Wagle SR, Foster T, Lewkowicz M, Wong EYM, Đanić M, Mikov M, Mooranian A, Al-Salami H. Novel polysaccharides–bile acid–cyclodextrin gel systems and effects on cellular viability and bioenergetic parameters. Therapeutic Delivery. 2024;15(2):119-34.

5. **Kovacevic B**, Wagle SR, Ionescu CM, Jones M, Lewkowicz M, Wong EYM, Kojic S, Stojanovic G, Đanić M, Mikov M, Mooranian A, Al-Salami H. Novel hydrogel comprising non-ionic copolymer with various concentrations of pharmacologically active bile acids for cellular injectable gel. Colloids and Surfaces B: Biointerfaces. 2023;222:113014.

6**. Kovacevic B**, Jones M, Wagle SR, Ionescu CM, Foster T, Đanić M, Mikov M, Mooranian A, Al-Salami H. Influence of poly-L-ornithine-bile acid nano hydrogels on cellular bioactivity and potential pharmacological applications. *Therapeutic Delivery*. 2023;14(8):499-510.

7. **Kovacevic B,** Jones M, Wagle S, Ionescu C, Foster T, Đanić M, Mikov M, Mooranian A, Al-Salami H. The effect of deoxycholic acid-based hydrogels on hepatic, muscle and pancreatic beta cells. Therapeutic Delivery. 2024;15(1):41-54.

8. **Kovacevic B**, Wagle SR, Ionescu CM, Foster T, Đanić M, Mikov M, Mooranian A, Al-Salami H. The biocompatibility and the metabolic impact of thermoresponsive, bile acid-based nanogels on auditory and macrophage cell lines. European Journal of Pharmaceutics and Biopharmaceutics. 2023;190:248-57.

9. Pharmacological and bioenergetic effects of smart thermoresponsive polymer-bile acid enhanced nanogel on hearing cells
Kovacevic B, Wagle S, Ionescu C, Foster T, Đanić M, Mikov M, Mooranian A, Al-Salami H. Reactive and Functional Polymers: Under Review

10.
Kovacevic B, Wagle S, Ionescu C, Foster T, Đanić M, Mikov M, Mooranian A, Al-Salami H. Advanced smart-polymers-bile acid chemical nano-biotechnological effects on cyclodextrin-based nanogels for ear delivery and treatment of hearing loss. Advanced Healthcare Materials. 2024;13(16):2303149.

Conferences

The data findings from this thesis resulted in a data presentation at 3 different conferences:

- **Bozica Kovacevic**, Armin Mooranian, Hani Al-Salami. Pharmacological effects of bio-nanotechnological tissue-engineered transplants on an inflammatory disease model. Drug Delivery Australia, CRS, Australian Local Chapter, Advanced Materials in Drug Delivery, 18th and 19th November 2021. ***Best Poster Presentation.***
- **Bozica Kovacevic**, Susbin Wagle, Corina Ionescu, Dan Walker, Melissa Jones, Fola Oluyede, Armin Mooranian, Daniel Brown, and Hani Al-Salami. Addition of hyperbranched dendrimers to alginate-based hydrogel for biomedical application. International Conference on Medical and Biological Engineering (CMBEBIH), the EU, 2021
- **Bozica Kovacevic**, Daniel Walker, Corina Ionescu, Susbin Raj Wagle, Melissa Jones, Fola Oluyede, Armin Mooranian, Daniel Brown and Hani Al-Salami. The positive pharmacological impact of principal and metabolised bile acids on organoid-based injectable gel formulation. 2020 Drug Delivery Australia, Perth, November 2020

Hypothesis and Objectives

Hypothesis

Bile acids are pharmacologically beneficial in biocompatible hydrogel matrices for potential drug delivery.

Objectives

This thesis has two main objectives:

1. To screen potential bile acids from the literature for anti-inflammatory activities and evaluate their formulation suitability in terms of polymer compatibility and microencapsulation properties. Selected bile acids will proceed to further studies.

2. To design bile acid hydrogel capsules/scaffolds with optimal chemical and physical stability properties, focusing on biocompatibility and characterization. Incorporate selected bile acids into the hydrogels and investigate their effects on rheological properties and cellular bio-parameters.

Structure of the Thesis

This thesis consists of a total of 10 publications that cover the design and manufacture of bile acid-based hydrogels/nanogels, the investigation of hydrogel/nanogel's rheological properties and biocompatibility with five different cell lines.

Chapter 1: Introduction And Literary Review

The Contents Of This Chapter Are Covered By Publication 1 (Pages 22-35):

Kovacevic B, Jones M, Ionescu C, Walker D, Wagle S, Chester J, Foster T, Brown D, Mikov M, Mooranian A, Al-Salami H. The emerging role of bile acids as critical components in nanotechnology and bioengineering: Pharmacology, formulation optimizers and hydrogel-biomaterial applications. Biomaterials. 2022;283:121459.

Chapter 1 discusses the role of bile acids as critical components in nanotechnology and bioengineering, explores existing and future applications of bile acids and provides a synopsis of their role in advanced, novel therapeutic delivery systems.

This chapter achieved the following objective:

1. through searching the literature, potential bile acids will be screened for anti-inflammatory activities. Selected bile acids will then be examined for formulation suitability in terms of polymer compatibility and their microencapsulation properties. Several bile acids will be selected for further studies.

Chapter 2: Sodium Alginate And Bile Acid-Based Hydrogels: Rheological Properties And Biocompatibility

Chapters 2-4 achieved the following objective:

2. Biocompatibility and characterisation of bile acid hydrogels: design of hydrogel capsules/scaffolds with optimum chemical and physical stability properties. Selected bile acids will be incorporated with the hydrogels, and their effects on rheological properties and cellular bio-parameters will be investigated.

The contents of this chapter are covered by publication 2 (pages 38-52), publication 3 (pages 54-61), publication 4 (pages 63-85), and publication 5 (pages 87-97):

Publication 2 (pages 38-52):

Kovacevic B, Ionescu CM, Jones M, Wagle SR, Lewkowicz M, Đanić M, Mikov M, Mooranian A, Al-Salami H. The Effect of Deoxycholic Acid on Chitosan-Enabled Matrices for Tissue Scaffolding and Injectable Nanogels. Gels. 2022;8(6):358.

Sub-objective (1): to design and create hydrogels utilising sodium alginate, various concentrations of chitosan and deoxycholic acid and to examine the shear stress, viscosity, surface tension, torque, microstructure, and zeta potential of hydrogels. Additionally, the hydrogels were incubated with 3 different cell lines (AML 12, C2C12 and NIT-1). Their impact on viability in normal and hypoxic conditions and their impact on bioenergetic parameters was investigated.

Publication 3 (pages 54-61):

Kovacevic B, Ionescu CM, Wagle SR, Jones M, Lewkowicz M, Wong EYM, Đanić M, Mikov M, Mooranian A, Al-Salami H. Impact of Novel Teflon-DCA Nanogel Matrix on Cellular Bioactivity. Journal of Pharmaceutical Sciences. 2023;112(3):700-7.

Sub-objective (2): to design and create hydrogels utilising sodium alginate, polytetrafluoroethylene, and various concentrations of deoxycholic acid and to examine the shear stress, viscosity, surface tension, torque, microstructure, and zeta potential of hydrogels. Additionally, the hydrogels were incubated with 3 different cell lines (AML 12, C2C12 and NIT-1). Their impact on viability in normal and hypoxic conditions and their impact on bioenergetic parameters was investigated.

Publication 4 (pages 63-85):

Kovacevic B, Ionescu CM, Jones M, Wagle SR, Foster T, Lewkowicz M, Wong EYM, Đanić M, Mikov M, Mooranian A, Al-Salami H. Novel polysaccharides–bile acid–cyclodextrin gel systems and effects on cellular viability and bioenergetic parameters. Therapeutic Delivery. 2024;15(2):119-34.

Sub-objective (3): to design and create hydrogels utilising sodium alginate, pectin, and various concentrations of deoxycholic acid and beta-cyclodextrin, and to examine the shear stress, viscosity, surface tension, torque, microstructure, and zeta potential of hydrogels. Additionally, the hydrogels were incubated with 3 different cell lines (AML 12, C2C12 and NIT-1). Their impact on viability in normal and hypoxic conditions and their impact on bioenergetic parameters was investigated.

Publication 5 (pages 87-97):

Kovacevic B, Wagle SR, Ionescu CM, Jones M, Lewkowicz M, Wong EYM, Kojic S, Stojanovic G, Đanić M, Mikov M, Mooranian A, Al-Salami H. Novel hydrogel comprising non-ionic copolymer with various concentrations of pharmacologically active bile acids for cellular injectable gel. Colloids and Surfaces B: Biointerfaces. 2023;222:113014.

Sub-objective (4): to design and create hydrogels utilising sodium alginate, poloxamer 407, and various concentrations of deoxycholic acid, and to examine the shear stress, viscosity, surface tension, torque, microstructure, and zeta potential of hydrogels. Additionally, the hydrogels were incubated with 3 different cell lines (AML 12, C2C12 and NIT-1). Their impact on viability in normal and hypoxic conditions and their impact on bioenergetic parameters was investigated.

Chapter 3: Poloxamer 407 And Bile Acid-Based Hydrogels: Rheological Properties And Biocompatibility

The contents of this chapter are covered by publication 6 (pages 100-121) and publication 7 (pages 123-136):

Publication 6 (pages 100-121):

Kovacevic B, Jones M, Wagle SR, Ionescu CM, Foster T, Đanić M, Mikov M, Mooranian A, Al-Salami H. Influence of poly-L-ornithine-bile acid nano hydrogels on cellular bioactivity and potential pharmacological applications. *Therapeutic Delivery*. 2023;14(8):499-510.

Sub-objective (5): to design and create hydrogels utilising poloxamer 407, poly-L-ornithine, ursodeoxycholic acid, chenodeoxycholic acid, deoxycholic acid, taurocholic acid, and lithocholic acid and to examine the shear stress, viscosity, surface tension, torque, microstructure, and zeta potential of hydrogels. Additionally, the hydrogels were incubated with 3 different cell lines (AML 12, C2C12 and NIT-1). Their impact on viability in normal and hypoxic conditions and their impact on bioenergetic parameters were investigated.

Publication 7 (pages 123-136):

Kovacevic B, Jones M, Wagle S, Ionescu C, Foster T, Đanić M, Mikov M, Mooranian A, Al-Salami H. The effect of deoxycholic acid-based hydrogels on hepatic, muscle and pancreatic beta cells. Therapeutic Delivery. 2024;15(1):41-54.

Sub-objective (6): to design and create hydrogels utilising poloxamer 407, deoxycholic acid and polysaccharides (starch, pectin, acacia, carboxymethylcellulose and methyl 2-hydroxyethyl cellulose) and to examine the shear stress, viscosity, surface tension, torque,

microstructure, and zeta potential of hydrogels. Additionally, the hydrogels were incubated with 3 different cell lines (AML 12, C2C12 and NIT-1). Their impact on viability in normal and hypoxic conditions and their impact on bioenergetic parameters was investigated.

Chapter 4: Poloxamer 407 And Bile Acid-Based Nanogels For Inner Ear Delivery: Rheological Properties And Biocompatibility

The contents of this chapter are covered by publication 8 (pages 142-151), publication 9 (pages 153-169) and publication 10 (pages 171-181):

Publication 8 (pages 142-151):

Kovacevic B, Wagle SR, Ionescu CM, Foster T, Đanić M, Mikov M, Mooranian A, Al-Salami H. The biocompatibility and the metabolic impact of thermoresponsive, bile acid-based nanogels on auditory and macrophage cell lines. European Journal of Pharmaceutics and Biopharmaceutics. 2023;190:248-57.

Sub-objective (7): to design and create nanogels utilising poloxamer 407, polyvinyl alcohol, deoxycholic acid, lithocholic acid and ursodeoxycholic acid and to examine the shear stress, viscosity, surface tension, torque, microstructure, and zeta potential of nanogels. Additionally, the nanogels were incubated with 2 different cell lines (HEI-OC1 and RAW264.7) and their impact on viability, total intracellular reactive oxygen species, as well as their impact on bioenergetic parameters, was investigated.

Publication 9 (pages 153-169):

Pharmacological and bioenergetic effects of smart thermoresponsive polymer-bile acid enhanced nanogel on hearing cells

Kovacevic B, Wagle S, Ionescu C, Foster T, Đanić M, Mikov M, Mooranian A, Al-Salami H. Reactive and Functional Polymers

Sub-objective (8): to design and create nanogels utilising poloxamer 407, Tyloxapol, and deoxycholic acid and to examine the shear stress, viscosity, surface tension, torque, and zeta potential of nanogels. Additionally, the nanogels were incubated with 2 different cell lines (HEI-OC1 and RAW264.7), and their impact on viability and bioenergetic parameters was investigated.

Publication 10 (pages 171-181):

Advanced smart-polymers-bile acid chemical nano-biotechnological effects on cyclodextrin-based nanogels for ear delivery and treatment of hearing loss
Kovacevic B, Wagle S, Ionescu C, Foster T, Đanić M, Mikov M, Mooranian A, Al-Salami H.
Journal:

Sub-objective (9): to design and create nanogels utilising poloxamer 407, polyvinyl alcohol and deoxycholic acid and to examine the shear stress, viscosity, surface tension, torque, microstructure, and zeta potential of nanogels. Additionally, the nanogels were incubated with 2 different cell lines (HEI-OC1 and RAW264.7) and their impact on viability, total intracellular reactive oxygen species, inflammatory profile, macrophage polarisation as well as nanogel impact on bioenergetic parameters was investigated.

Chapter 5: General Discussion and Conclusion, Limitations and Future Perspective

Table of Contents

Declaration 2

Acknowledgement 3

Abstract 4

List of Publications 6

Conferences 9

Hypothesis and Objectives 10

Structure of the Thesis 11

Chapter 1 21

Chapter 2 37

Chapter 3 99

Chapter 4 141

Chapter 5 183

Appendix A 187

Appendix B 189

Chapter 1

Introduction And Literary Review

Chapter 1

Introduction And Literary Review

The Contents Of This Chapter Are Covered By Publication 1 (Pages 22-35):

Kovacevic B, Jones M, Ionescu C, Walker D, Wagle S, Chester J, Foster T, Brown D, Mikov M, Mooranian A, Al-Salami H. The emerging role of bile acids as critical components in nanotechnology and bioengineering: Pharmacology, formulation optimizers and hydrogel-biomaterial applications. Biomaterials. 2022;283:121459.

Chapter 1 discusses the role of bile acids as critical components in nanotechnology and bioengineering, explores existing and future applications of bile acids and provides a synopsis of their role in advanced, novel therapeutic delivery systems.

This chapter achieved the following objective:

1. through searching the literature, potential bile acids will be screened for anti-inflammatory activities. Selected bile acids will then be examined for formulation suitability in terms of polymer compatibility and their microencapsulation properties. Several bile acids will be selected for further studies.

Biomaterials 283 (2022) 121450

Contents lists available at ScienceDirect

Biomaterials

journal homepage: www.elsevier.com/locate/biomaterials

The emerging role of bile acids as critical components in nanotechnology and bioengineering: Pharmacology, formulation optimizers and hydrogel-biomaterial applications

Bozica Kovacevic [a,b], Melissa Jones [a,b], Corina Ionescu [a,b], Daniel Walker [a,b], Susbin Wagle [a,b], Jacqueline Chester [a,b], Thomas Foster [a,b], Daniel Brown [c], Momir Mikov [d], Armin Mooranian [a,b,**], Hani Al-Salami [a,b,*]

[a] The Biotechnology and Drug Development Research Laboratory, Curtin Medical School & Curtin Health Innovation Research Institute, Curtin University, Bentley, Perth, WA, 6102, Australia
[b] Hearing Therapeutics Department, Ear Science Institute Australia, Queen Elizabeth II Medical Centre, Nedlands, Perth, WA, 6009, Australia
[c] Curtin Medical School & Curtin Health Innovation Research Institute, Curtin University, Bentley, Perth, WA, 6102, Australia
[d] Department of Pharmacology, Toxicology and Clinical Pharmacology, Faculty of Medicine, University of Novi Sad, Hajdak Veljkova 3, 21101, Novi Sad, Serbia

ARTICLE INFO

Keywords:
Bile acids
Nanotechnology
Biomaterials
Transplantation
Inflammation
Bioprinting

ABSTRACT

The role of endogenous bile acids as lipid stabilizers aiding uptake of lipophilic nutrients via micelle formation and saponification effects is well documented and precedes their growing applications in pharmaceutical sciences. Their utility stems from their unique physico-chemical profile and ability to modulate immune cell signalling pathways. It has been shown that bile acids alter specific receptor-mediated pathways of cellular respiration and metabolism, providing potential clinical therapies for cardio-metabolic disorders such as diabetes mellitus, hypercholesterolemia, and heart disease. Additionally, some bile acids exert profound anti-oxidant, anti-inflammatory and immunosuppressant properties, and are effective at reducing blood pressure and alleviating hypertension.

Their unique amphoteric properties and proven ability as permeability enhancers make them a desirable pharmaceutical excipient. When incorporated with various carbohydrates, polymers, hydrogels and/or polyelectrolytes to form micro- or nano-capsules, they provide enhanced thermodynamic, osmotic and structural stability, and cater for controlled delivery via specific tissue targeting, pH dependant release and temperature guided sol-gel complexation. Additionally, due to their immunosuppressant properties, they enhance the immunogenicity of encapsulated cells, increasing the feasibility of bioartificial organs as transplantable therapeutics.

This review explores existing and future applications of bile acids and provides a synopsis of their role in advanced, novel therapeutic delivery systems.

1. Introduction

Many diseases and traumas can cause irreparable damage to the tissue through acute or chronic insults, resulting in a complete or partial lack of function. For example, the autoimmune component of Type 1 diabetes is responsible for destruction to insulin-secreting beta cells, rendering endocrine parts of the pancreas non-functional, while acute ischemic insults in any tissue decrease its functionality and limit survival. So far, while there are instances of successful mitigation of complete or partial tissue dysfunction (thyroid hormone replacement therapy in case of removed thyroid gland), the majority of organ failures and terminal stages of progressive chronic diseases require deteriorated tissue to be replaced or repaired, usually through organ transplantation. An alternative to surgery is the utilization of injectable cell delivery

* Corresponding author. The Biotechnology and Drug Development Research Laboratory, Curtin Medical School & Curtin Health Innovation Research Institute, Curtin University, Bentley, Perth, WA 6102, Australia.
** Corresponding author. The Biotechnology and Drug Development Research Laboratory, Curtin Medical School & Curtin Health Innovation Research Institute, Curtin University, Bentley, Perth, WA 6102, Australia.
E-mail addresses: a.mooranian@curtin.edu.au (A. Mooranian), hani.al-salami@curtin.edu.au (H. Al-Salami).

https://doi.org/10.1016/j.biomaterials.2022.121450
Received 1 July 2021; Received in revised form 27 February 2022; Accepted 4 March 2022
Available online 12 March 2022
0142-9612/

systems. However, this kind of therapy has many obstacles: the host's immune response and subsequent inflammation [1,2]. In the case of diabetes, pancreas transplantation has substantial surgical complication risk and requires life-long immunosuppression [3]. Alternatively, islet transplantation, a low risk procedure, can achieve durable insulin independence only in a minority of patients and does not exclude a risk of associated immunosuppressive related complications, like infections, cancer, and organ-system toxicity. Furthermore, there is a rapid decline in islet viability and function post-transplantation [4–6]. An alternative approach that avoids the need for an immunosuppressant regime, would be delivering cells in a semipermeable immunostatic device or matrix. This technology would permit the physiological function of the pancreas while protecting the injected cells from the immune response. Current strategies involve using numerous biomaterials as a cell-supporting structure, with a promising versatility regarding biomaterial's mechanical properties and biodegradation, ability to interact with biomolecules, and the possibility of controlled drug release from within the material. While there is a great deal of research available in terms of tissue engineering and regenerative medicine [7–10], the focus of this review would be on the role of bile acids (BAs) as possible excipient enhancer within common biomaterials in terms of the impact on the cell viability, interactions within biological environment and effects on mechanical and rheological properties of the matrix.

1.1. BILE ACIDS: formation and biological activities

BAs are amphiphilic compounds found in the human body as part of bile. Bile, secreted by the liver, is a multicomponent fluid containing water, electrolytes, and other organic molecules such as bile salts, cholesterol, phospholipids, and bilirubin [11–15]. BAs have a role in the emulsification and absorption of dietary lipids, liposoluble medicines, and vitamins from the ileum due to their amphiphilic properties [16]. Recent findings suggest their broader role in maintaining healthy gut content, endocrine functions, controlling lipid absorption, and the immune response [17,18]. Disrupted homeostasis and the primary/secondary ratio have been linked to inflammation and diabetes development and progression [19,20].

Primary BAs (e.g., cholic acid (CA) and chenodeoxycholic acid (CDCA)) are synthesized via two different pathways: classic (neutral) or alternative (acidic). The classic BA pathway yields the vast majority (around 90%) of BAs in humans, converting cholesterol to 7α-hydroxycholesterol via the CYP7A1 enzyme. Subsequent conversion of 7α-hydroxycholesterol with HSD3B7 to CDCA and HSD3B7 and CYP8B1 to CA completes the classic, primary BA synthesis [21]. In the alternative BA pathway, cholesterol is oxidized by CYP27A1, then hydroxylated by the CYP7B1 enzyme to generate CDCA.

BAs are further conjugated with glycine or taurine, with a ratio of 3 to 1, respectively, utilizing BA-CoA synthetase (BACS) and BA coenzyme A-amino acid *N*-acyltransferase (BAAT) [21,22]. Hepatocytes excrete BAs into bile canaliculi through a bile salt export pump (BSEP/ABCB11) [23]. Compared to free BAs, conjugated BAs have lower pKa, increased water solubility, and lose the ability to passively cross cell membranes which cause a reduction in cytotoxic potential [16,24]. In addition, bile salts are hydrophilic, zwitterionic compounds at physiological pH [25], able to form micelles due to their amphoteric nature [26].

Cholangiocytes (bile duct epithelial cells) excrete bicarbonate in the presence of bile salts to line the bile ducts with a protective layer and create a drainage system for BAs [21]. As part of the bile, bile salts are secreted in the duodenum (stimulated by cholecystokinin). In the duodenum, when mixed with nutrients, bile salts decrease the surface tension of lipid droplets, enabling enzymatic hydrolysis of fats by lipases [21]. Bile salts are later reabsorbed in the terminal ileum. Conjugated BAs are taken into cells by active transport via an apical sodium-dependent BA transporter (ASBT). On entering, BAs are bound to cytosolic ileal BA binding protein IBABP, transported through the cell, and exported to portal bloodstream via organic solute transporters (OSTs), α/β.

BAs from portal circulation are taken up by basolateral transport systems in hepatocytes, for conjugated BAs by Na^+-taurocholate co-transporting polypeptide [NTCP]/SLC10A1, and for unconjugated BAs by organic anion transporters [OATPs]/SLCO/SLC21 [23,27]. Enterohepatic reuptake of BAs is highly efficient, as shown by the distinct difference in BA levels in portal blood (10–80 μM) compared to low levels of BA (2–10 μM) that can be found in systematic circulation, with the amount and type of present BAs dependent on meal and circadian rhythm [16,28]. Enterohepatic circulation occurs approximately 12-times a day with an efficacy of 95% [29,30]. The BAs that are not reabsorbed in the ileum pass through to the colon, where they are deconjugated and dehydroxylated by the gut microbiota into secondary BAs–lithocholic acid (LCA) and deoxycholic acid (DCA), from CDCA and CA respectively [21] (Fig. 1.). Systemic and local biological effects of secondary BAs added to cell delivery matrix are stated in more detail later in this text.

Enterohepatic circulation is tightly regulated. BAs enter hepatocytes from portal circulation via NTCP(SLC10A1) and OATPs (SLCO/SLC21). NTCP is responsible for the majority of BAs uptake (about 90%). It is downregulated by BAs, hormones (oestrogen and prolactin), and pro-inflammatory cytokines [32]. BAs in hepatocytes activate several nuclear receptors needed for tight regulation between BAs synthesis, uptake, and excretion, with Farnesoid-X-Receptor alpha (FXRα, NR1H4) being the primary receptor. FXRα activation has a hepatoprotective role in the case of BAs build-up. FXRα promotes transcription of a small heterodimer partner (SHP), which in turn inhibits nuclear receptors needed for activation of CYP7A1, including liver X receptor (LXR), liver receptor homolog (LHR-1), and hepatocyte nuclear factor 4α (HNF-4α). This pathway inhibits BA synthesis and further BA accumulation in hepatocytes. LRH-1 and HNF-4α are crucial modulators of the BA pool, as they inhibit CYP8B1 and subsequent synthesis of CA [21,33,34]. FXRα is a key modulator of BSEP, as it upregulates BSEP expression and subsequent secretion of BAs to bile canaliculi. Furthermore, FXRα promotes alternative basolateral transporters of BA, OST-α/β, and ATP binding cassette transporters, including multidrug resistance-associated protein MRP3 and MRP4 [35]. The alternative export pathway is also mediated by constitutive androstane receptor (CAR, NR111), vitamin D receptor (VDR, NR113), pregnane X receptor (PXR, NR112) and peroxisome proliferator-activate receptor alpha (PPARα, NR1C1). They all promote MRP3, while CAR and PPARα increase the expression of MRP4 and detoxification enzymes [32].

In enterocytes, nuclear receptors regulate several transport systems, including ABST. ABST is controlled by a negative feedback loop via FXRα and SHP, inhibiting BAs uptake. FXRα activation promotes both IBABP and OSTα/β, promoting BAs export [36]. Furthermore, the BA-mediated activation of FXRα leads to the secretion of FGF19 (FGF15 in mice), a member of the fibroblast growth family. FGF19 secreted in the intestine suppresses ASBT expression in a paracrine manner, suppresses BA synthesis through inhibition of CYP7A1 in hepatocytes, and facilitates gallbladder refilling [36]. In addition, FGF19 has a role in metabolism in an insulin-independent manner, as it upregulates glycogen synthesis, but it does not induce lipogenesis (Fig. 2.) [36].

In addition to regulating its production and secretion, a post-prandial surge of BAs in the liver and intestine and a lesser amount in the kidney, muscle, and adipose tissue activates signals for energy storage. It has also been shown that BAs have a regulatory role in the circadian rhythm of metabolism [37,38].

1.2. BILE ACIDS: physico-chemical properties

BAs have different chemical structures, compared to typical aliphatic surfactants, mainly due to the presence of the steroid nucleus. Steroid structures are planar, rigid, and hydrophobic, with 2–4 hydroxyl groups attached [39]. Position, number and α or β orientation of hydroxyl groups and conjugation determine hydrophobicity and detergent

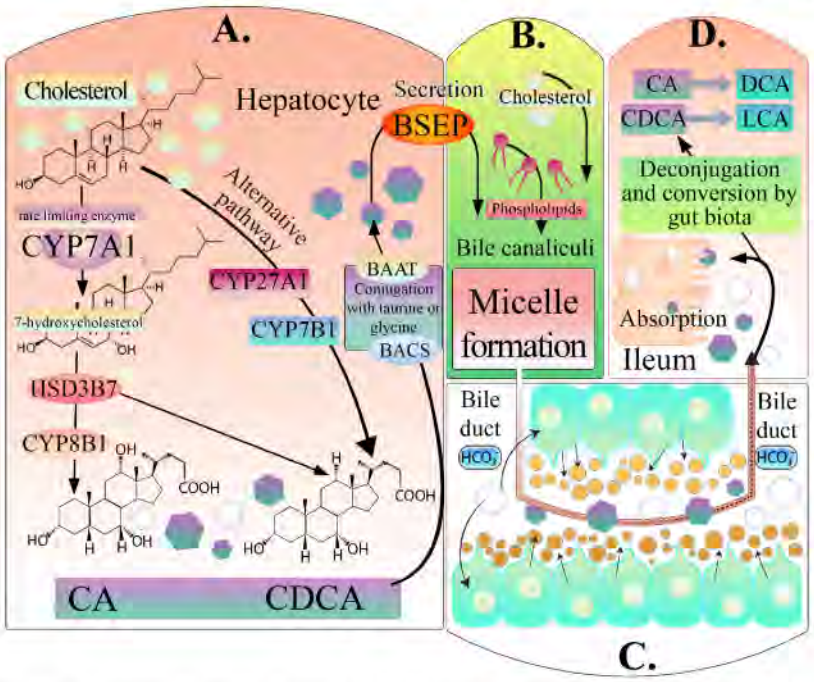

Fig. 1. A diagram outlining homeostasis and uptake of endogenous bile acids in mammals in a) hepatocytes, b) bile canaliculi, c) bile duct, and d) ileum.

properties of BAs [40–43]. Hydroxyl groups found on the concave α side make it hydrophilic, while the methyl group on the convex β side promotes hydrophobic behaviour [44,45]. Hydrophobicity decreases in the following order: LCA > DCA > CDCA > CA > UDCA > MCA [46]. Due to their aliphatic nature, BAs can form polymolecular aggregates (micelles) above critical micellar concentration (CMC). Depending on the structure and type of BA, each micelle can have anywhere from 4 to 50 molecules [47]. CMC largely depends on hydrophilic/hydrophobic balance in a molecule, i.e. number of hydroxyl groups and their stereospecific position in a molecule [48]. BAs (in the form of bile salts) first create primary micelles, with hydrophobic sides of the molecule turned to each other and hydrophilic ones to the water. Hydroxyl groups on primary micelles form hydrogen bonds at the higher concentration, creating elongated secondary micelles, disc-like and helical micelles. Secondary micelles are disordered and dynamic in various irregular shapes, but experiments show a preference for ellipsoids or elongated, cylindrical shapes [49]. Because of the molecule's rigidity and complex distribution of hydrophilic and hydrophobic groups, BAs have a specific self-assembly behaviour at high concentrations. Aggregation tendencies are inversely related to hydrophobicity. In an aqueous environment, when their solubility is lowered, by decreasing pH or solvent polarity, BAs aggregate as needle shaped crystals. When a controlled lowering of solubility is performed, BA's aggregates can self-assemble into fibrils that form a self-assembled fibrillary network or tubular structures, depending on BA and experimental conditions. The fibril network immobilizes the surrounding solvent via surface tension, allowing for gel formation [50,51]. At the neutral pH, a fraction of carboxylate groups in BAs is in the protonated form, decreasing repulsion between molecules, which allows for the formation of stabilizing bonds, including hydrogen bonds. Based on this, DCA can form gels in water solution, while its conjugated forms and LCA require the addition of salts to promote gelation. Gelation can be triggered by the addition of multivalent cations –alkaline earth, lanthanide, and transition-metal ions. Even luminescent gels can be made by combining DCA and europium nitrate [50].

BAs and their derivatives promote paracellular and transcellular drug absorption by widening tight junctions between cells and transport liposoluble drugs through membranes in the form of micelles [52]. BAs increase membrane permeability through micelles and cell swelling in low concentrations. Still, at concentrations above CMC, they associate with membrane phospholipids, causing a membranolytic effect directly proportional to BA's enhancer effect [39]. Therefore, cytotoxicity of BAs decrease with an increase of CMC [53].

Based on specific and unique physicochemical characteristics of BAs, they are potential candidates for use in nanotechnology and bioengineering as formulation enhancers, in order to overcome challenges of cell delivery technology. Some of the major obstacles and variables for successful cell delivery will be briefly discussed in next section.

2. Challenges for cell delivery technologies

2.1. Transplantation sites

Desired characteristics of the transplantation site would include sufficient space for relatively large tissue volumes, enable low-risk transplantation procedures, and allow for non-invasive monitoring and access for retrieval [54]. An additional advantage would be venous drainage through the portal system due to portal tolerance, which has been associated with lower rejection rates of transplants than those with access to systematically drained organs [55,56]. The liver, kidney capsule, brain, testis, thymus, and intraperitoneal sites allowed engraftment of soft tissue like islets in murine models. The liver is a preferred site in humans, although other areas have been investigated

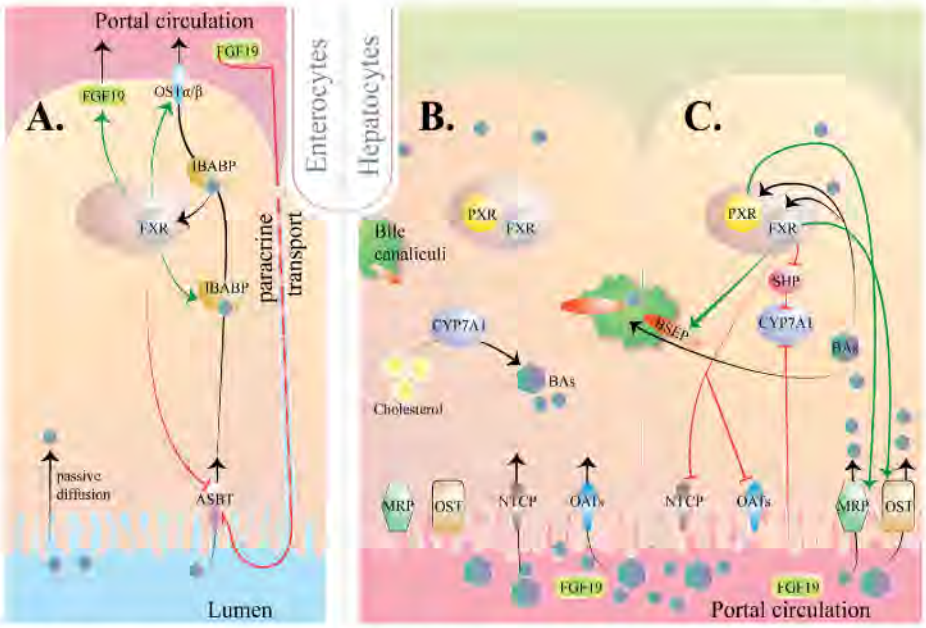

Fig. 2. Regulation of enterohepatic circulation at a) ileal site, b) uptake-oriented hepatocyte and c) excretion-oriented hepatocyte.

[54,57]. To improve the nutrient supply to the implant, efforts are made to improve the vascular supply in transplant sites by adding proangiogenic factors, endothelial cells, and/or placing the transplant close to a vascular network (such as omental blood supply) [58]. Precise geometrical manipulation of biomaterial enables the fabrication of complex and heterogeneous tissue constructs, including endothelial cells, to form capillaries to promote nutrient circulation and graft survival [59,60].

2.2. Inflammatory response, fibrosis, and graft failure

The elimination of foreign infectious agents by the immune system is usually achieved via phagocytosis and phagolysosomal digestion of the threat in a non-dangerous and reusable manner. While this approach works for bacterial, viral, and protozoal threats, it is ineffective in transplants entrapped in the biomaterial. Here, the immune system is mobilized on the biomaterial's surface to create a fibrous capsule, isolating and containing the threat. The foreign body response is achieved in several stages, starting with protein adsorption on the biomaterial's surface [61]. During the transplantation of the encapsulated material, tissues, including blood vessels, around the transplant site are damaged, causing a greater than normal concentration of plasma proteins in the area. Plasma proteins, first high mobility proteins like albumin, adhere to the surface of the biomaterial. They are in a constant dynamic state of continuous adsorption and desorption and increasingly become replaced by less mobile proteins with high affinities to specific sites. These include fibrinogen, fibronectin, vitronectin, and high molecular weight kininogen. Proteins create a provisional matrix, 2–5 nm thick, around the transplanted device [62]. Further interactions of immune cells are primarily with provisional matrix proteins, as they serve as a reservoir of cytokines and chemokines, adherence points and promoters of subsequent inflammation [63,64].

Inflammation can be defined as a protective response of the organism, triggered by pathogen-associated molecular patterns (PAMPs), in the case of invading pathogens, or endogenous stress signals, in case of tissue trauma. This process aims to recognize and eradicate the source of injury (pathogens), clearance of dead cells, and tissue repair [65]. However, due to complex molecular, physiological, and immunological responses included in the process of inflammation and their simultaneous nature, uncontrolled inflammation can lead to the development of inflammatory and autoimmune diseases and is contributing factor to the plethora of other diseases (diabetes, atherosclerosis, cancer) [66].

Inflammation is induced by activation of germline-encoded pattern-recognition receptors (PRRs) on myeloid cells, mainly macrophages, monocytes, neutrophils, dendritic cells, fibroblasts, lymphocytes and epithelial cells [67,68]. Activation of PPRs leads to the secretion of inflammatory cytokines and chemokines. The primary function of chemokines is to recruit immune cells, especially neutrophils, to the location of the infection, as they are crucial in phagocytosis and the elimination of pathogens [69,70]. TNF-γ cytokine's activate neutrophils [65]. Cytokines in the TNF family and IL-1β lead to local activation of macrophages and neutrophils via paracrine and autocrine signalling. At the same time, their high concentration exerts endocrine effects such as platelet activation, fever, fatigue, and loss of appetite [71]. Acute response proteins are released from hepatocytes in response to the detection of endotoxins via PPRs, and the presence of pro-inflammatory cytokines IL6, IL1β, TNFα, IL8 2, and IL-22 [72]. Cytokines activate endothelial cells to facilitate the migration of immune cells to the distressed tissue. Progressive changes in endothelium boost the vascular permeability of the microvasculature, increasing the amount of fluid exiting blood vessels. This effect leads to increased viscosity of blood, slowing down blood flow. Slow blood flow allows for increased, targeted migration of leucocytes (as they can more easily adhere to and migrate through the vascular wall), while increased capillary leakage brings plasma mediators to the injury site [73].

The secretion of cytokines in the circulations leads to the release of mediators of inflammation, such as prostaglandins, which act on the hypothalamus creating fatigue and fever [74]. In addition, mediators have a role in facilitating opsonisation through the initiation of inflammatory peptides (C3a and C5a) [75].

Migrated macrophages in damaged tissues differentiate into several phenotypes, broadly grouped as M1 and M2 phenotypes. M1 macrophages have a pivotal role in pro-inflammatory response and host defences [76]. The M1 phenotype is promoted by PAMPs, danger-associated molecular patterns (alarmins) like S100A9 and IL-1α, and pro-inflammatory cytokines including INF-γ and TNF [77]. Consecutively, M1 macrophages stimulate the production and activation of pro-inflammatory cytokines (IL-1, IL-6, IL-12, IL-23) and molecules involved in antigen presentation [78].

In foreign body response, migrated macrophages cannot eliminate threats (biomaterial) through usual mechanisms (phagocytosis). These 'frustrated' macrophages fuse in foreign body giant cells (FBGC) (up to several hundred μm large) with multiple nuclei. IL-4 and IL-13 have been detected as the most important signals for macrophage fusion [61, 79]. FBGC formation on biomaterial's surface is undesirable as they are the primary source of degradative enzymes, acids, and reactive oxygen species, leading to deterioration and transplant failure [80]. Furthermore, chronic inflammation and FBGC formation cause capsule formation around the device. Capsule formation is driven by pro-fibrotic and pro-angiogenic growth factors, including VEGF and TGF-β, secreted by M2 macrophages and other immune cells, fibroblasts and endothelial cells [81]. Fibroblasts and endothelial cells start depositing collagen and other ECM proteins, creating granulation tissue. Granulation tissue is composed of collagen fibres, fibroblasts, macrophages, and capillary sprouts. As the tissue matures, the percentage of collagen increases, while cellular elements decrease, finalizing formation of fibrous capsule. A fibrous capsule leads to the mechanical impairment of the transplant, and diminishes interaction of the transplant with surrounding environment, limiting nutrient supply [82].

2.3. Difficulties alleviating inflammatory response to grafts

Suppression of inflammation and return to homeostasis is an active process that employs complex negative autoregulatory loops [66]. Anti-inflammatory cytokines (Il-10, TGFβ, IL-37), released mainly from myeloid-derived suppressor cells and regulative T-cells, broadly suppress inflammation and production of pro-inflammatory cytokines [65, 83]. Receptor antagonists bind to receptors of pro-inflammatory cytokines and do not induce biological effects. This way, antagonist IL-1Ra binds to IL-1R, inhibiting cytokines IL-1α and IL-1β. Receptor decoys, such as cleaved extracellular domains of TNFR and IL-1R bind and neutralize pro-inflammatory cytokines, preventing them from binding to biologically active receptors [84]. Complement inhibitors, prostaglandins, and resolvins (lipid mediators) create a negative feedback loop that inhibits cytokine production. Polarization to the M2 phenotype of macrophages is triggered by cytokines IL-13 and IL-4 (M2a subtype), Toll-like receptors, and IL-1R ligands (M2b), and glucocorticoids, IL-10 and TNF β (M2c subtype). M2a, M2b, and M2c macrophages have individual and overlapping roles – M2a produces an anti-inflammatory, immune response, tissue fibrosis and wound healing, M2b participates in immunoregulation, while M2c has a role in immunosuppression, tissue repair and matrix remodelling [85,86]. The inflammatory reflex, via the vagus nerve, culminates in the release of acetylcholine from T-cells, which interacts with α7 nicotinic acetylcholine receptors on macrophages and inhibits the production of cytokines [87]. The resolution of inflammation is sparsely achieved in foreign body reactions, as cells surrounding a transplant continuously produce pro-inflammatory cytokines, and the biomaterial acts as the initiating agent [61].

3. Overview of cell delivery biomaterials and technologies

Potential cell therapies can be injected into the systemic circulation or directly to the damaged tissue as suspensions in appropriate media. Diverse cell populations have been introduced to the body via this route -bone-marrow-derived cells, myoblast populations, hepatocytes, differently differentiated embryonal stem cells, and others [88,89]. However, this type of transplantation is followed by immense cell death, extremely poor engraftment, and limited cell distribution in the tissues post-injection. All this has contributed to limited clinical success, especially in large volume tissues [9,90–95].

Structure-supporting constructs are engineered from biomaterials to exert more control over cell fate post-transplantation and to serve as equivalents of extracellular matrix (ECM). They enable the adhesion of cells of interest, regulate gene expression, reduce anoikis (apoptosis upon the loss of attachment to ECM), and contribute to tissue formation by allowing specific cell localization. Additionally, the interaction of biomaterial with the host's cells can have a beneficial effect, including the promotion of vascularization through newly transplanted tissue or protection from the immune system. This has led to FDA-approved therapies and clinical application in skin, cardiac, musculotendinous, and nerve reparation [9,96].

Cell-carrying constructs should support tissue formation, provide a stable environment with optimal nutrient and growth factors diffusion while simultaneously having immune-shielding effects, particularly in allografts and conditions with an autoimmune component. They traditionally include macroporous scaffolds, hydrogel entrapped cells, and their combination, made from different natural and synthetic materials. Decellularized ECM (dECM) has also been used as a possible biomaterial [97].

Encapsulation technology has been investigated to improve the viability and functionality of transplanted cells, including macroencapsulation in retrievable devices and bio-printed scaffolds and microencapsulation in hydrogel microspheres [94,98–101]. Furthermore, different forms of encapsulation are often combined; for example, scaffolds can be integrated into an injectable hydrogel, and microcapsules can be incorporated in scaffolds and injectable matrix [41,42, 101–106]. In addition, biomaterial based cellular encapsulation provides a protective 3D structural support for cell survival and function [5, 107] and a possible mechanical barrier between immunogenic cells and the immune system of the host while enabling sufficient function of transplanted cells [91,93,99–102,108–110].

3.1. Commonly used hydrogels in cell delivery and tissue engineering

Hydrogels are considered biomaterials for tissue engineering and cell delivery based on high water content, good mechanical properties, promising biocompatibility, and high permeability to oxygen, nutrients, and other water-soluble metabolites [111,112]. Hydrogels are polymeric networks with a 3D structure that is often cross-linked, characterized by a soft and rubbery consistency analogous to living tissue. Hydrogels can load water and other substances, including biological fluids [113,114]. This is associated with the presence of hydrophilic and hydrophobic groups in the polymeric chain, making water absorption from 10 to 99%, depending on the ratio of these groups [115,116]. Cross-links present in the hydrogel are needed to avoid dissolution in an aqueous environment [113,117]. However, there are problems linked to the gelation process, such as exogenous cytotoxicity of additive initiator, crosslinking agents or by-products formation, and poor gelation efficiency due to the use of light and radiation to initiate the crosslinking reaction [118–123]. Many different hydrogels (including their derivates and combinations) have been used in cell delivery (Table 1.).

The most commonly used hydrogel is alginate, which binds polyaminoacids at the surface, providing semi-permeable properties [162]. As shown by both clinical and preclinical studies, alginate is highly biocompatible [163,164]. It can form gels under physiological

Table 1
The most common natural polymers used in tissue engineering. Listed polymers include polymer derivates and combinations.

Polymers	Tissue	Form	Reference
Alginate	Islets	Microcapsules	[1,53,82,88,101,125,126]
	Bone	Scaffolds	[126]
	Bone	Microcapsules	[127]
	Cartilage	Scaffolds	[128]
	Cartilage	Scaffolds	[129]
	Cartilage	Injectable gel	[130]
	Stem cells	Microcapsules	[131]
Gelatine	Stem cells	Microcapsules	[132]
	Liver	Scaffolds	[133]
	Cartilage	Scaffolds	[134]
	Connective	Injectable gel	[135]
	Cardiac	Injectable gel	[136]
	Connective	Scaffolds	[137]
Collagen	Cartilage	Scaffolds	[138]
	Endothelial	Scaffolds	[139]
	Bone	Scaffolds	[140]
	Cartilage	Injectable gel	[141]
	Stem cells	Injectable gel	[142]
	Fibrocartilage	Injectable gel	[143]
	Stem cells	Microcapsules	[144]
Fibrin	Vascular	Microcapsules	[144]
	Stem cells	Injectable hydrogel	[145]
	Stem cells	Microcapsules	[146]
	Cartilage	Injectable hydrogel	[147]
	Vascular	Injectable hydrogel	[148]
	Stem cells	Scaffold	[149]
	Neural	Scaffold	[150]
	Stem cells	Scaffold	[151]
Hyaluronic acid	Connective tissue	Injectable hydrogel	[152]
	Cardiac	Injectable hydrogel	[153]
	Adipose	Injectable hydrogel	[154]
	Connective	Scaffold	[155]
	Stem cells	Microcapsules	[156]
Chitosan	Stem cells	Injectable hydrogel	[157]
	Stem cells	Scaffold	[158]
	Stem cells	Microcapsules	[159]
Agarose	Vascular	Microcapsules	[160]
	Stem cells	Microcapsules	[161]
	Cartilage	Scaffolds	[162]

environment, so it is widely used for encapsulation purposes and as a biostructure material [165]. Alginate can be harvested from algae or via bacterial cultures [166] and comprehensively consists of debranched homopolymeric regions of two different sugars -D-mannouranate (M-blocks) and L-guluronate (G-blocks), usually separated by regions of altering G – and M-blocks [167]. Alginate is water-soluble and able to be cross-linked by divalent ions. Most suitable for biomedical applications is Ca^{2+}, as opposed to the cellular toxicity of Ba^{2+} and Sr^{2+} [168]. Monovalent cations and Mg^{2+} do not induce gelation [169–174]. During cross-linking, the calcium ions react with G blocks (carboxyl groups) of two neighbouring chains creating an "egg box" orientation [168]. The M/G ratio, sequence, G-block length, and molecular weight are key parameters influencing the physicochemical properties of alginate and resulting hydrogels. Alginates with a higher concentration of G-blocks usually create stronger gels, while those with more M-blocks in their structure produce more flexible gels [175].

Fluctuations of pH in body fluids can make the surface of alginate more susceptible to adsorption of host proteins and inflammatory response [176]. Other polymers can be added to enhance alginate cell responsiveness, such as autologous platelet-rich plasma [177], gelatine [178] and gelatine methacryloyl (GelMA) [179]. It was reported that alginate modification, as a triazole derivate, could modulate populations of immune cells at the surface of the material, inhibiting and disrupting the fibrotic process [180–182].

Cells generally do not have receptors to recognize alginate, so proliferation and differentiation of some cells in alginate require signalling molecules [183]. Different agents are added to overcome certain shortcomings of the alginate system, such as ECM materials to stimulate cell growth [184] and oxygen generating biomaterials [185]. Finally, the addition of BAs is discussed as a possible molecule of interest to enhance cell viability and functionality within the alginate matrix.

Poloxamer 407 is another commonly used hydrogel. It consists of triblock chains, with polypropylene oxide (PPO) in the middle and two blocks of polyethylene oxide (PEO) on the sides. Based on specific properties (hydrophobic centre and hydrophilic sides), Poloxamer 407 is a surfactant capable of micelle formation, and at certain concentration and temperatures, it creates a reversible gel [186]. Thus, Poloxamer in the form of micelles has versatile roles, including drug delivery, surfactant, and crosslinker agent. Furthermore, Poloxamer 407 in the form of gel can be used in drug and cell delivery, as it is easily sterilized by filtration. Moreover, it can be modified to respond to external stimuli, like temperature, pH, light, wavelength, and magnetic fields [187,188]. Furthermore, Poloxamer is biocompatible and non-cytotoxic, and in combination with other polymers or alone, it is a prospective biomimetic material for cell delivery purposes [189,190].

3.2. Commonly used technologies in cell delivery and tissue engineering

3.2.1. Microencapsulation technology

Microencapsulation is a process that includes the envelopment of core material within a membrane, porous or impermeable, by various techniques to create particles in size of 1–1000 μm [167]. Microencapsulation techniques include emulsification and solvent evaporation, solvent extraction or phase inversion, interfacial polymerization, coacervation/phase separation, inotropic gelation, spray drying, and spray congealing. The choice of technique depends on the polymer, its properties, and the characteristics of the active compound [191]. One of the most widely used techniques is a vibrating-jet technique known as a vibrating nozzle technique (VNM) [167]. This technique utilizes the laminar breakup of liquid into droplets of equal size by a superimposed vibration; therefore, the frequency of vibration determines the number of droplets produced. Parameters include nozzle size, jet flow rate, vibration frequency, and electrode tension [191]. VNM effectively produces stable and homogeneous microcapsules using an encapsulator with various nozzle sizes, but it does not have high production yields. Adjustments in production flow rate by an increase in diameters or vibration frequency lead to higher production volumes, making a way to balance production amount with capsule size control [26].

Microcapsules can have various structures, enabling their use in different processes, classified into five types:

a) Mononuclear, simplest form, containing one enveloped core (usually a liquid),
b) Double/multi-shell walls, the extra shell is used for modification of microcapsule's stability or/and permeability,
c) Polynuclear microcapsule with two or more separate cores [167],
d) Microspheres (microbeads) – the most common type of capsules. Particles (and cells) are in a solid matrix without a distinctive membrane of microcapsule [192],
e) And irregular (non-spherical) shaped capsules [167].

The semipermeable membrane of a microcapsule prevents foreign particles such as antibodies or high weight molecules from damaging the encapsulated material while releasing encapsulated compounds in zero-order release [193,194]. This opens up the possibility of incorporating supporting molecules into a polymer matrix, such as anti inflammatory or antioxidant compounds [195]. Different natural (proteins,

carbohydrates, lipids, acacia gums), synthetic polymer materials, and their combinations can be used to produce microcapsules. The selection of polymer is significant for formulation properties and efficacy. For application in medical and biotechnological domains, the main focus is on alginate as a suitable polymer matrix [124,167,196].

Encapsulation can mitigate the shortage of donor tissue, allowing transplantation of allogeneic and xenogeneic cells [197]. Pluripotent stem cells have been proposed as an external source of cells [198–200]. However, the potential risk of neoplastic transformation should be considered. Manipulation steps needed for specific differentiation increase the risk of uncontrolled proliferation and atypical protein expression [198].

3.2.2. Bioprinting

Bioprinting is a printing technology that offers an advantage over microencapsulation as an easily retrievable transplant, in the form of cell-laden scaffolding structures, with defined macropores, mimicking the natural extracellular matrix of the tissue [201,202]. In addition, this technology is attractive for tissue engineering and other applications because of the high-throughput, digital control, and very precise placements of cells and biological factors to targeted locations [203]. The three most common bioprinting mechanisms are inkjet bioprinting, extrusion bioprinting, and laser bioprinting [204].

The hydrogel-cell suspension, bio-ink, is printed as a liquid solution, going through the dispensing and then gelation processes. However, the dispensing process often involves mechanical and thermal stress, affecting cell behaviour [205].

Bioprinting has the possibility of engineering a protective environment for cells by decreasing local inflammation and modulating the microenvironment in and around the device in a cytoprotective way [116]. This is not without difficulties, as cells within the device commonly suffer from necrosis and hypoxia, triggering the host immune system [98]. So far, biomaterials have had limited clinical success due to early graft rejection, fibrosis, and chemical instability, polymer biodegradation and limited permeability, and an associated reduction in viability and functionality of the cells [5,206,207]. Due to inflammatory reactions to the transplant, a collagenous fibrotic capsule can form around the transplant, which isolates it from the host, hindering metabolic exchange, cell signalling, healing and tissue-device integration, which further reduces transplantation success [54,181]. In the early stages of this reaction, neovascularization occurs, driven by induced expression of pro-angiogenic factors [208], which can possibly be utilized.

The functionality of bioprinted structures is determined by their properties, mainly macroporosity, microporosity, and interconnectivity. High macroporosity allows cell infiltration and colonisation of ECM. Pores' size and interconnectivity are linked to cell growth, proliferation, and migration, leading to faster vascularization and the formation of new tissue [202,209]. Microporosity is essential for efficient cell adhesion and spreading [210].

3.2.3. Injectable gels

Injectable gels are easy to manipulate and adjust based on the topography of the surrounding tissue, making them useful for numerous applications in cell and drug delivery. They are used as fillers for soft or dense tissues, promoting the physical integration of delivered cells. Minimally invasive application lessens the risks of associated complications, making injectable gels especially attractive for high-risk patients [211].

Gels are typically introduced to the system in the sol-to-gel transition phase as precursors, fully transitioning to hydrogel in the body. This effect is achieved via numerous physical or chemical stimuli or cross-linking reactions. The most common technique for *in situ* hydro gelations are physical associations within the polymer, including physical self-assembly, thermal gelation, ionic interactions, and photo polymerization [212,213]. Gels are preferable for cell injection, compared to low viscosity solutions like saline or cell culture media. They lessen the mechanical shear and extensional forces during the passage through a needle, mitigating damage to the cell membrane [214].

4. Cell delivery and bile acids: overview, impact and effects on transplanted cells and host

4.1. Effect of BA addition on hydrogel

The addition of BAs in the alginate matrix have been reported [41,94,99–101,108,109,215–218]. It is shown that BAs do not compromise the integrity of the alginate matrix [217]. One of the most studied BAs is ursodeoxycholic acid (UDCA). UDCA is the 7β-hydroxy isomer of CDCA, endogenously produced in humans in very small quantities (1–3% of human BA pool) by gut microbiota. UDCA is a hydrophilic BA with low toxicity, supplemented up to 40% of total BA pool in patients with several cholestatic liver diseases and GI tract diseases, including cholesterol gallstone, primary biliary cirrhosis and prophylaxis for colon cancer [219–222]. The addition of ursodeoxycholic acid (UDCA) reduces Zeta potential, suggesting a reduction in the surface charge, possibly through the chelation of positively charged ions [101]. Hydrophobic BA, like DCA, when added to the alginate matrix, reduces swelling, limits matrix erosion, and increases the matrix's mechanical strength [101,216]. A similar effect was observed with different BAs, including hydrophilic UDCA [94,109,215]. The incorporation of CA in a PVA based polymer network enhanced the hydrogel's mechanical stability and self-healing properties [223]. The increase of mechanical strength is favourable due to a possible reduction of shear cell stress during bioprinting and microencapsulation and subsequent reduction in inflammation and better cell viability and functionality.

4.2. Systemic and local biological effects of BA addition to cell delivery matrix

BAs, predominately hydrophilic ones (UDCA and TUDCA), have direct protective effects at the cellular and molecular levels, including improvement of defences against oxidative stress, inhibition of apoptosis, and stabilization of membranes [224]. It is reported that the addition of specific BAs can improve the viability and functionality of cells within the polymer [215], which is of major importance in cell delivery. This effect can be argued by the cell signalling effects of BA. BAs act as signalling molecules involved in a systematic regulation of several metabolic pathways through interaction with nuclear and cell membrane receptors [225].

BAs are ligands for five nuclear receptors: the vitamin D receptor (VDR, NR1H1), FXR (NR1H4), the pregnane X receptor (PXR, NR1H2), the constitutive androstane receptor (CAR, NR1H3), and the liver X receptor α (LXRα),(Fig. 3.) [226].

FXRα is a nuclear receptor expressed in the liver, kidney, adrenal gland, stomach, intestine, white adipose tissue, endothelial cells, vascular smooth muscle cells, pancreas, and immune system cells [225,227].

BAs can induce modulation of the immune system through anti-inflammatory effects via FXR activation – inhibition of activated B cells via nuclear factor kappa-light-chain (NF-kB)-enhancer leads to the downregulation of the synthesis of pro-inflammatory cytokines such as tumour necrosis factor (TNF)-α from monocytes and macrophages [12,228–230]. Therefore, biomaterial with constant and controlled release of BAs may influence monocytes and macrophages to lower pro-inflammation response to the transplanted device.

In the liver, FXR is shown to suppress excessive inflammation, as FXRα deplored mice spontaneously grow cancerous liver lesions [231]. The FXRα activation promotes hepatocytes proliferation and liver regeneration, inducing the transcription of pyruvate dehydrogenate kinase 4 (PDK4), which induces rapid biomass generation. Overexpression

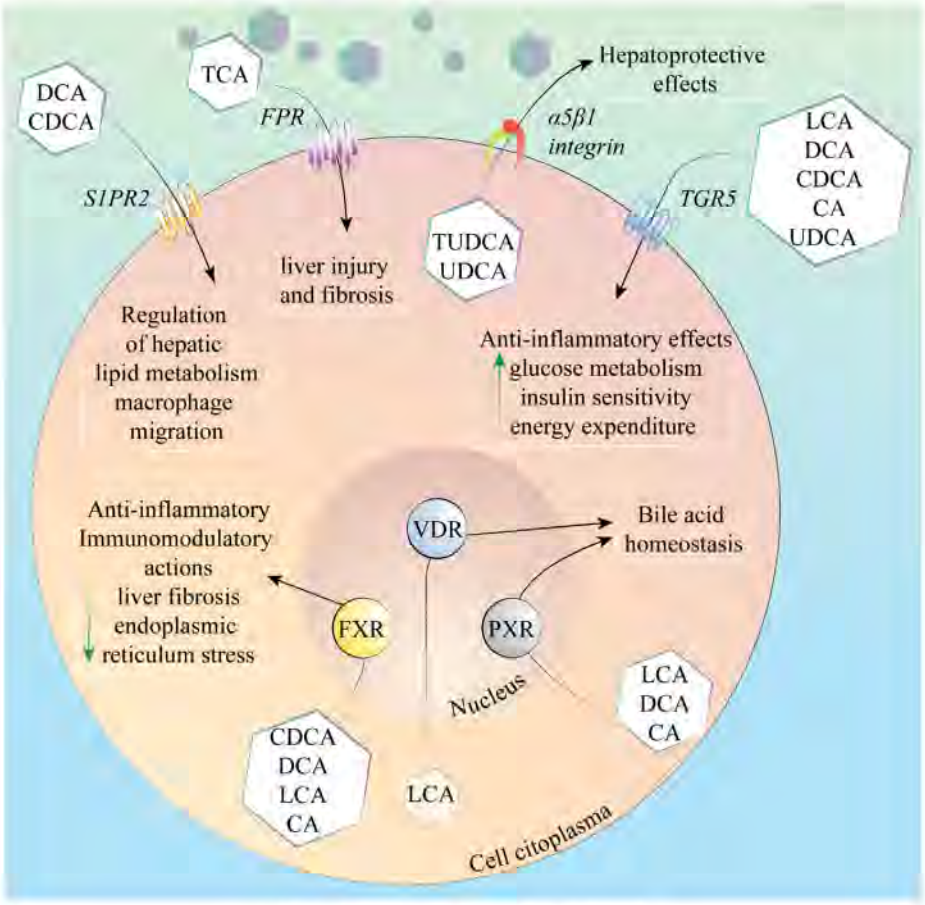

Fig. 3. Receptor-mediated bile acid biological activities.

of FXRα regulator, SIRT1, inhibits BA accumulation, leading to reduced hepatocyte proliferation [232], suggesting that BAs are essential for liver regeneration. In addition, FXRα inhibits hepatic stellate cells, responsible for the production of fibrotic factors and excess ECM proteins in liver fibrosis [233]. Based on this, cell delivery of hepatocytes within liver tissue may have several beneficial impacts of BAs addition to the graft. It promotes regeneration of heparocytes inside the device and limits liver fibrosis that may happen around the transplantation site, protecting the function of both graft and surrounding tissue.

Signalling pathways involving FXRα have a role in mitigating endoplasmic reticulum (ER) stress [234]. ER stress is caused by a hostile microenvironment characterized by oxygen and nutrient depravation and disturbed protein-folding capacity of ER. These conditions are prevalent within encapsulated cells. As a prolonged state of ER stress has a tumorigenic and metastatic capacity [235], alleviating this condition is of significant importance for normal tissue function within the graft. Particularly, UDCA is shown to decrease ER stress in endothelial cells caused by disturbed blood flow by inhibiting the activation of XBP-1 and CEBP homologous protein in the ER stress pathway, decreasing adhesion molecules' expression [236]. However, to reach nuclear receptors, BAs need to be readily released from the hydrogel matrix and not attached to it. Therefore, chemically binding BAs to matrix polymers may not promote FXRα related cell protection.

FXRα induces xenobiotic metabolism, adding to hepatoprotective behaviour [237]. During fasting, FXRα in hepatocytes promotes the expression of FGF21, a metabolically active member of the fibroblast growth family, and an inter-organ signalling molecule. FGF21 increases ketogenesis and fatty acid oxidation to improve insulin sensitivity and glucose uptake in white adipose tissue [238]. In addition, FXRα activation has been shown to decrease plasma lipoprotein levels by promoting lipoprotein clearance in the liver and inhibiting the synthesis of fatty acids and triglycerides [239].

BAs also activate several membrane-bound receptors TGR5 (GPBAR1), membrane α5β1 integrin, epidermal growth factor receptor, and sphingosine-1-phosphate receptor 2 [23,240,241]. TGR5 is expressed in brown adipose tissue, liver, gallbladder, intestine, muscle, selected areas of the central nervous system, and immune system cells [227]. TGR5, due to it's position as membrane-bound receptor, has a higher affinity to hydrophilic BAs and BAs salt [242]. TGR5 activation is followed by various effects, including anti inflammatory pathway

activation, improved glucose metabolism, gallbladder relaxation, improved intestinal motility, increased energy expenditure in brown adipose tissue, and increased insulin sensitivity [227]. Furthermore, In addition, TGR5 is expressed on $CD14^+$ monocytes and some macrophages, such as Kupffer cells, leading to the suppression of inflammation when activated [242]. Thus, TGR5 activation can potentially decrease inflammation around the transplant, synergistically with the anti-inflammatory response of FXRα.

Furthermore, TGR5 expressed in the bovine aorta endothelium produced nitric oxide (NO) in a dose-dependent manner in response to the administration of taurolithocholic acid [243]. NO is a known vasodilator, antioxidant, and anti-inflammatory agent, which inhibits various immunomodulatory cytokines secreted by macrophages, and down-regulates platelet aggregation and adherence [244]. The constant release of hydrophilic BAs or bile salts could affect the immune cells surrounding the transplant, mitigating inflammation of the transplant site. Systematic effects of added BAs would be limited by the placement of the transplant, in particular venous drainage. BAs going directly to the portal system would undergo hepatic reuptake, significantly reducing the amount that will appear in systematic circulation, thus limiting effects of added BAs on other organs. BAs also must be released in appropriately small concentrations so as not to affect hepatic feedback and secretion to the intestine. This is crucial, as injections of DCA and CDCA to rats (3 μg/rat/day) can increase permeability of brain blood barrier [245]. Hydrophobic bile acids induce cell death via intrinsic pathway by targeting mitochondria and via extrinsic pathway via death receptor-mediated apoptosis. Cell apoptosis was observed at lower concentrations lower than 100 μM, while necrosis at concentrations higher than 250 μM [246]. In contrast, hydrophilic UDCA was found to inhibit cytochrome c release and apoptosis induction at concentration of 500 μM [247]. Hydrophilic BAs are significant antioxidants as they raise glutathione levels, likely via higher expression of enzymes involved in glutathione synthesis (γ-glutamylcysteine synthetase and methionine S-adenosyltransferase) [248,249]. UDCA could be beneficial in for hepatocytes delivery, as it can elevate the amount of thiol-containing proteins such as metallothioneins, which can successfully scavenge the most highly reactive oxygen species, the hydroxyl radicals [248]. Regarding environment outside the trasnplantated graft, UDCA can decrease secretion of interleukins 2 and 4, TNF-α, interferon-γ from activated T lymphocytes, as well as immunoglobin production from B lymphocytes [230]. Finally, UDCA downregulates disturbed flow-induced inflammatory response consisting of monocyte adhesion to endothelial cells and endothelial cell apoptosis, which can be a beneficial feature for any implant [250].

BA's potentially have a beneficial effect on the vascularization of the transplant. CDCA improves angiogenesis by decreasing adhesion protein vascular endothelial cadherin (VE-cadherin) and promoting the expression of matrix metalloproteinases (MMP9) and vascular growth receptors (VEGFR1 and VEGFR 2) [251]. Vascular endothelial factor (VEGF) is a crucial angiogenesis regulator and agonist for VEGFR1 and VEGFR2. MMP9 increases the expression of VEGF and facilitate VEGF and VEGFR association [252]. In contrast, hydrophobic BAs (LCA and DCA) have detrimental effects on the vascular endothelium, and in high concentrations (above 25 μM), induce endothelial cell death, coiling, and shrinkage of newly formed vessels [251]. Activation of vasculature-specific FXRα improves lipid profile and influences vascular tension creating an anti atherosclerotic effect [24,253].

While theory on the topic may be encouraging (see Fig. 4), the benefits of BAs in cell delivery are still limited and studied on a small variety of cells and hydrogels (Table 2.). Therefore, further research is needed to determine the most suitable bile acid and its effect on the variety of different cells and transplant sites and impact on properties of hydrogel matrix.

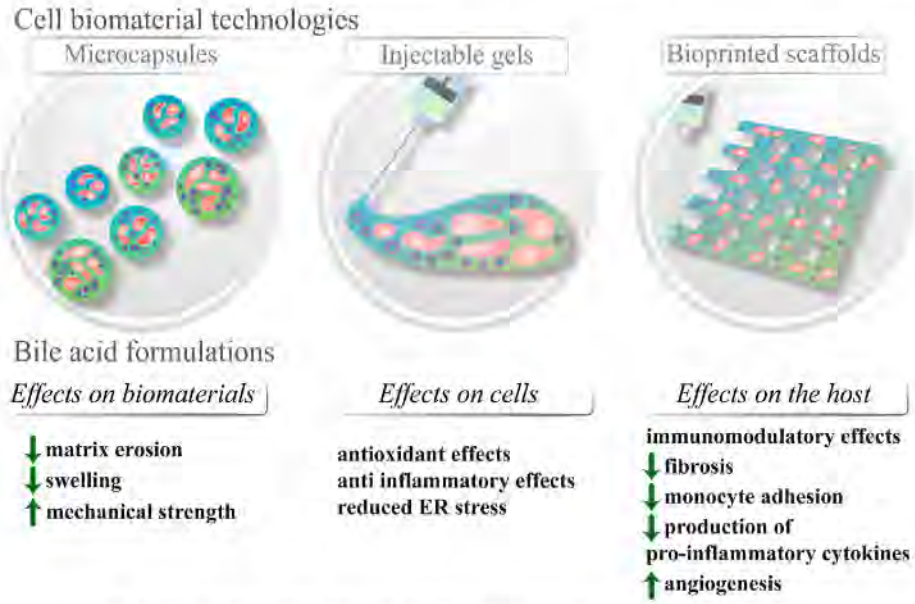

Fig. 4. Summary figure outlining bile acid's biological impact on transplanted graft and bioartificial roles.

Table 2
Studies using BA in cell delivery systems.

Bile acid	Polymer	Tissue	Form	Reference
UDCA	Alginate	Islets/β-cells	Microcapsules	[1,42,93,94,124,254]
CA	Alginate	B-cells	Microcapsules	[255]
TCA	Alginate	B-cells	Microcapsules	[256]

5. Conclusion

This review outlines the emerging role of BAs in the homeostasis of endocrine, gastrointestinal, immune, and cardio-metabolic biological systems, and how their unique pharmacological and physico-chemical properties contribute to potential roles in the new areas of biomaterials research, with a key focus on the creation of artificial organs. The ability of endogenous BAs to modify key cellular signalling pathways attributed to graft rejection, fibrosis, and tissue necrosis, could dramatically alter the science of transplantation and xenograft research, and perhaps re-examine the widespread use of immunosuppressants in clinical practice. Future research is needed to best guide the clinical manifestations of BA-mediated artificial organs, and to determine the benefits of BAs as pharmacological agents in the management of immune related disorders.

Data availability

All data is available upon request to the corresponding author.

Funding

H Al-Salami's work is partially supported by the European Union's Horizon 2020 SALSETH research and innovation programme under the Marie Sklodowska-Curie Grant agreement No. 872370. Al-Salami H has been and is currently receiving of funding from Beijing Nat-Med Biotechnology Co. Ltd and Glanis PTY Ltd.

Declaration of competing interest

The authors declare that they have no known competing financial interests or personal relationships that could have appeared to influence the work reported in this paper.

Acknowledgments

For their support, the authors acknowledge Australian Postgraduate Award & Curtin Research Scholarship.

References

[1] A. Mooranian, R. Negrulj, F. Arfuso, H. Al-Salami, Characterization of a novel bile acid-based delivery platform for microencapsulated pancreatic beta-cells, Artif Cells Nanomed Biotechnol 44 (1) (2016) 194–200.
[2] A.M. Rokstad, I. Lacik, P. de Vos, B.L. Strand, Advances in biocompatibility and physico-chemical characterization of microspheres for cell encapsulation, Adv. Drug Deliv. Rev. 67–68 (2014) 111–130.
[3] R.W.G. Gruessner, A.C. Gruessner, The current state of pancreas transplantation, Nat. Rev. Endocrinol. 9 (2013) 555.
[4] A.M.J. Shapiro, C. Ricordi, B.J. Hering, H. Auchincloss, R. Lindblad, R. P. Robertson, et al., International trial of the edmonton protocol for islet transplantation, N. Engl. J. Med. 355 (13) (2006) 1318–1330.
[5] D.C. Hamilton, H.H. Shih, R.A. Schubert, S.A. Michie, P.N. Staats, D.L. Kaplan, et al., A silk-based encapsulation platform for pancreatic islet transplantation improves islet function in vivo, Journal of Tissue Engineering and Regenerative Medicine 11 (3) (2017) 887–895.
[6] A.M. Shapiro, M. Pokrywczynska, C. Ricordi, Clinical pancreatic islet transplantation, Nat. Rev. Endocrinol. 13 (5) (2017) 268–277.
[7] A. Ovsianikov, A. Khademhosseini, V. Mironov, The synergy of scaffold-based and scaffold-free tissue engineering strategies, Trends Biotechnol. 36 (2018).
[8] A. Khademhosseini, R. Langer, A decade of progress in tissue engineering, Nat. Protoc. 11 (10) (2016) 1775–1781.
[9] D.J. Mooney, H. Vandenburgh, Cell delivery mechanisms for tissue repair, Cell Stem Cell 2 (3) (2008) 205–213.
[10] A. Lee, A.R. Hudson, D.J. Shiwarski, J.W. Tashman, T.J. Hinton, S. Yerneni, et al., 3D bioprinting of collagen to rebuild components of the human heart, Science 365 (6452) (2019) 482–487.
[11] S.M. Houten, M. Watanabe, J. Auwerx, Endocrine functions of bile acids, EMBO J. 25 (7) (2006) 1419–1425.
[12] J. Prawitt, S. Caron, B. Staels, Bile acid metabolism and the pathogenesis of type 2 diabetes, Curr. Diabetes Rep. 11 (3) (2011) 160.
[13] R. Negrulj, A. Mooranian, H. Al-Salami, Potentials and limitations of bile acids in type 2 diabetes mellitus: applications of microencapsulation as a novel oral delivery system, Journal of Endocrinology and Diabetes Mellitus 1 (2013) 49–59.
[14] Mooranian A, Negrulj R, Chen-Tan N, Fakhoury M, Jones F, Arfuso F, et al., editors. NOVEL MULTICOMPARTMENTAL BILE ACID-BASED MICROCAPSULES FOR PANCREATIC beta-CELL TRANSPLANTATION. IPITA-IXA-CTS 2015 Joint Congress of the International-Pancreas-And-Islet-Transplantation-Association, International-Xenotransplantation-Association and Cell-Transplant-Society; 2015/11/01/; Melbourne, AUSTRALIA United States: LIPPINCOTT WILLIAMS & WILKINS.
[15] Mooranian A, Negrulj R, Chen-Tan N, Fakhoury M, Jones F, Arfuso F, et al., editors. Novel multicompartmental bile acid-based microcapsules for pancreatic beta-cell transplantation. IPITA/IXA/CTS Joint Congress; 2015/11/01/; Melbourne, AUSTRALIA United States: WILEY-BLACKWELL.
[16] J.M. Donkers, R.L.P. Roscam Abbing, S.F.J. van de Graaf, Developments in bile salt based therapies: a critical overview, Biochem. Pharmacol. 161 (2019) 1–13.
[17] G. Perdigon, C. Maldonado Galdeano, J.C. Valdez, M. Medici, Interaction of lactic acid bacteria with the gut immune system, Eur. J. Clin. Nutr. 56 (Suppl 4) (2002) S21–S26.
[18] H.J. Wu, Ivanov II, J. Darce, K. Hattori, T. Shima, Y. Umesaki, et al., Gut-residing segmented filamentous bacteria drive autoimmune arthritis via T helper 17 cells, Immunity 32 (6) (2010) 815–827.
[19] A.S. Hassan, M.T. Subbiah, Effect of diabetes during pregnancy on maternal and neonatal bile acid metabolism in the rat, Proc Soc Exp Biol Med 165 (3) (1980) 490–495.
[20] A.B. Thomson, Unidirectional flux rate of cholesterol and fatty acids into the intestine of rats with drug-induced diabetes mellitus: effect of variations in the effective resistance of the unstirred water layer and the bile acid micelle, J. Lipid Res. 21 (6) (1980) 687–698.
[21] T.W.H. Pols, L.G. Noriega, M. Nomura, J. Auwerx, K. Schoonjans, The bile acid membrane receptor TGR5: a valuable metabolic target, Dig. Dis. 29 (1) (2011) 37–44.
[22] S. Takahashi, T. Fukami, Y. Masuo, C.N. Brocker, C. Xie, K.W. Krausz, et al., Cyp2c70 is responsible for the species difference in bile acid metabolism between mice and humans, JLR (J. Lipid Res.) 57 (12) (2016) 2130–2137.
[23] M. Trauner, C.D. Fuchs, E. Halilbasic, G. Paumgartner, New therapeutic concepts in bile acid transport and signaling for management of cholestasis, Hepatology 65 (4) (2017) 1393–1404.
[24] T. Vasavan, E. Ferraro, E. Ibrahim, P. Dixon, J. Gorelik, C. Williamson, Heart and bile acids – clinical consequences of altered bile acid metabolism, Biochim. Biophys. Acta (BBA) - Mol. Basis Dis. 1864 (4) (2018) 1345–1355. Part B.
[25] I. Makino, K. Shinozaki, K. Yoshino, S. Nakagawa, [Dissolution of cholesterol gallstones by long-term administration of ursodeoxycholic acid], Nihon Shokakibyo Gakkai zasshi = The Japanese journal of gastro-enterology 72 (6) (1975) 690–702.
[26] Negrulj R, Mooranian A, Al-Salami H. Potentials and Limitations of Bile Acids in Type 2 Diabetes Mellitus: Applications of Microencapsulation as a Novel Oral Delivery System2013. 49-59 p.
[27] P.A. Dawson, T. Lan, A. Rao, Bile acid transporters, JLR (J. Lipid Res.) 50 (12) (2009) 2340–2357.
[28] Y.-K.J. Zhang, G.L. Guo, C.D. Klaassen, Diurnal variations of mouse plasma and hepatic bile acid concentrations as well as expression of biosynthetic enzymes and transporters, PLoS One 6 (2) (2011), e16683.
[29] D.M. Small, R.H. Dowling, R.N. Redinger, The enterohepatic circulation of bile salts, Arch. Intern. Med. 130 (4) (1972) 552–573.
[30] M. Wagner, G. Zollner, M. Trauner, Nuclear bile acid receptor farnesoid X receptor meets nuclear factor-κB: new insights into hepatic inflammation, Hepatology 48 (5) (2008) 1383–1386.
[31] J.M. Ridlon, D.-J. Kang, P.B. Hylemon, Bile salt biotransformations by human intestinal bacteria, JLR (J. Lipid Res.) 47 (2) (2006) 241–259.
[32] E. Halilbasic, T. Claudel, M. Trauner, Bile acid transporters and regulatory nuclear receptors in the liver and beyond, J. Hepatol. 58 (1) (2013) 155–168.
[33] C. Mataki, B.C. Magnier, S.M. Houten, J.-S. Annicotte, C. Argmann, C. Thomas, et al., Compromised intestinal lipid absorption in mice with a liver-specific deficiency of liver receptor homolog 1, Mol. Cell Biol. 27 (23) (2007) 8330–8339.
[34] Y.K. Lee, D.R. Schmidt, C.L. Cummins, M. Choi, L. Peng, Y. Zhang, et al., Liver receptor homolog-1 regulates bile acid homeostasis but is not essential for feedback regulation of bile acid synthesis, Mol. Endocrinol. 22 (6) (2008) 1345–1356.
[35] C.Y. Han, Update on FXR biology: promising therapeutic target? Int. J. Mol. Sci. 19 (7) (2018) 2069.
[36] S. Kir, S.A. Beddow, V.T. Samuel, P. Miller, S.F. Previs, K. Suino-Powell, et al., FGF19 as a postprandial, insulin-independent activator of hepatic protein and glycogen synthesis, Science 331 (6024) (2011) 1621–1624.
[37] U. Beuers, M. Trauner, P. Jansen, R. Poupon, New paradigms in the treatment of hepatic cholestasis: from UDCA to FXR, PXR and beyond, J. Hepatol. 62 (1, Supplement) (2015) S25–S37.

[38] G. Le Martelot, T. Claudel, D. Gatfield, O. Schaad, B. Kornmann, G. Lo Sasso, et al., REV-ERBalpha participates in circadian SREBP signaling and bile acid homeostasis, PLoS Biol 7 (9) (2009) e1000181–e.
[39] M. Stojančević, N. Pavlović, S. Goločorbin-Kon, M. Mikov, Application of bile acids in drug formulation and delivery, Front. Life Sci. 7 (3–4) (2013) 112–122.
[40] Y. Qi, C. Jiang, J. Cheng, K.W. Krausz, T. Li, J.M. Ferrell, et al., Bile acid signaling in lipid metabolism: metabolomic and lipidomic analysis of lipid and bile acid markers linked to anti-obesity and anti-diabetes in mice, Biochim. Biophys. Acta Mol. Cell Biol. Lipids 1851 (1) (2015) 19–29.
[41] A. Mooranian, R. Negrulj, H. Al-Salami, Primary bile acid chenodeoxycholic acid-based microcapsules to examine β-cell survival and the inflammatory response, BioNanoScience 6 (2) (2016) 103–109.
[42] A. Mooranian, R. Negrulj, H. Al-Salami, The impact of allylamine-bile acid combinations on cell delivery microcapsules in diabetes, J. Microencapsul. 33 (6) (2016) 569–574.
[43] A. Mooranian, R. Negrulj, M. Mikov, S. Golocorbin-Kon, F. Arfuso, H. Al-Salami, Novel chenodeoxycholic acid-sodium alginate matrix in the microencapsulation of the potential antidiabetic drug, probucol. An in vitro study, J. Microencapsul. 32 (6) (2015) 589–597.
[44] H. Sugioka, Y. Moroi, Micelle formation of sodium cholate and solubilization into the micelle, Biochim. Biophys. Acta 1394 (1) (1998) 99–110.
[45] L. Galantini, M.C. di Gregorio, M. Gubitosi, L. Travaglini, J.V. Tato, A. Jover, et al., Bile salts and derivatives: rigid unconventional amphiphiles as dispersants, carriers and superstructure building blocks, Curr. Opin. Colloid Interface Sci. 20 (3) (2015) 170–182.
[46] A. Di Ciaula, G. Garruti, R. Lunardi Baccetto, E. Molina-Molina, L. Bonfrate, D. Q. Wang, et al., Bile acid physiology, Ann. Hepatol. 16 (Suppl. 1: s3–105) (2017) s4–s14.
[47] C. Darkoh, L.M. Lichtenberger, N. Ajami, E.J. Dial, Z.D. Jiang, H.L. DuPont, Bile acids improve the antimicrobial effect of rifaximin, Antimicrobial agents and chemotherapy 54 (9) (2010) 3618–3624.
[48] D. Wustner, A. Herrmann, P. Muller, Head group-independent interaction of phospholipids with bile salts. A fluorescence and EPR study, J. Lipid Res. 41 (3) (2000) 395–404.
[49] D. Madenci, S.U. Egelhaaf, Self-assembly in aqueous bile salt solutions, Curr. Opin. Colloid Interface Sci. 15 (1) (2010) 109–115.
[50] M.C. di Gregorio, L. Travaglini, A. Del Giudice, J. Cautela, N.V. Pavel, L. Galantini, Bile salts: natural surfactants and precursors of a broad family of complex amphiphiles, Langmuir 35 (21) (2019) 6803–6821.
[51] M. Zhang, C. Fives, K.C. Waldron, X.X. Zhu, Self-assembly of a bile acid dimer in aqueous solutions: from nanofibers to nematic hydrogels, Langmuir 33 (4) (2017) 1084–1089.
[52] V. Stepanov, K. Stankov, M. Mikov, The bile acid membrane receptor TGR5: a novel pharmacological target in metabolic, inflammatory and neoplastic disorders, J. Recept. Signal Transduct. Res. 33 (4) (2013) 213–223.
[53] A. Mooranian, R. Tackechi, E. Jamieson, G. Morahan, H. Al-Salami, Innovative microcapsules for pancreatic β-cells harvested from mature double-transgenic mice: cell imaging, viability, induced glucose-stimulated insulin measurements and proinflammatory cytokines analysis, Pharmaceut. Res. 34 (6) (2017) 1217–1223.
[54] A.R. Pepper, B. Gala-Lopez, R. Pawlick, S. Merani, T. Kin, A.M.J. Shapiro, A prevascularized subcutaneous device-less site for islet and cellular transplantation, Nat. Biotechnol. 33 (2015) 518.
[55] D.M. Berman, R.D. Molano, C. Fotino, U. Ulissi, J. Gimeno, A.J. Mendez, et al., Bioengineering the endocrine pancreas: intraomental islet transplantation within a biologic resorbable scaffold, Diabetes 65 (5) (2016) 1350.
[56] N. Fotino, C. Fotino, A. Pileggi, Re-engineering islet cell transplantation, Pharmacol. Res. 98 (2015) 76–85.
[57] A.C. Farney, D.E. Sutherland, E.C. Opara, Evolution of islet transplantation for the last 30 years, Pancreas 45 (1) (2016) 8–20.
[58] E.S. O'Sullivan, A. Vegas, D.G. Anderson, G.C. Weir, Islets transplanted in immunoisolation devices: a review of the progress and the challenges that remain, Endocr. Rev. 32 (6) (2011) 827–844.
[59] N. Ashammakhi, S. Ahadian, I. Pountos, S.-K. Hu, N. Tellisi, P. Bandaru, et al., In situ three-dimensional printing for reparative and regenerative therapy, Biomed. Microdevices 21 (2) (2019) 42.
[60] Y. Wang, X. Huang, Y. Shen, R. Hang, X. Zhang, Y. Wang, et al., Direct writing alginate bioink inside pre-polymers of hydrogels to create patterned vascular networks, J. Mater. Sci. 54 (10) (2019) 7883–7892.
[61] R. Klopfleisch, F. Jung, The pathology of the foreign body reaction against biomaterials, J. Biomed. Mater. Res. 105 (3) (2017) 927–940.
[62] L. Zhang, Z. Cao, T. Bai, L. Carr, J.R. Ella-Menye, C. Irvin, et al., Zwitterionic hydrogels implanted in mice resist the foreign-body reaction, Nat. Biotechnol. 31 (6) (2013) 553–556.
[63] T.H. Barker, A.J. Engler, The provisional matrix: setting the stage for tissue repair outcomes, Matrix Biol. 60–61 (2017) 1–4.
[64] K.R. Chandorkar Y, B. Basu, The foreign body response demystified, ACS Biomater. Sci. Eng. 5 (1) (2019) 19–44.
[65] M.G. Netea, F. Balkwill, M. Chonchol, F. Cominelli, M.Y. Donath, E. J. Giamarellos-Bourboulis, et al., A guiding map for inflammation, Nat. Immunol. 18 (8) (2017) 826–831.
[66] I. Afonina, Z. Zhong, M. Karin, R. Beyaert, Limiting inflammation - the negative regulation of NF-B and the NLRP3 inflammasome, Nat. Immunol. 18 (2017) 861–869.
[67] A. Iwasaki, R. Medzhitov, Toll-like receptor control of the adaptive immune responses, Nat. Immunol. 5 (10) (2004) 987–995.
[68] S. Akira, S. Uematsu, O. Takeuchi, Pathogen recognition and innate immunity, Cell 124 (4) (2006) 783–801.
[69] P. Scapini, O. Marini, C. Tecchio, M.A. Cassatella, Human neutrophils in the saga of cellular heterogeneity: insights and open questions, Immunol. Rev. 273 (1) (2016) 48–60.
[70] K. Eyerich, V. Dimartino, A. Cavani, IL-17 and IL-22 in immunity: driving protection and pathology, Eur. J. Immunol. 47 (4) (2017) 607–614.
[71] C.A. Dinarello, Historical insights into cytokines, Eur. J. Immunol. 37 (S1) (2007) S34–S45.
[72] W. Schrödl, R. Büchler, S. Wendler, P. Reinhold, P. Muckova, J. Reindl, et al., Acute phase proteins as promising biomarkers: perspectives and limitations for human and veterinary medicine, Proteonomics Clin. Appl. 10 (11) (2016) 1077–1092.
[73] M.M. Markiewski, J.D. Lambris, The role of complement in inflammatory diseases from behind the scenes into the spotlight, Am. J. Pathol. 171 (3) (2007) 715–727.
[74] E.C. Shattuck, M.P. Muehlenbein, Human sickness behavior: ultimate and proximate explanations, Am. J. Phys. Anthropol. 157 (1) (2015) 1–18.
[75] P.A. Ward, The harmful role of c5a on innate immunity in sepsis, J Innate Immun 2 (5) (2010) 439–445.
[76] S. Gordon, A. Pluddemann, Tissue macrophages: heterogeneity and functions, BMC Biol 15 (1) (2017) 53.
[77] P.M.-K. Tang, D.J. Nikolic-Paterson, H.-Y. Lan, Macrophages: versatile players in renal inflammation and fibrosis, Nat. Rev. Nephrol. 15 (3) (2019) 144–158.
[78] S.V. Kalish, S.V. Lyamina, E.A. Usanova, E.B. Manukhina, N.P. Larionov, I. Y. Malyshev, Macrophages reprogrammed in vitro towards the M1 phenotype and activated with LPS extend lifespan of mice with ehrlich ascites carcinoma, Med Sci Monit Basic Res 21 (2015) 226–234.
[79] S. Lin, B. Zhang, M.J. Skoumal, B. Ramunno, X. Li, C. Wesdemiotis, et al., Antifouling poly(β-peptoid)s, Biomacromolecules 12 (7) (2011) 2573–2582.
[80] J.M. Anderson, A.K. McNally, Biocompatibility of implants: lymphocyte/macrophage interactions, Semin. Immunopathol. 33 (3) (2011) 221–233.
[81] T.J. Koh, L.A. DiPietro, Inflammation and wound healing: the role of the macrophage, Expet Rev. Mol. Med. 13 (2011) e23.
[82] P. DiEgidio, H.I. Friedman, R.G. Gourdie, A.E. Riley, M.J. Yost, R.L. Goodwin, Biomedical implant capsule formation: lessons learned and the road ahead, Ann. Plast. Surg. 73 (4) (2014) 451–460.
[83] W. Ouyang, S. Rutz, N.K. Crellin, P.A. Valdez, S.G. Hymowitz, Regulation and functions of the IL-10 family of cytokines in inflammation and disease, Annu. Rev. Immunol. 29 (2011) 71–109.
[84] C.A. Dinarello, IL-1: discoveries, controversies and future directions, Eur. J. Immunol. 40 (3) (2010) 599–606.
[85] M.G. Kim, S.C. Kim, Y.S. Ko, H.Y. Lee, S.K. Jo, W. Cho, The role of M2 macrophages in the progression of chronic kidney disease following acute kidney injury, PLoS One 10 (12) (2015), e0143961.
[86] K.L. Spiller, R.R. Anfang, K.J. Spiller, J. Ng, K.R. Nakazawa, J.W. Daulton, et al., The role of macrophage phenotype in vascularization of tissue engineering scaffolds, Biomaterials 35 (15) (2014) 4477–4488.
[87] U. Andersson, K.J. Tracey, Reflex principles of immunological homeostasis, Annu. Rev. Immunol. 30 (1) (2012) 313–335.
[88] A. Mooranian, R. Negrulj, H. Al-Salami, Alginate-deoxycholic acid interaction and its impact on pancreatic B-cells and insulin secretion and potential treatment of type 1 diabetes, Journal of Pharmaceutical Innovation 11 (2) (2016) 156–161.
[89] A. Mooranian, N. Zamani, G. Luna, H. Al-Sallami, M. Mikov, S. Golocorbin-Kon, et al., Bile acid-polymer-probucol microparticles: protective effect on pancreatic beta-cells and decrease in type 1 diabetes development in a murine model, Pharmaceut. Dev. Technol. 24 (10) (2019) 1272–1277.
[90] H. Caplan, S.D. Olson, A. Kumar, M. George, K.S. Prabhakara, P. Wenzel, et al., Mesenchymal stromal cell therapeutic delivery: translational challenges to clinical application, Front. Immunol. 10 (2019) 1645.
[91] G. Almeida-Porada, A.J. Atala, C.D. Porada, Therapeutic mesenchymal stromal cells for immunotherapy and for gene and drug delivery, Mol Ther Methods Clin Dev 16 (2020) 204–224.
[92] A. Mooranian, R. Negrulj, F. Arfuso, H. Al-Salami, Characterization of a novel bile acid-based delivery platform for microencapsulated pancreatic beta-cells, Artificial Cells, Nanomedicine, and Biotechnology 44 (1) (2016) 194–200.
[93] A. Mooranian, R. Negrulj, H. Al-Salami, G. Morahan, E. Jamieson, Designing anti-diabetic β-cells microcapsules using polystyrenic sulfonate, polyallylamine, and a tertiary bile acid: morphology, bioenergetics, and cytokine analysis, Biotechnol. Prog. 32 (2) (2016) 501–509.
[94] A. Mooranian, R. Negrulj, H. Al-Salami, The incorporation of water-soluble gel matrix into bile acid-based microcapsules for the delivery of viable β-cells of the pancreas, in diabetes treatment: biocompatibility and functionality studies, Drug Delivery and Translational Research 6 (1) (2016) 17–23.
[95] A. Mooranian, R. Negrulj, H. Al-Salami, Viability and topographical analysis of microencapsulated β-cells exposed to a biotransformed tertiary bile acid: an ex vivo study, Int. J. Nano Biomaterials (IJNBM) 6 (2) (2016) 74–82.
[96] T. Hoffman, A. Khademhosseini, R. Langer, Chasing the paradigm: clinical translation of 25 Years of tissue engineering, Tissue Eng. 25 (9–10) (2019) 679–687.
[97] G. Mazza, K. Rombouts, A. Rennie Hall, L. Urbani, T. Vinh Luong, W. Al-Akkad, et al., Decellularized human liver as a natural 3D-scaffold for liver bioengineering and transplantation, Sci. Rep. 5 (1) (2015) 13079.
[98] X. Liu, S.-S.D. Carter, M.J. Renes, J. Kim, D.M. Rojas-Canales, D. Penko, et al., Development of a coaxial 3D printing platform for biofabrication of implantable islet-containing constructs, Advanced Healthcare Materials 8 (7) (2019) 1801181.

[99] A. Mooranian, R. Negrulj, R. Takechi, E. Jamieson, G. Morahan, H. Al-Salami, Electrokinetic potential-stabilization by bile acid-microencapsulating formulation of pancreatic β-cells cultured in high ratio poly-L-ornithine-gel hydrogel colloidal dispersion: applications in cell-biomaterials, tissue engineering and biotechnological applications, Artificial Cells, Nanomedicine, and Biotechnology 46 (6) (2018) 1156–1162.
[100] A. Mooranian, R. Negrulj, F. Arfuso, H. Al-Salami, Characterization of a novel bile acid-based delivery platform for microencapsulated pancreatic β-cells, Artificial Cells, Nanomedicine, and Biotechnology 44 (1) (2016) 194–200.
[101] A. Mooranian, R. Negrulj, E. Jamieson, G. Morahan, H. Al-Salami, Biological assessments of encapsulated pancreatic β-cells: their potential transplantation in diabetes, Cell. Mol. Bioeng. 9 (4) (2016) 530–537.
[102] W. Leong, T.T. Lau, D.-A. Wang, A temperature-cured dissolvable gelatin microsphere-based cell carrier for chondrocyte delivery in a hydrogel scaffolding system, Acta Biomater. 9 (5) (2013) 6459–6467.
[103] J.E. Mealy, J.J. Chung, H.-H. Jeong, D. Issadore, D. Lee, P. Atluri, et al., Injectable granular hydrogels with multifunctional properties for biomedical applications, Adv. Mater. 30 (20) (2018) 1705912.
[104] Negrulj Mooranian, H. Al-Salami, The effects of ionic gelation- vibrational jet flow technique in fabrication of microcapsules incorporating β-cell: applications in type-1 diabetes, Curr. Diabetes Rev. 13 (1) (2017) 91–96.
[105] R. Negrulj, A. Mooranian, N. Chen-Tan, H.S. Al-Salami, M. Mikov, S. Golocorbin-Kon, et al., Swelling, mechanical strength, and release properties of probucol microcapsules with and without a bile acid, and their potential oral delivery in diabetes, Artificial Cells, Nanomedicine, and Biotechnology 44 (5) (2016) 1290–1297.
[106] A. Mooranian, R. Negrulj, N. Chen-Tan, M. Fakhoury, F. Arfuso, F. Jones, et al., Advanced bile acid-based multi-compartmental microencapsulated pancreatic beta-cells integrating a polyelectrolyte-bile acid formulation, for diabetes treatment, Artificial Cells, Nanomedicine, and Biotechnology 44 (2) (2016) 588–595.
[107] J.C. Stendahl, D.B. Kaufman, S.I. Stupp, Extracellular matrix in pancreatic islets: relevance to scaffold design and transplantation, Cell Transplant. 18 (1) (2009) 1–12.
[108] A. Mooranian, N. Zamani, M. Mikov, S. Goločorbin-Kon, G. Stojanovic, F. Arfuso, et al., Novel nano-encapsulation of probucol in microgels: scanning electron micrograph characterizations, buoyancy profiling, and antioxidant assay analyses, Artificial Cells, Nanomedicine, and Biotechnology 46 (sup3) (2018) S741–S747.
[109] A. Mooranian, R. Negrulj, H. Al-Salami, The influence of stabilized deconjugated ursodeoxycholic acid on polymer-hydrogel system of transplantable NIT-1 cells, Pharmaceut. Res. 33 (5) (2016) 1182–1190.
[110] J.D. Weaver, D.M. Headen, M.D. Hunckler, M.M. Coronel, C.L. Stabler, A. J. García, Design of a vascularized synthetic poly(ethylene glycol) macroencapsulation device for islet transplantation, Biomaterials 172 (2018) 54–65.
[111] Y. Li, J. Rodrigues, H. Tomás, Injectable and biodegradable hydrogels: gelation, biodegradation and biomedical applications, Chem. Soc. Rev. 41 (6) (2012) 2193–2221.
[112] D. Seliktar, Designing cell-compatible hydrogels for biomedical applications, Science 336 (6085) (2012) 1124–1128.
[113] F.M. Croisfelt, L.L. Tundisi, J.A. Ataide, E. Silveira, E.B. Tambourgi, A.F. Jozala, et al., Modified-release topical hydrogels: a ten-year review, J. Mater. Sci. 54 (16) (2019) 10963–10983.
[114] E.S. Dragan, Design and applications of interpenetrating polymer network hydrogels. A review, Chem. Eng. J. 243 (2014) 572–590.
[115] Y. Samchenko, Z. Ulberg, O. Korotych, Multipurpose smart hydrogel systems, Adv. Colloid Interface Sci. 168 (1) (2011) 247–262.
[116] K. Deligkaris, T.S. Tadele, W. Olthuis, A. van den Berg, Hydrogel-based devices for biomedical applications, Sensor. Actuator. B Chem. 147 (2) (2010) 765–774.
[117] W.E. Hennink, C.F. van Nostrum, Novel crosslinking methods to design hydrogels, Adv. Drug Deliv. Rev. 64 (2012) 223–236.
[118] S. Bian, M. He, J. Sui, H. Cai, Y. Sun, J. Liang, et al., The self-crosslinking smart hyaluronic acid hydrogels as injectable three-dimensional scaffolds for cells culture, Colloids Surf. B Biointerfaces 140 (2016) 392–402.
[119] A. Mooranian, N. Zamani, R. Takechi, H. Al-Sallami, M. Mikov, S. Goločorbin-Kon, et al., Probucol-poly(meth)acrylate-bile acid nanoparticles increase IL-10, and primary bile acids in prediabetic mice, Ther. Deliv. 10 (9) (2019) 563–571.
[120] A. Mooranian, N. Zamani, G. Luna, H. Al-Sallami, M. Mikov, S. Goločorbin-Kon, et al., Bile acid-polymer-probucol microparticles: protective effect on pancreatic β-cells and decrease in type 1 diabetes development in a murine model, Pharmaceut. Dev. Technol. 24 (10) (2019) 1272–1277.
[121] J.C.L. Mamo, V. Lam, E. Brook, A. Mooranian, H. Al-Salami, N. Fimognari, et al., Probucol prevents blood–brain barrier dysfunction and cognitive decline in mice maintained on pro-diabetic diet, Diabetes Vasc. Dis. Res. 16 (1) (2019) 87–97.
[122] A. Mooranian, N. Zamani, M. Mikov, S. Goločorbin-Kon, G. Stojanovic, F. Arfuso, et al., Novel nano-encapsulation of probucol in microgels: scanning electron micrograph characterizations, buoyancy profiling, and antioxidant assay analyses. Artificial Cells, Nanomedicine and Biotechnology 46 (sup3) (2018) S741–S747.
[123] A. Mooranian, N. Zamani, M. Mikov, S. Goločorbin-Kon, G. Stojanovic, F. Arfuso, et al., Eudragit®-based microcapsules of probucol with a gut-bacterial processed secondary bile acid, Ther. Deliv. 9 (11) (2018) 811–821.
[124] A. Mooranian, R. Takechi, E. Jamieson, G. Morahan, H. Al-Salami, The effect of molecular weights of microencapsulating polymers on viability of mouse-cloned pancreatic beta-cells: biomaterials, osmotic forces and potential applications in diabetes treatment, Pharmaceut. Dev. Technol. 23 (2) (2018) 145–150.
[125] A. Cañibano-Hernández, L. Saenz del Burgo, A. Espona-Noguera, G. Orive, R. M. Hernández, J. Ciriza, et al., Hyaluronic acid enhances cell survival of encapsulated insulin-producing cells in alginate-based microcapsules, Int. J. Pharm. 557 (2019) 192–198.
[126] C.K. Kuo, P.X. Ma, Ionically crosslinked alginate hydrogels as scaffolds for tissue engineering: Part 1. Structure, gelation rate and mechanical properties, Biomaterials 22 (6) (2001) 511–521.
[127] P. Wang, Y. Song, M.D. Weir, J. Sun, L. Zhao, C.G. Simon, et al., A self-setting iPSMSC-alginate-calcium phosphate paste for bone tissue engineering, Dent. Mater. 32 (2) (2016) 252–263.
[128] H.V. Almeida, B.N. Sathy, I. Dudurych, C.T. Buckley, F.J. O'Brien, D.J. Kelly, Anisotropic shape-memory alginate scaffolds functionalized with either type I or type II collagen for cartilage tissue engineering, Tissue Eng. 23 (1–2) (2016) 55–68.
[129] C.-C. Wang, K.-C. Yang, K.-H. Lin, H.-C. Liu, F.-H. Lin, A highly organized three-dimensional alginate scaffold for cartilage tissue engineering prepared by microfluidic technology, Biomaterials 32 (29) (2011) 7118–7126.
[130] W. Chen, C. Li, M. Peng, B. Xie, L. Zhang, X. Tang, Autologous nasal chondrocytes delivered by injectable hydrogel for in vivo articular cartilage regeneration, Cell Tissue Bank. 19 (1) (2018) 35–46.
[131] J. Wu, G. Li, T. Ye, G. Lu, R. Li, L. Deng, et al., Stem cell-laden injectable hydrogel microspheres for cancellous bone regeneration, Chem. Eng. J. 393 (2020) 124715.
[132] Z. Münoz, H. Shih, C.-C. Lin, Gelatin hydrogels formed by orthogonal thiol–norbornene photochemistry for cell encapsulation, Biomaterials Science 2 (8) (2014) 1063–1072.
[133] T. Billiet, E. Gevaert, T. De Schryver, M. Cornelissen, P. Dubruel, The 3D printing of gelatin methacrylamide cell-laden tissue-engineered constructs with high cell viability, Biomaterials 35 (1) (2014) 49–62.
[134] H.A. Awad, M. Quinn Wickham, H.A. Leddy, J.M. Gimble, F. Guilak, Chondrogenic differentiation of adipose-derived adult stem cells in agarose, alginate, and gelatin scaffolds, Biomaterials 25 (16) (2004) 3211–3222.
[135] S. Sakai, K. Hirose, K. Taguchi, Y. Ogushi, K. Kawakami, An injectable, in situ enzymatically gellable, gelatin derivative for drug delivery and tissue engineering, Biomaterials 30 (20) (2009) 3371–3377.
[136] A.M. Sisso, M.O. Boit, C.A. DeForest, Self-healing injectable gelatin hydrogels for localized therapeutic cell delivery, J. Biomed. Mater. Res. 108 (5) (2020) 1112–1121.
[137] B. Ruozi, B. Parma, M.A. Croce, G. Tosi, L. Bondioli, S. Vismara, et al., Collagen-based modified membranes for tissue engineering: influence of type and molecular weight of GAGs on cell proliferation, Int. J. Pharm. 378 (1) (2009) 108–115.
[138] S.-H. Park, S.R. Park, S.I. Chung, K.S. Pai, B.-H. Min, Tissue-engineered cartilage using fibrin/hyaluronan composite gel and its in vivo implantation, Artif. Organs 29 (10) (2005) 838–845.
[139] E.C. Chan, S.-M. Kuo, A.M. Kong, W.A. Morrison, G.J. Dusting, G.M. Mitchell, et al., Three dimensional collagen scaffold promotes intrinsic vascularisation for tissue engineering applications, PLoS One 11 (2) (2016) e0149799–e.
[140] J. Elango, J. Zhang, B. Bao, K. Palaniyandi, S. Wang, W. Wenhui, et al., Rheological, biocompatibility and osteogenesis assessment of fish collagen scaffold for bone tissue engineering, Int. J. Biol. Macromol. 91 (2016) 51–59.
[141] Y. Gao, B. Li, W. Kong, L. Yuan, L. Guo, C. Li, et al., Injectable and self-crosslinkable hydrogels based on collagen type II and activated chondroitin sulfate for cell delivery, Int. J. Biol. Macromol. 118 (2018) 2014–2020.
[142] S. Huang, Y. Li, X. Wang, X. Ma, X. Zhang, Injectable co-gels of collagen and decellularized vascular matrix improve MSC-based therapy for acute kidney injury, J. Biomater. Sci. Polym. Ed. 28 (18) (2017) 2186–2195.
[143] Y. Moriguchi, B. Borde, C. Berlin, C. Wipplinger, S.R. Sloan, S. Kirnaz, et al., In vivo annular repair using high-density collagen gel seeded with annulus fibrosus cells, Acta Biomater. 79 (2018) 230–238.
[144] A.Y. Rioja, R. Tiruvannamalai Annamalai, S. Paris, A.J. Putnam, J.P. Stegemann, Endothelial sprouting and network formation in collagen- and fibrin-based modular microbeads, Acta Biomater 29 (2016) 33–41.
[145] J.H. Ryu, I.-K. Kim, S.-W. Cho, M.-C. Cho, K.-K. Hwang, H. Piao, et al., Implantation of bone marrow mononuclear cells using injectable fibrin matrix enhances neovascularization in infarcted myocardium, Biomaterials 26 (3) (2005) 319–326.
[146] S. Gerecht, J.A. Burdick, L.S. Ferreira, S.A. Townsend, R. Langer, G. Vunjak-Novakovic, Hyaluronic acid hydrogel for controlled self-renewal and differentiation of human embryonic stem cells, in: Proceedings of the National Academy of Sciences, vol. 104, 2007, pp. 11298–11303 (27).
[147] H.V. Almeida, R. Eswaramoorthy, G.M. Cunniffe, C.T. Buckley, F.J. O'Brien, D. J. Kelly, Fibrin hydrogels functionalized with cartilage extracellular matrix and incorporating freshly isolated stromal cells as an injectable for cartilage regeneration, Acta Biomater. 36 (2016) 55–62.
[148] R.T. Annamalai, T. Naik, H. Prout, A.J. Putnam, J.P. Stegemann, Biofabrication of injectable fibrin microtissues for minimally-invasive therapies: application of surfactants, Biomed. Mater. 13 (4) (2018), 045005.
[149] X. Xue, Y. Yan, Y. Ma, Y. Yuan, C. Li, X. Lang, et al., Stem-cell therapy for esophageal anastomotic leakage by autografting stromal cells in fibrin scaffold, STEM CELLS Translational Medicine 8 (6) (2019) 548–556.
[150] S. England, A. Rajaram, D.J. Schreyer, X. Chen, Bioprinted fibrin-factor XIII-hyaluronate hydrogel scaffolds with encapsulated Schwann cells and their in vitro characterization for use in nerve regeneration, Bioprinting 5 (2017) 1–9.

[151] F. Seyedi, A. Farsinejad, S.N. Nematollahi-Mahani, Fibrin scaffold enhances function of insulin producing cells differentiated from human umbilical cord matrix-derived stem cells, Tissue Cell 49 (2) (2017) 227–232. Part B).
[152] X.Z. Shu, K. Ghosh, Y. Liu, F.S. Palumbo, Y. Luo, R.A. Clark, et al., Attachment and spreading of fibroblasts on an RGD peptide-modified injectable hyaluronan hydrogel, J. Biomed. Mater. Res. 68 (2) (2004) 365–375.
[153] A.C. Gaffey, M.H. Chen, C.M. Venkataraman, A. Trubelja, C.B. Rodell, P.V. Dinh, et al., Injectable shear-thinning hydrogels used to deliver endothelial progenitor cells, enhance cell engraftment, and improve ischemic myocardium, J. Thorac. Cardiovasc. Surg. 150 (5) (2015) 1268–1276.
[154] H. Tan, C.M. Ramirez, N. Miljkovic, H. Li, J.P. Rubin, K.G. Marra, Thermosensitive injectable hyaluronic acid hydrogel for adipose tissue engineering, Biomaterials 30 (36) (2009) 6844–6853.
[155] F. Zamboni, M. Keays, S. Hayes, A.B. Albadarin, G.M. Walker, P.A. Kiely, et al., Enhanced cell viability in hyaluronic acid coated poly(lactic-co-glycolic acid) porous scaffolds within microfluidic channels, Int. J. Pharm. 532 (1) (2017) 595–602.
[156] Z. Li, M. Leung, R. Hopper, R. Ellenbogen, M. Zhang, Feeder-free self-renewal of human embryonic stem cells in 3D porous natural polymer scaffolds, Biomaterials 31 (3) (2010) 404–412.
[157] R.T. Annamalai, X. Hong, N.G. Schott, G. Tiruchinapally, B. Levi, J.P. Stegemann, Injectable osteogenic microtissues containing mesenchymal stromal cells conformally fill and repair critical-size defects, Biomaterials 208 (2019) 32–44.
[158] J. Zhang, X. Lu, G. Feng, Z. Gu, Y. Sun, G. Bao, et al., Chitosan scaffolds induce human dental pulp stem cells to neural differentiation: potential roles for spinal cord injury therapy, Cell Tissue Res. 366 (1) (2016) 129–142.
[159] S.M. Dang, S. Gerecht-Nir, J. Chen, J. Itskovitz-Eldor, P.W. Zandstra, Controlled, scalable embryonic stem cell differentiation culture, Stem Cell. 22 (3) (2004) 275–282.
[160] A.Y. Rioja, E.L.H. Daley, J.C. Habif, A.J. Putnam, J.P. Stegemann, Distributed vasculogenesis from modular agarose-hydroxyapatite-fibrinogen microbeads, Acta Biomater 55 (2017) 144–152.
[161] R. Tiruvannamalai Annamalai, D.R. Mertz, E.L. Daley, J.P. Stegemann, Collagen Type II enhances chondrogenic differentiation in agarose-based modular microtissues, Cytotherapy 18 (2) (2016) 263–277.
[162] P. de Vos, M. Spasojevic, B.J. de Haan, M.M. Faas, The association between in vivo physicochemical changes and inflammatory responses against alginate based microcapsules, Biomaterials 33 (22) (2012) 5552–5559.
[163] P. Soon-Shiong, R.E. Heintz, N. Merideth, Q.X. Yao, Z. Yao, T. Zheng, et al., Insulin independence in a type 1 diabetic patient after encapsulated islet transplantation, Lancet 343 (8903) (1994) 950–951.
[164] A.M. Rokstad, O.L. Brekke, B. Steinkjer, L. Ryan, G. Kollarikova, B.L. Strand, et al., Alginate microbeads are complement compatible, in contrast to polycation containing microcapsules, as revealed in a human whole blood model, Acta Biomater. 7 (6) (2011) 2566–2578.
[165] B.E. Larsen, J. Bjørnstad, E.O. Pettersen, H.H. Tønnesen, J.E. Melvik, Rheological characterization of an injectable alginate gel system, BMC Biotechnol. 15 (1) (2015) 29.
[166] C.S. Lee, J.P. Gleghorn, N. Won Choi, M. Cabodi, A.D. Stroock, L.J. Bonassar, Integration of layered chondrocyte-seeded alginate hydrogel scaffolds, Biomaterials 28 (19) (2007) 2987–2993.
[167] M. Whelehan, I.W. Marison, Microencapsulation using vibrating technology, J. Microencapsul. 28 (8) (2011) 669–688.
[168] E.A. Nunamaker, E.K. Purcell, D.R. Kipke, In vivo stability and biocompatibility of implanted calcium alginate disks, J. Biomed. Mater. Res. 83 (4) (2007) 1128–1137.
[169] M. George, T.E. Abraham, Polyionic hydrocolloids for the intestinal delivery of protein drugs: alginate and chitosan–a review, J. Contr. Release 114 (1) (2006) 1–14.
[170] S.R. Wagle, B. Kovacevic, D. Walker, C.M. Ionescu, M. Jones, G. Stojanovic, et al., Pharmacological and advanced cell respiration effects, enhanced by toxic human-bile nano-pharmaceuticals of probucol cell-targeting formulations, Pharmaceutics 12 (8) (2020) 1–17.
[171] A. Mooranian, N. Zamani, R. Takechi, G. Luna, M. Mikov, S. Goločorbin-Kon, et al., Modulatory nano/micro effects of diabetes development on pharmacology of primary and secondary bile acids concentrations, Curr. Diabetes Rev. 16 (8) (2020) 900–909.
[172] A. Mooranian, N. Zamani, M. Mikov, S. Goločorbin-Kon, G. Stojanovic, F. Arfuso, et al., A second-generation micro/nano capsules of an endogenous primary unmetabolised bile acid, stabilized by Eudragit-alginate complex with antioxidant compounds, Saudi Pharmaceut. J. 28 (2) (2020) 165–171.
[173] A. Mooranian, S. Raj Wagle, B. Kovacevic, R. Takechi, J. Mamo, V. Lam, et al., Bile acid bio-nanoencapsulation improved drug targeted-delivery and pharmacological effects via cellular flux: 6-months diabetes preclinical study, Sci. Rep. 10 (1) (2020).
[174] S. Mathavan, C.M. Ionescu, B. Kovacevic, M. Mikov, S. Golocorbin-Kon, A. Mooranian, et al., Histological effects of pharmacologically active human bile acid nano/micro-particles in Type-1 diabetes, Ther. Deliv. 11 (3) (2020) 157–171.
[175] B. Amsden, N. Turner, Diffusion characteristics of calcium alginate gels, Biotechnol. Bioeng. 65 (5) (1999) 605–610.
[176] P. de Vos, B.J. de Haan, J.A.A.M. Kamps, M.M. Faas, T. Kitano, Zeta-potentials of alginate-PLL capsules: a predictive measure for biocompatibility? J. Biomed. Mater. Res. 80A (4) (2007) 813–819.
[177] N. Faramarzi, I.K. Yazdi, M. Nabavinia, A. Gemma, A. Fanelli, A. Caizzone, et al., Patient-specific bioinks for 3D bioprinting of tissue engineering scaffolds, Adv Healthc Mater 7 (11) (2018), e1701347.
[178] N. Taira, K. Ino, J. Robert, H. Shiku, Electrochemical printing of calcium alginate/gelatin hydrogel, Electrochim. Acta 281 (2018) 429–436.
[179] C. Colosi, S.R. Shin, V. Manoharan, S. Massa, M. Costantini, A. Barbetta, et al., Microfluidic bioprinting of heterogeneous 3D tissue constructs using low-viscosity bioink, Adv. Mater. 28 (4) (2016) 677–684.
[180] A.J. Vegas, O. Veiseh, M. Gürtler, J.R. Millman, F.W. Pagliuca, A.R. Bader, et al., Long-term glycemic control using polymer-encapsulated human stem cell–derived beta cells in immune-competent mice, Nat. Med. 22 (2016) 306.
[181] A.J. Vegas, O. Veiseh, J.C. Doloff, M. Ma, H.H. Tam, K. Bratlie, et al., Combinatorial hydrogel library enables identification of materials that mitigate the foreign body response in primates, Nat. Biotechnol. 34 (2016) 345.
[182] R. Lindstedt, V.V.D.A. Ruggiero, S. Manganello, F. Petronzelli, M.A. Stasi, et al., The immunosuppressor st1959, a 3,5-diaryl-s-triazole derivative, inhibits T cell activation by reducing NFAT nuclear residency, Int. J. Immunopathol. Pharmacol. 22 (1) (2009) 29–42.
[183] T. Andersen, P. Auk-Emblem, M. Dornish, 3D cell culture in alginate hydrogels, Microarrays 4 (2) (2015) 133–161.
[184] A.M. Westman, R.L. Goldstein, G. Bradica, S.M. Goldman, M.A. Randolph, J. P. Gaut, et al., Decellularized extracellular matrix microparticles seeded with bone marrow mesenchymal stromal cells for the treatment of full-thickness cutaneous wounds, J. Biomater. Appl. 33 (8) (2019) 1070–1079.
[185] M.M. Coronel, R. Geusz, C.L. Stabler, Mitigating hypoxic stress on pancreatic islets via in situ oxygen generating biomaterial, Biomaterials 129 (2017) 139–151.
[186] A. Fakhari, M. Corcoran, A. Schwarz, Thermogelling properties of purified poloxamer 407, Heliyon 3 (8) (2017), e00390.
[187] P. Zarrintaj, Z. Ahmadi, M. Reza Saeb, M. Mozafari, Poloxamer-based stimuli-responsive biomaterials, in: Materials Today: Proceedings, vol. 5, 2018, pp. 15516–15523 (7, Part 3).
[188] G. Dumortier, J.L. Grossiord, F. Agnely, J.C. Chaumeil, A review of poloxamer 407 pharmaceutical and pharmacological characteristics, Pharmaceut. Res. 23 (12) (2006) 2709–2728.
[189] L.-S. Yap, M.-C. Yang, Evaluation of hydrogel composing of Pluronic F127 and carboxymethyl hexanoyl chitosan as injectable scaffold for tissue engineering applications, Colloids Surf. B Biointerfaces 146 (2016) 204–211.
[190] E. Inyang, V. Abhyankar, B. Chen, M. Cho, Modulation of in vitro brain endothelium by mechanical trauma: structural and functional restoration by poloxamer 188, Sci. Rep. 10 (1) (2020).
[191] R. Dorati, I. Genta, T. Modena, B. Conti, Microencapsulation of a hydrophilic model molecule through vibration nozzle and emulsion phase inversion technologies, J. Microencapsul. 30 (6) (2013) 559–570.
[192] V. Nedović, in: R. Willaert (Ed.), Fundamentals of Cell Immobilisation Biotechnology, Springer Netherlands, Dordrecht, 2004.
[193] G. Orive, R.M. Hernandez, A. Rodriguez Gascon, R. Calafiore, T.M. Chang, P. de Vos, et al., History, challenges and perspectives of cell microencapsulation, Trends Biotechnol 22 (2) (2004) 87–92.
[194] A. Murua, A. Portero, G. Orive, R.M. Hernández, M. de Castro, J.L. Pedraz, Cell microencapsulation technology: towards clinical application, J. Contr. Release 132 (2) (2008) 76–83.
[195] A. Mooranian, S. Raj Wagle, B. Kovacevic, R. Takechi, J. Mamo, V. Lam, et al., Bile acid bio-nanoencapsulation improved drug targeted-delivery and pharmacological effects via cellular flux: 6-months diabetes preclinical study, Sci. Rep. 10 (1) (2020) 106.
[196] A.J. Vegas, O. Veiseh, M. Gurtler, J.R. Millman, F.W. Pagliuca, A.R. Bader, et al., Long-term glycemic control using polymer-encapsulated human stem cell-derived beta cells in immune-competent mice, Nat. Med. 22 (3) (2016) 306–311.
[197] A.J. Ryan, H.S. O'Neill, G.P. Duffy, F.J. O'Brien, Advances in polymeric islet cell encapsulation technologies to limit the foreign body response and provide immunoisolation, Curr. Opin. Pharmacol. 36 (2017) 66–71.
[198] S. Pellegrini, L. Piemonti, V. Sordi, Pluripotent stem cell replacement approaches to treat type 1 diabetes, Curr. Opin. Pharmacol. 43 (2018) 20–26.
[199] B. Ludwig, S. Ludwig, A. Steffen, Y. Knauf, B. Zimerman, S. Heinke, et al., Favorable outcome of experimental islet xenotransplantation without immunosuppression in a nonhuman primate model of diabetes, in: Proceedings of the National Academy of Sciences, vol. 114, 2017, p. 11745 (44).
[200] M. Mandai, A. Watanabe, Y. Kurimoto, Y. Hirami, C. Morinaga, T. Daimon, et al., Autologous induced stem-cell–derived retinal cells for macular degeneration, N. Engl. J. Med. 376 (11) (2017) 1038–1046.
[201] S. Duin, K. Schütz, T. Ahlfeld, S. Lehmann, A. Lode, B. Ludwig, et al., 3D bioprinting of functional islets of langerhans in an alginate/methylcellulose hydrogel blend, Advanced Healthcare Materials 8 (7) (2019) 1801631.
[202] S. Pina, V.P. Ribeiro, C.F. Marques, F.R. Maia, T.H. Silva, R.L. Reis, et al., Scaffolding strategies for tissue engineering and regenerative medicine applications, Materials 12 (11) (2019) 1824.
[203] X. Cui, G. Gao, Y. Qiu, Accelerated myotube formation using bioprinting technology for biosensor applications, Biotechnol. Lett. 35 (3) (2013) 315–321.
[204] G. Gao, X. Cui, Three-dimensional bioprinting in tissue engineering and regenerative medicine, Biotechnol. Lett. 38 (2) (2016) 203–211.
[205] A. Blaeser, D.F. Duarte Campos, U. Puster, W. Richtering, M.M. Stevens, H. Fischer, Controlling shear stress in 3D bioprinting is a key factor to balance printing resolution and stem cell integrity, Advanced Healthcare Materials 5 (3) (2016) 326–333.
[206] A. Kerby, E.S. Jones, P.M. Jones, A.J. King, Co-transplantation of islets with mesenchymal stem cells in microcapsules demonstrates graft outcome can be improved in an isolated-graft model of islet transplantation in mice, Cytotherapy 15 (2) (2013) 192–200.

[207] B. Ludwig, B. Zimerman, A. Steffen, K. Yavriants, D. Azarov, A. Reichel, et al., A novel device for islet transplantation providing immune protection and oxygen supply, Horm. Metab. Res. 42 (13) (2010) 918–922.
[208] M.J. van Amerongen, G. Molema, J. Plantinga, H. Moorlag, M.J. van Luyn, Neovascularization and vascular markers in a foreign body reaction to subcutaneously implanted degradable biomaterial in mice, Angiogenesis 5 (3) (2002) 173–180.
[209] X. Xiao, W. Wang, D. Liu, H. Zhang, P. Gao, L. Geng, et al., The promotion of angiogenesis induced by three-dimensional porous beta-tricalcium phosphate scaffold with different interconnection sizes via activation of PI3K/Akt pathways, Sci. Rep. 5 (2015) 9409.
[210] Q.L. Loh, C. Choong, Three-Dimensional scaffolds for tissue engineering applications: role of porosity and pore size, Tissue Eng. B Rev. 19 (6) (2013) 485–502.
[211] S. Pina, V.P. Ribeiro, C.F. Marques, F.R. Maia, T.H. Silva, R.L. Reis, et al., Scaffolding strategies for tissue engineering and regenerative medicine applications, Materials 12 (11) (2019).
[212] S.A. Burke, M. Ritter-Jones, B.P. Lee, P.B. Messersmith, Thermal gelation and tissue adhesion of biomimetic hydrogels, Biomed. Mater. 2 (4) (2007) 203–210.
[213] T. Führmann, R.Y. Tam, B. Ballarin, B. Coles, I. Elliott Donaghue, D. van der Kooy, et al., Injectable hydrogel promotes early survival of induced pluripotent stem cell-derived oligodendrocytes and attenuates longterm teratoma formation in a spinal cord injury model, Biomaterials 83 (2016) 23–36.
[214] B.A. Aguado, W. Mulyasasmita, J. Su, K.J. Lampe, S.C. Heilshorn, Improving viability of stem cells during syringe needle flow through the design of hydrogel cell carriers, Tissue Eng. 18 (7–8) (2011) 806–815.
[215] A. Mooranian, R. Negrulj, F. Arfuso, H. Al-Salami, The effect of a tertiary bile acid, taurocholic acid, on the morphology and physical characteristics of microencapsulated probucol: potential applications in diabetes: a characterization study, Drug Deliv Transl Res 5 (5) (2015) 511–522.
[216] R. Negrulj, A. Mooranian, N. Chen-Tan, H.S. Al-Sallami, M. Mikov, S. Golocorbin-Kon, et al., Swelling, mechanical strength, and release properties of probucol microcapsules with and without a bile acid, and their potential oral delivery in diabetes, Artificial Cells, Nanomedicine, and Biotechnology 44 (5) (2016) 1290–1297.
[217] A. Mooranian, R. Negrulj, H. Al-Salami, Flow vibration-doubled concentric system coupled with low ratio amine to produce bile acid-macrocapsules of beta-cells, Ther. Deliv. 7 (3) (2016) 171–178.
[218] A. Mooranian, N. Zamani, R. Takechi, H. Al-Sallami, M. Mikov, S. Golocorbin-Kon, et al., Pharmacological effects of nanoencapsulation of human-based dosing of probucol on ratio of secondary to primary bile acids in gut, during induction and progression of type 1 diabetes, 2018, pp. 1–7.
[219] J.M. Ridlon, J.S. Bajaj, The human gut sterolbiome: bile acid-microbiome endocrine aspects and therapeutics, Acta Pharm. Sin. B 5 (2) (2015) 99–105.
[220] L. Serfaty, Chemoprevention of colorectal cancer with ursodeoxycholic acid: Pro, Clinics and Research in Hepatology and Gastroenterology 36 (2012) S53–S60.
[221] M.J. Perez, O. Briz, Bile-acid-induced cell injury and protection, World J. Gastroenterol. 15 (14) (2009) 1677–1689.
[222] K. Dilger, S. Hohenester, U. Winkler-Budenhofer, B.A.J. Bastiaansen, F.G. Schaap, C. Rust, et al., Effect of ursodeoxycholic acid on bile acid profiles and intestinal detoxification machinery in primary biliary cirrhosis and health, J. Hepatol. 57 (1) (2012) 133–140.
[223] Y.-G. Jia, J. Jin, S. Liu, L. Ren, J. Luo, X.X. Zhu, Self-healing hydrogels of low molecular weight poly(vinyl alcohol) assembled by host–guest recognition, Biomacromolecules 19 (2) (2018) 626–632.
[224] G. Paumgartner, U. Beuers, Ursodeoxycholic acid in cholestatic liver disease: mechanisms of action and therapeutic use revisited, Hepatology 36 (3) (2002) 525–531.
[225] F.S. Di Leva, C. Festa, A. Carino, S. De Marino, S. Marchianò, D. Di Marino, et al., Discovery of ((1,2,4-oxadiazol-5-yl)pyrrolidin-3-yl)ureidyl derivatives as selective non-steroidal agonists of the G-protein coupled bile acid receptor-1, Sci. Rep. 9 (1) (2019) 2504.
[226] S. Fiorucci, E. Distrutti, Bile acid-activated receptors, intestinal microbiota, and the treatment of metabolic disorders, Trends Mol. Med. 21 (11) (2015) 702–714.
[227] F. Kuipers, V.W. Bloks, A.K. Groen, Beyond intestinal soap—bile acids in metabolic control, Nat. Rev. Endocrinol. 10 (2014) 488.
[228] B. Renga, A. Mencarelli, P. Vavassori, V. Brancaleone, S. Fiorucci, The bile acid sensor FXR regulates insulin transcription and secretion, Biochim. Biophys. Acta (BBA) - Mol. Basis Dis. 1802 (3) (2010) 363–372.
[229] C. Thomas, J. Auwerx, K. Schoonjans, Bile acids and the membrane bile acid receptor TGR5–connecting nutrition and metabolism, Thyroid : official journal of the American Thyroid Association. 18 (2) (2008) 167–174.
[230] A. Zarrinpar, R. Loomba, Review article: the emerging interplay among the gastrointestinal tract, bile acids and incretins in the pathogenesis of diabetes and non-alcoholic fatty liver disease, Aliment. Pharmacol. Ther. 36 (10) (2012) 909–921.
[231] I. Kim, K. Morimura, Y. Shah, Q. Yang, J.M. Ward, F.J. Gonzalez, Spontaneous hepatocarcinogenesis in farnesoid X receptor-null mice, Carcinogenesis 28 (5) (2007) 940–946.
[232] Y. Xie, H. Wang, X. Cheng, Y. Wu, L. Cao, M. Wu, et al., Farnesoid X receptor activation promotes cell proliferation via PDK4-controlled metabolic reprogramming, Sci. Rep. 6 (2016) 18751.
[233] T. Tsuchida, S.L. Friedman, Mechanisms of hepatic stellate cell activation, Nat. Rev. Gastroenterol. Hepatol. 14 (7) (2017) 397–411.
[234] X. Liu, G.L. Guo, B. Kong, D.B. Hilburn, S.C. Hubchak, S. Park, et al., Farnesoid X receptor signaling activates the hepatic X-box binding protein 1 pathway in vitro and in mice, Hepatology 68 (1) (2018) 304–316.
[235] J.R. Cubillos-Ruiz, S.E. Bettigole, L.H. Glimcher, Tumorigenic and immunosuppressive effects of endoplasmic reticulum stress in cancer, Cell 168 (4) (2017) 692–706.
[236] Y. Calmus, J. Guechot, P. Podevin, M.T. Bonnefis, J. Giboudeau, R. Poupon, Differential effects of chenodeoxycholic and ursodeoxycholic acids on interleukin 1, interleukin 6 and tumor necrosis factor-alpha production by monocytes, Hepatology 16 (3) (1992) 719–723.
[237] T. Matsubara, F. Li, F.J. Gonzalez, FXR signaling in the enterohepatic system, Mol. Cell. Endocrinol. 368 (1–2) (2013) 17–29.
[238] C. Tezze, V. Romanello, M. Sandri, FGF21 as modulator of metabolism in health and disease, Front. Physiol. 10 (419) (2019).
[239] T.Q. de Aguiar Vallim, E.J. Tarling, P.A. Edwards, Pleiotropic roles of bile acids in metabolism, Cell Metabol. 17 (5) (2013) 657–669.
[240] H. Gohlke, B. Schmitz, A. Sommerfeld, R. Reinehr, D. Haussinger, alpha5 beta1-integrins are sensors for tauroursodeoxycholic acid in hepatocytes, Hepatology 57 (3) (2013) 1117–1129.
[241] E. Studer, X. Zhou, R. Zhao, Y. Wang, K. Takabe, M. Nagahashi, et al., Conjugated bile acids activate the sphingosine-1-phosphate receptor 2 in primary rodent hepatocytes, Hepatology 55 (1) (2012) 267–276.
[242] K. Yoneno, T. Hisamatsu, K. Shimamura, N. Kamada, R. Ichikawa, M.T. Kitazume, et al., TGR5 signalling inhibits the production of pro-inflammatory cytokines by in vitro differentiated inflammatory and intestinal macrophages in Crohn's disease, Immunology 139 (1) (2013) 19–29.
[243] T. Kida, Y. Tsubosaka, M. Hori, H. Ozaki, T. Murata, Bile acid receptor TGR5 agonism induces NO production and reduces monocyte adhesion in vascular endothelial cells, Arterioscler. Thromb. Vasc. Biol. 33 (7) (2013) 1663–1669.
[244] T. Dimitris, K Costas Anna-Maria, P. Tentolouris Nikolaos, S. Christodoulos, The role of nitric oxide on endothelial function, Curr. Vasc. Pharmacol. 10 (1) (2012) 4–18.
[245] M. Quinn, M. McMillin, C. Galindo, G. Frampton, H.Y. Pae, S. DeMorrow, Bile acids permeabilize the blood brain barrier after bile duct ligation in rats via Rac1-dependent mechanisms, Dig. Liver Dis. 46 (6) (2014) 527–534.
[246] A.P. Rolo, C.M. Palmeira, K.B. Wallace, Mitochondrially mediated synergistic cell killing by bile acids, Biochim. Biophys. Acta (BBA) - Mol. Basis Dis. 1637 (1) (2003) 127–132.
[247] C.M. Palmeira, A.P. Rolo, Mitochondrially-mediated toxicity of bile acids, Toxicology 203 (1) (2004) 1–15.
[248] H. Mitsuyoshi, T. Nakashima, Y. Sumida, T. Yoh, Y. Nakajima, H. Ishikawa, et al., Ursodeoxycholic acid protects hepatocytes against oxidative injury via induction of antioxidants, Biochem. Biophys. Res. Commun. 263 (2) (1999) 537–542.
[249] C.M. Rodriguez-Ortigosa, R.N. Cincu, S. Sanz, F. Ruiz, J. Quiroga, J. Prieto, Effect of ursodeoxycholic acid on methionine adenosyltransferase activity and hepatic glutathione metabolism in rats, Gut 50 (5) (2002) 701–706.
[250] J. Chung, K.H. Kim, S.C. Lee, S.H. An, K. Kwon, Ursodeoxycholic acid (UDCA) exerts anti-atherogenic effects by inhibiting endoplasmic reticulum (ER) stress induced by disturbed flow, Mol Cells 38 (10) (2015) 851–858.
[251] S. Kundu, S. Bansal, K.M. Muthukumarasamy, C. Sachidanandan, R.K. Motiani, A. Bajaj, Deciphering the role of hydrophobic and hydrophilic bile acids in angiogenesis using in vitro and in vivo model systems, MedChemComm 8 (12) (2017) 2248–2257.
[252] J. Vandooren, P.E. Van den Steen, G. Opdenakker, Biochemistry and molecular biology of gelatinase B or matrix metalloproteinase-9 (MMP-9): the next decade, Crit. Rev. Biochem. Mol. Biol. 48 (3) (2013) 222–272.
[253] J. Hageman, H. Herrema, A.K. Groen, F. Kuipers, A role of the bile salt receptor FXR in atherosclerosis, Arterioscler. Thromb. Vasc. Biol. 30 (8) (2010) 1519–1528.
[254] A. Mooranian, R. Negrulj, R. Takechi, E. Jamieson, G. Morahan, H. Al-Salami, New biotechnological microencapsulating methodology utilizing individualized gradient-screened jet laminar flow techniques for pancreatic β-cell delivery: bile acids support cell energy-generating mechanisms, Mol. Pharm. 14 (8) (2017) 2711–2718.
[255] A. Mooranian, R. Negrulj, S. Mathavan, J. Martinez, J. Sciarretta, N. Chen-Tan, et al., An advanced microencapsulated system: a platform for optimized oral delivery of antidiabetic drug-bile acid formulations, Pharmaceut. Dev. Technol. 20 (6) (2015) 702–709.
[256] A. Mooranian, N. Zamani, M. Mikov, S. Goločorbin-Kon, G. Stojanovic, F. Arfuso, et al., Stability and biological testing of taurine-conjugated bile acid antioxidant microcapsules for diabetes treatment, Ther. Deliv. 10 (2) (2019) 99–106.

Chapter 2

Sodium Alginate And Bile Acid-Based Hydrogels: Rheological Properties And Biocompatibility

Chapter 2

Sodium Alginate And Bile Acid-Based Hydrogels: Rheological Properties And Biocompatibility

The contents of this chapter are covered by publication 2 (pages 38-52), publication 3 (pages 54-61), publication 4 (pages 63-85), and publication 5 (pages 87-97).

Publication 2 (pages 38-52):

Kovacevic B, Ionescu CM, Jones M, Wagle SR, Lewkowicz M, Đanić M, Mikov M, Mooranian A, Al-Salami H. The Effect of Deoxycholic Acid on Chitosan-Enabled Matrices for Tissue Scaffolding and Injectable Nanogels. Gels. 2022;8(6):358.

Sub-objective (1): to design and create hydrogels utilising sodium alginate, various concentrations of chitosan and deoxycholic acid and to examine the shear stress, viscosity, surface tension, torque, microstructure, and zeta potential of hydrogels. Additionally, the hydrogels were incubated with 3 different cell lines (AML 12, C2C12 and NIT-1). Their impact on viability in normal and hypoxic conditions and their impact on bioenergetic parameters was investigated.

gels

MDPI

Article

The Effect of Deoxycholic Acid on Chitosan-Enabled Matrices for Tissue Scaffolding and Injectable Nanogels

Bozica Kovacevic [1,2], Corina Mihaela Ionescu [1,2], Melissa Jones [1,2], Susbin Raj Wagle [1,2], Michael Lewkowicz [1,2], Maja Danić [3], Momir Mikov [3], Armin Mooranian [1,2,*] and Hani Al-Salami [1,2,*]

1 The Biotechnology and Drug Development Research Laboratory, Curtin Medical School and Curtin Health Innovation Research Institute, Curtin University, Perth, WA 6102, Australia; bozica.kovacevic@postgrad.curtin.edu.au (B.K.); cionescu@postgrad.curtin.edu.au (C.M.I.); melissa.a.jones@postgrad.curtin.edu.au (M.J.); susbinraj.wagle@postgrad.curtin.edu.au (S.R.W.); mikhael.lewkowicz@graduate.curtin.edu.au (M.L.)

2 Hearing Therapeutics Department, Ear Science Institute Australia, Queen Elizabeth II Medical Centre, Perth, WA 6009, Australia

3 Department of Pharmacology, Toxicology and Clinical Pharmacology, Faculty of Medicine, University of Novi Sad, 21101 Novi Sad, Serbia; maja.djanic@mf.uns.ac.rs (M.D.); momir.mikov@mf.uns.ac.rs (M.M.)

* Correspondence: a.mooranian@curtin.edu.au (A.M.); hani.al-salami@curtin.edu.au (H.A.-S.)

Abstract: The pathophysiology of a multitude of diseases is influenced by bioenergetic dysfunction. Healthy mitochondria are presented as essential for the regulation and function of multiple cell types, including the cells of relevance for this research: pancreatic beta cells, muscle cells, and liver cells. Hence, effects of hydrogels (particularly nanogels) on bioenergetics needs to be taken into account when designing optimum delivery matrices. Several polymers have been suggested for use in hydrogels and nanogels, with focus on chitosan due to its range of beneficial properties. Bile acids have emerged as beneficial excipients, including deoxycholic acid, which can increase membrane permeability of cells. Nanogels were manufactured containing various concentrations of chitosan and deoxycholic acid in addition to the staple sodium alginate. Nanogels then underwent an array of analysis including rheological studies and in vitro cell work assessing viability, hypoxia, and the bioenergetic profiles. Overall, deoxycholic acid showed enhanced gel strength although this resulted in slightly lower cell viability and impacted bioenergetic profiles. Results from this study showed the benefits of deoxycholic acid; however, this was found to be less suitable for cell delivery matrices and is perhaps more beneficial for drug-delivery systems.

Keywords: bile acid; deoxycholic acid; chitosan; hydrogel; nanogel; biomaterial; bioenergetics

Citation: Kovacevic, B.; Ionescu, C.M.; Jones, M.; Wagle, S.R.; Lewkowicz, M.; Danić, M.; Mikov, M.; Mooranian, A.; Al-Salami, H. The Effect of Deoxycholic Acid on Chitosan-Enabled Matrices for Tissue Scaffolding and Injectable Nanogels. *Gels* **2022**, *8*, 358. https://doi.org/10.3390/gels8060358

Academic Editor: Mazeyar Parvinzadeh Gashti

Received: 9 May 2022
Accepted: 27 May 2022
Published: 7 June 2022

1. Introduction

Mitochondria are capable of transforming caloric intake into molecular energy adenosine triphosphate (ATP), metabolically active compounds, thermal energy, and oxidants. They are highly responsive to their environment and oxidative stress. Therefore, it is no surprise that the pathophysiology of many diseases, including diabetes, hearing loss, obesity, cancer, neurodegenerative and cardiovascular diseases, are underlined by bioenergetic dysfunction. Furthermore, mitochondria are essential in modulating reactive oxygen species (ROS) and controlling cellular apoptosis. However, they are sensitive to increased levels of ROS and reactive nitrogen species (RNS) in addition to calcium, endoplasmic reticulum stress, and the presence of modified proteins [1–4]. Damaged mitochondria can cause significant damage to the host cell, releasing an inappropriate amount of ROS and calcium. This in turn damages the surrounding mitochondria by furthering calcium overload and ROS damage [1].

Muscle cells form highly energy-demanding tissue, with the molecular energy in the form of ATP needed to support its function, mainly for actin–myosin contractions.

Skeletal muscle defects are linked to reduced mitochondrial calcium uptake and oxygen consumption rate [5]. Reduced oxidative phosphorylation (OXPHOS) leads to changes in cellular bioenergetics, shifting metabolism to the fatty acid pathway [6].

Mitochondrial disorders underline some of the most common liver disorders, including non-alcoholic fatty liver disease, non-alcoholic steatohepatitis, fibrosis, and steatosis [7]. Hepatocytes with increased mitochondrial matrix ROS are susceptible to mitochondrial DNA damage. ROS activate signalling factors (adenosine monophosphate-activated protein kinase (AMPK) and c-Jun N-terminal kinase (JNK)) involved in disease progression [7–10].

Mitochondria are essential for insulin secretion from pancreatic beta cells. Beta cells sense glucose concentration by coupling glycolysis to OXPHOS and the citric acid cycle to produce more ATP. This action increases the ATP-to-ADP ratio, leading to inhibition of ATP-inhibiting potassium channels, increased calcium influx, and subsequent exocytosis of insulin vesicles [11]. Mitochondrial disorders in OXPHOS and the citric acid cycle lead to a loss of sensitivity in glucose-stimulated insulin secretion. This is associated with insulin resistance and type 2 diabetes [12].

Therefore, healthy mitochondria are a prerequisite for any tissue function and survival, especially ones encapsulated or embedded in an artificial, extracellular matrix mimicking the environment of tissue replacement devices. Conditions within these vehicles are hypoxic, with uneven oxygen and glucose supply, requiring robust bioenergetics metabolism for tissue to preserve its functionality and viability [13–15].

Various polymers are used in cell delivery systems, including nanogels and nanogels, with natural origins, such as chitosan. Chitosan is a cationic linear polymer comprised of two subunits—D glucosamine and N-acetyl-D glucosamine, connected by a glycosidic bond [16]. It is biocompatible, biodegradable, and mucoadhesive, with antioxidant, antimicrobial, and immune-modulating properties, making it a prime candidate for pharmaceutical and cosmetic applications [17]. Chitosan has been used as a controlled drug-delivery system, including both time-controlled and response-stimulated release systems [18]. It has been used as a vehicle for a broad range of pharmaceuticals, including antibiotic, anaesthetic, hypotensive, and chemotherapeutic drugs [19]. Some therapeutical forms include wound dressings [20] and self-healing injectable nanogels [21]. Zhou et al. used a novel crosslinking model to 3D print chitosan scaffold suitable for tissue engineering [22]. By utilising different crosslinking agents, including other polymers, to obtain interpenetrating (IPN) and semi-interpenetrating polymer networks (semi-IPN), it is possible to modulate the self-healing, degradation, and mechanical properties of chitosan hydro/nano-gels [18].

Bile acids are emerging excipients in different pharmacologic and tissue engineering systems [23]. Naturally occurring secondary bile acid, namely deoxycholic acid (DCA), was found to exert positive and stabilising effects on nanogel capsules for oral delivery of a hydrophobic drug [24]. Majimbi et al. observed greater bioavailability of cannabinol when administered in the form of DCA-enhanced microcapsules [25]. Li et al. designed DCA-based micelles for targeted drug delivery of an antitumor agent [26]. The same bile acid was used as part of micelles for drug and gene for cancer therapy [27]. Furthermore, DCA was used as part of poly-l-lysine nanoparticles for the pH-sensitive release of curcumin [28].

DCA is known to enhance membrane permeability and interfere with normal gap junction function [29]. Higher than physiological concentrations can cause local low-grade inflammation and aggravate intestinal tumorigenesis, induce dysbiosis, and disrupt bile acid metabolism in the liver [30–32]. Therefore, formulation optimisation is crucial to avoid DCA-associated risks while maintaining the best-performing environment for cells.

Different cells require individual micro and macro environments with a variety of specific variables, so creating one universal cell delivery system would be incredibly challenging, hence our reasoning for investigating novel DCA-nanogels on three cell lines (muscle, liver, and pancreatic beta cells) to observe the effects on different tissues. Moreover, we examined different concentrations within the complex nanogel to better understand DCA's effect on cellular viability and mitochondrial metabolism. Five different formulations were made, labelled F1 to F5. F1 is made from water-soluble gel and sodium alginate (SA),

while F2 contains chitosan in addition to water-soluble gel and SA. Formulations F3, F4, and F5 are made from water-soluble gel, SA, chitosan, and DCA in different concentrations, with F3 having the lowest and F5 containing the highest DCA concentration.

2. Results and Discussion

Formulations with DCA have increased shear stress on higher shear rates, while F1 and F2 show similar, lower values (Figure 1a). Viscosity values for all formulations show a similar trend of decreasing viscosity with increasing shear rate (Figure 1b). Surface tension (Figure 1c) of formulations with DCA show a significant increase compared to DCA-free formulations (F1 and F2). The addition of chitosan (F2) to the gel-alginate matrix (F1) decreases surface tension. Torque results follow the trend of shear stress, with F5 exhibiting the highest torque at high rpm (Figure 1d). Similar to shear stress, DCA-free formulations F1 and F2 follow the same trend and exhibit the lowest values at high rpm among all gels. Zeta potential was successfully measured only for DCA-free gels, and they do not statistically significantly differ from one another (Figure 1e).

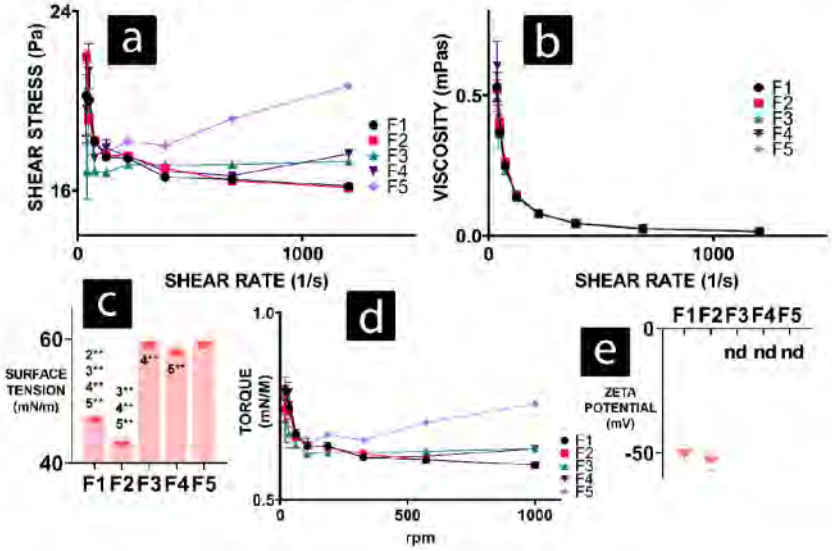

Figure 1. Rheology results of F1 to F5 formulations presented as values of (**a**) shear stress, (**b**) viscosity, (**c**) surface tension, (**d**) torque, and (**e**) zeta potential. $p < 0.01$ (*) or $p < 0.05$ (**).

All formulations exhibited shear-thinning/thixtropic/non-Nitonion behaviour (Figure 1a,b) characterised by viscous flow under shear stress [33]. Shear-thinning gels are found to be cytoprotective during the injection process and manufacturing of 3D-printed scaffolds. They are preferred to shear thickening gels or Newtonian fluids in cell delivery applications [34]. Shear stress and torque values (Figure 1a,d) show elastic tendencies for F5, a formulation with the highest percentage of DCA. DCA-free formulations (F1 and F2) exhibit the least shear or torque stress (Figure 1a,d). This suggests that DCA is integral in increasing the strength of inter-gel bonds, mainly between chitosan and sodium alginate. This is further observed with surface tension (Figure 1c). DCA-free gels have a smaller surface tension compared to formulations with DCA, suggesting that there are higher energy bonds in the presence of DCA.

SEM images of freeze-dried samples show overall similar surface topography (Figure 2). F1 formulations show the smoothest morphology, (Figure 2a) while addition of chitosan (Figure 2b) results in uneven surface topography. Presence of DCA in gel matrix leads to irregular surface morphology as well as different inner morphology (Figure 2c–e). Surface morphology may be linked to presence of DCA in nanogel matrix, as irregularities in morphology seem the most prevalent in F5 (Figure 2e).

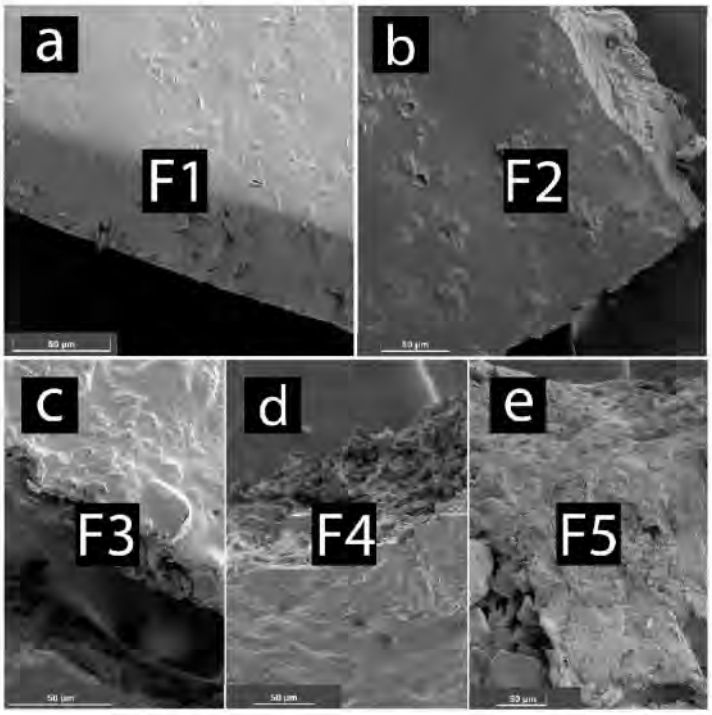

Figure 2. SEM images showing surface morphology of freeze-dried nanogels: (**a**) F1, (**b**) F2, (**c**) F3, (**d**) F4, and (**e**) F5.

Viability of hepatic, AML-12 cells in gels was preserved only at F2 compared to the control (C) (Figure 3a). All the other formulations had significantly lower viability in normal conditions after 24 h incubation, compared with control. The beneficial effect of chitosan on liver tissue is documented in the literature, which can explain high viability in the presence of chitosan enriched F2, as chitosan had a protective effect against CCl_4-induced hepatic fibrosis [35]. Furthermore, Lee et al. constructed a bio-artificial liver chip from chitosan microfibers [36]. The viability of C2C12 decreased compared to gel-free control for all formulations, but it showed no significant difference between different DCA concentrations (F3, F4, and F5) and the chitosan-enhanced formulation (F2) (Figure 3b). NIT-1 cells showed only a significant difference between the gel-free control and F2, with F2 increasing viability (Figure 3c).

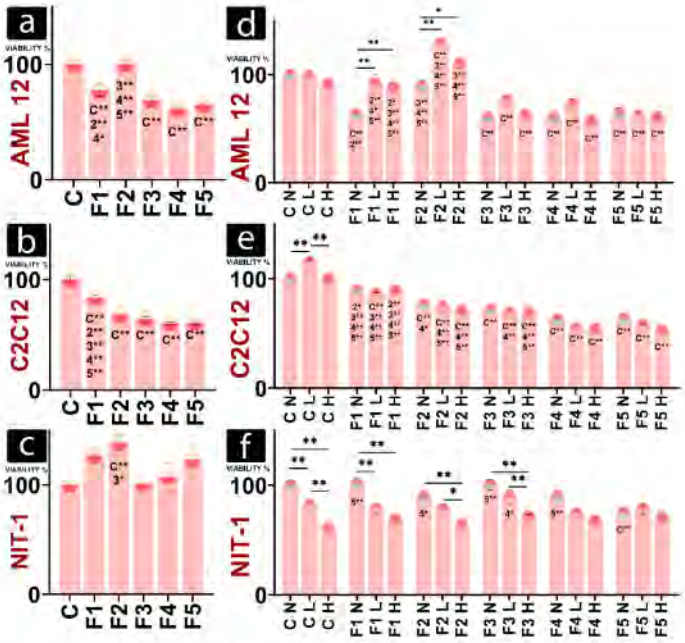

Figure 3. Viability of AML12 (**a**), C2C12 (**b**), and NIT-1 (**c**) under normal conditions. Viability of hepatic (**d**), muscle (**e**), and pancreatic beta cells (**f**) under different hypoxic conditions, where N, non-hypoxic control environment; L, lower hypoxic environment; and H, higher hypoxic environment. $p < 0.01$ (*) or $p < 0.05$ (**).

Different hypoxic conditions did not significantly affect the viability of gel-free hepatic cells or the viability of cells in the presence of DCA-enriched gels (Figure 3d). Viabilities of AML-12 showed increased values under hypoxia than in non-hypoxic conditions for F1 and F2. Within different hypoxic conditions, values follow a similar trend to data obtained in normal conditions, with increased viability for F2 and decreased for F3, F4, and F5 (Figure 3d), suggesting the positive effect of chitosan.

Gel-free muscle cells were the only ones to respond to hypoxia, with increased viability in lower hypoxia (Figure 3e). This is in accordance with the study by Sakushima et al., who found that slight hypoxia induces proteins needed for muscle hypertrophy and differentiation [37]. Cells in the presence of gels did not respond to hypoxia and showed no significant change in viability under hypoxia. Within the same hypoxic conditions, muscle cells followed the same declining trend as those in normal conditions, with a significant decrease in viability compared to control cells.

Control NIT-1 cells responded to hypoxic conditions in accordance with the severity of hypoxia (Figure 3f). The viability decreased with the increase of hypoxia. This trend was also observed with F1, F2, and F3, while cells in the presence of F4 and F5 had no significant changes in viability regardless of the environment (Figure 3f). Higher viability in the presence of F2, observed in normal conditions (Figure 3c), was not present under the hypoxic or the control environment (Figure 3f). This may suggest that high concentrations of DCA can induce hypoxic conditions or impair aerobic metabolism in NIT-1 cells.

Hepatic cells in a normal environment showed an increase in oxygen consumption in F1 and F2 (Figure 4a). For DCA gels (F3, F4, F5), an increase in extracellular acidification rate (ECAR) is prominent without an increase in OCR, suggesting a shift to glycolic metabolism (Figure 4a). In Figure 3b, the maximal oxygen consumption rate (OCR) is established as 100% to visually show allocated OCR for different functions within cells in the presence of different gels. Gel-free cells show the highest percentage of OCR allocated to ATP production, with minimal proton leak. F1 has a similar % of non-mitochondrial OCR (NM OCR) with decreased ATP production but increased spare capacity and proton leak. F2 has similar ATP production to F1, but spare capacity is negligible, and proton leak is further increased. F3 shows a substantial increase in non-mitochondrial OCR, while ATP production is deficient. Spare capacity is preserved similarly to gel-free control, and proton leak is insignificant.

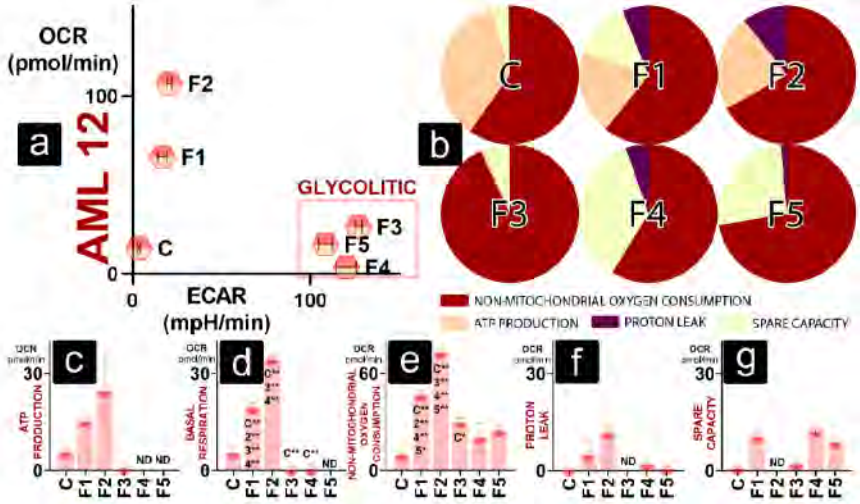

Figure 4. Bioenergetics of AML 12 cells showing (**a**) metabolic profile in normal conditions; (**b**) maximal OCR established as 100% and the oxygen consumption allotted between non-mitochondrial OCR, ATP-linked OCR, proton-leak-linked OCR, and spare-capacity-linked OCR; OCR values for (**c**) ATP production, (**d**) basal respiration, (**e**) non-mitochondrial oxygen consumption, (**f**) proton leak, and (**g**) spare capacity. $p < 0.01$ (*) or $p < 0.05$ (**).

In contrast to F3, the fraction of NM OCR of F4 is similar to one of the control free cells (C). F5 shows a higher percentage of NM OCR to F4, but, similar to F4, its OCR is mainly allocated for NM OCR and spare capacity (Figure 4b). ATP production is not observed; however, the spare capacity fraction for F4 is several-fold higher than the same fraction of gel-free cells.

ATP production for hepatic cells did not significantly differ amongst groups due to the high variability of data. Cells in the presence of F4 and F5 have no detectable ATP-production-linked OCR (Figure 4c). However, OCR values for basal respiration follow the trend seen in Figure 3a, with F1 and F2 showing a significant increase in OCR compared to the control, and F3 and F4 had a significant decrease compared to the same variable. Basal respiration of cells in F5 was of non-detectable levels (Figure 4d). Figure 4e shows that an increase in NM OCR features in an increase of total OCR for F1 and F2, which is significantly higher than the control levels. F3 also shows a significant increase in non-mitochondrial

OCR, while levels found in F4 and F5 were not significantly different to levels of the control (Figure 4e). While values for proton leak and spare-capacity-linked OCR were detected in most groups, they showed no statistical significance compared to the control cells or between different gels groups (Figure 4f,g).

Muscle cells in a normal environment reflect a trend present with hepatic cells—F1 and F2 show an increase in total OCR, while F3, F4, and F5 have increased ECAR and lower total OCR than the control (Figure 5a). However, OCR allocation is different between C2C12 and AML 12 cells. Control cells allocate most of the OCR for non-mitochondrial OCR, ATP production, and proton leak (Figure 5b). F2 and F3 follow that pattern with an increase in NM OCR and decreased ATP production. F3 presents a higher fraction of NM OCR than the control and DCA-free formulations, with smaller ATP production and proton leak. The spare capacity fraction of F3 is more considerable than its proton leak fraction. Maximal OCR allocation of F4 shows high NM OCR and the highest fraction of proton leak of all the formulations. Mitochondrial OCR in F5 is modest and reserved just for spare-capacity-linked OCR, while most oxygen is linked with NM OCR (Figure 5b).

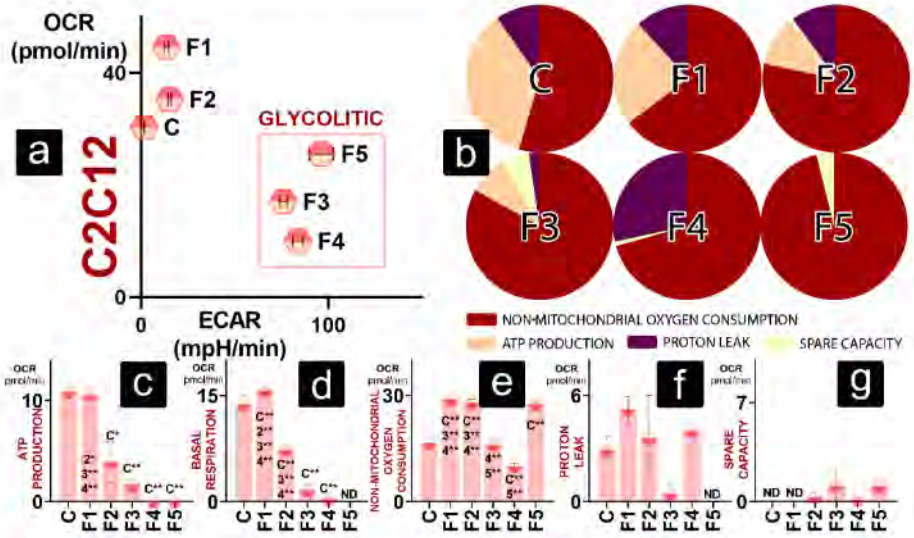

Figure 5. Bioenergetics of C2C12 cells showing (**a**) metabolic profile in normal conditions; (**b**) maximal OCR established as 100% and the oxygen consumption allotted between non-mitochondrial OCR, ATP-linked OCR, proton-leak-linked OCR, and spare-capacity-linked OCR; OCR values for (**c**) ATP production, (**d**) basal respiration, (**e**) non-mitochondrial oxygen consumption, (**f**) proton leak, and (**g**) spare capacity. $p < 0.01$ (*) or $p < 0.05$ (**).

As observed in Figure 5c, only F1 retained ATP production comparable to that of the control. All the other groups (F2, F3, F4, and F5) had significantly decreased ATP-production-linked OCR. OCR linked with basal respiration follows a similar trend (Figure 5d). NM OCR is higher for F1, F2, and F5 than the control, while F3 has comparable and F4 lower values (Figure 5e). Similar to AML 12, values for proton-leak- and spare-capacity-linked OCR were detected for most groups, but no statistical difference was found (Figure 5f,g).

Pancreatic beta cells show an even more significant disparity between test formulations and the control; F1 and F2 with high total oxygen consumption; and F3, F4, and F5 with

a lower total OCR and higher ECAR (Figure 6a). Gel-free NIT-1 cells (Figure 1b) have a similar OCR for NM OCR and ATP production. The rest of the maximal OCR is utilised for proton leak. F1 has slightly increased NM OCR compared to the control and decreased proton leak, while ATP production OCR fraction seems to be retained. ATP production and proton leak consume similar percentages of oxygen in F2, with ATP production being lower than in control and F2. NM OCR is the dominant oxygen consumer for F3, F4, and F5. Next to non-mitochondrial OCR, oxygen is used for proton leak (F3) and spare capacity (F3, F4, and F5) (Figure 6b).

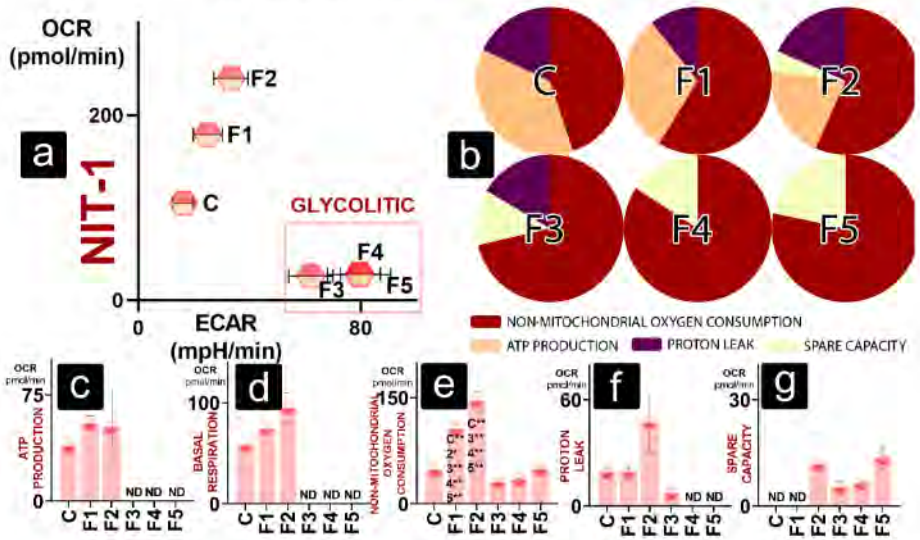

Figure 6. Bioenergetics of NIT-1 cells showing (**a**) metabolic profile in normal conditions; (**b**) maximal OCR established as 100% and the oxygen consumption allotted between non-mitochondrial OCR, ATP-linked OCR, proton-leak-linked OCR, and spare-capacity-linked OCR; OCR values for (**c**) ATP production, (**d**) basal respiration, (**e**) non-mitochondrial oxygen consumption, (**f**) proton leak, and (**g**) spare capacity. $p < 0.01$ (*) or $p < 0.05$ (**).

ATP-production-linked OCR was detected only for DCA-free cells (C, F1, and F2), with no statistical difference between groups (Figure 6c). A similar trend is observed with basal respiration (Figure 5d). NM OCR (Figure 5e) was the highest for cells in the presence of DCA-free gels (F1 and F2), which was significantly higher than in control and cells exposed to DCA gels (F3, F4, and F5). This illustrates that most of the increase in total OCR for F1 and F2 (Figure 6a) comes from increased NM OCR rather than mitochondrial respiration. Proton-leak- and spare-capacity-linked OCR showed no significant differences between groups (Figure 6f,g)

All three cell lines follow a similar bioenergetic pattern in the presence of DCA, shifting to anaerobic metabolism, with decreased ATP-linked OCR and increased percentage of spare-capacity-linked OCR and non-mitochondrial OCR.

Cells have enhanced glycolysis in a limited oxygen supply or if OXPHOS is impaired [38]. OXPHOS impairment is visible in the absence of ATP-linked OCR in cells exposed to DCA. ATP production in cells is driven by ATP synthetase, complex V of electron transport chain (ETC). In the seahorse Mito stress assay, ATP synthetase is inhibited by oligomycin, and ATP production OCR is calculated as a difference in OCR before and after

oligomycin injection. Oligomycin injection does not seem to be effective in most cells in the presence of DCA, suggesting prior ATP synthetase inhibition.

The main reasons behind compromised ATP production are damaged ETC, low substrate availability, and low ATP demand [3], meaning that DCA can exacerbate one or more of those conditions. Damaged ETC is characterised by high proton leak and low spare capacity. The injection of uncoupling agent (p-(trifluoromethoxy) phenylhydrazone FCCP) depletes mitochondrial membrane potential, allowing for uninhibited electron flow through ETC. The addition of FCCP estimates maximal OCR without dependence on ATP/ADP transport [39], as ATP/ADP translocator is dependent on proton gradient [40]. Therefore, spare capacity is the oxygen consumption available to cells during stress and increased ATP demand [39]. However, investigated cell types show no significant difference between proton-leak- and spare-capacity-linked OCR. This may suggest that DCA does not compromise ETC integrity.

Rheology studies (Figure 1) suggest increased bond strength within DCA gels, leading to thicker, more viscous gels. It is possible that oxygen and nutrients were unable to reach cells embedded in the DCA gel, leading to hypoxia. Hypoxic conditions lead to the stabilisation of hypoxia inducing factor HIF1 α. Hypoxia-inducing properties of $CoCl_2$, used in an assay to obtain results presented in Figure 3, rely on the exact HIF1 α mechanism [41]. Cells in non-hypoxic conditions in the presence of DCA mostly had unchanged viability to the cells treated to $CoCl_2$ (Figure 3d–f), so it can be argued that they were already hypoxic, with their HIF1 α stabilised prior to the $CoCl_2$ treatment. HIF1 α leads to the increased expression of enzymes needed for glycolysis, including glyceraldehyde-3-phosphate dehydrogenase [42,43]. HIF1 α also modulates pH in cells by enhancing lactic acid production [44]. Hypoxia and HIF1 α regulate the expression of ATPase Inhibitory Factor 1 (IF1) [45]. IF1 has pH-regulated binding to ATP synthetase, preferring the acidic environment available with an increase in glycolysis [46]. IF1 expression leads to the upregulation of aerobic glycolysis and inhibits ATP production in cells by inhibiting ATP synthase [47]. This may be the pathway responsible for glycolytic metabolism shift and absence of significant decrease in ATP-production-linked OCR in cells in the presence of DCA gels, as IF1 mimics the effects of oligomycin. Furthermore, IF1-mediated inhibition of ATP synthase leads to mitochondrial hyperpolarisation and the production of ROS [48]. However, in large amounts, ROS lead to lipid peroxidation, DNA damage, protein oxidation, ATP-synthase inhibition, mitochondria damage, and cell death [49]. This is concurrent with Yerushalmi et al., who found that glycochenodeoxycholic acid and hydrophobic bile acid, such as DCA, induces ROS generation and mitochondrial permeability transition in hepatocytes [50]. Excessive levels of hydrophobic bile acid stimulate mitochondria to release ROS, and high cytoplasmic ROS induces Ca^{2-} to exit the endoplasmic reticulum to the cytosol, where it further stimulates mitochondria to produce ROS [51]. This may be why NM OCR did not decrease together with OXPHOS in the presence of DCA (F3, F4, and F5) but increased in most cells (Figures 4e, 5e and 6e).

To further investigate the link between non-mitochondrial OCR, ATP-production-linked OCR in normal conditions and cell viability under normal and hypoxic conditions, we calculated linear regressions, presented in Figure 7a–s. For both hepatic and muscle cells, the fraction of NM OCR in basal respiration seems to be the best predictor of cell survivability in different hypoxic conditions (Figure 7c,i). With increased NM OCR fraction in basal cellular respiration, cell viability decreases no matter the conditions. Furthermore, actual NM OCR in pmol/min does not seem to indicate cell survival (Figure 7a,g,m). As ETC is a significant producer of ROS in cells [52,53], the rise in NM OCR following the increased OXPHOS does not seem to have a predictable negative impact on cell survival.

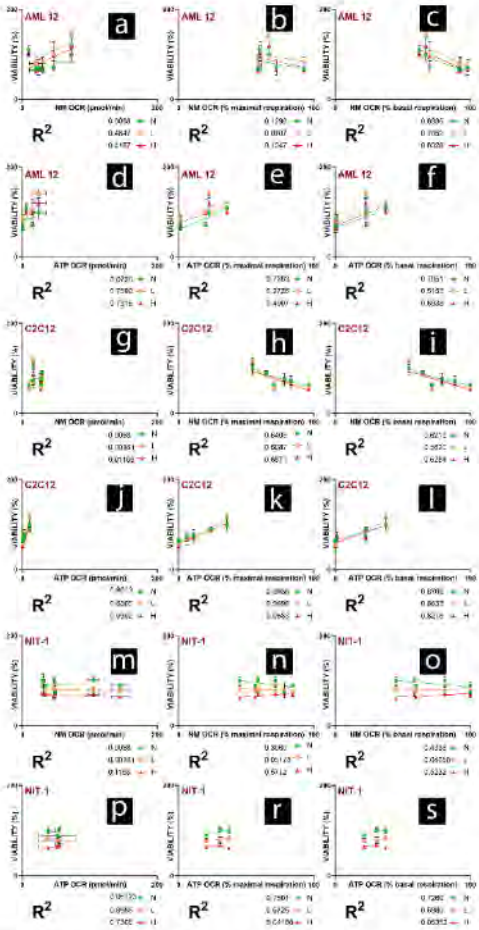

Figure 7. Relationships between bioenergetics in normoxic conditions and viability under normal, low, and high hypoxia. NM OCR, non-mitochondrial-linked OCR; ATP OCR, ATP-production-linked OCR. % maximal respiration—parameter is expressed as a % of maximal respiration, where value of maximal respiration linked OCR is 100%. % basal respiration—parameter is expressed as a % of basal respiration, where value of basal respiration linked OCR is 100%. Figure 7. shows the linear relationship of AML 12 cell viability and (**a**) NM OCR, (**b**) NM OCR as % of maximal respiration, (**c**) NM OCR as % of basal respiration, (**d**) ATP OCR, (**e**) ATP OCR as % of maximal respiration, (**f**) ATP OCR as % basal respiration. Figure 7. shows the linear relationship of C2C12 cell viability and (**g**) NM OCR, (**h**) NM OCR as % of maximal respiration, (**i**) NM OCR as % of basal respiration, (**j**) ATP OCR, (**k**) ATP OCR as % of maximal respiration, (**l**) ATP OCR as % basal respiration. Figure 7. shows the linear relationship of NIT-1 cell viability and (**m**) NM OCR, (**n**) NM OCR as % of maximal respiration, (**o**) NM OCR as % of basal respiration, (**p**) ATP OCR, (**r**) ATP OCR as % of maximal respiration, (**s**) ATP OCR as % basal respiration.

The ATP-production-linked OCR expressed as a % of basal respiration seems to be the best predictor of cell survival (Figure 7f,l,s). Cell survival is positively impacted with an increase of ATP production fraction of OCR in hypoxic and normoxic conditions. For the C2C12 cell line, a similar relationship is visible for the ATP-production-linked OCR expressed as % maximal respiration, probably because of minor spare capacity observed within these cells. High ATP-production-linked OCR in normal conditions seems to predict higher survival when cells are exposed to hypoxia. However, it does not seem to be directly correlated with NIT-1 and AML 12 survival in a normoxic environment (Figure 7d,p). NIT-1 cells have a positive impact on viability from increased ATP production fraction of OCR only in normal and mild hypoxia but not in the higher hypoxia (Figure 7i,s).

3. Conclusions

The addition of deoxycholic acid overall increased the strength of gels, increasing surface tension and shear stress, with retained shear-thinning properties. This significantly impacted three cell lines (muscle, liver, and pancreatic beta cells) that were subjected to novel DCA-enhanced nanogel delivery matrices. Gels with stronger bonds lead to slightly lowered viability and decreased aerobic respiration, with a noticeable shift in cellular metabolism to glycolysis. Therefore, these hydro/nanogels may be more suitable for drug delivery than cell delivery matrices.

4. Materials and Methods

4.1. Materials

Deoxycholic acid (DCA), sodium alginate (SA, low viscosity) and Poloxamer 407 were acquired from Sigma Chemical Co. (St. Louis, MO, USA). The gel (water-soluble) was acquired from the Australian Medical Association (Perth, Australia). Dulbecco's modified Eagle's medium (DMEM), foetal bovine serum (FBS), and needed supplements were acquired from Sigma Chemical Co. (MO, USA).

4.2. Cell Culture

AML 12 was cultured in DMEM with 10% FBS and further supplementation based on published protocol [54]. C2C12 were grown in DMEM (10% FBS and 1% penicillin-streptomycin) following protocol for non-differentiated myotubes [55]. NIT-1 were grown in DMEM (supplemented with 10% FBS, 5.5 mmol glucose), Sigma-Aldrich, MO, USA), and free amino acids following a published protocol [56]. The cells were incubated in a humidified atmosphere of 5% CO_2 at 37 °C. The media was changed every day for C2C12 and every other day for AML-12 and NIT-1.

4.3. Gel Preparation

Gels were prepared by mixing the water-soluble gel with sodium alginate (SA), chitosan, and DCA with deionised water under sterile conditions, following the formulations, as following. The water soluble gel (7%), SA (1.5%) and chitosan (0.3%) were used as appropriate, while DCA was used as (1.8, 2.2, and 2.4%) correspondingly, as described below.

For viability and hypoxia and seahorse assays, 20 µL of gel was added per well and left for 30 min under constant UV light. Freshly detached cells were added to gels and thoroughly mixed with a pipette. After mixing, the appropriate cell media was added. Each cell line was examined on a separate 96-well plate.

4.4. Rheology

A Visco-88 viscometer (Malvern Instruments, Malvern, UK) was utilised for viscosity, torque, shear stress, and shear rate measurements [56]. The Zeta potential was determent using a 3000HS Zetasizer (Malvern, UK). Surface tension was measured by a tensiometer (Sigma 703) [57]. All measurements were executed at room temperature.

4.5. Scanning Electron Microscopy (SEM)

Samples were freeze dried using Dynavac FD3 Freeze Dryer (Dynapumps, Seven Hills, Australia) for 48 h on −45 °C under vacuum. Afterwards, SEM (Zeiss Neon 40EsB FIBSEM, Carl Zeiss Microscopy GmbH, Jena, Germany) was utilised for surface morphology imaging [58].

4.6. Cell Viability Assay

A MTT (2,5-diphenyl-2,4,5-trimethylthiazol-2-yl) assay was used to observe the impact of nanogels on cell viability. Stock MTT solutions were prepared at 5 mg/mL within 24 h of use. All groups were treated in the same manner, including gel-free controls.

Following 24 h incubation, 20 µL of the stock MTT solution was added to each well containing cell-loaded nanogels or control wells. Resultant MTT-formazan was dissolved in 100 µL dimethyl sulfoxide (DMSO). The purple solution was then analysed via photometry at 550 nm in triplicates [59]. Obtained data were normalised and presented as a percentage, where 100% is the viability of cells in control wells.

4.7. Hypoxia Assays

Freshly detached cells were mixed with 80 µL of 50 µM or 100 µM solutions of $CoCl_2$ in an appropriate cell media and left for 20 min before mixing them with gels. After mixing, a further 100 µL of the $CoCl_2$-enriched media was added. After 24 h incubation, cell viability was assessed with the MTT assay [60].

4.8. Bioenergetic Parameters

After 24 h incubation, real-time mitochondrial activities were measured in hepatic, muscle, and pancreatic beta cells using a Seahorse Flux Analyser XF 96 (Agilent Technologies, Santa Clara, CA, USA) via an in-house-developed method [61,62].

4.9. Statistics

GraphPad Prism v9.3 (Graphpad, Inc., San Diego, CA, USA) for the data analysis, regressions, and one-way ANOVA/two-way ANOVA were conducted. Tukey HSD with post hoc comparisons of means was performed when the data were statistically significant. Data are shown as a mean ± SEM with $n = 3$, and the data were considered statistically significant at $p < 0.01$ (*) or $p < 0.05$ (**).

Author Contributions: Conceptualization, A.M., M.M. and H.A.-S.; data curation, B.K., C.M.I., S.R.W., M.L. and M.J.; formal analysis, B.K., C.M.I., M.J., S.R.W., M.L., M.D., M.M., A.M. and H.A.-S.; funding acquisition, A.M., M.M. and H.A.-S.; investigation, all authors.; methodology, B.K., C.M.I., S.R.W., M.L. and M.J.; project administration, M.Đ., M.M. and H.A.-S.; resources, A.M., M.M. and H.A.-S.; software B.K., C.M.I., M.J., S.R.W., M.L., M.Đ., M.M., A.M. and H.A.-S.; supervision, A.M., M.M. and H.A.-S.; validation, all authors; visualization, B.K., C.M.I., S.R.W., M.L. and M.J.; writing—original draft, B.K.; writing—review and editing, B.K., C.M.I., M.J., S.R.W., M.L., M.D., M.M., A.M. and H.A.-S. All authors have read and agreed to the published version of the manuscript.

Funding: The work is partially supported by the European Union Horizon 2020 research project and innovation program under the Marie Sklodowska-Curie Grant Agreement No 872370. Curtin Faculty ORS-WAHAI Consortium and the Australian National Health and Medical Research (APP9000597).

Institutional Review Board Statement: Not applicable.

Informed Consent Statement: Not applicable.

Data Availability Statement: The data presented in this study are available on request from the corresponding author. The data are not publicly available due to author property agreements.

Acknowledgments: The authors thank the technical researchers and Moore for their assistant. The authors acknowledge the Australian Postgraduate Award (APA) and Curtin Research Scholarship (CRS). The authors also acknowledge the Microscopy and Microanalysis Facility at Curtin University.

Conflicts of Interest: The authors declare no conflict of interest.

References

1. Dranka, B.P.; Hill, B.G.; Darley-Usmar, V.M. Mitochondrial reserve capacity in endothelial cells: The impact of nitric oxide and reactive oxygen species. *Free Radic. Biol. Med.* **2010**, *48*, 905–914. [CrossRef]
2. Higdon, A.N.; Benavides, G.A.; Chacko, B.K.; Ouyang, X.; Johnson, M.S.; Landar, A.; Zhang, J.; Darley-Usmar, V.M. Hemin causes mitochondrial dysfunction in endothelial cells through promoting lipid peroxidation: The protective role of autophagy. *Am. J. Physiol.-Heart Circ. Physiol.* **2012**, *302*, H1394–H1409. [CrossRef]
3. Hill, B.G.; Benavides, G.A.; Lancaster, J.R.; Ballinger, S.; Dell'Italia, L.; Zhang, J.; Darley-Usmar, V.M. Integration of cellular bioenergetics with mitochondrial quality control and autophagy. *Biol. Chem.* **2012**, *393*, 1485–1512. [CrossRef]
4. Abate, M.; Festa, A.; Falco, M.; Lombardi, A.; Luce, A.; Grimaldi, A.; Zappavigna, S.; Sperlongano, P.; Irace, C.; Caraglia, M.; et al. Mitochondria as playmakers of apoptosis, autophagy and senescence. *Semin. Cell Dev. Biol.* **2020**, *98*, 139–153. [CrossRef]
5. Cherardi, G.; Nogara, L.; Ciciliot, S.; Fadini, G.P.; Blaauw, B.; Braghetta, P.; Bonaldo, P.; De Stefani, D.; Rizzuto, R.; Mammucari, C. Loss of mitochondrial calcium uniporter rewires skeletal muscle metabolism and substrate preference. *Cell Death Differ.* **2019**, *26*, 362–381. [CrossRef]
6. Rossi, A.; Pizzo, P.; Filadi, R. Calcium, mitochondria and cell metabolism: A functional triangle in bioenergetics. *Biochim. Biophys. Acta (BBA)-Mol. Cell Res.* **2019**, *1866*, 1068–1078. [CrossRef]
7. Nie, H.; Yu, X.; He, H.; Zhou, L.; Li, Q.; Song, C.; Wang, D.; Ren, T.; Chen, Z.; Huang, H.; et al. Hepatocyte miR-33a mediates mitochondrial dysfunction and hepatosteatosis by suppressing NDUFA5. *J. Cell Mol. Med.* **2018**, *22*, 6285–6293. [CrossRef] [PubMed]
8. Lee, J.; Park, J.-S.; Roh, Y.S. Molecular insights into the role of mitochondria in non-alcoholic fatty liver disease. *Arch. Pharmacal Res.* **2019**, *42*, 935–946. [CrossRef]
9. Herzig, S.; Shaw, R.J. AMPK: Guardian of metabolism and mitochondrial homeostasis. *Nat. Rev. Mol. Cell Biol.* **2018**, *19*, 121–135. [CrossRef]
10. An, P.; Wei, L.-L.; Zhao, S.; Sverdlov, D.Y.; Vaid, K.A.; Miyamoto, M.; Kuramitsu, K.; Lai, M.; Popov, Y.V. Hepatocyte mitochondria-derived danger signals directly activate hepatic stellate cells and drive progression of liver fibrosis. *Nat. Commun.* **2020**, *11*, 2362. [CrossRef]
11. Wiederkehr, A.; Wollheim, C.B. Mitochondrial signals drive insulin secretion in the pancreatic β-cell. *Mol. Cell Endocrinol.* **2012**, *353*, 128–137. [CrossRef]
12. Tseng, W.-W.; Chu, C.-H.; Chang, C.; Lee, Y.-J.; Zhao, S.; Ho, Y.-P.; Wei, A.-C. Metabolic Regulation of Mitochondrial Morphologies in Pancreatic Beta Cells: Bioenergetics-Mitochondrial Dynamics Coupling. *bioRxiv* **2021**. [CrossRef]
13. Volkmer, E.; Drosse, I.; Otto, S.; Stangelmayer, A.; Stengele, M.; Kallukalam, B.C.; Mutschler, W.; Schieker, M. Hypoxia in Static and Dynamic 3D Culture Systems for Tissue Engineering of Bone. *Tissue Eng. Part A* **2008**, *14*, 1331–1340. [CrossRef]
14. Bland, E.; Dréau, D.; Burg, K.J.L. Overcoming hypoxia to improve tissue-engineering approaches to regenerative medicine. *J. Tissue Eng. Regen. Med.* **2013**, *7*, 505–514. [CrossRef]
15. Abudula, T.; Gauthaman, K.; Hammad, A.H.; Joshi Navare, K.; Alshahrie, A.A.; Bencherif, S.A.; Tamayol, A.; Memic, A. Oxygen-Releasing Antibacterial Nanofibrous Scaffolds for Tissue Engineering Applications. *Polymers* **2020**, *12*, 1233. [CrossRef] [PubMed]
16. Peers, S.; Montembault, A.; Ladavière, C. Chitosan hydrogels for sustained drug delivery. *J. Control. Release* **2020**, *326*, 150–163. [CrossRef]
17. Yang, J.; Shen, M.; Luo, Y.; Wu, T.; Chen, X.; Wang, Y.; Xie, J. Advanced applications of chitosan-based hydrogels: From biosensors to intelligent food packaging system. *Trends Food Sci. Technol.* **2021**, *110*, 822–832. [CrossRef]
18. Pellá, M.C.G.; Lima-Tenório, M.K.; Tenório-Neto, E.T.; Guilherme, M.R.; Muniz, E.C.; Rubira, A.F. Chitosan-based hydrogels: From preparation to biomedical applications. *Carbohydr. Polym.* **2018**, *196*, 233–245. [CrossRef]
19. Tian, B.; Hua, S.; Tian, Y.; Liu, J. Chemical and physical chitosan hydrogels as prospective carriers for drug delivery: A review. *J. Mater. Chem. B* **2020**, *8*, 10050–10064. [CrossRef]
20. Mukherjee, D.; Azamthulla, M.; Santhosh, S.; Dath, G.; Ghosh, A.; Natholia, R.; Anbu, J.; Teja, B.V.; Muzammil, K.M. Development and characterization of chitosan-based hydrogels as wound dressing materials. *J. Drug Deliv. Sci. Technol.* **2018**, *46*, 498–510. [CrossRef]
21. Xu, Y.; Li, Y.; Chen, Q.; Fu, L.; Tao, L.; Wei, Y. Injectable and Self-Healing Chitosan Hydrogel Based on Imine Bonds: Design and Therapeutic Applications. *Int. J. Mol. Sci.* **2018**, *19*, 2198. [CrossRef]
22. Zhou, L.; Ramezani, H.; Sun, M.; Xie, M.; Nie, J.; Lv, S.; Cai, J.; Fu, J.; He, Y. 3D printing of high-strength chitosan hydrogel scaffolds without any organic solvents. *Biomater. Sci.* **2020**, *8*, 5020–5028. [CrossRef]
23. Kovacevic, B.; Jones, M.; Ionescu, C.; Walker, D.; Wagle, S.; Chester, J.; Foster, T.; Brown, D.; Mikov, M.; Mooranian, A.; et al. The emerging role of bile acids as critical components in nanotechnology and bioengineering: Pharmacology, formulation optimizers and hydrogel-biomaterial applications. *Biomaterials* **2022**, *283*, 121459. [CrossRef]
24. Mooranian, A.; Zamani, N.; Mikov, M.; Goločorbin-Kon, S.; Stojanovic, G.; Arfuso, F.; Al-Salami, H. Eudragit®-based microcapsules of probucol with a gut-bacterial processed secondary bile acid. *Ther. Deliv.* **2018**, *9*, 811–821. [CrossRef]

25. Majumbi, M.; Brook, E.; Galettis, P.; Eden, E.; Al-Salami, H.; Mooranian, A.; Al-Sallami, H.; Lam, V.; Mamo, J.C.L.; Takechi, R. Sodium alginate microencapsulation improves the short-term oral bioavailability of cannabidiol when administered with deoxycholic acid. *PLoS ONE* **2021**, *16*, e0243858. [CrossRef]
26. Li, L.; Liang, N.; Wang, D.; Yan, P.; Kawashima, Y.; Cui, F.; Sun, S. Amphiphilic Polymeric Micelles Based on Deoxycholic Acid and Folic Acid Modified Chitosan for the Delivery of Paclitaxel. *Int. J. Mol. Sci.* **2018**, *19*, 3132. [CrossRef]
27. Chen, L.; Ji, F.; Bao, Y.; Xia, J.; Guo, L.; Wang, J.; Li, Y. Biocompatible cationic pullulan-g-deoxycholic acid-g-PEI micelles used to co-deliver drug and gene for cancer therapy. *Mater. Sci. Eng. C* **2017**, *70*, 418–429. [CrossRef]
28. Yang, D.H.; Kim, H.J.; Park, K.; Kim, J.K.; Chun, H.J. Preparation of poly-l-lysine-based nanoparticles with pH-sensitive release of curcumin for targeted imaging and therapy of liver cancer in vitro and in vivo. *Drug Deliv.* **2018**, *25*, 950–960. [CrossRef]
29. Gvoic, M.; Vukmirovic, S.; Al-Salami, H.; Mooranian, A.; Mikov, M.; Stankov, K. Bile acids as novel enhancers of CNS targeting antitumor drugs: A comprehensive review. *Pharm. Dev. Technol.* **2021**, *26*, 617–633. [CrossRef]
30. Liu, L.; Dong, W.; Wang, S.; Zhang, Y.; Liu, T.; Xie, R.; Wang, B.; Cao, H. Deoxycholic acid disrupts the intestinal mucosal barrier and promotes intestinal tumorigenesis. *Food Funct.* **2018**, *9*, 5588–5597. [CrossRef]
31. Xu, M.; Cen, M.; Shen, Y.; Zhu, Y.; Cheng, F.; Tang, L.; Hu, W.; Dai, N. Deoxycholic Acid-Induced Gut Dysbiosis Disrupts Bile Acid Enterohepatic Circulation and Promotes Intestinal Inflammation. *Dig. Dis. Sci.* **2021**, *66*, 568–576. [CrossRef]
32. Mroz, M.S.; Lajczak, N.K.; Goggins, B.J.; Keely, S.; Keely, S.J. The bile acids, deoxycholic acid and ursodeoxycholic acid, regulate colonic epithelial wound healing. *Am. J. Physiol. Gastrointest. Liver Physiol.* **2018**, *314*, G378–G387. [CrossRef]
33. Guvendiren, M.; Lu, H.D.; Burdick, J.A. Shear-thinning hydrogels for biomedical applications. *Soft Matter* **2012**, *8*, 260–272. [CrossRef]
34. Uman, S.; Dhand, A.; Burdick, J.A. Recent advances in shear-thinning and self-healing hydrogels for biomedical applications. *J. Appl. Polym. Sci.* **2020**, *137*, 48668. [CrossRef]
35. Wang, Z.F.; Wang, M.Y.; Yu, D.H.; Zhao, Y.; Xu, H.M.; Zhong, S.; Sun, W.Y.; He, Y.F.; Niu, J.Q.; Gao, P.J.; et al. Therapeutic effect of chitosan on CCl4-induced hepatic fibrosis in rats. *Mol. Med. Rep.* **2018**, *18*, 3211–3218. [CrossRef]
36. Lee, K.H.; Shin, S.J.; Kim, C.-B.; Kim, J.K.; Cho, Y.W.; Chung, B.G.; Lee, S.-H. Microfluidic synthesis of pure chitosan microfibers for bio-artificial liver chip. *Lab A Chip* **2010**, *10*, 1328–1334. [CrossRef]
37. Sakushima, K.; Yoshikawa, M.; Osaki, T.; Miyamoto, N.; Hashimoto, T. Moderate hypoxia promotes skeletal muscle cell growth and hypertrophy in C2C12 cells. *Biochem. Biophys. Res. Commun.* **2020**, *526*, 921–927. [CrossRef] [PubMed]
38. Sánchez-Aragó, M.; Formentini, L.; Cuezva, J.M. Mitochondria-Mediated Energy Adaption in Cancer: The H+-ATP Synthase-Geared Switch of Metabolism in Human Tumors. *Antioxid. Redox Signal.* **2012**, *19*, 285–298. [CrossRef]
39. Dranka, B.P.; Benavides, G.A.; Diers, A.R.; Giordano, S.; Zelickson, B.R.; Reily, C.; Zou, L.; Chatham, J.C.; Hill, B.G.; Zhang, J.; et al. Assessing bioenergetic function in response to oxidative stress by metabolic profiling. *Free Radic. Biol. Med.* **2011**, *51*, 1621–1635. [CrossRef]
40. Kunji, E.R.S.; Aleksandrova, A.; King, M.S.; Majd, H.; Ashton, V.L.; Cerson, E.; Springett, R.; Kibalchenko, M.; Tavoulari, S.; Crichton, P.G.; et al. The transport mechanism of the mitochondrial ADP/ATP carrier. *Biochim. Biophys. Acta (BBA) Mol. Cell Res.* **2016**, *1863*, 2379–2393. [CrossRef] [PubMed]
41. Lopez-Sánchez, L.M.; Jimenez, C.; Valverde, A.; Hernandez, V.; Peñarando, J.; Martinez, A.; Lopez-Pedrera, C.; Muñoz-Castañeda, J.R.; De la Haba-Rodriguez, J.R.; Aranda, E.; et al. CoCl2, a Mimic of Hypoxia, Induces Formation of Polyploid Giant Cells with Stem Characteristics in Colon Cancer. *PLoS ONE* **2014**, *9*, e99143. [CrossRef] [PubMed]
42. Lazarev, V.F.; Guzhova, I.V.; Margulis, B.A. Glyceraldehyde-3-phosphate Dehydrogenase is a Multifaceted Therapeutic Target. *Pharmaceutics* **2020**, *12*, 416. [CrossRef]
43. Krasnov, G.S.; Dmitriev, A.A.; Snezhkina, A.V.; Kudryavtseva, A.V. Deregulation of glycolysis in cancer: Glyceraldehyde-3-phosphate dehydrogenase as a therapeutic target. *Expert Opin. Ther. Targets* **2013**, *17*, 681–693. [CrossRef]
44. Chiche, J.; Ricci, J.-E.; Pouysségur, J. Tumor hypoxia and metabolism—Towards novel anticancer approaches. *Ann. D'endocrinologie* **2013**, *74*, 111–114. [CrossRef]
45. Martínez-Reyes, I.; Cuezva, J.M. The H(+)-ATP synthase: A gate to ROS-mediated cell death or cell survival. *Biochim. Biophys. Acta* **2014**, *1837*, 1099–1112. [CrossRef]
46. García-Bermúdez, J.; Cuezva, J.M. The ATPase Inhibitory Factor 1 (IF1): A master regulator of energy metabolism and of cell survival. *Biochim. Biophys. Acta (BBA)-Bioenerg.* **2016**, *1857*, 1167–1182. [CrossRef] [PubMed]
47. Sánchez-Cenizo, L.; Formentini, L.; Aldea, M.; Ortega, Á.D.; García-Huerta, P.; Sánchez-Aragó, M.; Cuezva, J.M. Up-regulation of the ATPase Inhibitory Factor 1 (IF1) of the Mitochondrial H+-ATP Synthase in Human Tumors Mediates the Metabolic Shift of Cancer Cells to a Warburg Phenotype. *J. Biol. Chem.* **2010**, *285*, 25308–25313. [CrossRef]
48. Sánchez-Aragó, M.; Formentini, L.; Martínez-Reyes, I.; García-Bermúdez, J.; Santacatterina, F.; Sánchez-Cenizo, L.; Willers, I.M.; Aldea, M.; Nájera, L.; Juarránz, Á.; et al. Expression, regulation and clinical relevance of the ATPase inhibitory factor 1 in human cancers. *Oncogenesis* **2013**, *2*, e46. [CrossRef]
49. Zhao, R.Z.; Jiang, S.; Zhang, L.; Yu, Z.B. Mitochondrial electron transport chain, ROS generation and uncoupling (Review). *Int. J. Mol. Med.* **2019**, *44*, 3–15. [CrossRef] [PubMed]
50. Yerushalmi, B.; Dahl, R.; Devereaux, M.W.; Gumpricht, E.; Sokol, R.J. Bile acid-induced rat hepatocyte apoptosis is inhibited by antioxidants and blockers of the mitochondrial permeability transition. *Hepatology* **2001**, *33*, 616–626. [CrossRef]

51. Tabas, I.; Ron, D. Integrating the mechanisms of apoptosis induced by endoplasmic reticulum stress. *Nat. Cell Biol.* **2011**, *13*, 184–190. [CrossRef]
52. Dröse, S.; Brandt, U. Molecular Mechanisms of Superoxide Production by the Mitochondrial Respiratory Chain. In *Mitochondrial Oxidative Phosphorylation: Nuclear Encoded Genes, Enzyme Regulation, and Pathophysiology*; Kadenbach, B., Ed.; Springer: New York, NY, USA, 2012; pp. 145–169.
53. Zhang, Y.; Wong, H.S. Are mitochondria the main contributor of reactive oxygen species in cells? *J. Exp. Biol.* **2021**, *224*, jeb221606. [CrossRef] [PubMed]
54. Fang, S.; Yu, X.; Ding, H.; Han, J.; Feng, J. Effects of intracellular iron overload on cell death and identification of potent cell death inhibitors. *Biochem. Biophys. Res. Commun.* **2018**, *503*, 297–303. [CrossRef]
55. Manabe, Y.; Miyatake, S.; Takagi, M.; Nakamura, M.; Okeda, A.; Nakano, T.; Hirshman, M.F.; Goodyear, L.J.; Fujii, N.L. Characterization of an Acute Muscle Contraction Model Using Cultured C2C12 Myotubes. *PLoS ONE* **2013**, *7*, e52592. [CrossRef]
56. Wagle, S.R.; Kovacevic, B.; Ionescu, C.M.; Walker, D.; Jones, M.; Carey, L.; Takechi, R.; Mikov, M.; Mooranian, A.; Al-Salami, H. Pharmacological and Biological Study of Microencapsulated Probucol-Secondary Bile Acid in a Diseased Mouse Model. *Pharmaceutics* **2021**, *13*, 1223. [CrossRef]
57. Wagle, S.R.; Kovacevic, B.; Walker, D.; Ionescu, C.M.; Jones, M.; Stojanovic, G.; Kojic, S.; Mooranian, A.; Al-Salami, H. Pharmacological and Advanced Cell Respiration Effects, Enhanced by Toxic Human-Bile Nano-Pharmaceuticals of Probucol Cell-Targeting Formulations. *Pharmaceutics* **2020**, *12*, 708. [CrossRef] [PubMed]
58. Mathavan, S.; Ionescu, C.M.; Kovacevic, B.; Mikov, M.; Golocorbin-Kon, S.; Mooranian, A.; Dass, C.R.; Al-Salami, H. Formulation buoyancy of nanoencapsulated gliclazide using primary, conjugated and deconjugated bile acids. *Ther. Deliv.* **2019**, *10*, 573–583. [CrossRef]
59. Mooranian, A.; Foster, T.; Ionescu, C.M.; Carey, L.; Walker, D.; Jones, M.; Wagle, S.R.; Kovacevic, B.; Chester, J.; Johnstone, E.; et al. The Effects of Primary Unconjugated Bile Acids on Nanoencapsulated Pharmaceutical Formulation of Hydrophilic Drugs: Pharmacological Implications. *Drug Des. Devel. Ther.* **2021**, *15*, 4423–4434. [CrossRef]
60. Li, Q.; Ma, R.; Zhang, M. CoCl2 increases the expression of hypoxic markers HIF-1α, VEGF and CXCR4 in breast cancer MCF-7 cells. *Oncol. Lett.* **2018**, *15*, 1119–1124. [CrossRef]
61. Mooranian, A.; Negrulj, R.; Al-Salami, H.; Morahan, G.; Jamieson, E. Designing anti-diabetic β-cells microcapsules using polystyrenic sulfonate, polyallylamine, and a tertiary bile acid: Morphology, bioenergetics, and cytokine analysis. *Biotechnol. Prog.* **2016**, *32*, 501–509. [CrossRef]
62. Wagle, S.R.; Walker, D.; Kovacevic, B.; Gedawy, A.; Mikov, M.; Golocorbin-Kon, S.; Mooranian, A.; Al-Salami, H. Micro-Nano formulation of bile-gut delivery: Rheological, stability and cell survival, basal and maximum respiration studies. *Sci. Rep.* **2020**, *10*, 7715. [CrossRef] [PubMed]

Publication 3 (pages 54-61):

Kovacevic B, Ionescu CM, Wagle SR, Jones M, Lewkowicz M, Wong EYM, Đanić M, Mikov M, Mooranian A, Al-Salami H. Impact of Novel Teflon-DCA Nanogel Matrix on Cellular Bioactivity. Journal of Pharmaceutical Sciences. 2023;112(3):700-7.

Sub-objective (2): to design and create hydrogels utilising sodium alginate, polytetrafluoroethylene, and various concentrations of deoxycholic acid and to examine the shear stress, viscosity, surface tension, torque, microstructure, and zeta potential of hydrogels. Additionally, the hydrogels were incubated with 3 different cell lines (AML 12, C2C12 and NIT-1). Their impact on viability in normal and hypoxic conditions and their impact on bioenergetic parameters was investigated.

Journal of Pharmaceutical Sciences 112 (2023) 700–709

Contents lists available at ScienceDirect

Journal of Pharmaceutical Sciences

journal homepage: www.jpharmsci.org

Pharmaceutics, Drug Delivery and Pharmaceutical Technology

Impact of Novel Teflon-DCA Nanogel Matrix on Cellular Bioactivity

Bozica Kovacevic[a,b], Corina Mihaela Ionescu[a,b], Susbin Raj Wagle[a,b], Melissa Jones[a,b], Michael Lewkowicz[a,b], Elaine Y.M. Wong[b], Maja Danić[c], Momir Mikov[c], Armin Mooranian[a,b,*], Hani Al-Salami[a,b,*]

[a] The Biotechnology and Drug Development Research Laboratory, Curtin Medical School & Curtin Health Innovation Research Institute, Curtin University, Bentley, Perth, WA 6102, Australia
[b] Hearing Therapeutics Department, Ear Science Institute Australia, Queen Elizabeth II Medical Centre, Nedlands, Perth, WA 6009, Australia
[c] Department of Pharmacology, Toxicology and Clinical Pharmacology, Faculty of Medicine, University of Novi Sad, Novi Sad, 21101, Serbia

ARTICLE INFO

Article history:
Received 16 August 2022
Revised 9 September 2022
Accepted 9 September 2022
Available online 21 September 2022

Keywords:
Bile acid
Deoxycholic acid
Teflon
Biocompatibility
Bioenergetics
Mitochondrial respiration

ABSTRACT

The biocompatibility and effects on cells' bioactivity of developed pharmaceuticals are crucial properties required to permit their safe delivery. Nanogel matrices offer a promising role in emerging pharmaceutics; however, it is crucial that they and their excipients do not demonstrate detrimental effects on the cells to which they interact. This study investigated the use of Teflon and the secondary bile acid deoxycholic acid in the formation of novel nanogel matrices. Each has properties which may be of benefit for the nanogels created and their use in the pharmaceutical industry. Rheological parameters and scanning electron microscopy studies were conducted. In order to assess the developed nanogels' impacts on cellular bioactivity, studies using Seahorse assays were conducted on three cell types, hepatic, muscle and pancreatic beta cells. Results demonstrated the addition of Teflon did not alter the morphological characteristics of resulting nanogels or the metabolic profiles of the cell lines. Interestingly, pancreatic beta cells highlighted the potential of Teflon to exert a protective profile from mitochondrial damage. Overall, the developed nanogels showed potentially promising profiles in certain studies conducted which may lead to future research.

Introduction

Rheological properties of matrices in close contact with tissue are crucial, as they are supposed to promote rather than inhibit inherent biological processes and cellular activity.[1,2] Krajina et al. showed that both fluidisation and stiffening of extracellular matrix (ECM) are necessary for tissue homeostasis, as mechanic cell-matrix interactions favour short-time stiffening and long-time fluidisation.[3] Furthermore, fluid shear induces gene expression via mechanotransduction.[4] Therefore, the nanogel matrix in contact with tissue has to show complex rheological properties associated with tissue growth and functions. Bile acids are one key excipient that can modify the rheological parameters of nanogels.

Bile acids (BA)s have shown to be compelling excipients in biotechnology due to their unique physico-chemistry and biological activity.[5] Mooranian et al. optimised post-transplantation inflammatory and glycaemic profiles of diabetic mice with islet-containing microcapsules. The transplant's high performance was aided by adding primary bile acid to the nanogel matrix.[6] The same group demonstrated improved stability and release profile of metformin encapsulated within the BA supplemented matrix. Mooranian et al. have shown that one bile acid, deoxycholic acid (DCA), displays unique properties in terms of stabilising nanogel matrices while simultaneously modifying fluid dynamics to cater for enhanced flow properties.[7] Therefore, we decided to add the secondary bile acid; DCA, in hopes of enhancing nanogel properties.

DCA is a valuable agent in polymer modification, as it allows for self-assembly behaviour and stable micelles.[8] DCA-modified chitosan is capable of self-assembly into cationic nanoparticles capable of co-delivering gene and anti-tumour compounds.[9] Furthermore, DCA-conjugated nanoparticles effectively increase the bioavailability of poorly water soluble antioxidants.[10] Also, injectable DCA is used in cosmetic surgeries as a minimally invasive, safe and effective treatment for lipolysis of submental fat.[11,12] However, DCA has been shown to induce a proinflammatory response in macrophages dose-dependently.[13] Therefore, DCA concentration in the nanogel matrix needs to be optimised in order to mitigate the less desirable and enhance the beneficial effects on cells. One polymer that has shown

* Corresponding authors.
E-mail addresses: a.mooranian@curtin.edu.au (A. Mooranian), h.al-salami@curtin.edu.au (H. Al-Salami).

https://doi.org/10.1016/j.xphs.2022.09.008
0022-3549/

promise in cellular delivery matrices is Polytetrafluoroethylene (PTFE, Teflon).

PTFE, Teflon is a thermally stable, hydrophobic, biologically inert material with an exceptionally low friction coefficient. Due to its versatile properties, it is used in various industries, from aerospace and automotive to food processing, biomedical and pharmaceutical industries.[14] It is commonly used as a medical implant due to its biocompatibility and inertness, including in facial surgeries, such as angioplasty catheters, joint implants and vocal cord disorders.[15] Modified PTFE may be a promising anti-thrombogenic biomaterial for narrow vascular grafts.[16]

We made novel nanogel matrices from ultra-soluble water gel, sodium alginate, and PTFE, featuring three different DCA concentrations. In order to assess their biocompatibility and effect on cells, we examined the viability of murine muscle, hepatic and pancreatic beta-cell lines after 24h incubation in nanogel presence. To further understand nanogel impact on cell metabolism, we utilised Seahorse mitochondrial stress test and viability after treatment with a hypoxic agent.

Methods

Materials

The water-soluble gel was purchased from the Australian Medical Association (Perth, Australia). Low viscosity sodium alginate (SA, 99%), polytetrafluoromethylene (PTFE, Teflon,) and deoxycholic acid (DCA, 99%) were purchased from Sigma Chemical Co (St. Louis, MO, USA). Dulbecco's modified Eagle's medium (DMEM), foetal bovine serum (FBS) and other required supplements were purchased from Sigma Chemical Co (St. Louis, MO, USA). The NIT-1 pancreatic β-cells were a generous donation from Professor Grant Morahan at the University of Western Australia. AML-12 (ATCC®, CRL-2254™) and C2C12 (ATCC®, CRL-1772™) cell lines were purchased from a commercial vendor, American Type Culture Collection (ATCC).

Methods

Nanogels were prepared based on Table 1. Water-soluble gel, SA, PTFE and DCA were added in appropriate amounts and dissolved in deionised water by constant mixing at room temperature overnight. Created nanogel were than stored in fridge and used within 24h.

Scanning electron microscope (SEM) micrographs were obtained from freeze-dried and platinum-coated nanogel samples using Zeiss Neon 40EsB FIBSEM, Carl Zeiss Microscopy GmbH, Jena, Germany. Freeze drying was carried out for 48h using Dynavac FD3 Freeze Dryer (Dynapumps, Seven Hills, Australia).

Rheological parameters were obtained from freshly made formulations using a Visco-88 viscometer (Malvern Instruments, Malvern, UK) for viscosity, shear stress, shear rate and torque. Aliquots of formulations were placed in instrument cap and results for above mentioned parameters were obtain at 8 different rotational speeds available on the viscometer. A tensiometer (Sigma 703) was used for the determination of surface tension by placing 5 ml of nanogels in instrument, utilizing du Nouy ring method. Zeta potential was measured using 3000HS Zetasizer (Malvern, UK) by putting samples in glass cuvette with square aperture. On the adjacent software, standard operation procedure was designed with 25 runs per measurement. All measuring processes were executed at room temperature, following established protocols,[17–23] All obtained data were in triplicates ($n = 3$).

C2C12 myoblast cell line was cultured in DMEM supplemented with 10% FBS and 1% penicillin-streptomycin. The media was changed every 24h. AML12 hepatocytes were cultured in DMEM supplemented with 10% FBS and 1% penicillin-streptomycin, with media change every 48h. NIT-1, pancreatic beta-cell murine line, was cultured in DMEM supplemented with 10% FBS, 5.5 mmol glucose and 1% penicillin-streptomycin. The media was changed every 48h.

Freshly made nanogel matrices were added to 96-well plates, 20 μl per well, and left for 30 min under UV light in sterile conditions before any further procedure. Freshly detached cells were counted and added to nanogels, followed by viability, hypoxia, and Seahorse assays. Cell count for each cell line was 6×10^4 cells per well. A viability assay was conducted with MTT (2,5-diphenyl-2,4,5-trimethylthiazol-2-yl) after 24h incubation with nanogels, as per established protocol.[18,21–27] Cells were mixed with appropriate media with 50 μM (lower hypoxia) or 100 μM (higher hypoxia) of CoCl2, and then added to the nanogels. After 24h incubation, viability was assessed by following an MTT assay. Data was normalised, and the viability of control cells without nanogel was presented as 100%. Cellular bioenergetics was assessed by Seahorse XF Cell Mito Stress Test using Seahorse Flux Analyser XF 96 (Seahorse Bioscience, USA), per established in-house developed protocol.[17,28–31] All obtained data was in triplicates ($n = 3$).

Statistical analysis was done by GraphPad Prism version 9.3 (Graphpad, Inc., USA). One-way ANOVA, two-way ANOVA, regression analysis, and Tukey HSD were utilised appropriate of data. All data is shown as mean ± SEM, with statistical significance defined as $p < 0.01$ (*) and $p < 0.05$ (**).

Results

Shear stress and torque curves follow a similar pattern, as shown in Fig. 1a and b. All samples show an initial dip at a low shear rate, with a gradual increase in shear rate afterwards. At the highest shear rate, for both shear stress and torque, the PTFE-free formulation has the highest value (F1), while F3 plateaus after the initial dip and shows the lowest values. All formulations have similar viscosity behaviour, with a non-linear decrease in viscosity in response to increased shear rate (Fig. 1c). Surface tension is the lowest in F5, a formulation with the highest DCA concentration. This contrasts with F3 and F4, which are significantly higher than DCA-free formulations (F1 and F2) (Fig. 1d).

Cells exposed to nanogel matrices had a different pattern of viability (Fig. 2). AML 12 cell line had consistently significantly lowered viability in the presence of nanogels, with the lowest viability observed with F2 and F5 (Fig. 2a). Unlike the previous viability pattern, C2C12 did not show a reduction in viability in the presence of

Table 1
Components of nanogel matrices.

Code	Water-soluble Gel (% w/w)	SA (% w/w)	PTFE (% w/w)	DCA (% w/w)
F1	6	1.4	0	0
F2	6	1.4	0.1	0
F3	6	1.4	0.1	2
F4	6	1.4	0.1	3.8
F5	6	1.4	0.1	4

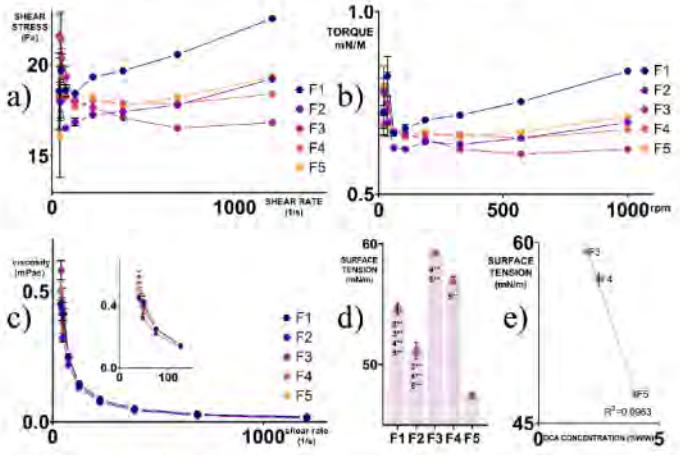

Figure 1. Rheological properties of formulations F1-F5, showing values for a) shear rate, b) torque, c) viscosity, d) surface tension, and e) zeta potential. One-way ANOVA, two-way ANOVA, regression analysis, and Tukey HSD were utilised appropriate of data. All data is shown as mean ± SEM, with statistical significance defined as $p < 0.01$ (*) and $p < 0.05$ (**).

DCA-free nanogels compared to the nanogel-free control C (Fig. 2b). However, the addition of DCA to nanogel matrix (F3, F4, and F5) significantly lowered the viability of muscle cells compared to DCA-free nanogels (F1 and F2) and nanogel-free control (C) (Fig. 2b). NIT-1 cells have an opposite viability pattern (Fig. 2c). The highest viability is observed in the presence of the highest DCA concentration (F5), while all formulations containing PTFE (F2) and PTFE and DCA (F3, F4 and F5) showed a significant increase in viability compared to nanogel-free control (C), and PTFE and DCA-free formulation (F1) (Fig. 2c).

When treated with a hypoxia-inducing agent, $CoCl_2$, control cells of hepatic and pancreatic cell lines show a lowering of viability in hypoxic conditions, except for muscle cells (Fig. 3). Uniform behaviour under hypoxic stress is observed for all cell lines within F5 nanogel, where the addition of a hypoxic agent does not significantly alter viability. AML-12 cells within F1, F2, and F3 show similar viability patterns, with increased viability under low hypoxia (Fig. 3a). However, with F4, this effect is seen in high hypoxic conditions rather than in lower hypoxic ones (Fig. 3a). Murine muscle cell line, C2C12, has a similar behaviour within the first two formulations (F1 and F2), with the exception that viability is the highest in higher hypoxia. In F3 and F4, normoxia outperforms hypoxia (Fig. 3b). The NIT-1 cell line does not have uniform viability patterns (Fig. 3c).

Unlike viability patterns, all cell lines show similar behaviours in terms of metabolism (Fig. 4a, Fig. 4d, and Fig. 4g). Nanogel-free cells (C) show aerobic metabolism, with a low extracellular acidification rate (ECAR) for all cell types. All cell types within F1 and F2 have similar aerobic metabolism, which favours oxygen consumption rate (OCR) over ECAR. Cells exposed to formulations with DCA (F3, F4, and F5) show a metabolic shift to anaerobic metabolism, with increased ECAR (Fig. 4a, d, and g). An increase in ECAR is significantly higher than in control cells, F1 and F2 in most cell lines, as presented in Fig. 4b, e, and h. A linear relationship between ECAR in normal conditions and viability in normoxia and different hypoxic conditions are calculated in Fig. 4c for AML 12 cell line, Fig. 4f for C2C12 and Fig. 4i for NIT-1 cells. Higher ECAR in normal conditions may predict a smaller decrease in low hypoxia for AML 12, but there is no relationship with viability in higher hypoxia or normoxia (Fig. 4c). Higher ECAR in normoxia is connected with lowered viability in all

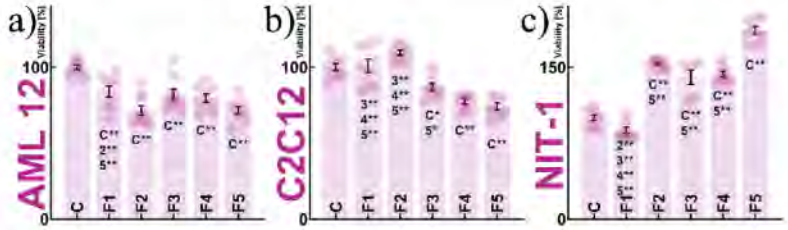

Figure 2. Results of viability assay for a) AML 12 cell line, b) C2C12 cell line, and c) NIT-1 cell line. One-way ANOVA, two-way ANOVA, and Tukey HSD were utilised appropriate of data. All data is shown as mean ± SEM, with statistical significance defined as $p < 0.01$ (*) and $p < 0.05$ (**).

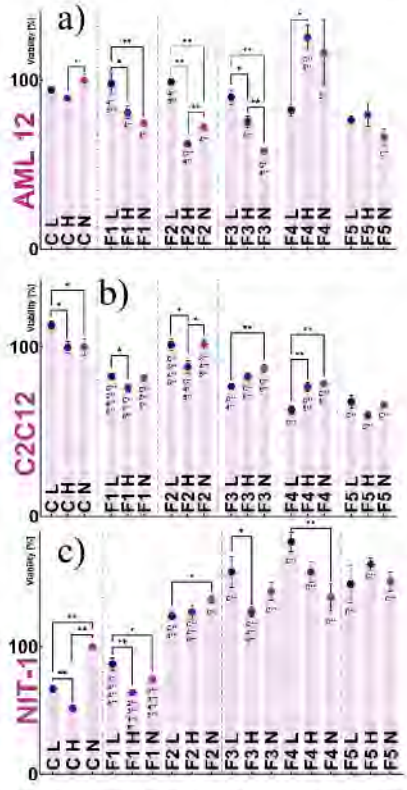

Figure 3. Results of viability values in different hypoxic conditions for a) AML 12; b) C2C12, and c) NIT-1. Hypoxic conditions are: N-normoxia, L-low hypoxia, H-high hypoxia. One-way ANOVA, two-way ANOVA, and Tukey HSD were utilised appropriate of data. All data is shown as mean ± SEM, with statistical significance defined as $p < 0.01$ (*) and $p < 0.05$ (**).

conditions for muscle cells (Fig. 4f). For NIT-1 cells, however, an increase in ECAR in normal conditions can result in an increase in viability under hypoxic conditions (Fig. 4i).

Cellular bioenergetics for AML-12 cells does not show a significant difference in ATP-production linked OCR for most formulations (Fig. 5a). Formulation F2 seems to be an exception, with decreased ATP production compared to nanogels with added DCA (F3 and F4). Spare capacity was the highest for the same cells within F1 (Fig. 5b), while proton leak was prominent for F2 and F3 (Fig. 5c). Non-mitochondrial oxygen production was increased for all formulations compared to nanogel-free control, with the exception of F4 (Fig. 5d). DCA enriched formulations (F3 and F4) showed a decrease in non-mitochondrial oxygen consumption compared to DCA-free formulations (F1 and F2) (Fig. 5d). In C2C12 cell line, DCA-free formulations (F1 and F2) have increased ATP production compared to nanogel-free control and DCA nanogels (F3 and F5) (Fig. 5e). A similar pattern is observed with non-mitochondrial oxygen consumption, with F1 and F2 showing a significant increase compared to nanogel-free control and DCA-nanogels (Fig. 5h). Spare capacity-linked OCR is not prominent in muscle cell line (Fig. 5f). Proton leak-linked OCR does not differ significantly among most groups, showing only an increase of F1 over F3 and F4 (Fig. 5g). NIT-1 cell line has a comparable pattern for most bioenergetic parameters. DCA-free formulations (F1 and F2) are significantly higher compared to nanogel-free control and DCA enriched nanogels (F3, F4, and F5) for ATP-production linked OCR (Fig. 5i), proton leak-linked OCR (Fig. 5k), and non-mitochondrial oxygen consumption (Fig. 5l). Spare capacity-linked OCR was not prominent for this cell line either (Fig. 5j).

The surface morphology of freeze-dried nanogels is shown in Fig. 6. All formulations show similar surface morphology, with an irregular, rough and cracking surface.

Discussion

The rheological properties demonstrate that all formulations have similar behaviour to non-Newtonian fluids, exhibiting pseudo-plastic and shear-thinning properties (Fig. 1). The addition of bile acid did not alter fluid behaviour, which is concurrent with a study by Wagle et al.[18, 28] Retained shear thinning characteristics are crucial for injectable delivery systems, as lower viscosity under high shear has a beneficial effect on cell viability.[32] PTFE addition to nanogel (F2) significantly lowered surface tension compared to the non-PTFE formulation (F1) (Fig. 1d), probably due to PTFE's hydrophobicity and low surface energy.[18] Surface tension (Fig. 1d) increased with the addition of DCA (F3), but surface tension seemed to decrease with an increase in DCA concentration, as there was a significant decrease in surface tension at the highest DCA concentration within the nanogel matrix (Fig. 1d, F5). A reduction in pH with the addition of DCA in the polymer matrix may be responsible for the increase in surface tension in F3 and F4 compared to F1 and F2, as alginate tends to increase hydrogen bonding with pH decrease.[33] This is also observed in viscosity values, as the highest viscosity under low shear is with F3 and F4 (Fig. 1c). However, a further increase in DCA concentration (F5) leads to a decrease in surface tension compared to F1 and F2 (Fig. 1d). An interaction between alginate and DCA may explain this. DCA can form dynamic micellar structures as an unconventional surfactant with a rigid steroid nucleus.[34,35]

Furthermore, it is established that micelles interact with polymers in aqueous solutions and lead to a reduction of surface tension.[36] However, this effect is most prominent after polymer saturation point (PSP), which describes surfactant concentrations needed to saturate polymer chains with bound micelles or surfactant molecules fully. An increase in surfactant concentrations leads to unbound micelles capable of interacting with surface area and lowering surface tension.[37] This effect may explain the linear relationship between the decrease in surface tension and the increase in DCA concentration within nanogels (Fig. 1e).

Rheological properties, mainly surface tension and viscosity of nanogel matrices, had a limited effect on cellular viability and bioenergetic parameters (Fig. 7). A positive linear relationship can be seen only for hepatic cell lines. Based on data obtained in previous assays, it seems that a slight increase in surface tension is correlated with an increase in ATP production and viability, but only for the AML 12 cell line. C2C12 and NIT-1 cell lines do not show an apparent relationship between surface tension and viability, as well as ATP production (Fig. 7a and b). An increase in viscosity, however, may affect both hepatic and pancreatic cell lines (Fig. 7c). Those two cell lines have a positive correlation between viscosity and cellular ECAR. Viscosity is a significant mechanical signal for cellular differentiation, migration and substrate mechanotransduction.[38,39] As the increased viscosity of nanogel may alter and/or decrease the flow of nutrients and oxygen to cells, cells may rely more on anaerobic metabolism (Fig. 7c).

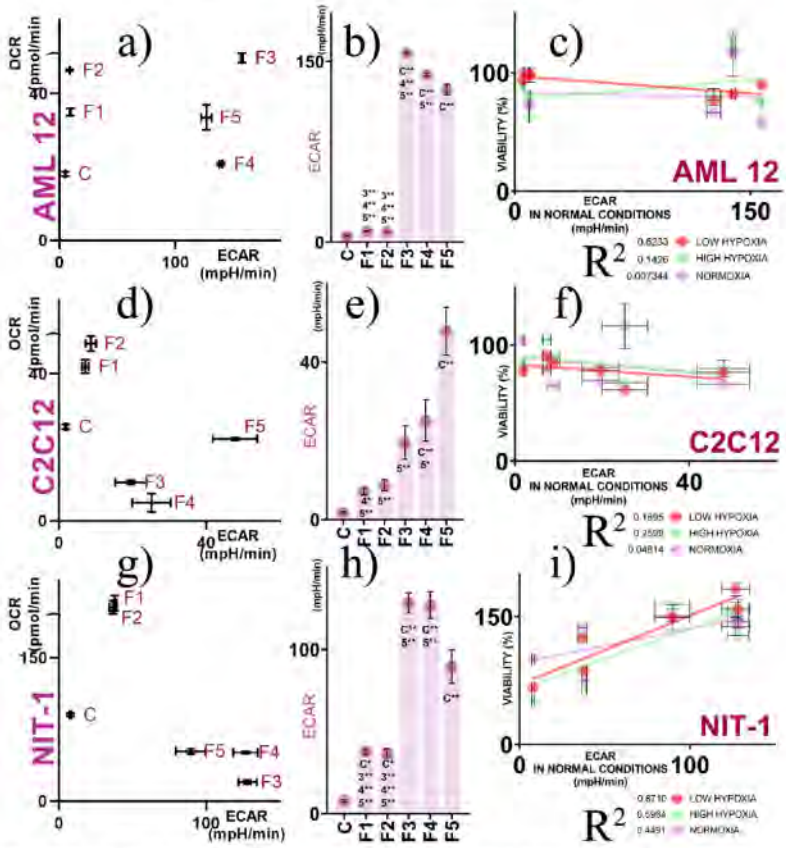

Figure 4. Metabolic profile of a) AML 12, d) C2C12, g) NIT-1 cells in normal conditions, with ECAR values in same environment for b) AML-12, e) C2C12, h) NIT-1. The relationship between ECAR in normal conditions and survival of cells in different hypoxic conditions is presented for c) AML-12, f) C2C12, and i) NIT-1. One-way ANOVA, two-way ANOVA, regression analysis, and Tukey HSD were utilised appropriate of data. All data is shown as mean ± SEM, with statistical significance defined as $p < 0.01$(*) and $p < 0.05$ (**).

The highest concentration of DCA (F5) lowered the viability of hepatocytes compared to DCA-free nanogel (F1) (Fig. 2a). DCA also negatively affected the viability of C2C12 (F3, F4, F5) compared to DCA-free nanogels (F1 and F2) (Fig. 2b). This may be linked with TGR5, a BA-responsive membrane receptor expressed universally in human and murine tissue.[40] TGR5 activation in hepatocytes modulates apoptosis.[41,42] BAs' effect on the cells may be concentration-dependent, with higher concentrations leading to additional cellular damage.[43] This may explain the lower viability of hepatocytes under F5 compared to DCA and PTFE-free nanogel (F1) (Fig. 2b). Abrigo et al. showed that TGR5 activation by DCA has a deleterious impact on muscle tissue,[44] adding to the low viability of C2C12 cells in the presence of F3, F4 and F5 (Fig. 2b). TGR5 activation in pancreatic beta cells leads to increased cAMP and Ca^{2+}, leading to insulin secretion.[45] However, improved viability of NIT-1 cells is present with F2, not just F3, F4 and F5, so it may suggest that PTFE, rather than DCA, is responsible for high viability (Fig. 2c).

High concentrations of DCA show similar effects to hypoxia, as presented within F5 nanogel for all cell lines under hypoxic conditions (Fig. 3). This is further supported by bioenergetic parameters presented in Figs. 4 and 5. Formulations with DCA (F3, F4 and F5) increased ECAR, i.e. level of substrate phosphorylation by glycolysis (Fig. 4) for all cell lines.[46] This is linked with decreased total OCR and ATP production-linked OCR for C2C12 and NIT-1 (Fig. 5e and i). Hepatocytes may preserve ATP production (Fig. 5a) due to the rapid metabolisation of DCA to less toxic glycodeoxycholic acid.[47] The shift to glycolytic metabolism in the presence of DCA is consistent with a previous study by Kovacevic et al.[17] This effect may be linked with DCA perturbation to the outer mitochondrial membrane, leading to altered metabolism, favouring glycolysis to oxidative

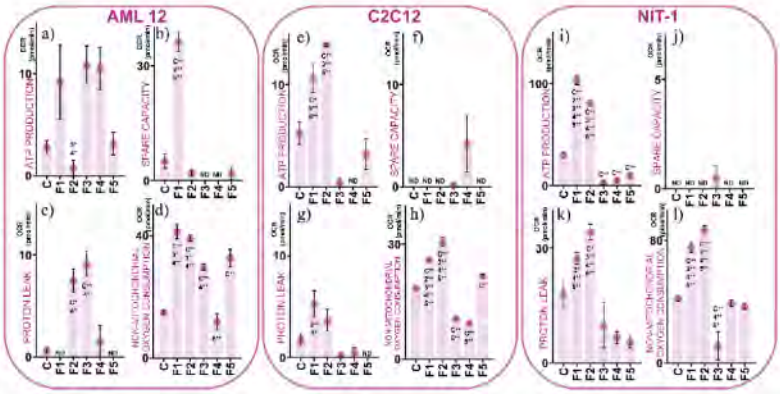

Figure 5. Cellular bioenergetics for AML-12 showing a) ATP-production linked OCR, b) spare capacity linked OCR, c) proton leak linked OCR, and d) non-mitochondrial oxygen consumption. Cellular bioenergetics for C2C12 showing e) ATP-production linked OCR, f) spare capacity linked OCR, g) proton leak linked OCR, and h) non-mitochondrial oxygen consumption. Cellular bioenergetics for NIT-1 showing i) ATP-production linked OCR, j) spare capacity linked OCR, k) proton leak linked OCR, and l) non-mitochondrial oxygen consumption. One-way ANOVA, two-way ANOVA, and Tukey HSD were utilised appropriate of data. All data is shown as mean ± SEM, with statistical significance defined as $p < 0.01$(*) and $p < 0.05$ (**).

phosphorylation.[43] However, glycolytic metabolism seems efficient enough to protect NIT-1 cells from hypoxia-induced decreased viability, as higher ECAR in normal conditions positively correlates to higher viability in mild hypoxia (Fig. 4i). This is not the case with AML12 and C2C12 cells (Fig. 4c and i). The addition of PTFE (F2) does not majorly alter the metabolic profile or viability of either cell line, compared to PTFE-free F1 (Fig. 4), except with NIT-1 cells (Figs. 2c and 3c). The addition of PTFE seems to have a protective effect on pancreatic cells in hypoxic conditions, as viability is increased in all environments compared to PTFE-free F1 and nanogel-free control (Fig. 3c). The exact mechanism is yet to be elucidated.

Conclusion

This study investigated the use of Teflon and the secondary bile acid in the formation of novel nanogels. Results showed that the addition of PTFE lowered surface tension of nanogels, but it did not change the morphological properties of freeze dried nanogel products. PTFE did not alter the metabolic profiles of the examined cell lines, being hepatic, muscle and pancreatic beta cells. Furthermore, it has been demonstrated by this study that PTFE may exert protective effect against mitochondrial damage in pancreatic beta cells. Hence, the addition of PTFE and bile acids in the development of nanogels

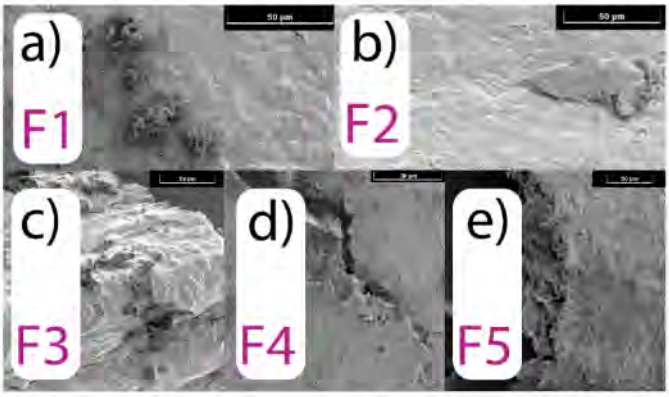

Figure 6. Surface morphology of freeze-dried nanogels, shown by SEM images. Formulations showed are a) A1, b) A2, c) A3, d) A4 and e) A5.

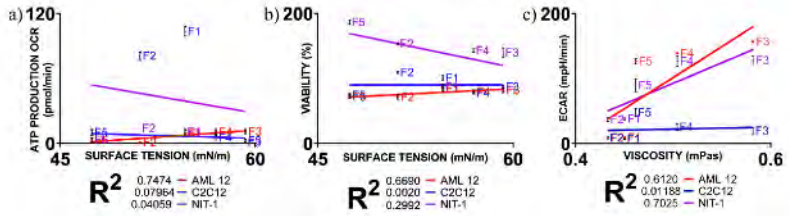

Figure 7. Linear correlations between a) surface tension and ATP production linked OCR of all three cell lines, b) surface tension and viability of all three cell lines, and c) viscosity and ECAR of all three cell lines.

may have beneficial properties and indicate their potential for future research.

Disclaimer

The work is partially supported by the European Union Horizon 2020 research project and in-novation program under the Marie Skłodowska-Curie Grant Agreement No 872370. Curtin Faculty ORS-WAHAI Consortium and the Australian National Health and Medical Research (APP9000597).

The author would like to thank Alex Moore for their contribution to this paper. The authors would like to acknowledge the Australian Postgraduate Award (APA) and Curtin Research Scholarship (CRS). The authors also acknowledge the Microscopy and Microanalysis Facility at Curtin University.

Hani Al-Salami reports financial support was provided by Australian National Health and Medical Research.

Availability of Data and Materials

The datasets generated and/or analysed during the current study are not publicly available, but are available from the corresponding author on reasonable request.

Declaration of Interests

The authors declare the following financial interests/personal relationships which may be considered as potential competing interests:

Hani Al-Salami reports financial support was provided by Australian National Health and Medical Research.

Reference

1. Caliari SR, Burdick JA. A practical guide to hydrogels for cell culture. *Nat Methods*. 2016;13(5):405–414.
2. Davidson MD, Prendergast ME, Ban E, et al. Programmable and contractile materials through cell encapsulation in fibrous hydrogel assemblies. *Sci Adv*. 2021;7(46):eabi8157.
3. Krajina BA, LeSavage BL, Roth JG, et al. Microrheology reveals simultaneous cell-mediated matrix stiffening and fluidization that underlie breast cancer invasion. *Sci Adv*. 2021;7(8):eabc1969.
4. Corrigan MA, Johnson GP, Stavenschi E, Riffault M, Labour M-N, Hoey DA. TRPV4 mediates oscillatory fluid shear mechanotransduction in mesenchymal stem cells in part via the primary cilium. *Sci Rep*. 2018;8(1):3824.
5. Kovacevic B, Jones M, Ionescu C, et al. The emerging role of bile acids as critical components in nanotechnology and bioengineering: Pharmacology, formulation optimizers and hydrogel-biomaterial applications. *Biomaterials*. 2022:121459.
6. Mooranian A, Ionescu CM, Wagle SR, et al. Polyelectrolytes formulated with primary unconjugated bile acid optimised pharmacology of bio-engineered implant. *Pharmaceutics*. 2021;13(10):1713.
7. Mooranian A, Foster T, Ionescu CM, et al. The effects of primary unconjugated bile acids on nanoencapsulated pharmaceutical formulation of hydrophilic drugs: pharmacological implications. *Drug Des Devel Ther*. 2021;15:4423–4434.
8. Yue L, Liu C, Li K, Deng L, Li J. Structure and properties of corn starch synthesized by using sulfobetaine and deoxycholic acid. *Int J Biol Macromol*. 2021;183:1293–1301.
9. Chen S, Deng J, Zhang L. M. Cationic nanoparticles self-assembled from amphiphilic chitosan derivatives containing poly(amidoamine) dendrons and deoxycholic acid as a vector for co-delivery of doxorubicin and gene. *Carbohydr Polym*. 2021;258:117706.
10. Yao W, Xu Z, Sun J, Liu J, Wei Y, Zou J. Deoxycholic acid-functionalised nanoparticles for oral delivery of rbein. *Eur J Pharm Sci*. 2021;159:105713.
11. Liu C, Li MR, Alster TS. Alternative cosmetic and medical applications of injectable deoxycholic acid: a systematic review. *Dermatol Surg*. 2021;47(11):1466–1472.
12. Cunha KS, Lima F, Cardoso RM. Efficacy and safety of injectable deoxycholic acid for submental fat reduction: a systematic review and meta-analysis of randomized controlled trials. *Expert Rev Clin Pharmacol*. 202.;14(3):383–397.
13. Yan F, Yan N, Wang H, et al. FXR-Deoxycholic acid TNF-α axis modulates acetaminophen-induced hepatotoxicity. *Toxicol Sci*. 2021;181(2):273–284.
14. Dhanumalayan E, Joshi GM. Performance properties and applications of polytetrafluoroethylene (PTFE)—a review. *Adv Compos Hybrid Mater*. 2018;1(2):247–268.
15. Reina Y, Auber F, Hocquet D, Herlem G. ePTFE functionalization for medical applications. *Mater Today Chem*. 2021;20:100412.
16. Yu C, Yang H, Wang L, Thomson JA, Turng L-S, Guan G. Surface modification of polytetrafluoroethylene (PTFE) with a heparin-immobilized extracellular matrix (ECM) coating for small diameter vascular grafts applications. *Mater Sci Eng*. 2021;128:112301.
17. Kovacevic B, Ionescu CM, Jones M, et al. The effect of deoxycholic acid on chitosan-enabled matrices for tissue scaffolding and injectable nanogels. *Gels*. 2022;8(6):358.
18. Jones M, Ionescu CM, Walker D, et al. Biguanide pharmaceutical formulations and the applications of bile acid–based nano delivery in chronic medical conditions. *Int J Mol Sci*. 2022;23(2).
19. Wagle SR, Kovacevic B, Ionescu CM, et al. Pharmacological and biological study of microencapsulated probucol-secondary bile acid in a diseased mouse model. *Pharmaceutics*. 2021;13(8).
20. Teofilovic B, Golocorbin-Kon S, Stilinovic N, et al. Pharmacological effects of novel microvesicles of basil on blood glucose and the lipid profile: a preclinical study. *Sci Rep*. 2021;11(1).
21. Mooranian A, Jones M, Ionescu CM, et al. Advancements in assessments of bio-tissue engineering and viable cell delivery matrices using bile acid-based pharmacological biotechnologies. *Nanomaterials*. 2021;11(7).
22. Mooranian A, Jones M, Ionescu CM, et al. Artificial cell encapsulation for biomaterials and tissue bio-nanoengineering: History, achievements, limitations, and future work for potential clinical applications and transplantation. *J Funct Biomater*. 2021;12(4).
23. Mooranian A, Ionescu CM, Wagle SR, et al. Chenodeoxycholic acid pharmacology in biotechnology and transplantable pharmaceutical applications for tissue delivery: an acute preclinical study. *Cells*. 2021;10(9).
24. Wagle SR, Walker D, Kovacevic B, et al. Micro-Nano formulation of bile gut delivery: rheological, stability and cell survival, basal and maximum respiration studies. *Sci Rep*. 2020;10(1):7715.
25. Mooranian A, Ionescu CM, Wagle SR, et al. Polyelectrolytes formulated with primary unconjugated bile acid optimised pharmacology of bio-engineered implant. *Pharmaceutics*. 2021;13(10).
26. Majumbi M, Brouk E, Galettis P, et al. Sodium alginate microencapsulation improves the short-term oral bioavailability of cannabidiol when administered with deoxycholic acid. *PLoS One*. 2021;16(6 June).
27. Carey L, Walker D, Jones M, et al. Bile acid permeation enhancement for inner ear cochlear drug pharmacological uptake: Bio-nanotechnologies in chemotherapy-induced hearing loss. *Nanomedicine*. 2021;12(12):807–819.

28. Mooranian A, Jones M, Ionescu CM, et al. Advancements in assessments of bio-tissue engineering and viable cell delivery matrices using bile acid-based pharmacological biotechnologies. *Nanomaterials*. 2021;11(7):1861.
29. Wagle SR, Kovacevic B, Ionescu CM, et al. Pharmacological and biological study of microencapsulated probucol-secondary bile acid in a diseased mouse model. *Pharmaceutics*. 2021;13(8):1223.
30. Mooranian A, Foster T, Ionescu CM, et al. Enhanced bilosomal properties resulted in optimum pharmacological effects by increased acidification pathways. *Pharmaceutics*. 2021;13(8).
31. Wagle SR, Kovacevic B, Walker D, et al. Pharmacological and advanced cell respiration effects, enhanced by toxic human-bile nano-pharmaceuticals of probucol cell-targeting formulations. *Pharmaceutics*. 2020;12(8):1–17.
32. Loebel C, Rodell CB, Chen MH, Burdick JA. Shear-thinning and self-healing hydrogels as injectable therapeutics and for 3D-printing. *Nat Protoc*. 2017;12(8):1521–1541.
33. Lee KY, Mooney DJ. Alginate: properties and biomedical applications. *Prog Polym Sci*. 2012;37(1):106–126.
34. Madenci D, Egelhaaf SU. Self-assembly in aqueous bile salt solutions. *Curr Opin Colloid Interface Sci*. 2010;15(2):109–115.
35. Mooranian A, Negrulj R, Al-Salami H. Alginate-deoxycholic acid interaction and its impact on pancreatic B-cells and insulin secretion and potential treatment of type 1 diabetes. *J Pharm Innov*. 2016;11(2):156–166.
36. Phan CM, Yusa S I, Honda T, Sharker KK, Hyde AE, Nguyen CV. Micelle and surface tension of double-chain cationic surfactants. *ACS Omega*. 2018;3(9):10907–10911.
37. Yang J, Pal R. Investigation of surfactant-polymer interactions using rheology and surface tension measurements. *Polymers*. 2020;12(10):2302.
38. Gonzalez-Molina J, Zhang X, Borghesan M, et al. Extracellular fluid viscosity enhances liver cancer cell mechanosensing and migration. *Biomaterials*. 2018;177:113–124.
39. Lee K, Chen Y, Li X, Kawazoe N, Yang Y, Chen G. Influence of viscosity on chondrogenic differentiation of mesenchymal stem cells during 3D culture in viscous gelatin solution embedded hydrogels. *J Mater Sci Technol*. 2021;63:1–8.
40. Keitel V, Stindt J, Häussinger D. Bile acid-activated receptors: GPBAR1 (TGR5) and other G protein-coupled receptors. In: Fiorucci S, Distrutti E, eds. *Bile Acids and Their Receptors*. Cham: Springer International Publishing; 2019:19–49.
41. Yang JI, Yoon J-E, Myung SJ, et al. Bile acid-induced TGR5-dependent c-Jun-N terminal kinase activation leads to enhanced caspase 8 activation in hepatocytes. *Biochem Biophys Res Commun*. 2007;361(1):156–161.
42. Holter MM, Chirikjian MK, Briere DA, et al. Compound 18 improves glucose tolerance in a hepatocyte TGR5-dependent manner in mice. *Nutrients*. 2020;12(7):2124.
43. Marques de Sousa TP, Castro R, Pinto S, et al. Deoxycholic acid modulates cell death signaling through changes in mitochondrial membrane properties. *J Lipid Res*. 2015;56.
44. Abrigo J, Gonzalez F, Aguirre F, et al. Cholic acid and deoxycholic acid induce skeletal muscle atrophy through a mechanism dependent on TGR5 receptor. *J Cell Physiol*. 2021;236(1):260–272.
45. Kumar DP, Rajagopal S, Mahavadi S, et al. Activation of transmembrane bile acid receptor TGR5 stimulates insulin secretion in pancreatic β cells. *Biochem Biophys Res Commun*. 2012;427(3):600–605.
46. Schmidt CA, Fisher-Wellman KH, Neufer PD. From OCR and ECAR to energy: perspectives on the design and interpretation of bioenergetics studies. *J Biol Chem*. 2021;297(4).
47. Oizumi K, Sekine S, Fukagai M, Susukida T, Ito K. Identification of bile acids responsible for inhibiting the bile salt export pump, leading to bile acid accumulation and cell toxicity in rat hepatocytes. *J Pharm Sci*. 2017;106(9):2412–2419.

Publication 4 (pages 63-85):

Kovacevic B, Ionescu CM, Jones M, Wagle SR, Foster T, Lewkowicz M, Wong EYM, Đanić M, Mikov M, Mooranian A, Al-Salami H. Novel polysaccharides–bile acid–cyclodextrin gel systems and effects on cellular viability and bioenergetic parameters. Therapeutic Delivery. 2024;15(2):119-34.

Sub-objective (3): to design and create hydrogels utilising sodium alginate, pectin, and various concentrations of deoxycholic acid and beta-cyclodextrin, and to examine the shear stress, viscosity, surface tension, torque, microstructure, and zeta potential of hydrogels. Additionally, the hydrogels were incubated with 3 different cell lines (AML 12, C2C12 and NIT-1). Their impact on viability in normal and hypoxic conditions and their impact on bioenergetic parameters was investigated.

Novel bile acid-cyclodextrin gel systems and effects on cellular oxidative phosphorylation and electron transport chain

Journal:	*Therapeutic Delivery*
Manuscript ID	TDE-2023-0063
Manuscript Type:	Research Article
Keywords:	bile acid, beta cyclodextrin, pectin, deoxycholic acid, mitochondrial respiration

Abstract

The novel hydrogel systems made from sodium alginate, pectin, beta-cyclodextrin and deoxycholic acid (DCA) were proposed as potential drug delivery matrices. To ensure biocompatibility, rheological parameters were examined, as well as hydrogels' effects on bioenergetic parameters and cellular viability on murine hepatic, and muscle and pancreatic beta cells. All hydrogels show non-Newtonian, shear thinning behaviour. Cells displayed various oxygen-dependent viability patterns, with the bile acid overall adversely affecting their biological activities. All cells performed best under normoxia, with pancreatic beta cells displaying the most profound oxygen-dependant viability behaviour. The addition of a moderate concentration of beta-cyclodextrin to the polymer matrix was tolerated by the cells.

Introduction

The extracellular matrix (ECM) can be described as a hydrated biopolymer network encasing cells in tissues. It is in dynamic equilibrium, constantly modifying and being modified by surrounding cells (1, 2). Furthermore, the viscoelastic properties of the ECM are important in modulating intracellular morphology and influencing cellular behaviour (3). ECM rheology describes strain-stress relations on a macroscopic scale. These are influenced mainly by the ECM fibre network consisting of proteins, collagen, elastin and fibronectin. Each has different rheological properties, adding to the complex ECM rheology required to support tissues in all homeostatic and healthy stages (1). Therefore, we hypothesised that in creating novel hydrogels that may be in direct contact with tissue, several polymer components should be included to achieve satisfactory hydrogel properties. The main components of this novel hydrogel system include sodium alginate, pectin, beta-cyclodextrin and deoxycholic acid.

Sodium alginate (SA) is a natural polysaccharide-based biopolymer investigated for various medical applications. Bahadoran et al. used SA as a component of a hydrogel-based scaffold for tissue regeneration and wound healing (4). Furthermore, Zhu et al. used SA to alleviate the side effects of bioactive glass implantation and promote soft tissue regeneration and immune response modulation (5). Lv et al. used SA as an injectable delivery system for the treatment of myocardial infarction (6), while Wagle et al. used SA as an oral delivery system for a lipophilic drug with low bioavailability in the treatment of diabetes (7). Similar to alginate, pectin is also a natural, polysaccharide-based biopolymer used in myriad applications and is compatible with a wide range of other polymers (8). Goel et al. used pectin as part of hydrogel to promote tissue integration of bioactive glass (9). Ghorbani et al. developed a complex polysaccharide-based injectable gel for tissue engineering using pectin (10). Furthermore, Morello et al. used pectin-based hydrogel as an artificial ECM to promote the growth of the spheroid tumour model (11). The versatility of applications in biomedical research illustrates good biocompatibility and favourable viscoelastic properties of alginate and pectin.

Beta-cyclodextrin (BCD) consists of seven glucose units arranged in a cyclical structure. Unlike pectin and SA, which share similar anionic properties and gelation mechanisms (12). BCD has a distinct polarisation structure between the hydrophilic exterior surface and hydrophobic interior cavity (13). It is widely used in the pharmaceutical industry as an important excipient to improve the solubilisation and stability of drugs (14). It is an important excipient for producing novel drug delivery systems, such as nanoparticles and nanogels (15, 16).

Deoxycholic acid (DCA) is a secondary bile acid naturally occurring in humans. Adding bile acids to the alginate polymer matrix results in decreased surface charge, increased mechanical stability and reduced matrix erosion (17). DCA is extensively used in cosmetic surgeries (18) and the pharmaceutical industry for the synthesis of novel anti-cancer molecules (19), oral nanocomplexes (20), and self-assembling nanoparticles for gene transfection (21). However, DCA may contribute to an inflammatory response and thus may act as a pro-inflammatory bile acid (22, 23); therefore, formulation optimisation is key in minimising DCA-potential adverse effects and inflammation.

To better understand the cytotoxicity of hydrogels, we examined mitochondrial parameters of three different cell lines, including murine liver, muscle and pancreatic beta cells. Furthermore, cellular viability was assessed after 24 hours incubation in hypoxic and normal conditions in hydrogel presence.

Methods

Materials

Sodium alginate (Low viscosity SA, 99%), pectin (99%), beta-cyclodextrin (99%) and deoxycholic acid (DCA, 99%) were purchased from Sigma Chemical Co (St. Louis, MO, USA) and Shanghai Soyoung Biotech. Inc. (Shanghai, China). The water-soluble gel was obtained from the Australian Medical Association (Metron, Perth, Australia). Dulbecco's modified Eagle's medium (DMEM), foetal bovine serum (FBS) and other necessary supplements and complementary substances were purchased from Sigma Chemical Co (St. Louis, MO, USA).

Cell culture

Hepatic cells, AML 12, were grown in DMEM with 10% FBS and further supplementation based on previously published protocols (22). Non-differentiated myotubes, C2C12, were cultured in DMEM with 10% FBS and 1% penicillin-streptomycin. Pancreatic beta cells, NIT-1, were grown in DMEM with supplemented 10% FBS, 5.5 mmol glucose (Sigma-Aldrich, St Louis, MO, USA) and free amino acids following a published protocol (7, 24-26). The cells were incubated in an atmosphere of 5% CO2 at 37°C. The media was changed every 24h for C2C12 and every 48h for AML-12 and NIT-1.

Hydrogel preparation

Hydrogels were prepared by stirring ingredients. with deionised water using homogenisation at room temperature. Freshly prepared hydrogels were stored at 4°C and used for further assays. Before tissue culture work, appropriate hydrogel aliquots were subjected to UV light for 20 minutes. In terms of hydrogels' components (excipients as %), they are the water-soluble gel, SA, pectin, β-cyclodextrin and DCA. Percentages of the water-soluble gel and SA in P1-P15, were 5 and 1.6, respectively. All formulations of P2-P15 had 0.25% of pectin. P3-8 had an incremental increase in β-cyclodextrin (2%, 4%, 6%, 8%, 10%, 12%), while P1-8 had no DCA, and P9-P15 had an incremental increase of DCA % (1-4).

Rheology

Freshly prepared hydrogels were assessed for viscosity, shear stress and torque using a Visco-88 viscometer (Malvern Instruments, Malvern, UK). The Zeta potential of hydrogels was obtained using a 3000HS Zetasizer (Malvern, UK). Hydrogels' surface tension was acquired by a tensiometer (Sigma 703, ATA Scientific, Caringbah, Australia) (27). All measurements were done at room temperature.

Cell viability assay

Cell viability of all three cell lines was assessed using an MTT (2,5-diphenyl-2,4,5-trimethylthiazol-2-yl) assay. After 24h incubation with 20 µL of hydrogels, 20 µL of the stock MTT solution (5 mg/mL) was added to wells containing cells hydrogels mixed with cells, and control, hydrogel-free well. MTT-formazan was then dissolved using 50 µL dimethyl sulfoxide (DMSO). The resulting purple solution was photometrically analysed at 550 nm in triplicates. Obtained cell viability data was normalised and presented as a percentage of hydrogel-free cells' viability, where 100% is the viability of cells in hydrogel-free wells.

Hypoxia assays

20 µL of cells (cell count $1x10^6$/ml for all cell types) were mixed with 50 µM or 100 µM solutions of $CoCl_2$ (80 µL) in a suitable cell media and incubated for 20 minutes before mixing with hydrogels. After

mixing, a further 100 µL of appropriate $CoCl_2$-supplemented media was added. Incubation lasted for 24h, after which cell viability was assessed using the MTT assay.

Bioenergetic parameters

Following 24h incubation with 20 µL of hydrogels, real-time mitochondrial activities of all cell types were assessed using a Seahorse Flux Analyser XF 96 (Agilent, CA, USA), utilising an in-house developed method (27, 28).

Statistics

The data analysis, regressions, and one-way ANOVA/two-way ANOVA were conducted using GraphPad Prism version 9.5 (Graphpad, Inc., MA, USA). Tukey's HSD (honestly significant difference) test, post hoc comparison of means was performed for statistically significant data. Data were shown as a mean ± SEM with $n = 3$, and the data were considered statistically significant at $p < .05$(*) or $p < .01$ (**). Only relevant comparisons of different groups were shown on the graphs.

Results

Bioenergetic parameters for control (C) hepatic cells show non-mitochondrial and ATP production-linked oxygen consumption rate (OCR), with the absence of proton leak-linked OCR (Figure 1a). Other groups show diverse metabolic profiles, with an increase in proton leak (all groups excluding P6, P7, P8 and P14). Non-mitochondrial oxygen consumption (NM-OCR) is the most dominant oxygen-using function within all groups, but it is above 90% in several outliers, including P4, P7 and P14. The percentage of ATP production linked OCR varies across groups (Figure 1a), and it is minimal (5% or less) or non-existent within groups P4, P5, P6, P7, P9, P10, P12, P13, P14 and P15. The energetic profile for all groups in normal conditions, excluding P6 which is altered compared to the metabolic profile of control (C) (Figure 1b). The majority of cells under the influence of BCD hydrogels have increased total OCR without a major increase in extracellular acidification rate (ECAR) (Figure 1b). Groups with DCA-enriched hydrogels (P9-P15) show a significant rise in ECAR compared to C and non-DCA groups (Figures 1b and 1c).

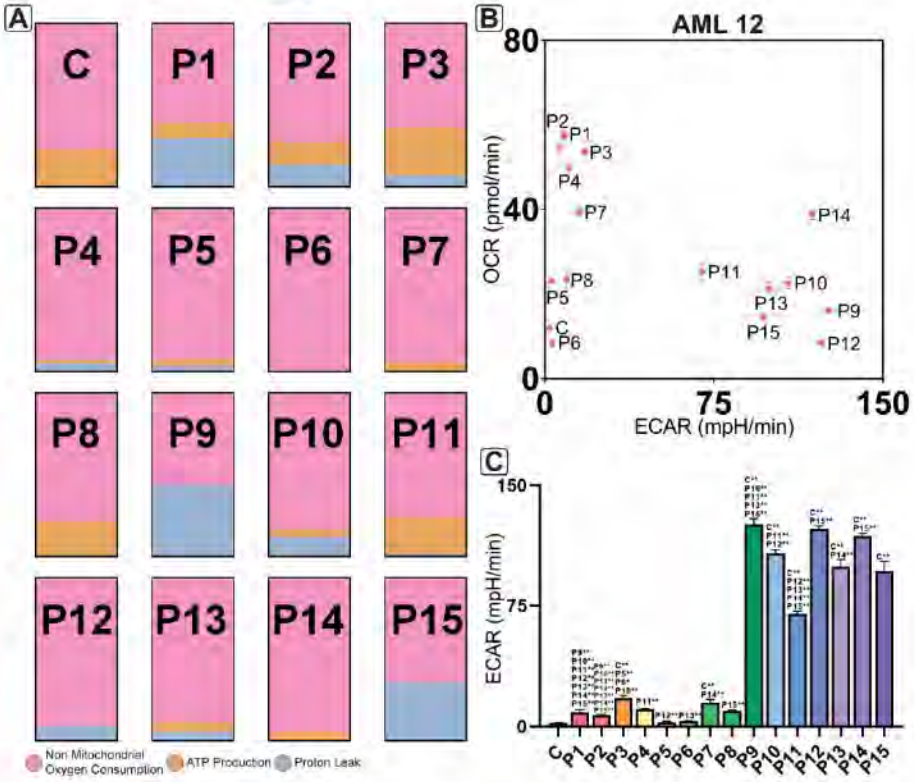

Figure 1. a) Bioenergetic profile of AML 12 cell line, with non-mitochondrial oxygen consumption, ATP production, and Proton Leak linked OCR are shown as a percentage of basal OCR; b) bioenergetic profile of AML 12 cells in normal conditions, prior to oligomycin injection; c) rates of ECAR for AML 12 cells in normal conditions.

The viability of AML 12 cells under hypoxic conditions is presented in Figure 2. Under lower hypoxic conditions, all test groups (except for P3) showed a significant decrease in viability compared to the gel-free control (Figure 2a.1). The introduction of pectin (P2) did not significantly impact the AML 12

viability compared to the gel matrix without it (P1) under lower hypoxic conditions. P4 seems an exception for higher viability of cells in the presence of a low concentration of BCD (P3, P5, and P6). With an increase of BCD to 10% and more (P7 and P8), cellular viability significantly drops compared to hydrogels with a lower concentration of BCD (Figure 2a.1). The viability of AML 12 cells seems to decrease in the presence of DCA, compared to equivalent hydrogels with BCD and without bile acid. In lower hypoxia, P3 has significantly higher viability compared to P10, P5 to P12 and P6 to P13. P4 seems to be an exception again, not being significantly different to P11. For BCD-free hydrogels (P2), the addition of DCA (P9) does not significantly change viability. Control hydrogels (P1 and P2) have substantially higher viability than the majority of hydrogels with DCA (Figure 2a.1).

Under high hypoxia (Figure 2.a2), there is a different viability pattern for AML 12 cells. All groups in the presence of hydrogels (except P15) are significantly lower than the hydrogel-free control. The addition of pectin (P2) negatively affected hepatic cells viability compared to pectin-free hydrogel (P1), but the addition of a small BCD concentration (2% in P3) seemed to increase the hepatic cells' viability. The same trend was observed in lower hypoxia, with increased viability of P3 compared to P2. In high hypoxia, P4 is lower than P3, similar to low hypoxia conditions, although P5 and P6 are still not significantly higher than P4 (Figure 2a.2), as in the case in lower hypoxia (Figure 2a.1). Furthermore, DCA does not have a major impact on cellular viability compared to equivalent DCA-free gels, except for P3, which is significantly higher than P10 (Figure 2a.2). Control gels (P1 and P2) show an interesting trend, with P1 being statistically not different to P3 and P9, while P2 is significantly lower compared to P1, and both P3 and P9, showing that low concentrations of BCD (P3) and DCA (P9) may help cell survival in hypoxic conditions, while in the presence of pectin-enriched hydrogel (P2), cells have lower viability. Lower DCA concentrations in hydrogels (P9) seem to outperform higher ones (P11, P12, and P14), with P15 being an outlier with out-of-trend high cellular viability (Figure 2a.2).

In normoxic conditions (Figure 2a.3), hepatic cells have a mostly statistically similar viability regardless of hydrogel group, with all groups in presence of hydrogels being significantly lower than hydrogel-free control.

Figure 2b compares AML-12 viability under different hypoxic conditions but in the presence of the same hydrogel. Hydrogel-free control (C) shows the highest viability under normoxia; however, control hydrogels (P1 and P2) show the highest cellular viability under low hypoxia. This trend continues with the addition of BCD for most groups (P3, P4, P5 and P6). The addition of DCA does not have a similar effect. In fact, for most of the hydrogels containing DCA, hypoxic conditions do not significantly affect the viability (P9, P10, P12, and P13). The present effect seems non-consistent, as P11 favours normoxia, P14 low hypoxia and P15 high hypoxia.

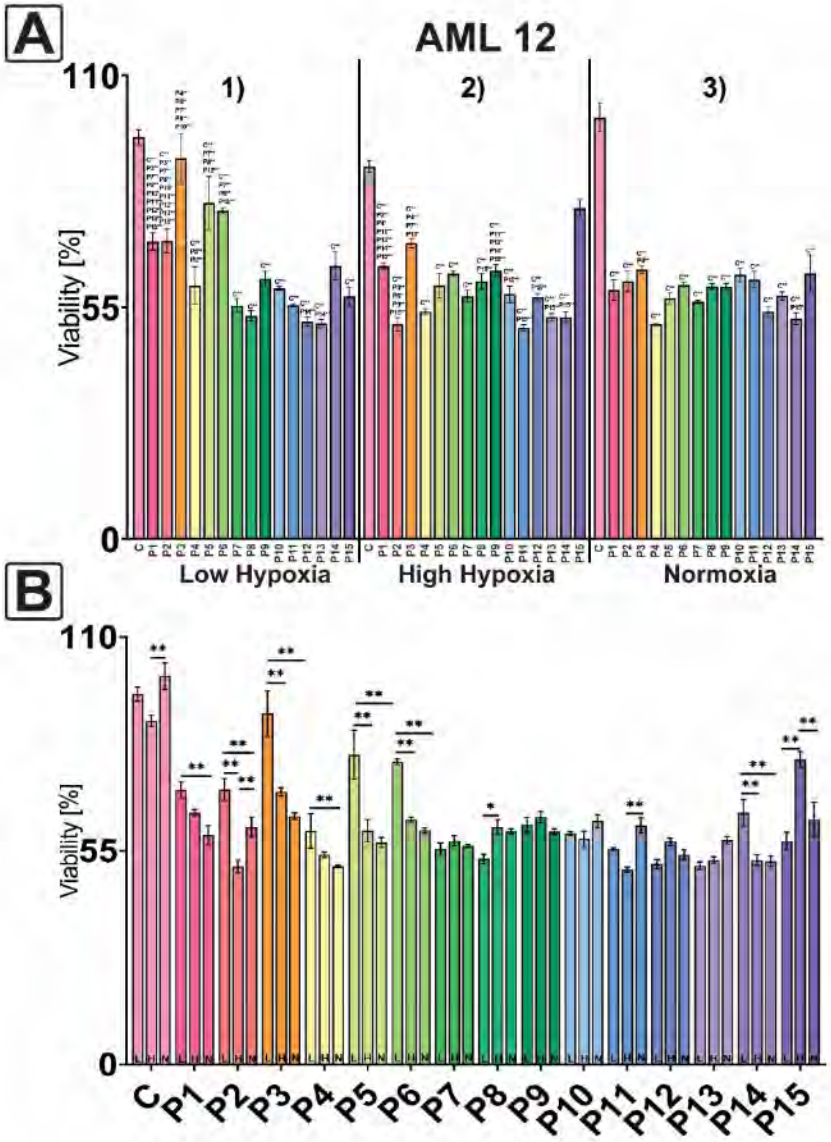

Figure 2. Viability under hypoxic conditions for AML 12 cells line, showing data with a) significance between different groups within some hypoxic conditions: 1) low hypoxia, 2) high hypoxia and 3) control conditions; and b) significance between the viability of cells exposed to the same hydrogel, but under different hypoxic conditions. L stands for low hypoxia, H for high hypoxia, and N for control conditions.

Bioenergetics of the C2C12 muscle cell line are presented in Figure 3. Similar to AML 12, the major component of OCR was NM-OCR consumption. The only notable exception is group P5, where proton leak is the major contributor to OCR. ATP production is similar for gel-free control (C), control gels (P1 and P3), and gels with the lowest amount of BCD (P3 and P4). Outside of these groups, ATP production is in decline or is not detectable.

Interestingly, P13 and P15 have retained ATP production, even though those gels have a very high concentration of DCA. Most groups have modified metabolism compared to gel-free control, with P10, P11, P12 and P13 showing a significant shift to glycolytic metabolism (Figure 3b). This is further observed in Figure 3c, showing ECAR values for each group. Inclusion of DCA in hydrogel matrix seems to increase ECAR in cells, as seen with significant difference between the same gel matrix with or without DCA in pairs; P3 and P10, P4 and P11, P5 and P12, P6 and P13 (Figure 3c).

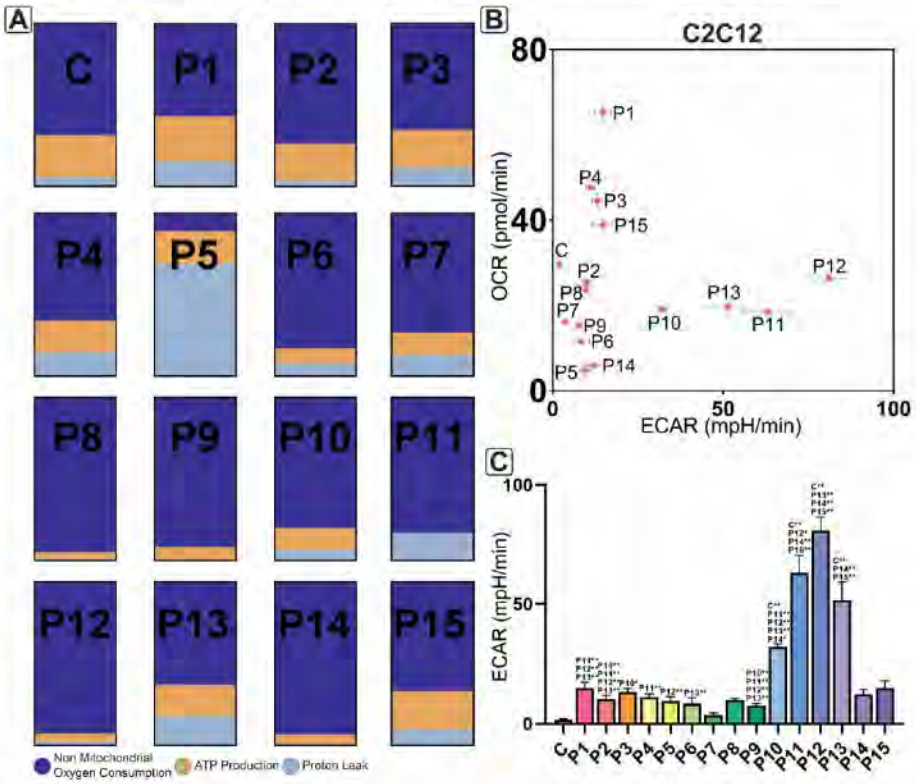

Figure 3. a) Bioenergetic profile of C2C12 cell line, with non-mitochondrial oxygen consumption, ATP production, and Proton Leak linked OCR are shown as a percentage of basal OCR; b) bioenergetic profile of C2C12 cells in normal conditions, prior to oligomycin injection; c) rates of ECAR for C2C12 cells in normal conditions.

The viability pattern for C2C12 cells is similar across both hypoxic conditions and normoxia (Figure 2a). Gel-free control shows significantly higher viability amongst most groups within all conditions, followed by control gels (P1 and P2) and gels with lower concentrations of BCD (P3, P4, P6). Gels with DCA seem to have decreased viability, with P15 having the lowest viability among all three conditions (Figure 4a).

In Figure 2.b data shows a difference in viability within the same hydrogel group but in different hypoxic conditions. The C2C12 cell line seems to have increased viability in low hypoxia when in absence of hydrogels (C). P3 and P11 follows this trend while P1, P4, P5, P7, P9 and P15 have high viability in normal conditions. For most groups that were incubated in the presence of DCA-enriched hydrogels, there is no statistically significant difference in viability between different hypoxic conditions (Figure 4b).

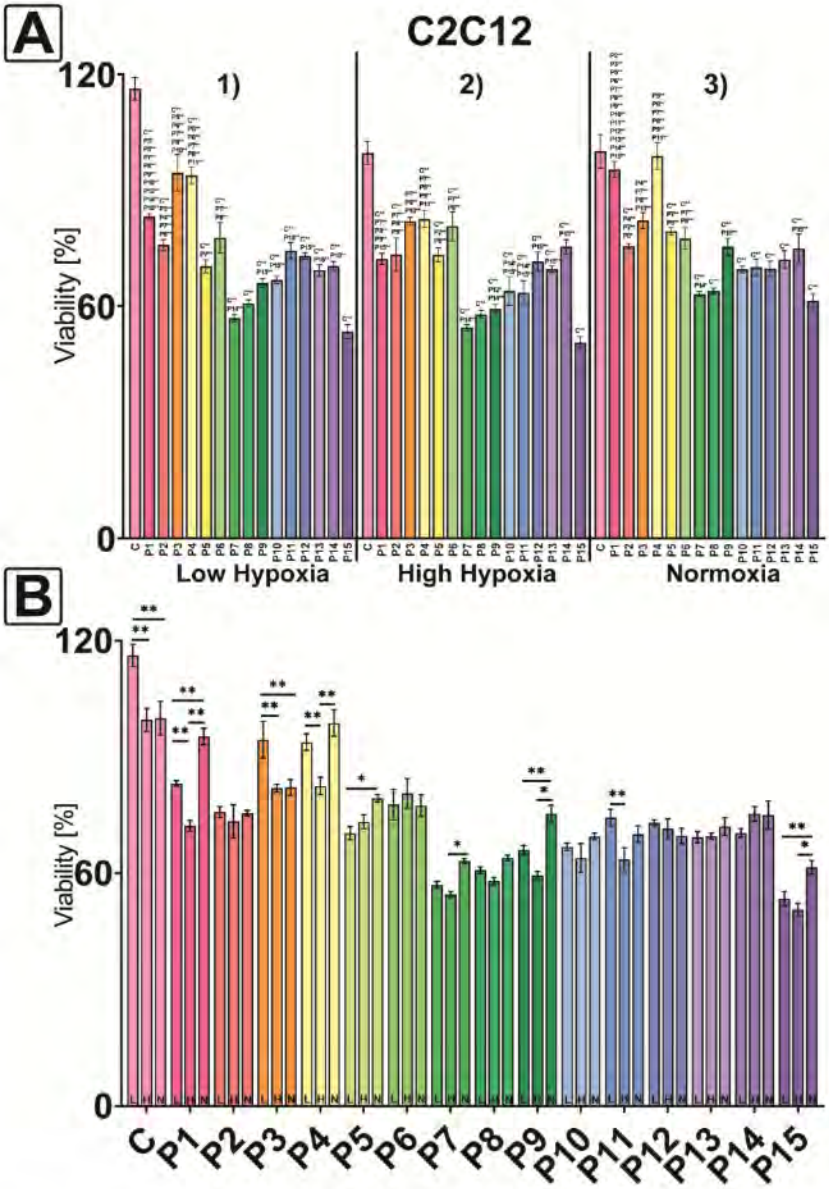

Figure 4. Viability under hypoxic conditions for C2C12 cells line, showing data with a) significance between different groups within the same hypoxic conditions: 1) low hypoxia, 2) high hypoxia and 3) control conditions; and b) significance between the viability of cells exposed to the same hydrogel, but under different hypoxic conditions. Cell viability is normalised to gel-free control in normal conditions being 100%. L stands for low hypoxia, H for high hypoxia, and N for control conditions.

Bioenergetics of NIT-1 cells are shown in figure 5. Similar to previous data sets, NM-OCR consumption seems dominant in total oxygen consumption for most groups (Figure 5a). ATP production is retained in control gels (P1 and P2), and in the majority of cells exposed to gels with BCD without DCA (P3-P6). Cells incubated with a hydrogel containing DCA (P9-P15), except for P11, have negligible (less than 5% of maximal respiration OCR) ATP production (Figure 5a). Control gels (P1 and P2), together with P3, have increased OCR in normal conditions compared to hydrogel-free gels (Figure 5b). There is a noticeable shift in cellular metabolism to glycolytic metabolism in the presence of DCA (Figure 5b). This trend is further illustrated in ECAR values (Figure 5c), with cells in the presence of DCA having significantly increased ECAR compared to the hydrogel-free control and a majority of DCA-free equivalent gels (P4 and P11, P5 and P12, P6 and P13, P7 and P14, P8 and P15).

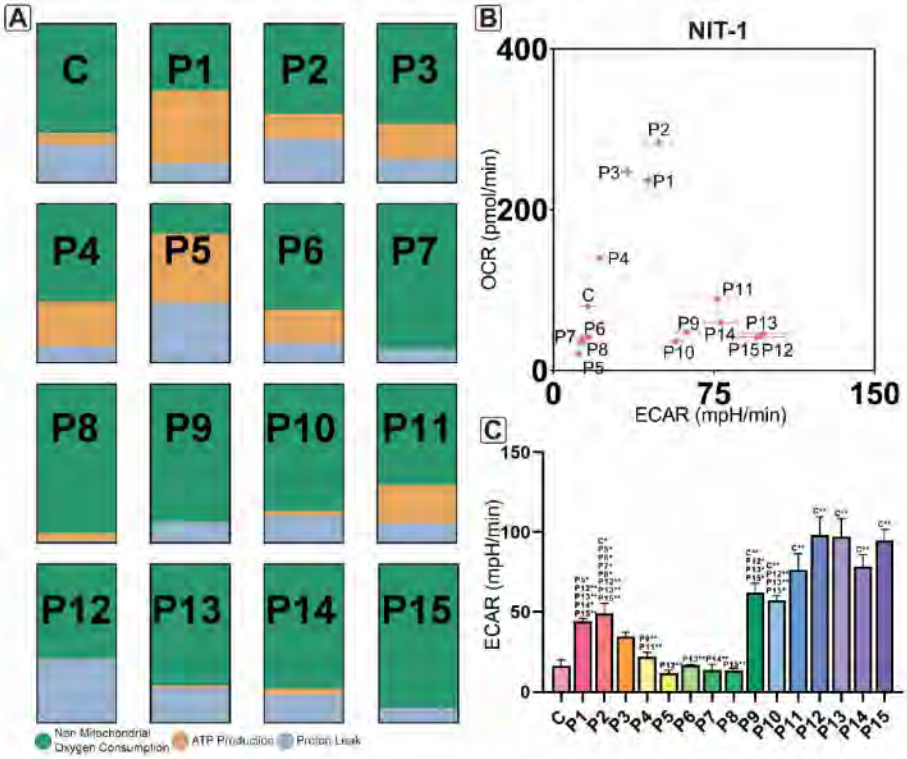

Figure 5. a) Bioenergetic profile of the NIT-1 cell line, with non-mitochondrial oxygen consumption, ATP production, and Proton Leak linked OCR are shown as a percentage of basal OCR; b) bioenergetic profile of NIT-1 cells in normal conditions, prior to oligomycin injection; c) rates of ECAR for NIT-1 cells in normal conditions.

The viability of NIT-1 shows different patterns in normoxia and hypoxic conditions (figure 6a). In low hypoxia, the majority of hydrogel-gel groups are not significantly varied from the hydrogel-free control (C) (Figure 6a.1). Furthermore, there are no significant differences between DCA-enriched hydrogels and their DCA-free equivalents (Figure 6a.1). In high hypoxia, cells show similar behaviour except for P12 and P14 which show increased viability compared to the control (C). P12 and P14 are the only groups that have a significant difference in viability compared to their DCA-free equivalent hydrogels P5 and P7, respectably (Figure 6a.2). Cellular viability in normoxia shows more variability (Figure 6a.3). Hydrogels with high concentrations of BCD (P5-P8) have a negative impact on NIT-1 cell viability.

Hydrogels with DCA leads to decreased viability in P10, P11, P13 and P15. Once again, P12 is an exception, as it shows increased viability compared to both hydrogel-free cells (C) and control P1 and P2 gels (Figure 6a.3).

Figure 6b shows relationships between the viability of cells incubated with the same hydrogel in different conditions. Gel-free control (C), control gels (P1 and P2), and cells exposed to hydrogels with a low concentration of BCD (P3 and P4) show the best viability in normal, non-hypoxic conditions. Interestingly, this is also the case with cells exposed to high concentrations of DCA (P12-P15), while cells exposed to lower DCA concentrations (P9-P11) do not show significant differences between viabilities regardless of conditions (Figure 6b).

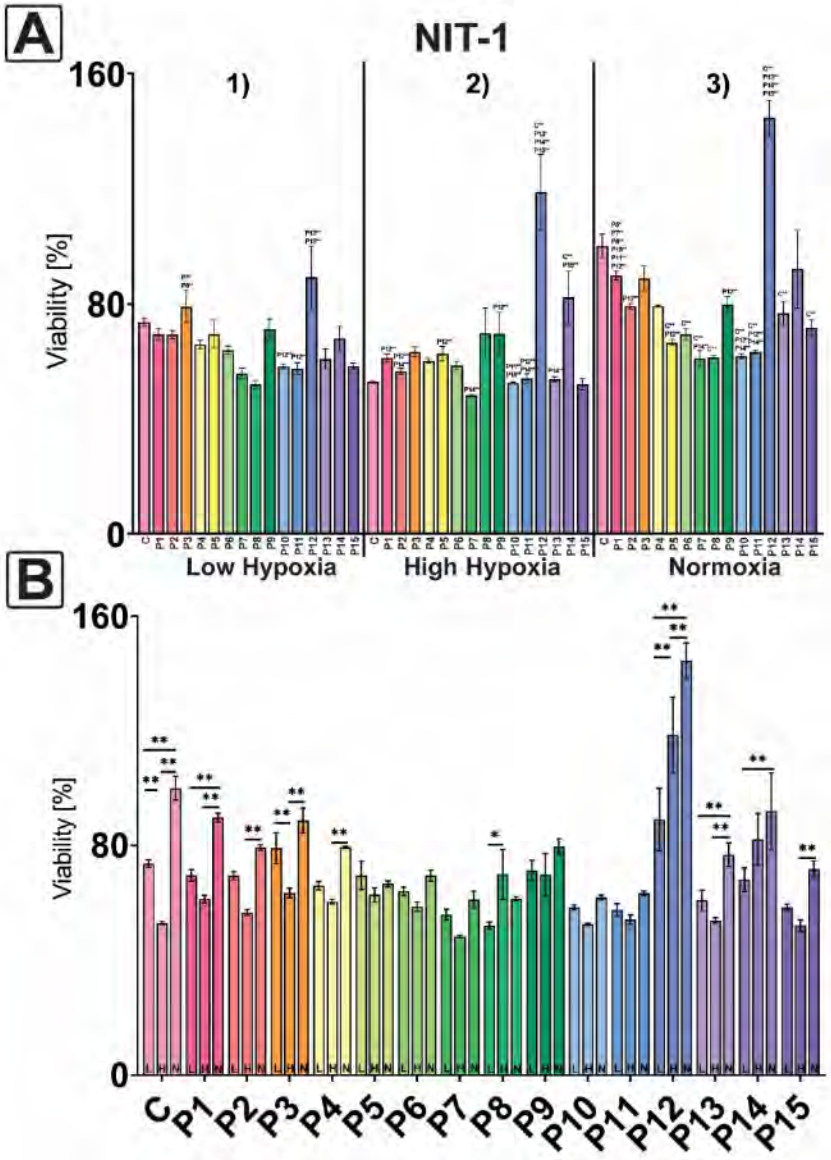

Figure 6. Viability under hypoxic conditions for NIT-1 cells line, showing data with a) significance between different groups within the same hypoxic conditions: 1) low hypoxia, 2) high hypoxia and 3) control conditions; and b) significance between the viability of cells exposed to the same hydrogel, but under different hypoxic conditions. Cell viability is normalised to gel-free control in normal conditions being 100%. L stands for low hypoxia, H for high hypoxia, and N for control conditions.

Figure 7. shows the energy profile of different cell lines. All cell lines show the most considerable variability in values for NM-OCR consumption. Variability in values for other categories (ATP production, proton leak and spare capacity) is not as pronounced.

Figure 7d shows the viability of all experimental cell lines in normal conditions after 24h incubation with hydrogels. Between cell lines, NIT-1 cells seem to have the best survivability overall, followed by the C2C12 cell line. AML-12 cells show significantly lower viability compared to other cell lines when exposed to most hydrogels.

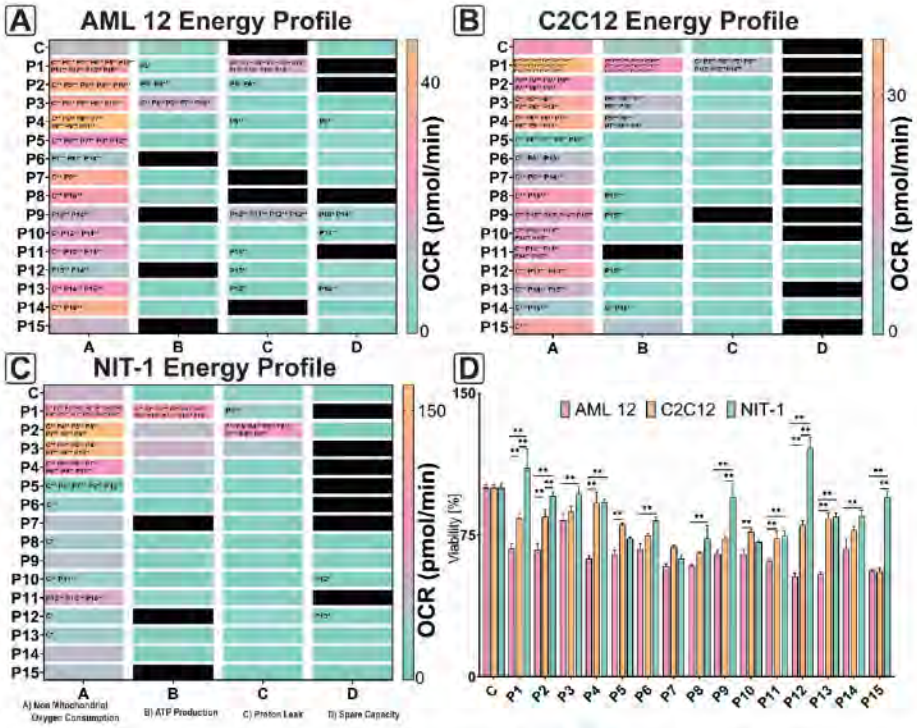

Figure 7. The energy profile is shown for a) AML-12 cells, b) C2C12 cells, and c) NIT-1 cells. D) Viability of different cell lines exposed to hydrogels was compared in normoxic conditions; 100% is viability for each cell line for cells not exposed to any hydrogel (C). Black fields represent undetected points.

Rheology studies (Figure 8) show non-Newtonian shear thinning behaviour for all hydrogels (Figure 8a-f). The addition of BCD or DCA in various concentrations does not seem to change this trend (Figure 8a-f). The shear rate seems to impact DCA-enriched hydrogels (Figure 8h). At a low shear rate, shear stress appears to stay consistent regardless of increasing DCA concentration in hydrogels. However, there is a difference in hydrogel behaviour at the highest shear rate. Hydrogels with concentrations up to 2% w/w of DCA have lower shear stress compared to the same hydrogels at the lowest shear rate. Shear stress values at different shear rates seem comparable, except for hydrogels with 3.5% w/w, which show an increase in shear stress at the highest shear rate. Surface tension values show an interesting trend with hydrogels with added DCA having consistently lower surface tension, compared to equivalent hydrogels without DCA (Figure 8g, pairs P3 and P10, P4 and P11, P5 and P12, P6 and P13, P7 and P14, and P8 and P15), probably due its surfactant nature. The addition of BCD also seems to increase surface tension compared to control hydrogels (P1 and P2) (Figure 8g).

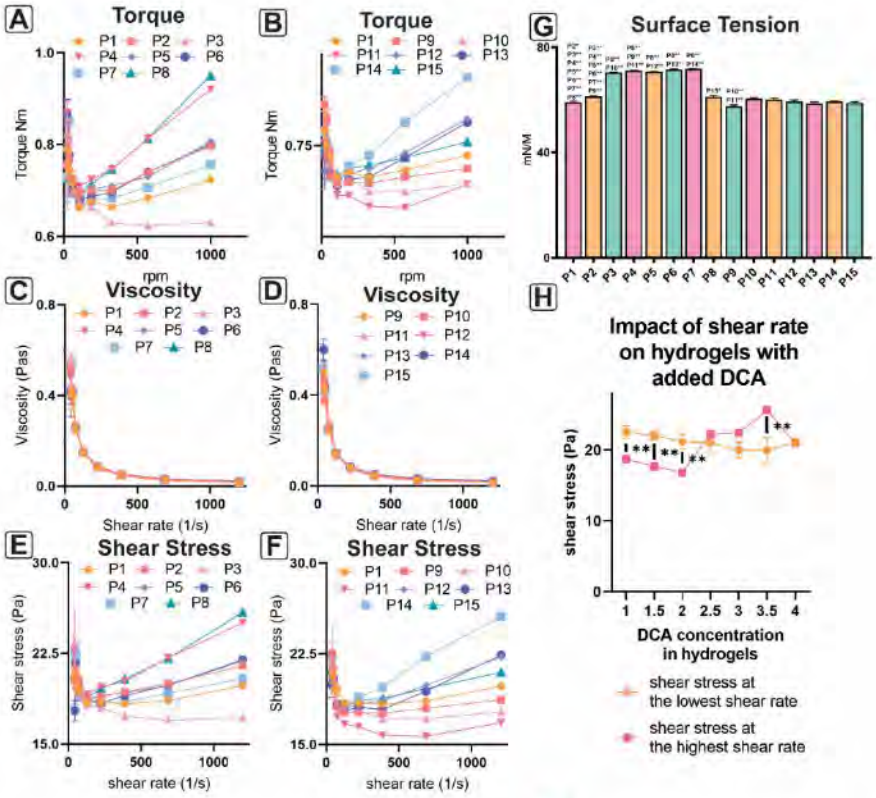

Figure 8. a) Torque values for control hydrogels (P1 and P2) and DCA free hydrogels (P3-P8); b) Torque values for control hydrogels (P1 and P2) and hydrogels with added DCA (P9-P15); c) Viscosity values for control hydrogels (P1 and P2) and DCA free hydrogels (P3-P8); d) Viscosity values for control hydrogels (P1 and P2) and hydrogels with added DCA (P9-P15); e) Shear stress values for control hydrogels (P1 and P2) and DCA free hydrogels (P3-P8); f) Shear stress values for control hydrogels (P1 and P2) and hydrogels with added DCA (P9-P15); g) Surface tension values for all hydrogels; h) Impact of shear rate on hydrogels with added DCA.

Discussion

Optimal rheological characteristics are imperative for suitable potential nanogel behaviour *in vivo*. Non-Newtonian fluid behaviour refers to the behaviour of the fluid to have lower viscosity at higher shear stress (29). Non-Newtonian hydrogels are ideal as they demonstrate more desirable properties for applications including drug delivery, injectability, and tissue fabrication (30). Furthermore, the ability of bile acids to lower surface tension has previously been reported in the literature (31). It is thought that bile acid lowers interface tension between the hydrogel and solution (32).

There seems to be a distinctive trend of increased ECAR within AML-12 cells exposed to hydrogels with DCA (Figure 1b and 1c). This may suggest a shift in metabolism to an anaerobic phenotype (33, 34). An increase in ECAR may be due to the presence of oxidative phosphorylation (OXPHOS) inhibitors (31), suggesting that DCA may be an OXPHOS inhibitor. Similar findings were observed within both C2C12 and NIT-1 cells (Figure 3c and 5c). This effect is aligned with studies done by Kovacevic et al., which show the same effect (35-37). There may be several explanations for this DCA-induced effect.

Nath proposes bile acids as external inducers in opening permeability transition pore in the mitochondrial membrane, leading to diverging of ATP-synthase function from an energy-conserving enzyme to an energy-dissipating structure (38). Rodrigues et al. observed a decrease in transmembrane potential in isolated hepatic mitochondria of mice fed with DCA. This was followed by increased peroxides production, superoxide anion and elevation in mitochondria-associated BAX protein levels (39). This may also explain increased and varied NM-OCR consumption in all three cell types (Figure 7a, 7b and 7c), as increased NM-OCR consumption linked OCR may be linked with increased ROS production (40, 41).

Furthermore, Schulz et al. reported mitochondrial toxicity of specific bile salts, suggesting that glycochenodeoxycholic acid and taurochenodeoxycholic acid target adenine nucleotide translocator which leads to the depletion of mitochondrial membrane potential and an increase of mitochondrial permeability in hepatocytes. However, this effect seems to be dose, time, and species dependent as both ursodeoxycholic acid, and tauroursodeoxycholic acid may be hepatoprotective (39, 42). Gao et al. observed DCA-induced inhibition of PINK1-mediated mitophagy and the activation of inflammatory pathways on steatotic hepatocytes, leading to cell death (43). PINK1 targets damaged mitochondria with depleted mitochondrial potential, leading to mitophagy (44). Therefore, PINK1 inhibition in mitochondria leads to an intracellular build-up of impaired mitochondria and consequent metabolic dysfunction.

For muscle cells, DCA activation of TGR5 has been proposed as a cause of mitochondrial dysfunction and a decrease in mitochondrial potential (45, 46). TGR5 receptor is present in pancreatic beta cells as well, and it is known to promote insulin secretion and glucose homeostasis (47, 48), and this interaction may influence slightly better viability of NIT-1 cells in the presence of DCA hydrogels, compared to AML-12 and C2C12 cells.

The various cell lines examined displayed oxygen-dependent viability patterns, with the bile acid overall adversely affecting their biological activities. The data shows that all cell types performed best under normoxia, with NIT-1 displaying the most profound oxygen-dependant viability behaviour. This could be attributed to the negligible hypoxic-defence mechanism of NIT-1 compared with AML-12 and C2C12; thus, it would be most impacted by the slightest variations in oxygen levels. Interestingly, the cytotoxic effect of hypoxia is not pronounced within all three cell types incubated with hydrogels with several different DCA concentrations (Figure 2b, 4b and 6b). Lower concentration of DCA may negate some of the toxic effects of hypoxia, as they may destabilise HIF-1α, leading to repression of hypoxic

responses in cells (49, 50). Furthermore, TGR5 may be involved in this process, leading to further anti-inflammatory cellular responses (51, 52). This effect has been observed by Mooranian et al., who found improved cellular viability, insulin secretion and reduced inflammatory response of encapsulated pancreatic beta cells when hydrophobic bile acid (chenodeoxycholic acid) is added to a polymer matrix (53).

BCD has concentration dependant cell toxicity, and is involved in cholesterol depletion in cells (54, 55). This study observed a similar dose-dependent effect on cells, showing that low concentration of BCD (up to 2%, P3) did not significantly alter cellular viability and bioenergetics of cells compared to BCD-free gel (P2).

Conclusion

This study examined three cell lines' cellular viability and bioenergetic parameters in the presence of fifteen different hydrogels with gradually increasing concentrations of beta-cyclodextrin and deoxycholic acid. The addition of a moderate concentration of beta-cyclodextrin to the polymer matrix may be tolerated by various cell types interacting with the matrix. Furthermore, low concentrations of DCA do not alter the rheological parameters of a polymer matrix and may be beneficial to some tissues to combat hypoxic effects. However, this effect is dose-dependent, and tissue-dependent, so determining the most idealistic formulation and its application are crucial.

Disclaimer

Funding: The work is partially supported by [redacted]

Data Availability Statement: The data presented in this study are available on request from the corresponding author. The data are not publicly available due to author property agreements.

Acknowledgments: The authors would like to acknowledge the [redacted]

Conflicts of Interest: The authors declare no conflict of interest

Reference

1. Sun B. The mechanics of fibrillar collagen extracellular matrix. Cell Reports Physical Science. 2021;2(8):100515.
2. Gupta M, Sarangi BR, Deschamps J, Nematbakhsh Y, Callan-Jones A, Margadant F, et al. Adaptive rheology and ordering of cell cytoskeleton govern matrix rigidity sensing. Nature Communications. 2015;6(1):7525.
3. Baker EL, Bonnecaze RT, Zaman MH. Extracellular matrix stiffness and architecture govern intracellular rheology in cancer. Biophys J. 2009;97(4):1013-21.
4. Bahadoran M, Shamloo A, Nokoorani YD. Development of a polyvinyl alcohol/sodium alginate hydrogel-based scaffold incorporating bFGF-encapsulated microspheres for accelerated wound healing. Scientific Reports. 2020;10(1):7342.
5. Zhu Y, Ma Z, Kong L, He Y, Chan HF, Li H. Modulation of macrophages by bioactive glass/sodium alginate hydrogel is crucial in skin regeneration enhancement. Biomaterials. 2020;256:120216.
6. Lv K, Li Q, Zhang L, Wang Y, Zhong Z, Zhao J, et al. Incorporation of small extracellular vesicles in sodium alginate hydrogel as a novel therapeutic strategy for myocardial infarction. Theranostics. 2019;9(24):7403-16.
7. Wagle SR, Kovacevic B, Ionescu CM, Walker D, Jones M, Carey L, et al. Pharmacological and biological study of microencapsulated probucol-secondary bile acid in a diseased mouse model. Pharmaceutics. 2021;13(8):1223.
8. Li D-q, Li J, Dong H-l, Li X, Zhang J-q, Ramaswamy S, et al. Pectin in biomedical and drug delivery applications: A review. International Journal of Biological Macromolecules. 2021;185:49-65.
9. Goel H, Gupta N, Santhiya D, Dey N, Bohidar HB, Bhattacharya A. Bioactivity reinforced surface patch bound collagen-pectin hydrogel. International Journal of Biological Macromolecules. 2021;174:240-53.
10. Ghorbani M, Roshangar L, Soleimani Rad J. Development of reinforced chitosan/pectin scaffold by using the cellulose nanocrystals as nanofillers: An injectable hydrogel for tissue engineering. European Polymer Journal. 2020;130:109697.
11. Morello G, Quarta A, Gaballo A, Moroni L, Gigli G, Polini A, et al. A thermo-sensitive chitosan/pectin hydrogel for long-term tumor spheroid culture. Carbohydrate Polymers. 2021;274:118633.
12. Cao L, Lu W, Mata A, Nishinari K, Fang Y. Egg-box model-based gelation of alginate and pectin: A review. Carbohydrate Polymers. 2020;242:116389.

13. Niu X, Mo Z, Yang X, Sun M, Zhao P, Li Z, et al. Advances in the use of functional composites of β-cyclodextrin in electrochemical sensors. Microchimica Acta. 2018;185(7):328.
14. Kurkov SV, Loftsson T. Cyclodextrins. International Journal of Pharmaceutics. 2013;453(1):167-80.
15. Kettel MJ, Hildebrandt H, Schaefer K, Moeller M, Groll J. Tenside-free Preparation of Nanogels with High Functional β-Cyclodextrin Content. ACS Nano. 2012;6(9):8087-93.
16. Gil ES, Wu L, Xu L, Lowe TL. β-Cyclodextrin-poly(β-Amino Ester) Nanoparticles for Sustained Drug Delivery across the Blood–Brain Barrier. Biomacromolecules. 2012;13(11):3533-41.
17. Kovacevic B, Jones M, Ionescu C, Walker D, Wagle S, Chester J, et al. The emerging role of bile acids as critical components in nanotechnology and bioengineering: Pharmacology, formulation optimizers and hydrogel-biomaterial applications. Biomaterials. 2022:121459.
18. Farina GA, Cherubini K, de Figueiredo MAZ, Salum FG. Deoxycholic acid in the submental fat reduction: A review of properties, adverse effects, and complications. Journal of Cosmetic Dermatology. 2020;19(10):2497-504.
19. Salomatina OV, Popadyuk II, Zakharenko AL, Zakharova OD, Chepanova AA, Dyrkheeva NS, et al. Deoxycholic acid as a molecular scaffold for tyrosyl-DNA phosphodiesterase 1 inhibition: A synthesis, structure–activity relationship and molecular modeling study. Steroids. 2021;165:108771.
20. Xin C, Liu S, Qu H, Wang Z. The novel nanocomplexes containing deoxycholic acid-grafted chitosan and oleanolic acid displays the hepatoprotective effect against CCl4-induced liver injury in vivo. International Journal of Biological Macromolecules. 2021;185:338-49.
21. Chen S, Deng J, Zhang L-M. Cationic nanoparticles self-assembled from amphiphilic chitosan derivatives containing poly(amidoamine) dendrons and deoxycholic acid as a vector for co-delivery of doxorubicin and gene. Carbohydrate Polymers. 2021;258:117706.
22. Mroz MS, Lajczak NK, Goggins BJ, Keely S, Keely SJ. The bile acids, deoxycholic acid and ursodeoxycholic acid, regulate colonic epithelial wound healing. American Journal of Physiology-Gastrointestinal and Liver Physiology. 2018;314(3):G378-G87.
23. Xu M, Cen M, Shen Y, Zhu Y, Cheng F, Tang L, et al. Deoxycholic Acid-Induced Gut Dysbiosis Disrupts Bile Acid Enterohepatic Circulation and Promotes Intestinal Inflammation. Digestive Diseases and Sciences. 2021;66(2):568-76.
24. Mooranian A, Raj Wagle S, Kovacevic B, Takechi R, Mamo J, Lam V, et al. Bile acid bio-nanoencapsulation improved drug targeted-delivery and pharmacological effects via cellular flux: 6-months diabetes preclinical study. Scientific Reports. 2020;10(1):106.
25. Mooranian A, Takechi R, Jamieson E, Morahan G, Al-Salami H. The effect of molecular weights of microencapsulating polymers on viability of mouse-cloned pancreatic beta-cells: biomaterials, osmotic forces and potential applications in diabetes treatment. Pharm Dev Technol. 2018;23(2):145-50.
26. Mooranian A, Zamani N, Mikov M, Goločorbin-Kon S, Stojanovic G, Arfuso F, et al. Stability and biological testing of taurine-conjugated bile acid antioxidant microcapsules for diabetes treatment. Therapeutic Delivery. 2019;10(2):99-106.
27. Wagle SR, Walker D, Kovacevic B, Gedawy A, Mikov M, Golocorbin-Kon S, et al. Micro-Nano formulation of bile-gut delivery: rheological, stability and cell survival, basal and maximum respiration studies. Sci Rep. 2020;10(1):7715.
28. Wagle SR, Kovacevic B, Walker D, Ionescu CM, Jones M, Stojanovic G, et al. Pharmacological and Advanced Cell Respiration Effects, Enhanced by Toxic Human-Bile Nano-Pharmaceuticals of Probucol Cell-Targeting Formulations. Pharmaceutics. 2020;12(8):708.
29. Yu I, Chen R. An experimental and numerical study on coaxial extrusion of a non-Newtonian hydrogel material. Journal of Manufacturing Science and Engineering. 2021;143(8).
30. Stojkov G, Niyazov Z, Picchioni F, Bose RK. Relationship between structure and rheology of hydrogels for various applications. Gels. 2021;7(4):255.
31. Luner PE. Wetting properties of bile salt solutions and dissolution media. Journal of pharmaceutical sciences. 2000;89(3):382-95.

32. Pavlović N, Goločorbin-Kon S, Đanić M, Stanimirov B, Al-Salami H, Stankov K, et al. Bile acids and their derivatives as potential modifiers of drug release and pharmacokinetic profiles. Frontiers in pharmacology. 2018;9:1283.
33. Divakaruni AS, Paradyse A, Ferrick DA, Murphy AN, Jastroch M. Chapter Sixteen - Analysis and Interpretation of Microplate-Based Oxygen Consumption and pH Data. In: Murphy AN, Chan DC, editors. Methods in Enzymology. 547: Academic Press; 2014. p. 309-54.
34. Monsour M, Gorsky A, Nguyen H, Castelli V, Lee J-Y, Borlongan CV. Enhancing oxidative phosphorylation over glycolysis for energy production in cultured mesenchymal stem cells. NeuroReport. 2022;33(15):635-40.
35. Kovacevic B, Wagle SR, Ionescu CM, Jones M, Lewkowicz M, Wong EYM, et al. Novel hydrogel comprising non-ionic copolymer with various concentrations of pharmacologically active bile acids for cellular injectable gel. Colloids and Surfaces B: Biointerfaces. 2023;222:113014.
36. Kovacevic B, Ionescu CM, Jones M, Wagle SR, Lewkowicz M, Đanić M, et al. The Effect of Deoxycholic Acid on Chitosan-Enabled Matrices for Tissue Scaffolding and Injectable Nanogels. Gels [Internet]. 2022; 8(6).
37. Kovacevic B, Ionescu CM, Wagle SR, Jones M, Lewkowicz M, Wong EYM, et al. Impact of Novel Teflon-DCA Nanogel Matrix on Cellular Bioactivity. Journal of Pharmaceutical Sciences. 2022.
38. Nath S. A Novel Conceptual Model for the Dual Role of FOF1-ATP Synthase in Cell Life and Cell Death. Biomol Concepts. 2020;11(1):143-52.
39. Rodrigues CMP, Fan G, Wong PY, Kren BT, Steer CJ. Ursodeoxycholic Acid May Inhibit Deoxycholic Acid-Induced Apoptosis by Modulating Mitochondrial Transmembrane Potential and Reactive Oxygen Species Production. Molecular Medicine. 1998;4(3):165-78.
40. Hill BG, Benavides GA, Lancaster JR, Ballinger S, Dell'Italia L, Zhang J, et al. Integration of cellular bioenergetics with mitochondrial quality control and autophagy. Biological Chemistry. 2012;393(12):1485-512.
41. Islam MN, Rauf A, Fahad FI, Emran TB, Mitra S, Olatunde A, et al. Superoxide dismutase: an updated review on its health benefits and industrial applications. Critical Reviews in Food Science and Nutrition. 2022;62(26):7282-300.
42. Schulz S, Schmitt S, Wimmer R, Aichler M, Eisenhofer S, Lichtmannegger J, et al. Progressive stages of mitochondrial destruction caused by cell toxic bile salts. Biochimica et Biophysica Acta (BBA) - Biomembranes. 2013;1828(9):2121-33.
43. Gao X, Ruan Y, Zhu X, Lin X, Xin Y, Li X, et al. Deoxycholic Acid Promotes Pyroptosis in Free Fatty Acid-Induced Steatotic Hepatocytes by Inhibiting PINK1-Mediated Mitophagy. Inflammation. 2022;45(2):639-50.
44. Eiyama A, Okamoto K. PINK1/Parkin-mediated mitophagy in mammalian cells. Current Opinion in Cell Biology. 2015;33:95-101.
45. Abrigo J, Olguín H, Gutierrez D, Tacchi F, Arrese M, Cabrera D, et al. Bile Acids Induce Alterations in Mitochondrial Function in Skeletal Muscle Fibers. Antioxidants. 2022;11(9):1706.
46. Abrigo J, Gonzalez F, Aguirre F, Tacchi F, Gonzalez A, Meza MP, et al. Cholic acid and deoxycholic acid induce skeletal muscle atrophy through a mechanism dependent on TGR5 receptor. Journal of Cellular Physiology. 2021;236(1):260-72.
47. Kumar DP, Rajagopal S, Mahavadi S, Mirshahi F, Grider JR, Murthy KS, et al. Activation of transmembrane bile acid receptor TGR5 stimulates insulin secretion in pancreatic β cells. Biochemical and Biophysical Research Communications. 2012;427(3):600-5.
48. Kumar DP, Asgharpour A, Mirshahi F, Park SH, Liu S, Imai Y, et al. Activation of Transmembrane Bile Acid Receptor TGR5 Modulates Pancreatic Islet α Cells to Promote Glucose Homeostasis *. Journal of Biological Chemistry. 2016;291(13):6626-40.
49. Phelan JP, Reen FJ, Dunphy N, O'Connor R, O'Gara F. Bile acids destabilise HIF-1α and promote anti-tumour phenotypes in cancer cell models. BMC Cancer. 2016;16(1):476.

50. Legendre C, Reen FJ, Woods DF, Mooij MJ, Adams C, O'Gara F. Bile Acids Repress Hypoxia-Inducible Factor 1 Signaling and Modulate the Airway Immune Response. Infection and Immunity. 2014;82(9):3531-41.
51. Wang Q, Wei S, Li L, Qiu J, Zhou S, Shi C, et al. TGR5 deficiency aggravates hepatic ischemic/reperfusion injury via inhibiting SIRT3/FOXO3/HIF-1α pathway. Cell Death Discovery. 2020;6(1):116.
52. Hanafi NI, Mohamed AS, Sheikh Abdul Kadir SH, Othman MHD. Overview of Bile Acids Signaling and Perspective on the Signal of Ursodeoxycholic Acid, the Most Hydrophilic Bile Acid, in the Heart. Biomolecules. 2018;8(4):159.
53. Mooranian A, Negrulj R, Al-Salami H. Primary Bile Acid Chenodeoxycholic Acid-Based Microcapsules to Examine β-cell Survival and the Inflammatory Response. BioNanoScience. 2016;6(2):103-9.
54. Castagne D, Fillet M, Delattre L, Evrard B, Nusgens B, Piel G. Study of the cholesterol extraction capacity of β-cyclodextrin and its derivatives, relationships with their effects on endothelial cell viability and on membrane models. Journal of Inclusion Phenomena and Macrocyclic Chemistry. 2009;63(3):225-31.
55. Kiss T, Fenyvesi F, Bácskay I, Váradi J, Fenyvesi É, Iványi R, et al. Evaluation of the cytotoxicity of β-cyclodextrin derivatives: Evidence for the role of cholesterol extraction. European Journal of Pharmaceutical Sciences. 2010;40(4):376-80.

Publication 5 (pages 87-97):

Kovacevic B, Wagle SR, Ionescu CM, Jones M, Lewkowicz M, Wong EYM, Kojic S, Stojanovic G, Đanić M, Mikov M, Mooranian A, Al-Salami H. Novel hydrogel comprising non-ionic copolymer with various concentrations of pharmacologically active bile acids for cellular injectable gel. Colloids and Surfaces B: Biointerfaces. 2023;222:113014.

Sub-objective (4): to design and create hydrogels utilising sodium alginate, poloxamer 407, and various concentrations of deoxycholic acid, and to examine the shear stress, viscosity, surface tension, torque, microstructure, and zeta potential of hydrogels. Additionally, the hydrogels were incubated with 3 different cell lines (AML 12, C2C12 and NIT-1). Their impact on viability in normal and hypoxic conditions and their impact on bioenergetic parameters was investigated.

Colloids and Surfaces B: Biointerfaces 222 (2023) 113014

Contents lists available at ScienceDirect

Colloids and Surfaces B: Biointerfaces

journal homepage: www.elsevier.com/locate/colsurfb

Novel hydrogel comprising non-ionic copolymer with various concentrations of pharmacologically active bile acids for cellular injectable gel

Bozica Kovacevic [a,b], Susbin Raj Wagle [a,b], Corina Mihaela Ionescu [a,b], Melissa Jones [a,b], Michael Lewkowicz [a,b], Elaine YM Wong [b], Sanja Kojic [c], Goran Stojanovic [c], Maja Đanić [d], Momir Mikov [d], Armin Mooranian [a,b,e,*], Hani Al-Salami [a,b,f,*]

[a] The Biotechnology and Drug Development Research Laboratory, Curtin Medical School & Curtin Health Innovation Research Institute, Curtin University, Bentley, Perth, WA 6102, Australia
[b] Hearing Therapeutics Department, Ear Science Institute Australia, Queen Elizabeth II Medical Centre, Nedlands, Perth, WA 6009, Australia
[c] Faculty of Technical Sciences, University of Novi Sad, Novi Sad, Serbia
[d] Department of Pharmacology, Toxicology and Clinical Pharmacology, Faculty of Medicine, University of Novi Sad, Novi Sad 21101, Serbia
[e] School of Pharmacy, University of Otago, Dunedin, Otago, New Zealand

ARTICLE INFO

Keywords:
Bile acids
Hydrogels
Hydrogels
Injectable gels
Matrices
Secondary bile acids

ABSTRACT

Deoxycholic acid (DCA) is a bile acid capable of forming micelles and modifying the properties of hydrogels. We incorporated DCA in sodium alginate (SA) and poloxamer 407 matrices creating novel DCA-copolymer hydrogel for therapeutic delivery. Hydrogels were assessed for common rheological properties. Biocompatibility and biological effect were examined on various cell lines. Cell viability was determent in normal and various hypoxic conditions, and full mitochondrial bioenergetic parameters were assessed in cell lines in order to illustrate hydrogel effects on survival, and cell metabolic profile within the hydrogels. Obtained data suggest that a low dose of DCA in permeable, biocompatible hydrogels can be beneficial for cells to combat hypoxic conditions.

1. Introduction

Hydrogels are three-dimensional networks of hydrophilic polymers within the liquid microenvironment. They mimic living tissues' softness and water content, making them prime materials for tissue engineering scaffolds, support structures for cell delivery, and potential effective matrices for drug delivery. Furthermore, the properties of hydrogels and nanogels are highly tuneable to specific applications [1,2]. Studies suggest an impactful role of amphiphilic molecules on hydrogels, mainly bile acids. Bile acids are canonically seen mainly as dietary emulsifiers, but recent research suggests they have a broader biological role [3–12]. Furthermore, Mooranian et al. successfully demonstrated the benefits of bile acids in an alginate matrix for cell encapsulation and drug delivery [13–25].

One of the possibly underutilised bile acids is deoxycholic acid (DCA). DCA is a secondary bile acid synthesised in the colon by gut biota from cholic acid [1]. DCA is common in the colon in normal conditions. It is currently used as a cosmetic agent to dissolve fat. However, elevated concentrations have been linked with inflammation, increased apoptosis of epithelial cells, and inhibition of wound healing of colon epithelium [26]. Excessive levels are also linked with disruptions in the intestinal mucosal barrier and the promotion of intestinal tumorigenesis [27].

DCA is a hydrophobic molecule with a steroid structure, capable of forming micelles and nanoparticles with polymers, notably polysaccharides [28,29]. DCA increases interaction with cell membranes in these structures and enhances cell permeation. Therefore, DCA conjugates are used in gene delivery as non-viral gene carriers with negligible toxicity [30]. Oh et al. used DCA–conjugated polyethyleneimine to deliver Heme Oxygenase-1, while Kim et al. used a similar complex as a cardiac siRNA-carrier [31,32].

DCA is also used in cosmetic surgery due to its higher affinity to adipocyte membranes than other cells' membranes. DCA injection to an area with redundant fat is a non-invasive, well-tolerated procedure with

* Corresponding authors at: The Biotechnology and Drug Development Research Laboratory, Curtin Medical School & Curtin Health Innovation Research Institute, Curtin University, Bentley, Perth, WA 6102, Australia
E-mail addresses: armin.mooranian@curtin.edu.au (A. Mooranian), hani.al-salami@curtin.edu.au (H. Al-Salami).

https://doi.org/10.1016/j.colsurfb.2022.113014
Received 17 August 2022; Received in revised form 19 October 2022; Accepted 8 November 2022
Available online 11 November 2022

much less risk than classic liposuction or cryolipolysis. This procedure is FDA-approved and successful in various sites [35–38].

We developed novel DCA based copolymer hydrogels using poloxamer 407 and alginate mix. Different poloxamer-alginate hydrogels are known, including alginate/poloxamer/silk fibroid hydrogel for cartilage tissue engineering by Liu et al. [56], while Moebus et al. engineered alginate/poloxamer microparticles for controlled protein release [57]. Recently, Popescu et al. separately modified alginate and poloxamer with photopolymerisation responsive moieties before cross-linking and demonstrated anti-inflammatory effects of alginate/poloxamer in wound treatment [58]. To our knowledge, DCA-based alginate/poloxamer hydrogels have not been reported in the literature so far.

As these hydrogels have potential use in cell delivery and tissue engineering, we assessed their rheology and biological impact on several cell lines, including viability and cellular respiration and survivability under stressful hypoxic conditions.

2. Methods

2.1. Materials

Poloxamer 407 (99%), deoxycholic acid (DCA, 99%) and sodium alginate (Low viscosity SA, 99%) were acquired from Sigma Chemical Co (St. Louis, MO, USA). Foetal bovine serum (FBS), Dulbecco's modified Eagle's medium (DMEM), and needed supplements and reagents were acquired from Sigma Chemical Co (St. Louis, MO, USA).

2.2. Hydrogel preparation

Seven formulations were prepared including control. Stock solutions were prepared for each formulation, consisting of SA (1.4%; formulations 1–7), poloxamer 407 (4.5%; formulations 2–7), and DCA (0.1%, 0.3%, 0.9%, 1.1% and 1.6%; formulations 3–7 respectively). All ingredients were measured and mixed with water. To completely dissolve them, they were put on 45 °C for 6 h, and mixed constantly. After SA completely dissolved, gels were stored at 4 °C. Gels were completely consumed within 2 days for pharmaceutical examinations and biological analyses. For biological assays, 20 μL of hydrogel was placed in a 96 well plate and left for 30 min under UV light. After that, freshly detached and separated cells were added to the hydrogels and thoroughly mixed. After mixing, appropriate cell media was added and mixed thoroughly for 1 min.

2.3. Rheology and liquid analysis measurements

Rheological parameters and relevant analyses were carried out using a Visco-88 viscometer (Malvern Panalytical/Instruments, Malvern, UK). Various rotation speeds and analytical parameters were used to measure each formulation's viscosity, shear stress, and rate in the instrument cap [39–41]. A sample for each formulation was prepared, mixed thoroughly, weighted and placed in the cap of the instrument as per manual guide and based on best practice, well established in our lab. A Mastersizer 3000 (Malvern, UK) to measure Z-potential values and particle size of the various formulations. Surface tension was also measured by a tensiometer (Sigma 703) as per manufacturer's guidelines and best practice [42]. All measurements were performed at room temperature and samples were freshly made prior to measurements.

2.4. SEM imaging

Hydrogel samples were freeze dried using Dynavac FD3 Freeze Dryer (Dynapumps, Seven Hills, Australia), for 96 h. Scanning electron microscope (SEM) imaging was done on freeze-dried and platinum-coated hydrogel samples by Zeiss Neon 40Esb FIBSEM, Carl Zeiss Microscopy GmbH, Jena, Germany [43–54].

2.5. Cell lines

Based on widely published protocols, a hepatic murine cell line (AML 12) was cultured in DMEM with 10% FBS and recommended supplements and conditions needed for best growth [55]. Similarly, muscle cell line (C2C12) were cultured in DMEM with 10% FBS based on well established and verified protocols [56]. The pancreatic β-cell line (NIT-1) was cultured based on well-established protocols in our laboratory, and was grown in DMEM with supplemented 10% FBS and 5.5 mmol glucose (all purchased from Sigma-Aldrich, MO, USA) with free amino acids supplied as per our protocols [46]. The cultured cells were incubated in a humidified 5% CO2 hemisphere at temperature of 37 °C. The media was changed approximately every 24 h (for C2C12) and 48 h timeframe (for AML-12 and NIT-1), respectively.

2.6. Cell viability

Multiple MTT (2,5-diphenyl-2,4,5-trimethylthiazol-2-yl) assays were carried out to assess mitochondrial activity as an index of cell viability, and to observe the impact of various hydrogels on cellular ability to proliferate, which was compared with control (no hydrogels). Cell viability was measured as a percentage of pre-intervention i.e. pre hydrogel intervention. Stock MTT solutions were prepared at a concentration of 5 mg/mL and were consumed within 24 h of preparation and used immediately after preparation. All groups treated with hydrogels were cultured, grown and interventions added in the exact same way, including controls.

One day after incubation of cells in each well and intervention application, 20 μL of MTT stock solution was added. Using a plate reader, MTT formazan (created by mitochondrial reductase) and dissolved in dimethyl sulfoxide (DMSO), was measured in each well, and correlated to mitochondrial reductase levels and hence, correlated with percentage of cell viability in each well based on our established protocols [41]. Obtained data were normalised and presented as a percentage of viable cells relevant to control.

2.7. Hypoxia assays

Cells were freshly detached and were mixed with different solutions of $CoCl_2$ in appropriate cell media and left for 20–30 min before incorporating them into the hydrogels. After mixing the cells and the hydrogels including control, the rest of the $CoCl_2$ enriched media was added. Cells were left to incubate for one day, and their viability was determent with a subsequent MTT assay. $CoCl_2$ concentrations used were 50 μM for low hypoxic conditions and 100 μM for high hypoxic conditions as appropriate [15,57].

2.8. Bioenergetic measurements

After one day incubation with the hydrogels, real-time mitochondrial and non-mitochondrial activities were measured in AML 12, C2C12, and NIT-1 cells using a Seahorse Flux Analyser XF 96 (Seahorse Bioscience, USA), using an in house developed method [39,58].

2.9. Statistics

Data were shown as a mean ± SEM with $n = 3$. For data statistical assessments, relevant correlation, regression, and one/two way ANOVA analyses were conducted with posthoc comparisons of means, as appropriate. Statistical software utilised was GraphPad Prism version 9.0 (GraphPad, Inc., USA), and the data were considered statistically significant at $p < 1\%$ or $< 5\%$.

3. Results and discussion

Different rheological parameters of DCA-based hydrogels are shown

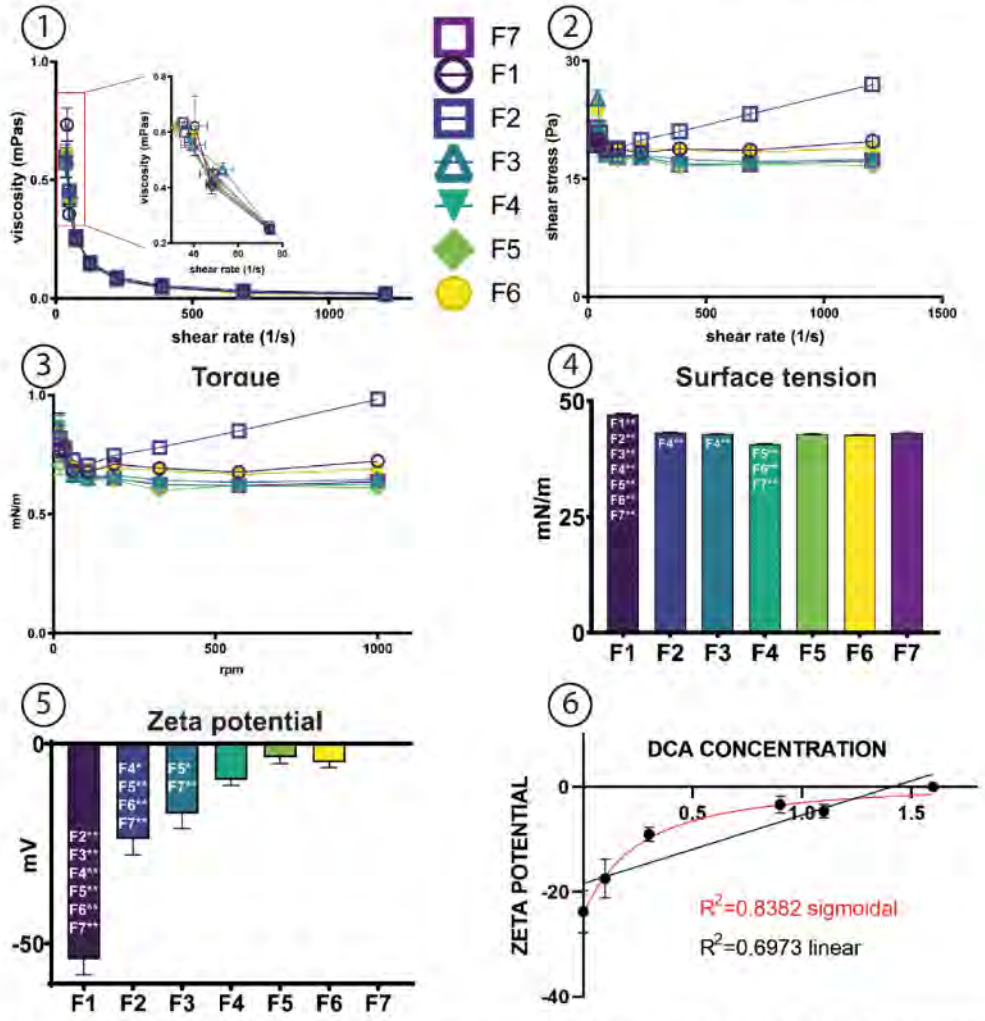

Fig. 1. Parameters of novel DCA-based hydrogels: 1) viscosity, 2) shear stress, 3) torque, 4) surface tension, 5) zeta potential, and 6) mathematical model of zeta potential and DCA concentration regression. Data are mean ± SEM, n = 3, ** $p < 0.05$ and * $p < 0.01$.

in Fig. 1. All hydrogels show a decrease in viscosity with an increase in shear rate suggesting that when shear stress is increased, shear flow follows and at the molecular level, the hydrogels are thinner and flow better (Figure 1.1). This is typical of the shear-thinning behaviour of non-Newtonian fluids. Under the shear-induced reorganisation, the polymeric network morphs into a more stretched conformation, decreasing its entanglement and lowering viscosity [59]. The addition of poloxamer 407 or different concentrations of DCA did not impact this ability nor significantly changed viscosity, suggesting that those molecules were incorporated into alginate's polymeric network. Non-Newtonian behaviour is confirmed by the values of shear stress (Figure 1.2) and torque (Figure 1.3). Alginate (F1) had the highest surface tension of all hydrogels, while the addition of DCA affected surface tension only in F4, with a significant decrease (Figure 1.4). Wagle et al. similarly noted no significant change in surface tension after adding bile acid to the polymer matrix [45]. F1 had the highest surface charge (Figure 1.5), while F7 had a neutral surface charge. The addition of poloxamer (F2) and DCA (F3, F4, F5, F6, F7) decreased the total charge. There seems to be a relationship between surface charge and DCA concentration (Figure 1.6). Different mathematical models were utilised to describe this effect, showing that the non-linear model fits better (84%). Bile-acids' amphiphilic nature can explain the DCA effect on polymers, and it is vital as Zeta potential directly affects cell survival. Polymers with considerable charges, especially positive charges, have more significant cell membrane interaction and lead to cell toxicity [60]. Therefore, DCA can have a beneficial effect on cell survival by reducing the surface charge.

Introduction of different materials to SA had profound impact on

hydrogel structure. As presented on Fig. 2, SEM micrographs of F1 (SA only) show smooth, thin and film-like structure (Figure 2.1, 2.2), with surface pores visible only at high magnification (Figure 2.3). Addition of poloxamer 407 to sodium alginate in F2 significantly modified hydrogel structure (Figure 2.4 and 2.5), leading to thicker, more robust structure with smother surface without visible pores (Figure 2.6). Introduction of DCA to SA-poloxamer 407 matrix modifies hydrogel structure even further (Figure 2.7 and 2.8), with appearance of small round particles on surface, or just beneath the surface of hydrogel (Figure 2.9). These particles seems to be around or less than 1 micrometre in diameter, and they appear toform clusters. A similar structure can be observed in other formulations with DCA (Figure 2.10-Figure 2.21). However, with increase of DCA concentration in formulations, there are some differences in particle appearance. F4 and F7 (Figure 2.12 and 2.21) have larger and more misshapen particle clusters, that seem less integrated into polymer matrix than those of F5 and F6 (Figure 2.15 and 2.16). Furthermore, particle clusters seem to be absent from outer, undisturbed surfaces (Figure 2.7, 2.10, 2.13, 2.16, 2.19), and may be underneath the external polymer layer (Figure 2.11). This is in concurrent with previous study done by Mooranian et al., which showed that bile acid is concentrated within the inner parts of alginate microcapsules, rather than staying on the surface [61].

The biological effects of DCA-based hydrogels are variable, as presented in Fig. 3 [1–3]. Even though it is one of the most commonly used polymers in cell delivery [16, 45, 62–64], alginate (F1) substantially decreased viability in all cell types. The addition of poloxamer 407 (F2) increased viability across all three cell lines, with high significance for AML 12 and C2C12. NIT-1 and C2C12 demonstrated similar behaviour in DCA hydrogels – F3 and F4 have higher viability, statistically not different from F2. In contrast, F5, F6 and F7 have similar low viability, suggesting that concentrations of 0.9 w/w% and above in hydrogel have a detrimental effect on the survival of muscle and pancreatic beta cells.

For hepatic cells, the impact of DCA hydrogels is different. The peak of viability is achieved with F5, significantly higher than with any other hydrogel formulation. Similar viability is seen among F3, F4 and F5, which are all significantly higher than F7. Hepatic cells benefited the most from DCA addition to hydrogel, having the highest viability within F5. Muscle and pancreatic beta cells experienced a significant unfavourable effect on survivability at the same concentration. As hydrophobic bile acid, DCA has been linked with hepatocyte apoptosis, promotion of ROS production, the release of cytochrome c and the cause of mitochondrial permeability transition [65]. This, at least within specific DCA concentrations, is not consistent with our findings; therefore, we decided to examine the cellular respiration of these cells and determine the impact DCA may have on ROS production and mitochondrial health.

Bioenergetics of AML 12 support the beneficial effect of F5 (Fig. 4). F5 showed favourable metabolic parameters compared to other hydrogels, including the highest maximal respiration in the presence of hydrogels (Figure 4.2), basal respiration (Figure 4.3), and ATP production (Figure 4.7), significantly not different to values of hydrogel free cells. Increased basal respiration is linked with increased ATP turnover, while high ATP production reflects high ATP demand consistent with a metabolically active cell. Increased maximal respiration is linked with increased mitochondrial mass, substrate availability and good integrity of the electron transport chain (ETC). Furthermore, proton leak (Figure 4.4) and non-mitochondrial oxygen consumption (Figure 4.5) were lower than free cells. Common proton leak further confirms good ETC and membrane integrity, while low non-mitochondrial oxygen consumption is linked with low extramitochondrial ROS.

In contrast, AML 12 in F2 have a high metabolism (Figure 4.1), but most oxygen consumption is consumed outside mitochondria, demonstrating high non-mitochondrial oxygen consumption (Figure 4.5). This is potentially linked with increased ROS levels in cytosol, possibly

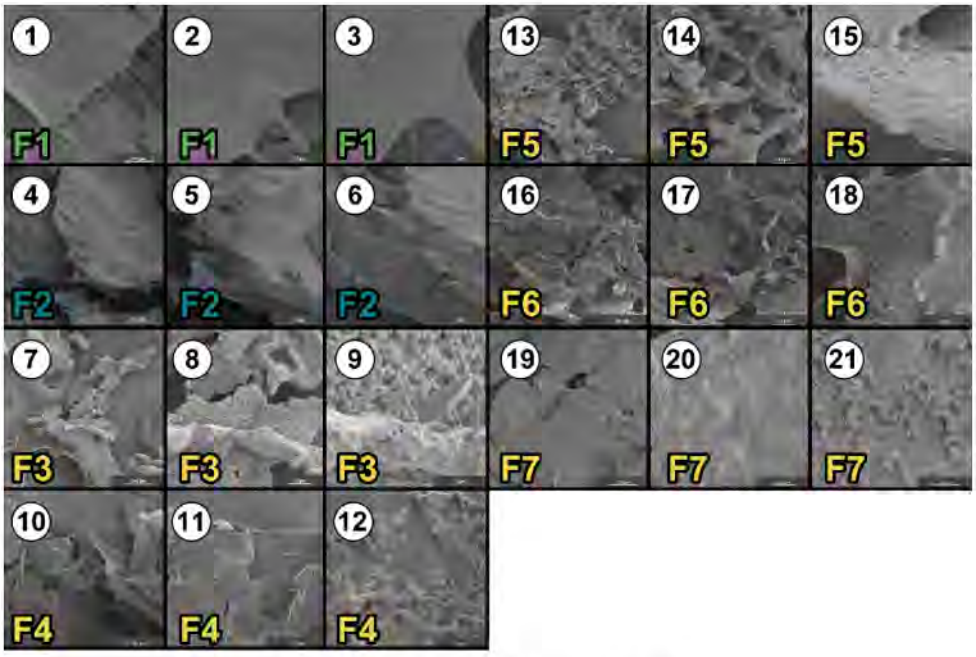

Fig. 2. Showing SEM micrographs of freeze dried hydrogels.

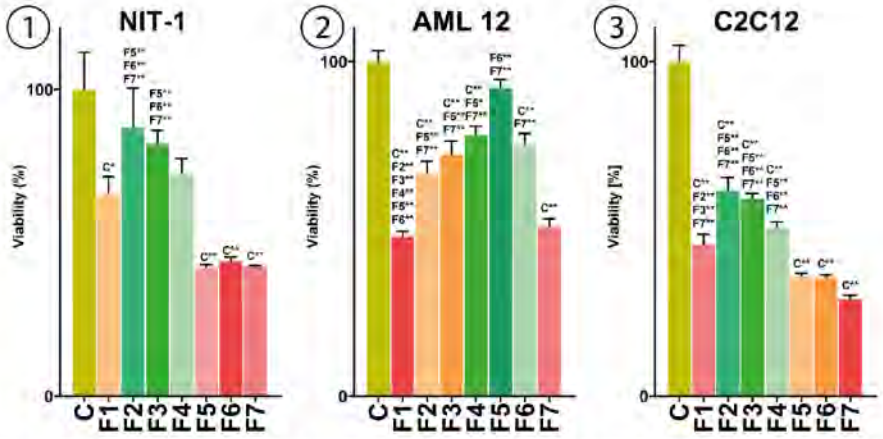

Fig. 3. Viability of 1) NIT-1 cells, 2) AML 12 cells, and 3) C2C12 cells in the presence of hydrogels after 24 h incubation. Data are mean ±SEM, n = 3, * $p < 0.05$ and ** $p < 0.01$.

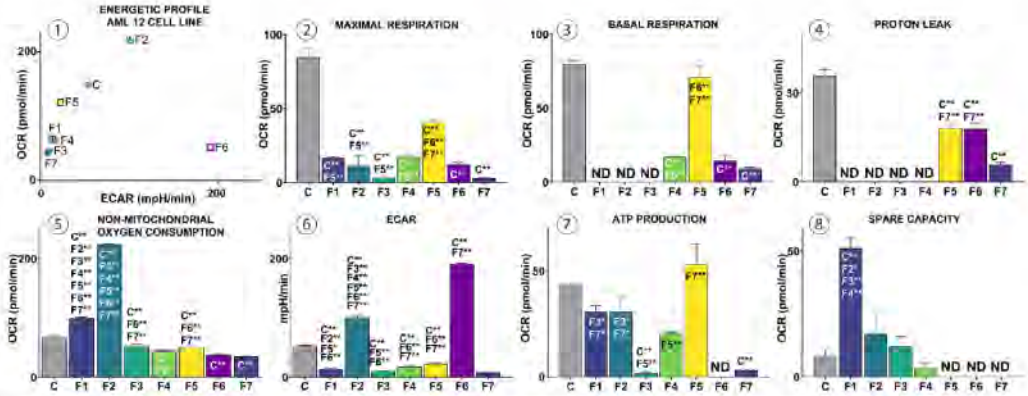

Fig. 4. Bioenergetics of AML 12 cell line showing 1) energetic profile, 2) maximal respiration, 3) basal respiration, 4) proton leak, 5) non-mitochondrial oxygen consumption, 6) extracellular acidification rate (ECAR), 7) ATP production, and 8) spare capacity. Data are mean ±SEM, n = 3, ** $p < 0.05$ and * $p < 0.01$.

originating from damaged mitochondria. Damage to the mitochondrion is further implicated by low maximal respiration and negligible basal respiration, possibly linked with poor ETC integrity, decreased mitochondrial mass and low substrate availability [66]. With all metabolic parameters taken together, cells in the presence of F2 seem to be consuming more oxygen than control. However, their damaged mitochondrial metabolism is likely to further acerbate cell hypoxia and ROS production, which might explain low viability in high oxygen consumption. ECAR values (Figure 4.6) seem to be tied with glycolytic metabolism, shifting cell bioenergetics to anaerobic metabolism. This is evident in cells within F6, with low maximal and basal respiration, negligible ATP production (Figure 4.7) and high ECAR. Based on this, it is possible that an increase of DCA levels above optimum (F5) leads to anaerobic adaptation (F6) and further to quiescent metabolism (F7) in hepatic cells (Figure 4.1). As non-mitochondrial oxygen consumption does not increase with every increase in DCA levels (Figure 4.5), it is possible that DCA is not connected with oxidation production, contrary to previous studies that linked DCA, to a certain extent, to increased free radical generation [67,68]. However, as seen above, the DCA effect is heavily concentration-dependent, and at higher concentrations, it may lead to a generation of free radicals and other physiological changes that play a role in such findings.

Energetic profile of C2C12 cells seems to be increased for most groups (except F7), compared to cell free control (Fig 5.1). F1 has non-measurable basal metabolism and ATP production, with most OCR used for non-mitochondrial oxygen consumption, suggesting that hypoxia and ROS generation cause low viability. Similarly to increased viability to F1, muscle cells in the presence of F2, F3, and F4 show favourable basal and maximal respiration (Figure 5.2 and 5.3), proton leak (Figure 5.4), and ATP production (Figure 5.7). F2 has the lowest non-mitochondrial oxygen consumption, which may have influenced the highest viability among all hydrogels (Figure 3.3). Low viability of highly metabolically active F5 can be linked with high proton leak and non-mitochondrial oxygen consumption, ROS generation, electron slippage and disrupted ETC integrity. High basal metabolism is the result of high proton leak. As proton leak is higher than ATP production, this shows stressed cells experiencing increased ROS generation and hypoxia. This is further confirmed with increased ECAR (Figure 5.7),

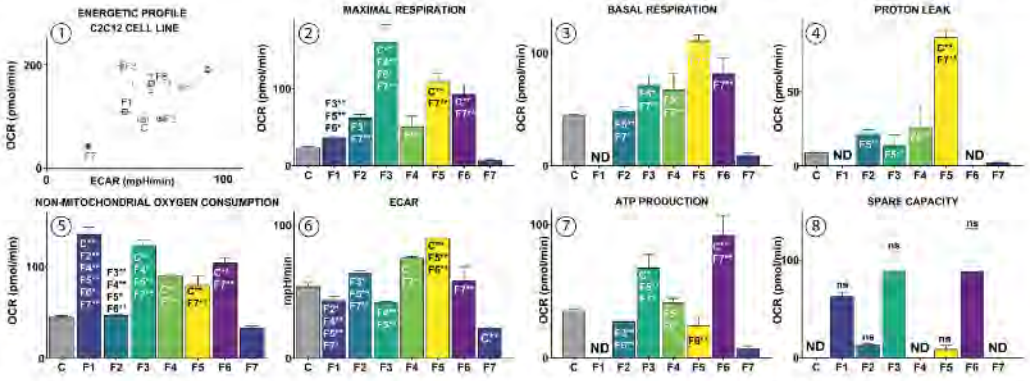

Fig. 5. Bioenergetics of C2C12 cell line showing 1) energetic profile, 2) maximal respiration, 3) basal respiration, 4) proton leak, 5) non-mitochondrial oxygen consumption, 6) extracellular acidification rate (ECAR), 7) ATP production, and 8) spare capacity. Data are mean ±SRM, n = 3, * $p < 0.05$ and * * $p < 0.01$.

suggesting a shift to anaerobic glycolysis due to substrate deficiency. Cells in F6 showed favourable bio-metabolic parameters, including increased maximal and basal respiration, ATP production and spare capacity, low proton leak and ECAR, similar to the control. However, F6 showed significantly higher non-mitochondrial oxygen consumption than control, suggesting high free radicals in the cytosol. This may contribute to low viability, despite seemingly healthy metabolism. F7 shows quiescent metabolism related to low viability, with high non-mitochondrial oxygen consumption compared to basal and maximal respiration and ATP production. High non-mitochondrial consumption rates were found within all cells exposed to DCA (F3, F4, F5, F6, F7), suggesting that high rates of free radicals are responsible for the low viability of muscle cells. This is concurrent with the recent study done by Abrigo et al., which observed the atrophic effect of DCA on C2C12 cells through activation of the TGR5 receptor and subsequent free radical generation [69].

The cellular metabolism of NIT-1 cells is shown in Fig. 6 (1-8). Pancreatic beta cells within F1, F2 and F3 hydrogels seem to have majorly increased oxygen consumption compared to control in normal conditions. High oxygen consumption might be a sign of substrate availability and increased metabolism and considers all oxygen demanding processes in a cell. However, the majority of that high oxygen demand seems to be used for non-mitochondrial oxygen consumption. Non mitochondrial oxygen consumption can vary from undetectable to 60% of oxygen consumption, depending on cell type. It is used for various processes in a cell, including lipid and collagen synthesis, DNA and histone demethylation and protein folding. However, increased values are suggested due to potential superoxide production by the NADPH oxidase (Nox) protein family in the plasma membrane [70,71]. Compared to the last three hydrogels, higher viability of F1, F2, F4, and F4 can be linked to basal respiration, as cells in the first four hydrogels managed to preserve detectable basal metabolism. In contrast, low viability F5, F6 and F7 had insignificant basal metabolism and meagre total oxygen consumption. NIT-1 cells within F7 hydrogel showed similar behaviour to AML-12 cells in F6, displaying visible elevated media acidification and shift to glycolytic metabolism that seems to have a significant impact on cellular performance, over time.

Because most cells retained some robustness of metabolism, the aim was to test their resilience in hydrogels under stressful hypoxic conditions. Conditions that mimic hypoxia were achieved through $CoCl_2$ cell exposure. Various cell lines respond differently to the presence of cobalt chloride. AML 12 control cells show a viability increase in the presence of low CoCl2 concentration, while, in contrast, C2C12 shows a decrease in viability under the same conditions but increases survivability in the presence of a more hypoxic reagent (Fig. 7, 1-12). Furthermore, control NIT-1 cells have a decrease in viability dependent on CoCl2 concentration. This disparity in cell responses is in line with a study done by

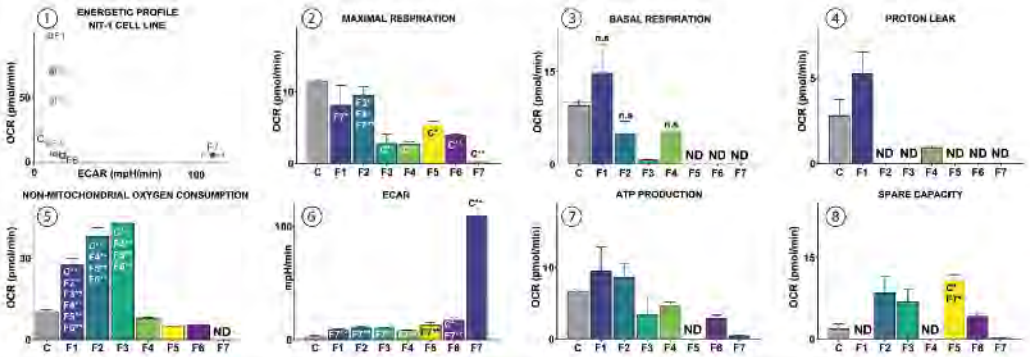

Fig. 6. Bioenergetics of NIT-1 cell line showing 1) energetic profile, 2) maximal respiration, 3) basal respiration, 4) proton leak, 5) non-mitochondrial oxygen consumption, 6) extracellular acidification rate (ECAR), 7) ATP production, and 8) spare capacity. Data are mean ± SEM, n = 3, * $p < 0.05$ and * * $p < 0.01$.

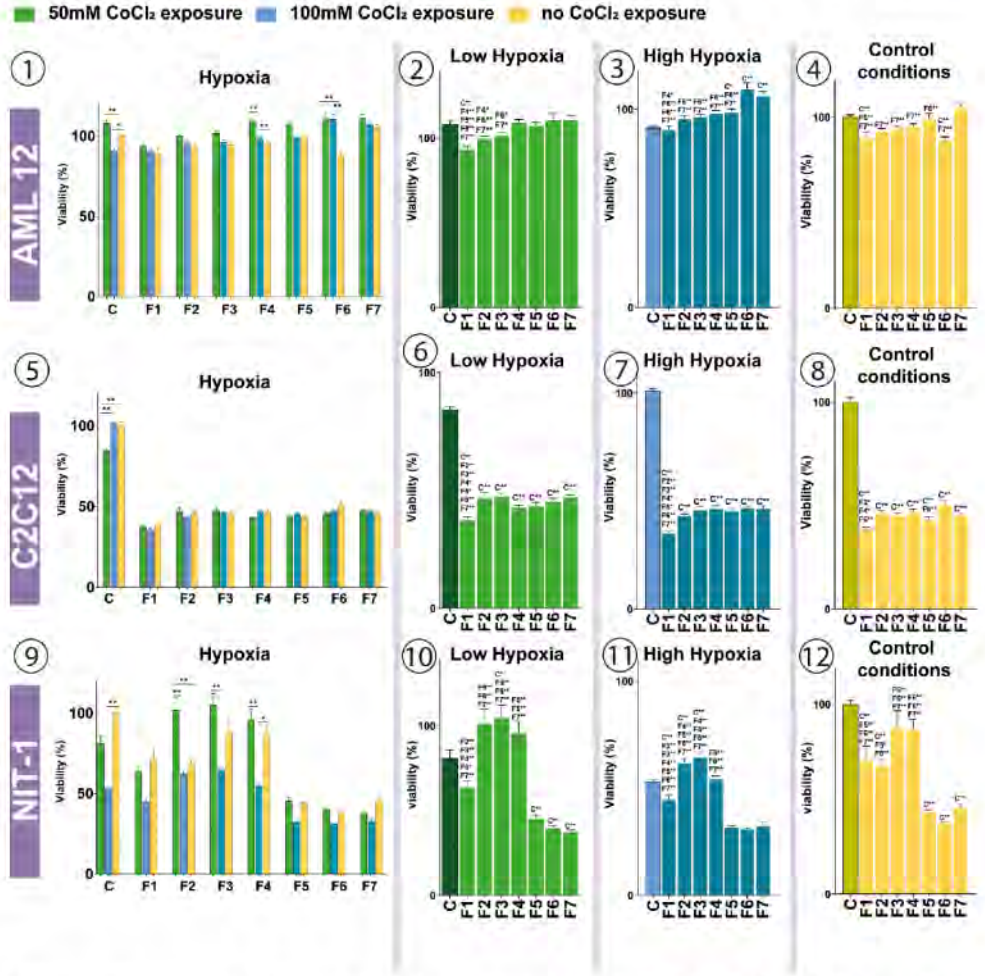

Fig. 7. Viability of 1) AML 12, 5) C2C12 and 9) NIT-1 under different hypoxic conditions. Viability of AML 12 under 2) low hypoxia, 3) high hypoxia, and 4) control conditions. Viability of C2C12 under 5,6) low hypoxia, 7) high hypoxia, and 8) control conditions. Viability of NIT-1 under 9,10) low hypoxia, 11) high hypoxia, and 12) control conditions. Data are mean ± SEM, n = 3, ** $p < 0.05$ and * $p < 0.01$.

Horev-Azaria et al., which demonstrated various affinities of different cell lines to cobalt [72].

Most hydrogels (F1, F2, F3, F5 and F6) modified AML-12 viability and kept it similar under all conditions (Figure 7.1), meaning they did not allow for an increase of viability in 50 μM $CoCl_2$ nor a significant decrease in 100 μM CoCl2. Since cells were treated with CoCl2 prior to mixing with hydrogel, and hydrogel's permeability, we assumed that it was not a physical barrier of hydrogel that protected cells from CoCl2 exposure. This suggests the protective effect of DCA-based hydrogels under stressful conditions. The best example can be seen within F6. AML 12 cells in F6 had significantly increased viability under hypoxic conditions compared to the control conditions. Furthermore, F6 decreased the viability of cells under control conditions compared to the control cells and increased it under harsher hypoxia. This may be explained by the promotion of glycolic metabolism by hydrogel, as shown above (Fig. 4), facilitating survival in hypoxic conditions.

Muscle cells have no significant difference in control conditions with 100 μM CoCl2. However, they have significantly higher viability in described conditions than viability in a lower hypoxic environment (50 μM CoCl2). Similarly to Figure 3.3, C2C12 cells have significantly reduced viability within all hydrogels in all conditions, with the lowest survivability detected within F1, suggesting that the addition of poloxamer (F2) and DCA may be more favourable to cell survival (Figure 7.6, 7.7, and 7.8). Hydrogels had a protective effect on C2C12, negating hypoxia effects on cells, similarly to the effect observed in AML 12.

Unlike hepatic or muscle cells, pancreatic beta cells retained a similar pattern of viability under different hypoxic conditions to control cells, with the lowest viability in the highest hypoxic environment. Hydrogels with poloxamer and lower concentrations of DCA -F2, F3, and F4, showed the best performance in hypoxic conditions, with increased

viability compared to non-hypoxic conditions.

In control conditions, viability within these hydrogels was not significantly different from viability in alginate (F1). Formulations with DCA concentrations above 0.3% w/w, F5, F6 and F7 have similar low viability under all conditions. F7 did not show better viability in hypoxic conditions regardless of high affinity to anaerobic metabolism (Figure 6.6), unlike AML 12 cells in F6. This can be explained by negligible mitochondrial metabolism in NIT-1 cells within F7 (Figures 6.2, 6.3 and 6.7), while AML 12 cells preserved basal and maximal respiration (Figures 4.2 and 4.3). This study used murine cell lines as part of preclinical data to evaluate hydrogels' cellular biocompatibility and overall cell performance with several well-established techniques.

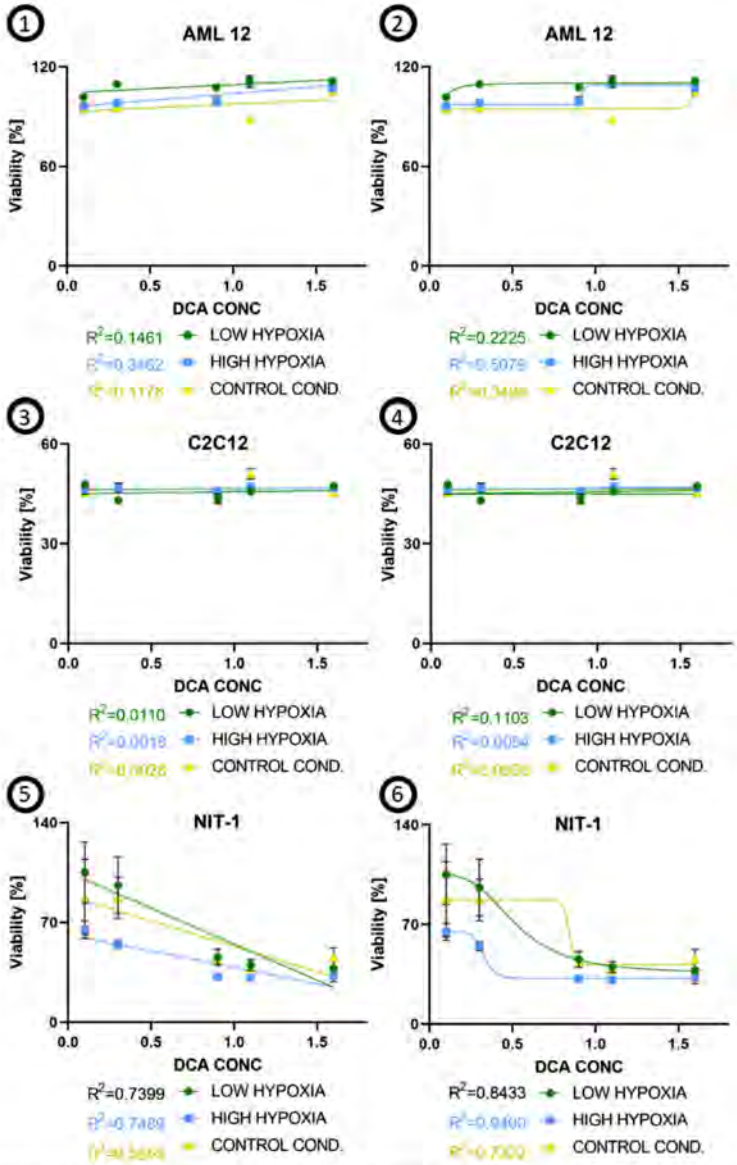

Fig. 8. Mathematical models of DCA concentration impact on cell viability under different hypoxic conditions 1) AML 12 cell line, linear model, 2) AML 12 cell line, non-linear model, 3) C2C12 cell line, linear model, 4) C2C12 cell line, non-linear model, 5) NIT-1 cell line, linear model, and 6) NIT-1 cell line, non-linear model. Data are mean ± SEM, n = 3, ** $p < 0.05$ and * $p < 0.01$.

Further research is required to expand the clinical significance of the proposed hydrogels.

To better understand the impact of DCA in hydrogels on various cell lines, we made different mathematical models, as some cells are more responsive to bile acids (Fig. 8, 1–6). There are no ideal and fully-described and in-depth established mathematical models that can fully explain the effects of bile acid on the viability of the cells at the various amounts of oxygen for AML 12 and C2C12 cells. Cells that showed better viability under hypoxic conditions (AML 12 and C2C12) were not critically responsive to DCA, indicating that cells that prefer hypoxia are not affected by an increase in DCA concentration. In contrast, DCA concentration has a growing impact with an increase in hypoxia in NIT-1 cells (Figures 8.5 and 8.6). Biodegradation of hydrogels and controlled release of DCA in cell media should have minimal impact, as poloxamer 407 is not biodegradable, and alginate was not cross-linked. Cross-linked alginate biodegrades in the body primarily by an ion exchange process, which results in the loss of divalent ions responsible for cross-linking alginate chains [73,74].

4. Conclusion

This study investigated novel DCA-based copolymer hydrogels regarding rheological properties and biological effects on murine hepatic, muscle and pancreatic beta cells. All hydrogels retained shear-thinning behaviour, while DCA concentration modified zeta potential. Lower concentrations of DCA in hydrogels are possibly linked with higher viability in all cells. In comparison, higher concentrations are mostly linked with high non-mitochondrial oxygen consumption, and cells seem to shift to anaerobic metabolism. This effect proved beneficial under hypoxic stress for hepatic and muscle cells, allowing for possible retainment of viability in a hypoxic environment. Pancreatic beta cells, in turn, were more sensitive to DCA impact under hypoxic conditions than in a normal environment. The unique ability of DCA to enable cells to withstand hypoxia conditions by readapting, reconditioning and restructuring their biocellular processes and effects, may help with preconditioning cells expected to undergo hypoxic stress, present in various drug delivery systems. Presented data suggest that a low dose of DCA in permeable, biocompatible hydrogels can be beneficial for cells to combat hypoxic conditions.

5. Disclaimer

The authors would like to acknowledge the Australian Postgraduate Award (APA) and Curtin Research Scholarship (CRS). The authors also acknowledge the Microscopy and Microanalysis Facility at Curtin University.

The work is partially supported by the European Union Horizon 2020 research project and innovation program under the Marie Sklodowska-Curie Grant Agreement No 872370. Curtin Faculty ORS-WAHAI Consortium and the Australian National Health and Medical Research (APP9000597).

CRediT authorship contribution statement

Conceptualization, A.M., M.M. and H.A.-S.; Data curation, B.K., C.M. I., S.R.W., M.L., M.J.; Formal analysis, All authors; Funding acquisition, A.M., M.M., E.YM.W., G.S. and H.A.-S.; Investigation, All authors; Methodology, B.K., C.M.I., S.R.W., M.L., and M.J.; Project administration, M.Đ., E.YM.W., S.K., M.M. and H.A.-S.; Resources, A.M., M.M. and H.A.-S.; Software, All authors; Supervision, A.M., M.M. and H.A.-S.; Validation, All authors.; Visualization, B.K., C.M.I., S.R.W., M.L., M.J; Writing—original draft, B.K.; Writing—review & editing, All authors. All authors have read and agreed to the published version of the manuscript.

Declaration of Competing Interest

The authors declare the following financial interests/personal relationships which may be considered as potential competing interests: Hani Al-Salami reports financial support was provided by European Union Horizon 2020 research project. Hani Al-Salami reports financial support was provided by Curtin Faculty ORS-WAHAI Consortium and the Australian National Health and Medical Research.

Data availability

Data will be made available on request.

Appendix A. Supporting information

Supplementary data associated with this article can be found in the online version at doi:10.1016/j.colsurfb.2022.113014.

References

[1] Y.S. Zhang, A. Khademhosseini, Advances in engineering hydrogels, Science 356 (6337) (2017) eaaf3627.
[2] H. Kamata, Y. Akagi, Y. Kayasuga-Kariya, Chung U-i, Sakai T. "Nonswellable" hydrogel without mechanical hysteresis, Science 343 (6173) (2014) 873–875.
[3] F. Kuipers, V.W. Bloks, A.K. Groen, Beyond intestinal soap—bile acids in metabolic control, Nat. Rev. Endocrinol. 10 (2014) 488.
[4] B. Kovacevic, M. Jones, C. Ionescu, D. Walker, S. Wagle, J. Chester, et al., The emerging role of bile acids as critical components in nanotechnology and bioengineering: pharmacology, formulation optimizers and hydrogel-biomaterial applications, Biomaterials (2022), 121459.
[5] A. Mooranian, M. Jones, D. Walker, C.M. Ionescu, S.R. Wagle, B. Kovacevic, et al., Pharmacological dose-effect profiles of various concentrations of humanised primary bile acid in encapsulated cells, Nanomaterials 12 (2022) 4.
[6] A. Mooranian, M. Jones, C.M. Ionescu, D. Walker, S.R. Wagle, B. Kovacevic, et al., Pharmaceutical formulation and polymer chemistry for cell encapsulation applied to the creation of a lab-on-a-chip bio-microsystem, Ther. Deliv. 13 (1) (2022) 51–66.
[7] A. Mooranian, C.M. Ionescu, D. Walker, M. Jones, S.R. Wagle, B. Kovacevic, et al., Single-cellular biological effects of cholesterol-catabolic bile acid-based nano/micro capsules as anti-inflammatory cell protective systems, Biomolecules 12 (2022) 1.
[8] A. Mooranian, C.M. Ionescu, S.R. Wagle, B. Kovacevic, D. Walker, M. Jones, et al., Taurine grafted micro-implants improved functions without direct dependency between interleukin-6 and the bile acid lithocholic acid in plasma, Biomedicines 10 (2022) 1.
[9] A. Mooranian, J. Chester, E. Johnston, C.M. Ionescu, D. Walker, M. Jones, et al., Reduced cytokine tumour necrosis factor by pharmacological intervention in a preclinical study, Biomolecules 12 (7) (2022) 877.
[10] S. Lazarević, M. Đanic, H. Al-Salami, A. Mooranian, M. Mikov, Gut microbiota metabolism of azathioprine: a new hallmark for personalized drug-targeted therapy of chronic inflammatory bowel disease, Front. Pharmacol. (2022) 13.
[11] B. Kovacevic, M. Jones, C. Ionescu, D. Walker, S. Wagle, J. Chester, et al., The emerging role of bile acids as critical components in nanotechnology and bioengineering: Pharmacology, formulation optimizers and hydrogel-biomaterial applications, Biomaterials (2022) 283.
[12] B. Kovacevic, C.M. Ionescu, S.R. Wagle, M. Jones, M. Lewkowicz, E.Y. Wong, et al., Impact of novel Teflon-DCA nanogel matrix on cellular bioactivity, J. Pharm. Sci. (2022).
[13] A. Mooranian, S. Raj Wagle, B. Kovacevic, R. Takechi, J. Mamo, V. Lam, et al., Bile acid bio-nanoencapsulation improved drug targeted-delivery and pharmacological effects via cellular flux: 6-months diabetes preclinical study, Sci. Rep. 10 (1) (2020) 106.
[14] A. Mooranian, R. Negrulj, R. Takechi, E. Jamieson, G. Morahan, H. Al-Salami, Electrokinetic potential-stabilization by bile acid-microencapsulating formulation of pancreatic β-cells cultured in high ratio poly-L-ornithine-gel hydrogel colloidal dispersion: applications in cell-biomaterials, tissue engineering and biotechnological applications, Artif. Cells, Nanomed., Biotechnol. 46 (6) (2018) 1156–1162.
[15] A. Mooranian, R. Negrulj, H. Al-Salami, The incorporation of water-soluble gel matrix into bile acid-based microcapsules for the delivery of viable β-cells of the pancreas, in diabetes treatment: biocompatibility and functionality studies, Drug Deliv. Transl. Res. 6 (1) (2016) 17–23.
[16] A. Mooranian, R. Negrulj, F. Arfuso, H. Al-Salami, Characterization of a novel bile acid-based delivery platform for microencapsulated pancreatic β-cells, Artif. Cells, Nanomed., Biotechnol. 44 (1) (2016) 194–200.
[17] A. Mooranian, R. Negrulj, E. Jamieson, G. Morahan, H. Al-Salami, Biological assessments of encapsulated pancreatic β-cells: their potential transplantation in diabetes. cellular and molecular, Bioengineering 9 (4) (2016) 530–537.

[18] B. Kovacevic, C.M. Ionescu, M. Jones, S.R. Wagle, M. Lewkowicz, M. Đanić, et al., The effect of deoxycholic acid on chitosan-enabled matrices for tissue scaffolding and injectable nanogels, Gels 8 (6) (2022) 358.
[19] M. Jones, C.M. Ionescu, D. Walker, S.R. Wagle, B. Kovacevic, J. Chester, et al., Biguanide pharmaceutical formulations and the applications of bile acid-based nano delivery in chronic medical conditions, Int. J. Mol. Sci. 23 (2022) 2.
[20] S.R. Wagle, B. Kovacevic, C.M. Ionescu, D. Walker, M. Jones, L. Carey, et al., Pharmacological and biological study of microencapsulated probucol-secondary bile acid in a diseased mouse model, Pharmaceutics 13 (2021) 8.
[21] A. Mooranian, M. Jones, C.M. Ionescu, D. Walker, S.R. Wagle, B. Kovacevic, et al., Advancements in assessments of bio-tissue engineering and viable cell delivery matrices using bile acid-based pharmacological biotechnologies, Nanomaterials 11 (2021) 7.
[22] A. Mooranian, M. Jones, C.M. Ionescu, D. Walker, S.R. Wagle, B. Kovacevic, et al., Artificial cell encapsulation for biomaterials and tissue bio-nanoengineering: History, achievements, limitations, and future work for potential clinical applications and transplantation, J. Funct. Biomater. 12 (2021) 4.
[23] A. Mooranian, C.M. Ionescu, S.R. Wagle, B. Kovacevic, D. Walker, M. Jones, et al., Chenodeoxycholic acid pharmacology in biotechnology and transplantable pharmaceutical applications for tissue delivery: An acute preclinical study, Cells 10 (2021) 9.
[24] A. Mooranian, C.M. Ionescu, S.R. Wagle, B. Kovacevic, D. Walker, M. Jones, et al., Probucol pharmacological and bio-nanotechnological effects on surgically transplanted graft due to powerful anti-inflammatory, anti-fibrotic and potential bile acid modulatory actions, Pharmaceutics 13 (2021) 8.
[25] A. Mooranian, C.M. Ionescu, S.R. Wagle, B. Kovacevic, D. Walker, M. Jones, et al., Polyelectrolytes formulated with primary unconjugated bile acid optimised pharmacology of bio-engineered implant, Pharmaceutics 13 (2021) 10.
[26] M.S. Mroz, N.K. Lajczak, B.J. Goggins, S. Keely, S.J. Keely, The bile acids, deoxycholic acid and ursodeoxycholic acid, regulate colonic epithelial wound healing, Am. J. Physiol. -Gastrointest. Liver Physiol. 314 (3) (2018) G378–G387.
[27] L. Liu, W. Dong, S. Wang, Y. Zhang, T. Liu, R. Xie, et al., Deoxycholic acid disrupts the intestinal mucosal barrier and promotes intestinal tumorigenesis, Food Funct. 9 (11) (2018) 5588–5597.
[28] L. Li, N. Liang, D. Wang, P. Yan, Y. Kawashima, F. Cui, et al., Amphiphilic polymeric micelles based on deoxycholic acid and folic acid modified chitosan for the delivery of paclitaxel, Int. J. Mol. Sci. 19 (10) (2018) 3132.
[29] J.Y. Lee, C. Crake, B. Teo, D. Carugo, M. de Saint Victor, A. Seth, et al., Ultrasound-Enhanced siRNA Delivery Using Magnetic Nanoparticle-Loaded Chitosan-Deoxycholic Acid Nanodroplets, Adv. Healthc. Mater. 6 (8) (2017) 1601246.
[30] S.Y. Chae, S. Son, M. Lee, M.-K. Jang, J.-W. Nah, Deoxycholic acid-conjugated chitosan oligosaccharide nanoparticles for efficient gene carrier, J. Control. Release 109 (1) (2005) 330–344.
[31] J. Oh, M.S. Lee, J.H. Jeong, M. Lee, Deoxycholic acid–conjugated polyethylenimine for delivery of heme oxygenase-1 gene in rat ischemic stroke model, J. Pharm. Sci. 106 (12) (2017) 3524–3532.
[32] D. Kim, J. Hong, H.-H. Moon, H.Y. Nam, H. Mok, J.H. Jeong, et al., Anti-apoptotic cardioprotective effects of SHP-1 gene silencing against ischemia–reperfusion injury: Use of deoxycholic acid-modified low molecular weight polyethyleneimine as a cardiac siRNA-carrier, J. Control. Release 168 (2) (2013) 125–134.
[33] E.D. Deeks, Deoxycholic acid: a review in submental fat contouring, Am. J. Clin. Dermatol. 17 (6) (2016) 701–707.
[34] B. Ascher, K. Hoffmann, P. Walker, S. Lippert, U. Wollina, B. Havlickova, Efficacy, patient-reported outcomes and safety profile of ATX-101 (deoxycholic acid), an injectable drug for the reduction of unwanted submental fat: results from a phase III, randomized, placebo-controlled study, J. Eur. Acad. Dermatol. Venereol. 28 (12) (2014) 1707–1715.
[35] J.R. Montes, E. Santos, A. Chillar, Jowl reduction with deoxycholic acid, Dermatol. Surg. 46 (1) (2020) 78–85.
[36] J. Liu, Q. Fang, H. Lin, X. Yu, H. Zheng, Y. Wan, Alginate-poloxamer/silk fibroin hydrogels with covalently and physically cross-linked networks for cartilage tissue engineering, Carbohydr. Polym. 247 (2020), 116593.
[37] K. Moebus, J. Siepmann, R. Bodmeier, Novel preparation techniques for alginate–poloxamer microparticles controlling protein release on mucosal surfaces, Eur. J. Pharm. Sci. 45 (3) (2012) 358–366.
[38] I. Popescu, M. Turtoi, D.M. Suflet, M.V. Dinu, R.N. Darie-Nita, M. Anghelache, et al., Alginate/poloxamer hydrogel obtained by thiol-acrylate photopolymerization for the alleviation of the inflammatory response of human keratinocytes, Int. J. Biol. Macromol. 180 (2021) 418–431.
[39] S.R. Wagle, B. Kovacevic, C.M. Ionescu, D. Walker, M. Jones, L. Carey, et al., Pharmacological and biological study of microencapsulated probucol-secondary bile acid in a diseased mouse model, Pharmaceutics 13 (8) (2021) 1223.
[40] A. Mooranian, T. Foster, C.M. Ionescu, D. Walker, M. Jones, S.R. Wagle, et al., Enhanced bilosomal properties resulted in optimum pharmacological effects by increased acidification pathways, Pharmaceutics 13 (2021) 8.
[41] A. Mooranian, T. Foster, C.M. Ionescu, L. Carey, D. Walker, M. Jones, et al., The effects of primary unconjugated bile acids on nanoencapsulated pharmaceutical formulation of hydrophilic drugs: Pharmacological implications, Drug Des., Dev. Ther. 15 (2021) 4423–4434.
[42] A. Mooranian, L. Carey, C.M. Ionescu, D. Walker, M. Jones, S.R. Wagle, et al., The effects of accelerated temperature-controlled stability systems on the release profile of primary bile acid-based delivery microcapsules, Pharmaceutics 13 (2021) 10.
[43] S.R. Wagle, D. Walker, B. Kovacevic, A. Gedawy, M. Mikov, S. Golocorbin-Kon, et al., Micro-Nano formulation of bile-gut delivery: rheological, stability and cell survival, basal and maximum respiration studies, Sci. Rep. 10 (2020) 1.
[44] S.R. Wagle, B. Kovacevic, D. Walker, C.M. Ionescu, U. Shah, G. Stojanovic, et al., Alginate-based drug oral targeting using bio-micro/nano encapsulation technologies, Expert Opin. Drug Deliv. 17 (10) (2020) 1361–1376.
[45] S.R. Wagle, B. Kovacevic, D. Walker, C.M. Ionescu, M. Jones, G. Stojanovic, et al., Pharmacological and advanced cell respiration effects, enhanced by toxic human-bile nano-pharmaceuticals of probucol cell-targeting formulations, Pharmaceutics 12 (8) (2020) 708.
[46] A. Mooranian, N. Zamani, M. Mikov, S. Goločorbin-Kon, G. Stojanovic, F. Arfuso, et al., A second-generation micro/nano capsules of an endogenous primary un-metabolised bile acid, stabilized by Eudragit-alginate complex with antioxidant compounds, Saudi Pharm. J. 28 (2) (2020) 165–171.
[47] A. Mooranian, R. Negrulj, F. Arfuso, Al-Salami H. Multicompartmental, multilayered probucol microcapsules for diabetes mellitus: Formulation characterization and effects on production of insulin and inflammation in a pancreatic β-cell line. Artificial Cells, Nanomed., Biotechnol. 44 (7) (2016) 1642–1653.
[48] A. Mooranian, R. Negrulj, F. Arfuso, H. Al-Salami, Characterization of a novel bile acid-based delivery platform for microencapsulated pancreatic beta-cells, Artif. Cells, Nanomed., Biotechnol. 44 (1) (2016) 194–200.
[49] A. Mooranian, R. Negrulj, H. Al-Salami, G. Morahan, E. Jamieson, Designing anti-diabetic β-cells microcapsules using polystyrenic sulfonate, polyallylamine, and a tertiary bile acid: Morphology, bioenergetics, and cytokine analysis, Biotechnol. Prog. 32 (2) (2016) 501–509.
[50] A. Mooranian, R. Negrulj, H. Al-Salami, Primary bile acid chenodeoxycholic acid-based microcapsules to examine β-cell survival and the inflammatory response, BioNanoScience 6 (2) (2016) 103–109.
[51] A. Mooranian, R. Negrulj, S. Mathavan, J. Martinez, J. Sciarretta, N. Chen-Tan, et al., Stability and release kinetics of an advanced gliclazide-cholic acid formulation: the use of artificial-cell microencapsulation in slow release targeted oral delivery of antidiabetics, J. Pharm. Innov. 9 (2014) 150–157.
[52] A. Mooranian, R. Negrulj, N. Chen-Tan, G.F. Watts, F. Arfuso, H. Al-Salami, An optimized probucol microencapsulated formulation integrating a secondary bile acid (deoxycholic acid) as a permeation enhancer, Drug Des., Dev. Ther. 8 (2014) 1673–1683.
[53] A. Mooranian, R. Negrulj, N. Chen-Tan, H.S. Al-Sallami, Z. Fang, T.K. Mukkur, et al., Microencapsulation as a novel delivery method for the potential antidiabetic drug, Probucol, Drug Des., Dev. Ther. 8 (2014) 1221–1230.
[54] A. Mooranian, R. Negrulj, N. Chen-Tan, H.S. Al-Sallami, Z. Fang, T. Mukkur, et al., Novel artificial cell microencapsulation of a complex gliclazide-deoxycholic bile acid formulation: a characterization study, Drug Des., Dev. Ther. 8 (2014) 1003–1012.
[55] M. Yuan, Z. Sun, R.K. Manthari, Y. Zhao, Q. Guo, K. Yang, et al., Arsenic-induced autophagy regulates apoptosis in AML-12 cells, Toxicol. Vitr. 72 (2021), 105074.
[56] Y. Manabe, S. Miyatake, M. Takagi, M. Nakamura, A. Okeda, T. Nakano, et al., Characterization of an Acute Muscle Contraction Model Using Cultured C2C12 Myotubes, PLOS ONE 7 (12) (2013), e52592.
[57] Q. Li, R. Ma, M. Zhang, CoCl2 increases the expression of hypoxic markers HIF-1α, VEGF and CXCR4 in breast cancer MCF-7 cells, Oncol. Lett. 15 (1) (2018) 1119–1124.
[58] S.R. Wagle, D. Walker, B. Kovacevic, A. Gedawy, M. Mikov, S. Golocorbin-Kon, et al., Micro-nano formulation of bile-gut delivery: rheological, stability and cell survival, basal and maximum respiration studies, Sci. Rep. 10 (1) (2020) 7715.
[59] M. Guvendiren, H.D. Lu, J.A. Burdick, Shear-thinning hydrogels for biomedical applications, Soft Matter 8 (2) (2012) 260–272.
[60] X.-R. Shao, X.-Q. Wei, X. Song, L.-Y. Hao, X.-X. Cai, Z.-R. Zhang, et al., Independent effect of polymeric nanoparticle zeta potential/surface charge, on their cytotoxicity and affinity to cells, Cell Prolif. 48 (4) (2015) 465–474.
[61] A. Mooranian, R. Negrulj, H. Al-Salami, Flow vibration-doubled concentric system coupled with low ratio amine to produce bile acid-macrocapsules of β-cells, Ther. Deliv. 7 (3) (2016) 171–178.
[62] A. Mooranian, R. Negrulj, H. Al-Salami, The Influence of Stabilized Deconjugated Ursodeoxycholic Acid on Polymer-Hydrogel System of Transplantable NIT-1 Cells, Pharm. Res. 33 (5) (2016) 1182–1190.
[63] Q. Liu, A. Chiu, L.-H. Wang, D. An, M. Zhong, A.M. Smink, et al., Zwitterionically modified alginates mitigate cellular overgrowth for cell encapsulation, Nat. Commun. 10 (1) (2019) 5262.
[64] M.A. Bochenek, O. Veiseh, A.J. Vegas, J.J. McGarrigle, M. Qi, E. Marchese, et al., Alginate encapsulation as long-term immune protection of allogeneic pancreatic islet cells transplanted into the omental bursa of macaques, Nat. Biomed. Eng. 2 (11) (2018) 810–821.
[65] S. Wei, X. Ma, Y. Zhao, Mechanism of hydrophobic bile acid-induced hepatocyte injury and drug discovery, Front Pharm. 11 (2020) 1084.
[66] B.G. Hill, G.A. Benavides, J.R. Lancaster, S. Ballinger, L. Dell'Italia, J. Zhang, et al., Integration of cellular bioenergetics with mitochondrial quality control and autophagy, Biol. Chem. 393 (12) (2012) 1485–1512.
[67] A. Hino, M. Morita, M. Une, K. Fujimura, T. Kuramoto, Effects of deoxycholic acid and its epimers on lipid peroxidation in isolated rat hepatocytes, J. Biochem. 129 (5) (2001) 683–689.
[68] C.M.P. Rodrigues, G. Fan, P.Y. Wong, B.T. Kren, C.J. Steer, Ursodeoxycholic acid may inhibit deoxycholic acid-induced apoptosis by modulating mitochondrial transmembrane potential and reactive oxygen species production, Mol. Med. 4 (3) (1998) 165–178.
[69] J. Abrigo, F. Gonzalez, F. Aguirre, F. Tacchi, A. Gonzalez, M.P. Meza, et al., Cholic acid and deoxycholic acid induce skeletal muscle atrophy through a mechanism dependent on TGR5 receptor, J. Cell. Physiol. 236 (1) (2021) 260–272.

[70] P.M. Herst, M.V. Berridge, Cell surface oxygen consumption: a major contributor to cellular oxygen consumption in glycolytic cancer cell lines, Biochim. Et. Biophys. Acta (BBA) - Bioenerg. 1767 (2) (2007) 170–177.
[71] R.S. Banh, C. Iorio, R. Marcotte, Y. Xu, D. Cojocari, A.A. Rahman, et al., PTP1B controls non-mitochondrial oxygen consumption by regulating RNF213 to promote tumour survival during hypoxia, Nat. Cell Biol. 18 (7) (2016) 803–813.
[72] L. Horev-Azaria, C.J. Kirkpatrick, R. Korenstein, P.N. Marche, O. Maimon, J. Ponti, et al., Predictive toxicology of cobalt nanoparticles and ions: comparative in vitro study of different cellular models using methods of knowledge discovery from data, Toxicol. Sci. 122 (2) (2011) 489–501.
[73] H. Tan, C.M. Ramirez, N. Miljkovic, H. Li, J.P. Rubin, K.G. Marra, Thermosensitive injectable hyaluronic acid hydrogel for adipose tissue engineering, Biomaterials 30 (36) (2009) 6844–6853.
[74] M.K. Joo, M.H. Park, B.G. Choi, B. Jeong, Reverse thermogelling biodegradable polymer aqueous solutions, J. Mater. Chem. 19 (33) (2009) 5891–5905.

Chapter 3

Poloxamer 407 And Bile Acid-Based Hydrogels: Rheological Properties And Biocompatibility

Chapter 3

Poloxamer 407 And Bile Acid-Based Hydrogels: Rheological Properties And Biocompatibility

The contents of this chapter are covered by publication 6 (pages 100-121) and publication 7 (pages 123-136).

Publication 6 (pages 100-121):

Kovacevic B, Jones M, Wagle SR, Ionescu CM, Foster T, Đanić M, Mikov M, Mooranian A, Al-Salami H. Influence of poly-L-ornithine-bile acid nano hydrogels on cellular bioactivity and potential pharmacological applications. *Therapeutic Delivery*. 2023;14(8):499-510.

Sub-objective (5): to design and create hydrogels utilising poloxamer 407, poly-L-ornithine, ursodeoxycholic acid, chenodeoxycholic acid, deoxycholic acid, taurocholic acid, and lithocholic acid and to examine the shear stress, viscosity, surface tension, torque, microstructure, and zeta potential of hydrogels. Additionally, the hydrogels were incubated with 3 different cell lines (AML 12, C2C12 and NIT-1). Their impact on viability in normal and hypoxic conditions and their impact on bioenergetic parameters was investigated.

Influence of poly-L-ornithine-bile acid hydrogels on cellular bioactivity

Journal:	*Therapeutic Delivery*
Manuscript ID	TDE-2023-0034.R2
Manuscript Type:	Research Article
Keywords:	biomaterial, poly-L-ornithine, bioenergetics, deoxycholic acid

Influence of poly-L-ornithine-bile acid hydrogels on cellular bioactivity

Abstract

Aims: Cellular bioactivity and pathophysiological changes associated with chronic disorders are considered pivotal detrimental factors when developing novel formulations for biomedical applications.

Methods: This paper investigates the use of bile acids and synthetic polypeptide poly-L-ornithine (PLO) in formulations and their impacts on a variety of cell lines, with a particular focus on their cellular bioactivity.

Results: The hepatic cell line was the most negatively affected by the presence of PLO, while the muscle and beta-pancreatic cell lines did not show as profound of a negative impact of PLO on cellular viability. PLO was the least disruptive regarding mitochondrial function for muscle and beta cells.

Conclusion: The addition of bile acids generally decreased mitochondrial respiration and altered bioenergetic parameters in all cell lines.

Keywords: poly-L-ornithine; bile acid; poloxamer 407; biocompatibility; bioenergetics; pancreatic beta cells; muscle cells; hepatic cells.

Summary Points:

- Formulations with Poloxamer 407, poly-L-ornithine and different bile acids have non-Newtonian shear-thinning behaviour.
- The hepatic cell line was the most negatively affected by the presence of poly-L-ornithine, while the muscle and beta-pancreatic cell lines did not show as profound of a negative impact of poly-L-ornithine on cellular viability.
- Poly-L-ornithine was the least disruptive regarding mitochondrial function for muscle and beta cells.
- The addition of bile acids generally decreased mitochondrial respiration and altered bioenergetic parameters in all cell lines.

Plain Language Summary

In our study, we made special gels using two kinds of materials and different acids found in bile. We wanted to see how these gels affected different cells like muscles, liver, and pancreatic beta cells. The gels we made had good traits needed for injections. Liver cells didn't enjoy the new materials very much. Adding bile acids to the materials changed how the cells acted for all cell types we looked at.

Introduction

Biomaterial matrices have significant potential applications in various medical therapies, ranging from wearable and implantable drug-delivery devices to tissue engineering and novel organ-on-chip systems [1-3]. Biomaterial matrices have different structures, and they are made from a wide range of synthetic and naturally occurring biocompatible materials, including from a protein in silkworm cocoon to decellularised skeletal muscle, depending upon the desired application [4,5]. However, they are often in need of optimisation to achieve desirable results.

Polycations are versatile polymers, often used as a backbone to graft polymers due to an accessible carboxyl- or amino-group on the monomer [6]. Poly-L-ornithine (PLO) is a synthetic cationic polypeptide. Brown et al. modified PLO and poly-L-lysine (PLL) to create amphiphilic polymers capable of assembling into vesicles in the presence of cholesterol for *in vitro* and *in vivo* gene delivery [7,8]. More recently, Pan et al. synthesised a hyperbranched polymer with polyethyleneimine core and peripheral PLO branches, which may emerge as a novel antibiotic agent, as it showed effective microbial biofilm disruption and microbicidal activity [9]. Furthermore, PLO exerts biological effects on cells, as was demonstrated by Ge et al., who showed that PLO might influence the differentiation of neural stem/progenitor cells [10]. As part of a polymer matrix, PLO has been used to coat alginate microcapsules. This resulted in an increase in the microcapsules' mechanical strength and membrane thickness, leading to better biocompatibility and viability of encapsulated cells [11]. Bile acids that are endogenously produced in humans have been proposed to be beneficial in nano-gels.

Bile acids (BA)s are emerging as promising novel excipients for biomaterials, and they are proposed to reduce polymer swelling and matrix erosion and increase mechanical strength [12]. Furthermore, BAs are biologically active compounds with various effects and applications. Their disbalance has been implicated in certain diseases, including dysbiosis, Crohn's disease, obesity, and cancer progression in gastrointestinal tissues [13]. BAs' structure is distinctly classified as surfactants, with a rigid steroid backbone and convex hydrophobic and concave hydrophilic areas. BA originate from cholesterol, and in mammals, BA are classified as C24-5β-bile acids. BA have a steroid nucleus comprised of four fused carbon rings, consisting of three 6-carbon rings and one 5-carbon ring [14]. The number, position and orientation of hydroxyl groups are crucial for the overall hydrophilicity level. These properties allow BAs to self-assemble into micelles and even further into more complex supramolecular aggregates, such as gels or nanotubes [15]. Therefore, BAs can be a valuable addition to new biomaterial formulations. However, each BA has a different structure and subsequent rheological and biological effects.

Chenodeoxycholic acid (CDCA) is a primary BA, which can be converted into its 7β epimer (UDCA), or dehydroxylated into lithocholic acid (LCA) [16]. CDCA is a biologically active BA and may be implicated in mitochondrial function and energy expenditure [17]. Broeders et al. showed that CDCA increases the activity of brown adipose tissue in humans through increased mitochondrial uncoupling via the TGR5 receptor [17]. CDCA is an effective long-term treatment for Cerebrotendinous xanthomatosis, a rare disorder caused by a mutation in CYP27A1 [18]. Furthermore, it may be a viable treatment for impaired intestinal epithelial barrier [19], progression of acute myeloid leukaemia [20] and insulin resistance [21]. CDCA has been found to act synergistically with antibiotics against Methicillin-resistant *Staphylococcus aureus* (MRSA) [22].

One of the most studied and promising BAs is ursodeoxycholic acid (UDCA). UDCA is a hydrophilic bile acid essential for lipid metabolism and regulation of intestinal barrier integrity. It is long established as a drug for hepatobiliary disorders and has clinical benefits, most prominently in treatment for intrahepatic cholestasis of pregnancy (17, 18). Furthermore, due to UDCA's peculiar antioxidant, anti-inflammatory and, depending on the tissue, pro and anti-apoptotic properties, it may be a helpful chemo-protecting or chemotherapeutic agent (15, 16).

Taurocholic acid (TCA) is taurine-conjugated cholic acid [12]. This bile salt has been associated with numerous health conditions and biological effects. Tian et al. observe that a high serum level of TCA is correlated with the severity of drug-induced liver injury [23]. Furthermore, TCA may contribute to liver inflammation and fibrosis [24], ileal permeability [25], and when metabolised by specific microbiome colonies, it may show carcinogen and tumour-promoter effects [26]. TCA-related mechanisms have been implicated in aiding chemoresistance [27] and inhibiting the response to interferon-α therapy in patients with hepatitis B [28]. Despite such negatives, TCA has also been shown to have protective effects against age-related macular degeneration [29]. In addition, local TCA application in the distal colon has been proposed as a novel treatment for obesity and type 2 diabetes management [30]. As a delivery system, TCA-conjugated nanoparticles may be promising oral agents for the targeted delivery of anticancer drugs [31].

Deoxycholic acid (DCA) is an endogenously produced secondary BA. It is widely used in dermatology for the effective, non-invasive treatment of submental fat [32]. DCA has been shown to induce gut dysbiosis, leading to subsequent intestinal inflammation. Furthermore, it may induce cellular senescence in hepatic stellate cells [33]. On the other hand, Lin et al. suggest that DCA may act as a tumour-suppressive factor in gallbladder cancer [34]. DCA, however, has extensive usage in the drug delivery space. DCA has been used as a molecular steroid scaffold for anticancer drugs [35], as part of derivatised steroids for possible new imagining materials [36], as a conjugate with the anticancer agent to enable targeted hepatic delivery [37], and for the synthesis of transfersomes for percutaneous delivery [38].

LCA is a secondary BA, which is, along with DCA, known to induce DNA damage, oxidative stress and inflammation, posing a risk factor for colon cancer [39]. Furthermore, there are studies that LCA may have more adverse effects, ranging from inducing endoplasmic reticulum stress [40], depletion of intracellular antioxidants [41], skin inflammation [42], and hepatotoxicity [43]. However, DCA may also be protective in breast cancer [44,45], be involved in an anti-inflammatory effect on liver fibrosis [46], inhibit epithelial apoptosis [47], and exert a protective effect on intestinal epithelium via the activation of vitamin D receptors [48].

To characterise the effects of PLO alone and in combination with different BAs (UDCA, CDCA, TCA, DCA and LCA), we examined the cellular viability of three different cell lines in normoxia and hypoxia, as well as bioenergetic, oxygen consumption rate (OCR) linked parameters. We chose the AML12 cell line for a model of hepatotoxicity, the NIT-1 cell as a model for oxidative damage, and the C2C12 cell line to assess the preliminary damage done to the muscle if the hydrogels were to be administered intramuscularly.

Methods

Materials

Poloxamer 407, PLO, and bile acids (UDCA, CDCA, TCA, DCA, LCA) were purchased from Sigma Chemical Co (St. Louis, MO, USA).

Dulbecco's modified Eagle's medium (DMEM), foetal bovine serum (FBS) and other necessary substances were purchased from Sigma Chemical Co (St. Louis, MO, USA). AML12 and C2C12 cell lines were purchased from ATCC (Manassas, VA, USA). The NIT-1 cell line was a generous gift from The University of Western Australia and St. Vincent's Institute of Medical Research. All cell lines were grown as per previously established protocols [49-53].

Formulation preparation

Poloxamer 407, PLO and BAs were mixed with deionised water using homogenisation at room temperature. The hydrogels were prepared using a cold process to dissolve poloxamer 407 in water, adding cold water (5-10°C) to powder poloxamer 407, mixing and leaving at 4°C overnight to fully dissolve, without taking anything from the hydrogel system. Poloxamer 407 was chosen as a gelation agent for formulations due to its thermoresponsive nature and ability to solubilise bile acids. Formulations were stored at 4°C and used for further assays. For tissue culture assays, appropriate aliquots were subjected to UV light for 20 minutes. Excipients as %w/w are 0.5 PLO and 2.5 Poloxamer 407 for all formulations (F1-F6), with 0.3% of UDCA, CDCA, TCA, DCA and LCA in F1, F2, F3, F4, and F5, respectively. Poloxamer 407 was chosen due to the resulting viscosity of the formulations.

Rheology

Room temperature acclimated formulations were assessed for shear stress, viscosity, and torque by a Visco-88 viscometer (Malvern Instruments, Malvern, UK). The 3000HS Zetasizer (Malvern, UK) was used for zeta potential measurements. Surface tension measurements were performed by a tensiometer (Sigma 703, ATA Scientific, Caringbah, Australia) [50].

Cell viability assay

Cell viability was measured using an MTT (2,5-diphenyl-2,4,5-trimethylthiazol-2-yl) assay for C2C12, AML12 and NIT-1 cell lines. 180 µL of media containing cells ($2x10^5$ cells/ml) was incubated with 20 20 µL of formulations for 24 hours. The established protocol was followed [54], and obtained data was normalised as % of control cells' viability (no formulation added), with control cells being 100%.

Hypoxia assays

An appropriate number of cells in normoxic cell media were mixed with a cell-free CoCl2 media solution to achieve 50 µM (lower hypoxia) or 100 µM (higher hypoxia) solutions in wells [55]. Cells were exposed to CoCl2 for 20 minutes before formulations were added. Cells and formulations were incubated for 24h, followed by an MTT assay to assess viability in different hypoxic conditions. Data is presented as % of control cells' viability in normoxia.

Mitochondrial respiration

All three cell lines were treated with 20 µL of appropriate formulation and incubated for 24h. Following incubation, mitochondrial parameters were assessed with a Seahorse Flux Analyser XF 96 (Agilent, CA, USA), using Seahorse XF Cell Mito Stress Test Kit [56,57].

Statistical Analysis

The data analysis, one-way ANOVA and post hoc comparison of means were conducted using GraphPad Prism version 9.5 (Graphpad, Inc., MA, USA). Data are presented as a mean ± SEM with n = 3, and the data were considered statistically significant at $p < 0.05$(*) or $p < 0.01$ (**).

Results

Formulations had distinctive effects on C2C12, AML12 and NIT-1 cell lines (Figure 1a). The hepatic cell line had a significant drop in viability in the presence of all formulations, especially when compared to the viabilities of C2C12 and NIT-1 cell lines (Figure 1a). C2C12 cells have a superior viability compared to NIT-1 cells in most formulations, excluding F3 and F5. Within those two groups, C2C12 and NIT-1 viability, no significant difference exists (Figure 1a).

Regarding surface tension studies, only F4 and F5 had significantly different values to the BA-free formulation (F6) (Figure 1b). It seems that hydrophobic bile acids (DCA-F4 and LCA-F5) are able to lower surface tension in this system, unlike UDCA (F1), CDCA (F2) and TCA (F3). Adding BAs to the PLO system resulted in changes, with CDCA (F2) and TCA (F3) formulations having the lowest zeta charge. However, there is no significantly alteration of Zeta potential between formulations (Figure 1c).

Logarithmic graphs of shear stress (Figure 1d), torque (Figure 1e) and viscosity (Figure 1f) suggest that all formulations have non-Newtonian, shear thinning behaviour. Adding BAs (F1-F5) to the PLO-poloxamer 407 system (F6) does not appear to alter overall fluid behaviour.

Figure 1. shows a) viability of different cell lines in the presence of formulations, b) the surface tension of formulations, c) the zeta potential of formulations, d) shear stress values, e) torque values, and f) viscosity values of formulations.

The viability of C2C12 cells was demonstrated to be slightly retained compared to the formulation-free control (C) (Figure 2a). Cellular viability in the presence of F3 (TCA and PLO) and F6 (PLO) is not statistically different to C. However, groups F1, F2, F4, and F5 have significantly lower viability than C. F1, and F5 are lower than F6, suggesting that UDCA (F1) and LCA (F5) may have a negative effect on the viability of muscle cells.

The viability of C2C12 cells in different hypoxic conditions is shown in Figure 2b. Formulation-free cells (C) show a gradual decrease in viability consistent with increased $CoCl_2$ concentration. This trend is only preserved within group F1 to a certain degree, while other groups show either no effect from hypoxia on viability (F4, F5 and F6), or a slight increase in viability in hypoxia conditions (F2 and F3) (Figure 2b). Unlike the previous figure, the viability in normal conditions (C, under N) is significantly higher than in most groups, including F6. The only exception, again, is F3. The same trend is observed in lower hypoxia, with all groups but F3 having lowered viability compared to the control (C). In the higher hypoxic conditions, the presence of formulations did not have an as pronounced effect, with a majority of groups (F1, F2, F4 and F6) having no significant difference to the formulation-free control (C). Cellular viability in the presence of F5 significantly decreased in higher hypoxia, compared to C. F3 in high hypoxia, interestingly outperformed all other groups, including C (Figure 2b).

The energetic phenotype of C2C12 shows a decrease in overall oxygen consumption (OCR) (Figure 2c), with F2 and F5 having very little OCR. F6 shows an increased extracellular acidification rate (ECAR), which may lead to slightly more glycolytic metabolism than C (Figure 2c). This decrease in overall OCR is evident in decreased OCR-linked parameters across groups (Figures 2d, 2e and 2f). F6 has preserved ATP production and lower proton leak than C but increased non-mitochondrial oxygen consumption rate (NM-OCR) (Figure 2e, 2f and 2d). F3, although the best performing in terms of viability, has

decreased ATP production compared to the control but also significantly decreased proton leak and NM-OCR (Figure 2e, 2f and 2d).

Figure 2. shows a) viability of C2C12 cells in the presence of formulations, b) the viability of the same cell line in N (normoxia), L (Lower hypoxia) and H (higher hypoxia), c) metabolic phenotype, d) non-mitochondrial oxygen consumption, e) ATP production, and f) proton leak, all for C2C12 cell line.

Following a trend from Figure 1a, and unlike in the previous cell line, PLO had a profound negative effect on AML12 cells (Figure 3a). All groups had a statistically lowered viability compared to C (Figure 3a). UCDA (F1) and CDCA (F2) seem to have the most adverse effect on AML12 cells, while F3 (TCA) and F6 are the best-performing formulations (Figure 3a). In hypoxia, AML12 follows a similar trend of significantly lowered viability compared to C (Figure 3b). Control cells perform the best in normoxia, and this is similar within the worst-performing groups, F1 and F2. Groups F3, F4 and F6 have unexpectedly high viability in one of the hypoxic conditions, while for F5, hypoxia does not significantly affect viability (Figure 3b). F3 outperforms other formulations in lower hypoxia, while in higher hypoxia, F4 and F6 have the highest viability (Figure 3b).

OCR is shown as the lowest for F1 and F2, while F5 substantially increases ECAR in AML12 cells (Figure 3c). NM-OCR is preserved for most groups (F2, F3, F4 and F5) compared to C, with F6 significantly increasing (Figure 3d). ATP production is variable and sporadic, being below detection for F2, F4 and F6 (Figure 3e). Proton leak is present within almost all groups and is not significantly different from C (Figure 3f).

Figure 3. shows a) viability of AML12 cells in the presence of formulations, b) the viability of the same cell line in N (normoxia), L (Lower hypoxia) and H (higher hypoxia), c) metabolic phenotype, d) non-mitochondrial oxygen consumption, e) ATP production, and f) proton leak, all for AML12 cell line.

Pancreatic beta cells (NIT-1 cells) show sensitivity to PLO and PLO-bile acid combinations (Figure 4a). There is a significant decrease in viability among all groups compared to the formulation-free control (C) (Figure 4a). Of all formulations, F2 (CDCA) has the most adverse effect on NIT-1 cells (Figure 4a). F3 (TCA) shows a tentative increase in viability compared to PLO only (F6). The hypoxia assay shows a slightly more positive trend, with F1, F4, F5 and F6 not having significantly different viabilities in normoxia compared to C. Furthermore, F3, in normoxia, shows higher viability than C (Figure 4b). Most groups (F1, F3, F4, and F6) follow the viability trend of C, with cellular viability being the highest in normoxia. In low hypoxia, F3 shows increased viability compared to C, and F1, F2 and F4 show a decrease (Figure 4b). In high hypoxia, the only groups not to be lower than C are F3 and F6 (Figure 4b).

Regarding bioenergetic parameters, F6 shows an increase in both OCR and ECAR compared to C (Figure 4c). The other formulations have lower OCR and ECAR than C, a result especially observed in F1 and F2 (Figure 4c). Values for NM-OCR are variable, ranging from F6, which has NM-OCR higher than the control, F4, which is not statistically different, to F1, F2, F3 and F5, which are significantly lower than C (Figure 4d). ATP production is suppressed in the presence of BAs (F1-F5) (Figure 4e). On the contrary, F6 shows higher ATP production than C (Figure 4e). Proton leak-linked OCR is similarly suppressed in the presence of BAs (F1-F4) and retained in F6 (Figure 4f).

Figure 4. shows a) viability of NIT-1 cells in the presence of formulations, b) the viability of the same cell line in N (normoxia), L (Lower hypoxia) and H (higher hypoxia), c) metabolic phenotype, d) non-mitochondrial oxygen consumption, e) ATP production, and f) proton leak, all for NIT-1 cell line.

Discussion

In previous studies by Marciel et al., PLO and its coacervates showed Newtonian fluid behaviour [58]. On the contrary, our study found that the PLO systems examined have non-Newtonian, shear thinning behaviour (Figure 1f). However, PLO formulations in this study have Poloxamer 407 as part of the system. Poloxamer 407 was added to aid the solubilisation of BAs in the aqueous environment. Poloxamer 407 is known to have non-Newtonian shear thinning fluid behaviour [59] and is probably responsible for the overall shear thinning properties of the studied PLO systems. Shear-thinning fluid behaviour is desirable in terms of drug delivery, as it was found to be beneficial during the extrusion of hydrogels via needle or nozzle [60]. Therefore, Poloxamer 407 was added to ensure the shear-thinning behaviour of resulting formulations, as a gelation agent and to aid the solubilisation of bile acids in the aqueous environment .

The hydrophobic BAs, DCA (F4) and LCA (T5), lead to a slight decrease in surface tension compared to BA-free formulation (F6) (Figure 1b). As all other system components are hydrophilic (both PLO and poloxamer 407), DCA and LCA may lead to a disruption in hydrophilic interactions between poloxamer 407, PLO and water. Furthermore, DCA and LCA may have increased interactions on the systems' surface, leading to a decrease in surface tension [61].

Hepatic cells (AML12) seem to be the most vulnerable to PLO, with the addition of UDCA (F1) and CDCA (F2) lowering viability further (Figure 1a and Figure 3a). L-ornithine is an intermediary molecule in urea and glutamine synthesis occurring in the hepatocytes (51). It can be metabolised in the liver from poly-L-ornithine [62]. AML12 cells are capable of expressing major hepatic CYP enzymes involved in metabolic detoxification [63]. However, increased CYP protein levels may increase ROS levels in hepatic cells [64]. An increase in ROS levels may be responsible for high levels of non-mitochondrial oxygen consumption (Figure 3d), despite the decrease in cellular viability. A high non-mitochondrial oxygen consumption rate is linked to increased cellular ROS presence [65]. Furthermore, PLO does not protect hepatic cells from hypoxic effects (Figure 3b).

The presence of PLO did not significantly impact the viability of muscle cells, (F6, Figure 2a). Results indicated PLO alters cellular metabolism making it more resistant to hypoxia (F6, Figure 2b). This effect is also similar in the presence of hydrophobic DCA (F4) and LCA (F5), where the addition of a hypoxic agent did not create a difference in cellular viability (Figure 2b). PLO may increase muscle glutamine synthesis (55) and contribute to the high viability of C2C12 cells. Additionally, PLO did not interfere with ATP production (F6, Figure 2e), it decreased proton leak (F6, Figure 2f), and slightly increased non-mitochondrial oxygen consumption rate, compared to control cells (Figure 2d), showing the best-preserved mitochondrial function of all groups, compared to control cells.

The addition of BAs significantly impacts the viability of C2C12 cells (Figure 2a), although this observation was not as profound as on AML12 cells (Figure 3a). Furthermore, adding BAs showed a decreased cellular metabolism (Figure 2c), especially ATP production-linked oxygen consumption (Figure 2e). Similar findings were found in previous studies [51-53]. Xiao et al. linked hydrophobic BAs to a dose-dependent muscle contraction, increased H_2O_2 production, lipid peroxidation and increased free radical formation in muscle cells [66]. Furthermore, Abrigo et al. reported decreased

mitochondrial mass and metabolic dysfunction of skeletal muscle fibres in the presence of BAs (59), which aligns with our findings.

The pancreatic beta cells have an increased metabolism in the presence of PLO (F6 Figure 4c). The cellular viability is slightly decreased in the presence of PLO (F6, Figure 4a), and the response to hypoxia is preserved (Figure 4b). Interestingly, PLO did not only increase non-mitochondrial oxygen consumption (Figure 4d) but ATP production, too (Figure 4e). Proton leak, linked to disruption of the electron transport chain, did not significantly change in the presence of PLO (F6, Figure 4f). Luca et al. demonstrated a beneficial biocompatibility of alginate/PLO systems for rat islets [67]. Hilberg et al. used PLO as a stabilising agent in alginate microcapsules to optimise islets' viability and insulin secretion [68].

Regarding BAs, CDCA (F2) decreased NIT-1 viability the most, with TCA (F3) having the most negligible impact on cellular viability (Figure 4a). CDCA also impaired the hypoxic response (F2, Figure 4b) and bioenergetic parameters of NIT-1 cells (Figure 4c), which is in contrast with the findings of Mooranian et al., who reported the beneficial impact of CDCA on pancreatic beta cells [69]. However, that study was done in a microcapsule system, where CDCA may have a more indirect effect on cells as a stabilising agent of the microcapsule matrix. The addition of a conjugated BA (TCA) (F3) to the PLO matrix slightly improved the viability of NIT-1 cells (Figure 4a), which is aligned with a study done on TCA-alginate microcapsules, where the addition of TCA improved beta cell survival in hyperglycaemic conditions and lowered pro-inflammatory markers [70]. The addition of BAs (F1-F5) decreased cellular metabolism in all categories (Figure 4c-4f), which is consistent with previous findings [51-53].

There are several limitations to this study, including only one time point of investigation for cellular parameters, and used only three immortalised cell lines. Study also lacks prolonged stability, determination and morphology studies for examined hydrogels. Further research is needed to address these limitations.

Conclusion

Different cell lines showed diverse bioenergetic responses to the PLO and PLO-BA systems. The hepatic cell line was the most negatively affected by the presence of PLO, while the muscle and beta-pancreatic cell lines did not show as profound of a negative impact of PLO on cellular viability. PLO was the least disruptive regarding mitochondrial function for muscle and beta cells. The addition of bile acids generally decreased mitochondrial respiration and altered bioenergetic parameters in all cell lines. Further studies are necessary to elucidate the exact mechanism involved in BA's impact on cellular biometabolism.

Reference

1. D'Costa K, Kosic M, Lam A, Moradipour A, Zhao Y, Radisic M. Biomaterials and Culture Systems for Development of Organoid and Organ-on-a-Chip Models. *Annals of Biomedical Engineering*, 48(7), 2002-2027 (2020).
2. Mitrousis N, Fokina A, Shoichet MS. Biomaterials for cell transplantation. *Nature Reviews Materials*, 3(11), 441-456 (2018).
3. Kar A, Ahamad N, Dewani M, Awasthi L, Patil R, Banerjee R. Wearable and implantable devices for drug delivery: Applications and challenges. *Biomaterials*, 283, 121435 (2022).
4. Philips C, Terrie L, Thorrez L. Decellularized skeletal muscle: A versatile biomaterial in tissue engineering and regenerative medicine. *Biomaterials*, 283, 121436 (2022).
5. Liu J, Shi L, Deng Y *et al.* Silk sericin-based materials for biomedical applications. *Biomaterials*, 287, 121638 (2022).
6. Zhao L, Li N, Wang K, Shi C, Zhang L, Luan Y. A review of polypeptide-based polymersomes. *Biomaterials*, 35(4), 1284-1301 (2014).
7. Brown MD, Schätzlein A, Brownlie A *et al.* Preliminary Characterization of Novel Amino Acid Based Polymeric Vesicles as Gene and Drug Delivery Agents. *Bioconjugate Chemistry*, 11(6), 880-891 (2000).
8. Brown MD, Gray AI, Tetley L *et al.* In vitro and in vivo gene transfer with poly(amino acid) vesicles. *Journal of Controlled Release*, 93(2), 193-211 (2003).
9. Pan M, Lu C, Zheng M *et al.* Unnatural Amino-Acid-Based Star-Shaped Poly(l-Ornithine)s as Emerging Long-Term and Biofilm-Disrupting Antimicrobial Peptides to Treat Pseudomonas aeruginosa-Infected Burn Wounds. *Advanced Healthcare Materials*, 9(19), 2000647 (2020).
10. Ge H, Tan L, Wu P *et al.* Poly-L-ornithine promotes preferred differentiation of neural stem/progenitor cells via ERK signalling pathway. *Scientific Reports*, 5(1), 15535 (2015).
11. Darrabie MD, Kendall WF, Opara EC. Characteristics of Poly-l-Ornithine-coated alginate microcapsules. *Biomaterials*, 26(34), 6846-6852 (2005).
12. Kovacevic B, Jones M, Ionescu C *et al.* The emerging role of bile acids as critical components in nanotechnology and bioengineering: Pharmacology, formulation optimizers and hydrogel-biomaterial applications. *Biomaterials*, 283, 121459 (2022).
13. Shansky Y, Bespyatykh J. Bile Acids: Physiological Activity and Perspectives of Using in Clinical and Laboratory Diagnostics. *Molecules*, 27(22), 7830 (2022).
14. Chiang JY. Bile acid metabolism and signaling. *Compr Physiol*, 3(3), 1191-1212 (2013).
15. Galantini L, di Gregorio MC, Gubitosi M *et al.* Bile salts and derivatives: Rigid unconventional amphiphiles as dispersants, carriers and superstructure building blocks. *Current Opinion in Colloid & Interface Science*, 20(3), 170-182 (2015).
16. Fiorucci S, Distrutti E. Chenodeoxycholic Acid: An Update on Its Therapeutic Applications. In: *Bile Acids and Their Receptors.* Fiorucci, S, Distrutti, E (Eds.) (Springer International Publishing, Cham, 2019) 265-282.
17. Broeders Evie PM, Nascimento Emmani BM, Havekes B *et al.* The Bile Acid Chenodeoxycholic Acid Increases Human Brown Adipose Tissue Activity. *Cell Metabolism*, 22(3), 418-426 (2015).
18. Verrips A, Dotti MT, Mignarri A, Stelten BML, Verma S, Federico A. The safety and effectiveness of chenodeoxycholic acid treatment in patients with cerebrotendinous xanthomatosis: two retrospective cohort studies. *Neurological Sciences*, 41(4), 943-949 (2020).
19. Song M, Ye J, Zhang F *et al.* Chenodeoxycholic Acid (CDCA) Protects against the Lipopolysaccharide-Induced Impairment of the Intestinal Epithelial Barrier Function via the FXR-MLCK Pathway. *Journal of Agricultural and Food Chemistry*, 67(32), 8868-8874 (2019).

20. Liu J, Wei Y, Jia W *et al.* Chenodeoxycholic acid suppresses AML progression through promoting lipid peroxidation via ROS/p38 MAPK/DGAT1 pathway and inhibiting M2 macrophage polarization. *Redox Biology*, 56, 102452 (2022).
21. Bazzari FH, Abdallah DM, El-Abhar HS. Chenodeoxycholic Acid Ameliorates AlCl3-Induced Alzheimer's Disease Neurotoxicity and Cognitive Deterioration via Enhanced Insulin Signaling in Rats. *Molecules*, 24(10), 1992 (2019).
22. Cui K, Yang W, Liu S *et al.* Synergistic Inhibition of MRSA by Chenodeoxycholic Acid and Carbapenem Antibiotics. *Antibiotics*, 12(1), 71 (2023).
23. Tian Q, Yang R, Wang Y *et al.* A High Serum Level of Taurocholic Acid Is Correlated With the Severity and Resolution of Drug-induced Liver Injury. *Clinical Gastroenterology and Hepatology*, 19(5), 1009-1019.e1011 (2021).
24. Mancinelli R, Ceci L, Kennedy L *et al.* The Effects of Taurocholic Acid on Biliary Damage and Liver Fibrosis Are Mediated by Calcitonin-Gene-Related Peptide Signaling. *Cells*, 11(9), 1591 (2022).
25. Liu H, Kohmoto O, Sakaguchi A *et al.* Taurocholic acid, a primary 12α-hydroxylated bile acid, induces leakiness in the distal small intestine in rats. *Food and Chemical Toxicology*, 165, 113136 (2022).
26. Wolf PG, Gaskins HR, Ridlon JM *et al.* Effects of taurocholic acid metabolism by gut bacteria: A controlled feeding trial in adult African American subjects at elevated risk for colorectal cancer. *Contemporary Clinical Trials Communications*, 19, 100611 (2020).
27. Yang C, Yuan H, Gu J *et al.* ABCA8-mediated efflux of taurocholic acid contributes to gemcitabine insensitivity in human pancreatic cancer via the S1PR2-ERK pathway. *Cell Death Discovery*, 7(1), 6 (2021).
28. Xun Z, Lin J, Yu Q *et al.* Taurocholic acid inhibits the response to interferon-α therapy in patients with HBeAg-positive chronic hepatitis B by impairing CD8+ T and NK cell function. *Cellular & Molecular Immunology*, 18(2), 461-471 (2021).
29. Warden C, Barnett JM, Brantley MA. Taurocholic acid inhibits features of age-related macular degeneration in vitro. *Experimental Eye Research*, 193, 107974 (2020).
30. Wu T, Bound MJ, Standfield SD *et al.* Effects of rectal administration of taurocholic acid on glucagon-like peptide-1 and peptide YY secretion in healthy humans. *Diabetes, Obesity and Metabolism*, 15(5), 474-477 (2013).
31. Khatun Z, Nurunnabi M, Reeck GR, Cho KJ, Lee Y-k. Oral delivery of taurocholic acid linked heparin–docetaxel conjugates for cancer therapy. *Journal of Controlled Release*, 170(1), 74-82 (2013).
32. Liu C, Li MK, Alster TS. Alternative Cosmetic and Medical Applications of Injectable Deoxycholic Acid: A Systematic Review. *Dermatologic Surgery*, 47(11) (2021).
33. Nguyen PT, Kanno K, Pham QT *et al.* Senescent hepatic stellate cells caused by deoxycholic acid modulates malignant behavior of hepatocellular carcinoma. *Journal of Cancer Research and Clinical Oncology*, 146(12), 3255-3268 (2020).
34. Lin R, Zhan M, Yang L *et al.* Deoxycholic acid modulates the progression of gallbladder cancer through N6-methyladenosine-dependent microRNA maturation. *Oncogene*, 39(26), 4983-5000 (2020).
35. Salomatina OV, Popadyuk II, Zakharenko AL *et al.* Deoxycholic acid as a molecular scaffold for tyrosyl-DNA phosphodiesterase 1 inhibition: A synthesis, structure–activity relationship and molecular modeling study. *Steroids*, 165, 108771 (2021).
36. Agarwal DS, Prakash Singh R, Jha PN, Sakhuja R. Fabrication of deoxycholic acid tethered α-cyanostilbenes as smart low molecular weight gelators and AIEE probes for bio-imaging. *Steroids*, 160, 108659 (2020).
37. Xiao L, Yu E, Yue H, Li Q. Enhanced Liver Targeting of Camptothecin via Conjugation with Deoxycholic Acid. *Molecules*, 24(6), 1179 (2019).

38. Leonyza A, Surini S. Optimization of sodium deoxycholate-based transfersomes for percutaneous delivery of peptides and proteins. *International Journal of Applied Pharmaceutics*, 11(5), 329-332 (2019).
39. Han Y, Haraguchi T, Iwanaga S *et al.* Consumption of Some Polyphenols Reduces Fecal Deoxycholic Acid and Lithocholic Acid, the Secondary Bile Acids of Risk Factors of Colon Cancer. *Journal of Agricultural and Food Chemistry*, 57(18), 8587-8590 (2009).
40. Chao S, Xiaojun L, Haizhen W *et al.* Lithocholic acid activates mTOR signaling inducing endoplasmic reticulum stress in placenta during intrahepatic cholestasis of pregnancy. *Life Sciences*, 218, 300-307 (2019).
41. Hu J, Zhang Y, Yi S *et al.* Lithocholic acid inhibits dendritic cell activation by reducing intracellular glutathione via TGR5 signaling. *Int J Biol Sci*, 18(11), 4545-4559 (2022).
42. Xiao W, Chen M, Peng Q *et al.* Lithocholic acid promotes rosacea-like skin inflammation via G protein-coupled bile acid receptor 1. *Biochimica et Biophysica Acta (BBA) - Molecular Basis of Disease*, 1868(12), 166563 (2022).
43. Woolbright BL, Li F, Xie Y *et al.* Lithocholic acid feeding results in direct hepato-toxicity independent of neutrophil function in mice. *Toxicology Letters*, 228(1), 56-66 (2014).
44. Kovács P, Csonka T, Kovács T *et al.* Lithocholic Acid, a Metabolite of the Microbiome, Increases Oxidative Stress in Breast Cancer. *Cancers*, 11(9), 1255 (2019).
45. Mikó E, Vida A, Kovács T *et al.* Lithocholic acid, a bacterial metabolite reduces breast cancer cell proliferation and aggressiveness. *Biochimica et Biophysica Acta (BBA) - Bioenergetics*, 1859(9), 958-974 (2018).
46. Shao J, Ge T, Tang C, Wang G, Pang L, Chen Z. Synergistic anti-inflammatory effect of gut microbiota and lithocholic acid on liver fibrosis. *Inflammation Research*, 71(10), 1389-1401 (2022).
47. Lajczak-McGinley NK, Porru E, Fallon CM *et al.* The secondary bile acids, ursodeoxycholic acid and lithocholic acid, protect against intestinal inflammation by inhibition of epithelial apoptosis. *Physiological Reports*, 8(12), e14456 (2020).
48. Yao B, He J, Yin X, Shi Y, Wan J, Tian Z. The protective effect of lithocholic acid on the intestinal epithelial barrier is mediated by the vitamin D receptor via a SIRT1/Nrf2 and NF-κB dependent mechanism in Caco-2 cells. *Toxicology Letters*, 316, 109-118 (2019).
49. Mooranian A, Raj Wagle S, Kovacevic B *et al.* Bile acid bio-nanoencapsulation improved drug targeted-delivery and pharmacological effects via cellular flux: 6-months diabetes preclinical study. *Scientific Reports*, 10(1), 106 (2020).
50. Wagle SR, Walker D, Kovacevic B *et al.* Micro-Nano formulation of bile-gut delivery: rheological, stability and cell survival, basal and maximum respiration studies. *Sci Rep*, 10(1), 7715 (2020).
51. Kovacevic B, Ionescu CM, Jones M *et al.* The Effect of Deoxycholic Acid on Chitosan-Enabled Matrices for Tissue Scaffolding and Injectable Nanogels. In: *Gels*. (Ed.^(Eds) (2022)
52. Kovacevic B, Ionescu CM, Wagle SR *et al.* Impact of Novel Teflon-DCA Nanogel Matrix on Cellular Bioactivity. *Journal of Pharmaceutical Sciences*, (2022).
53. Kovacevic B, Wagle SR, Ionescu CM *et al.* Novel hydrogel comprising non-ionic copolymer with various concentrations of pharmacologically active bile acids for cellular injectable gel. *Colloids and Surfaces B: Biointerfaces*, 222, 113014 (2023).
54. Mooranian A, Foster T, Ionescu CM *et al.* Enhanced Bilosomal Properties Resulted in Optimum Pharmacological Effects by Increased Acidification Pathways. *Pharmaceutics*, 13(8), 1184 (2021).
55. Li Q, Ma R, Zhang M. CoCl2 increases the expression of hypoxic markers HIF-1α, VEGF and CXCR4 in breast cancer MCF-7 cells. *Oncol Lett*, 15(1), 1119-1124 (2018).
56. Mooranian A, Ionescu CM, Walker D *et al.* Single-Cellular Biological Effects of Cholesterol-Catabolic Bile Acid-Based Nano/Micro Capsules as Anti-Inflammatory Cell Protective Systems. *Biomolecules*, 12(1), 73 (2022).

57. Wagle SR, Kovacevic B, Walker D *et al.* Pharmacological and Advanced Cell Respiration Effects, Enhanced by Toxic Human-Bile Nano-Pharmaceuticals of Probucol Cell-Targeting Formulations. *Pharmaceutics*, 12(8), 708 (2020).
58. Marciel AB, Srivastava S, Tirrell MV. Structure and rheology of polyelectrolyte complex coacervates. *Soft Matter*, 14(13), 2454-2464 (2018).
59. Rohani Rad E, Vahabi H, Formela K, Saeb MR, Thomas S. Injectable poloxamer/graphene oxide hydrogels with well-controlled mechanical and rheological properties. *Polymers for Advanced Technologies*, 30(9), 2250-2260 (2019).
60. Uman S, Dhand A, Burdick JA. Recent advances in shear-thinning and self-healing hydrogels for biomedical applications. *Journal of Applied Polymer Science*, 137(25), 48668 (2020).
61. He S, Liang W, Cheng K-L, Fang J, Wu S-T. Bile acid–surfactant interactions at the liquid crystal/aqueous interface. *Soft Matter*, 10(26), 4609-4614 (2014).
62. Vong LB, Ibayashi Y, Lee Y, Ngo D-N, Nishikawa Y, Nagasaki Y. Poly(ornithine)-based self-assembling drug for recovery of hyperammonemia and damage in acute liver injury. *Journal of Controlled Release*, 310, 74-81 (2019).
63. Ren S, Sun G, Wu Z *et al.* mmu-miR-199a-5p regulates CYP2B10 through repression of E4BP4 in mouse AML-12 hepatocytes. *Xenobiotica*, 51(10), 1101-1109 (2021).
64. Nesnow S, Grindstaff RD, Lambert G *et al.* Propiconazole increases reactive oxygen species levels in mouse hepatic cells in culture and in mouse liver by a cytochrome P450 enzyme mediated process. *Chemico-Biological Interactions*, 194(1), 79-89 (2011).
65. Hill BG, Benavides GA, Lancaster JR *et al.* Integration of cellular bioenergetics with mitochondrial quality control and autophagy. *Biological Chemistry*, 393(12), 1485-1512 (2012).
66. Xiao Z-L, Rho AK, Biancani P, Behar J. Effects of bile acids on the muscle functions of guinea pig gallbladder. *American Journal of Physiology-Gastrointestinal and Liver Physiology*, 283(1), G87-G94 (2002).
67. Luca G, Calafiore R, Basta G *et al.* Improved function of rat islets upon co-microencapsulation with Sertoli's cells in alginate/poly-L-ornithine. *AAPS PharmSciTech*, 2(3), 15 (2001).
68. Hillberg AL, Kathirgamanathan K, Lam JBB, Law LY, Garkavenko O, Elliott RB. Improving alginate-poly-L-ornithine-alginate capsule biocompatibility through genipin crosslinking. *Journal of Biomedical Materials Research Part B: Applied Biomaterials*, 101B(2), 258-268 (2013).
69. Mooranian A, Negrulj R, Al-Salami H. Primary Bile Acid Chenodeoxycholic Acid-Based Microcapsules to Examine β-cell Survival and the Inflammatory Response. *BioNanoScience*, 6(2), 103-109 (2016).
70. Mooranian A, Negrulj R, Arfuso F, Al-Salami H. The effect of a tertiary bile acid, taurocholic acid, on the morphology and physical characteristics of microencapsulated probucol: potential applications in diabetes: a characterization study. *Drug Delivery and Translational Research*, 5(5), 511-522 (2015).

Figure and table legends

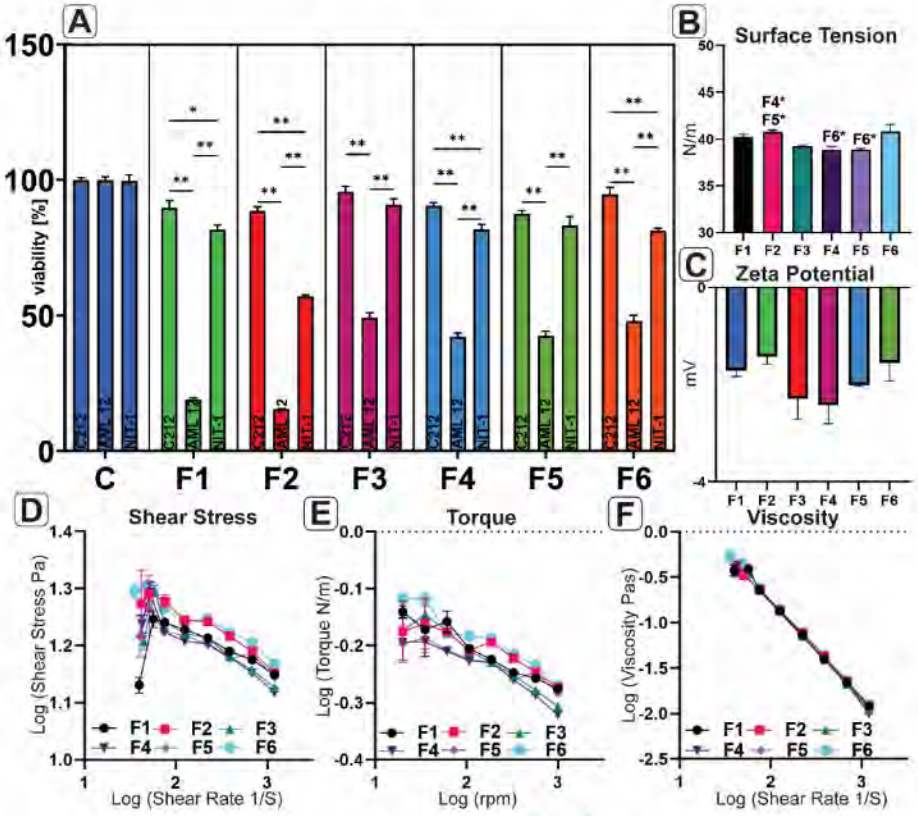

Figure 1. shows a) viability of different cell lines in the presence of formulations, b) the surface tension of formulations, c) the zeta potential of formulations, d) shear stress values, e) torque values, and f) viscosity values of formulations.

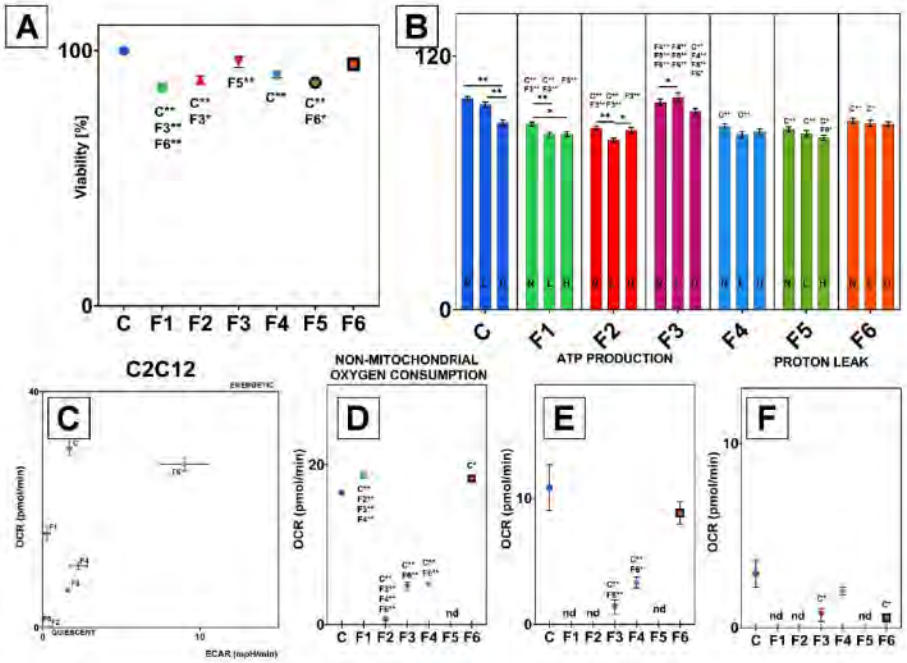

Figure 2. shows a) viability of C2C12 cells in the presence of formulations, b) the viability of the same cell line in N (normoxia), L (Lower hypoxia) and H (higher hypoxia), c) metabolic phenotype, d) non-mitochondrial oxygen consumption, e) ATP production, and f) proton leak, all for C2C12 cell line.

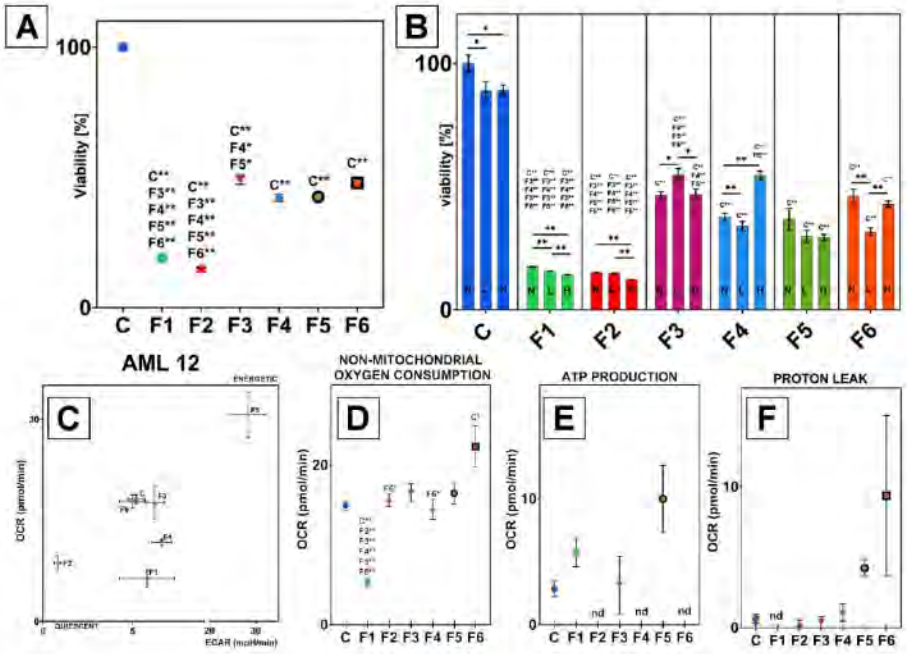

Figure 3. shows a) viability of AML12 cells in the presence of formulations, b) the viability of the same cell line in N (normoxia), L (Lower hypoxia) and H (higher hypoxia), c) metabolic phenotype, d) non-mitochondrial oxygen consumption, e) ATP production, and f) proton leak, all for AML12 cell line.

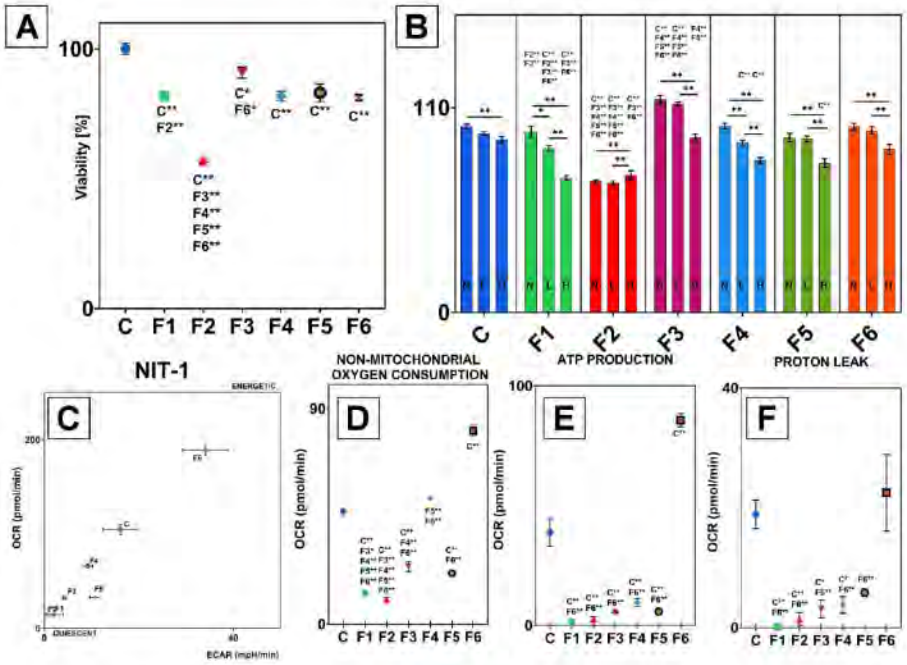

Figure 4. shows a) viability of NIT-1 cells in the presence of formulations, b) the viability of the same cell line in N (normoxia), L (Lower hypoxia) and H (higher hypoxia), c) metabolic phenotype, d) non-mitochondrial oxygen consumption, e) ATP production, and f) proton leak, all for NIT-1 cell line.

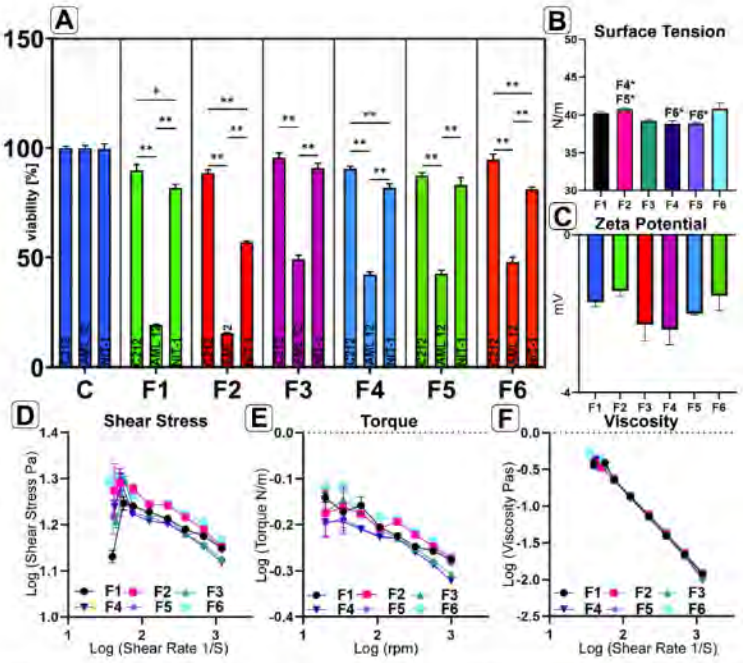

Figure 1. shows a) viability of different cell lines in the presence of formulations, b) the surface tension of formulations, c) the zeta potential of formulations, d) shear stress values, e) torque values, and f) viscosity values of formulations.

212x188mm (300 x 300 DPI)

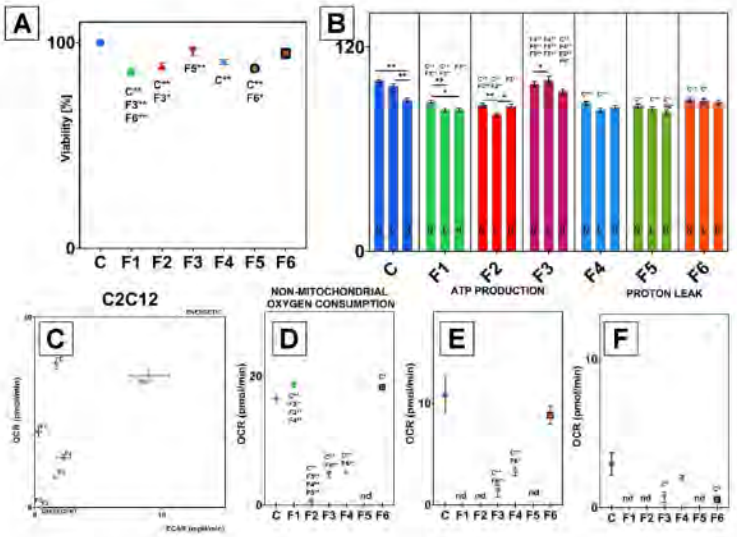

Figure 2. shows a) viability of C2C12 cells in the presence of formulations, b) the viability of the same cell line in N (normoxia), L (Lower hypoxia) and H (higher hypoxia), c) metabolic phenotype, d) non-mitochondrial oxygen consumption, e) ATP production, and f) proton leak, all for C2C12 cell line.

685x501mm (72 x 72 DPI)

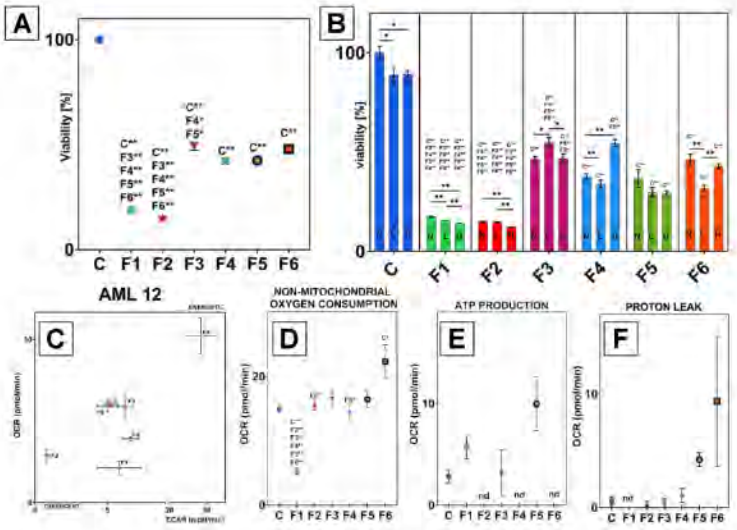

Figure 3. shows a) viability of AML12 cells in the presence of formulations, b) the viability of the same cell line in N (normoxia), L (Lower hypoxia) and H (higher hypoxia), c) metabolic phenotype, d) non-mitochondrial oxygen consumption, e) ATP production, and f) proton leak, all for AML12 cell line.

685x501mm (72 x 72 DPI)

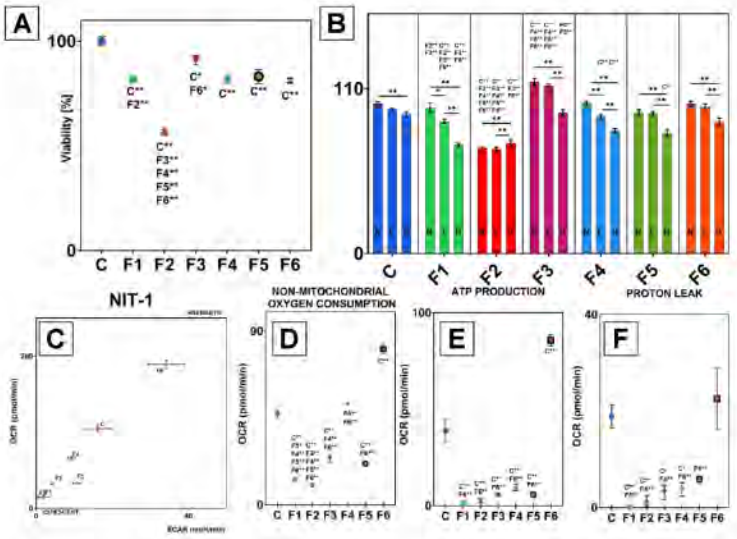

Figure 4. shows a) viability of NIT-1 cells in the presence of formulations, b) the viability of the same cell line in N (normoxia), L (Lower hypoxia) and H (higher hypoxia), c) metabolic phenotype, d) non-mitochondrial oxygen consumption, e) ATP production, and f) proton leak, all for NIT-1 cell line.

685x501mm (72 x 72 DPI)

Publication 7 (pages 123-136):

Kovacevic B, Jones M, Wagle S, Ionescu C, Foster T, Đanić M, Mikov M, Mooranian A, Al-Salami H. The effect of deoxycholic acid-based hydrogels on hepatic, muscle and pancreatic beta cells. Therapeutic Delivery. 2024;15(1):41-54.

Sub-objective (6): to design and create hydrogels utilising poloxamer 407, deoxycholic acid and polysaccharides (starch, pectin, acacia, carboxymethylcellulose and methyl 2-hydroxyethyl cellulose) and to examine the shear stress, viscosity, surface tension, torque, microstructure, and zeta potential of hydrogels. Additionally, the hydrogels were incubated with 3 different cell lines (AML 12, C2C12 and NIT-1). Their impact on viability in normal and hypoxic conditions and their impact on bioenergetic parameters was investigated.

The effects of polysaccharide and deoxycholic acid-based hydrogels on hepatic, muscle and pancreatic beta cells

Journal:	*Therapeutic Delivery*
Manuscript ID	TDE-2023-0054
Manuscript Type:	Research Article
Keywords:	hydrogel, deoxycholic acid, pancreatic beta cells, cellulose, polysaccharide

Abstract
Hydrogels are essential for a diverse range of biomedical applications. Polysaccharides have notable cell protective properties, while bile acids have a vast biological effect. Bile acids are amphoteric molecules with stabilising effects on common polymers.

Novel hydrogels containing poloxamer 407, polysaccharides (starch, pectin, acacia, carboxymethyl and methyl 2-hydroxyethyl cellulose) and deoxycholic acid were examined for biological effects on hepatic, muscle, and pancreatic beta cells.

Including deoxycholic acid in hydrogels had limited effects depending on the tissue, mainly detrimental to cellular survival and bioenergetics. Further research is needed as proposed hydrogels may be helpful for cell delivery systems of pancreatic beta cells but may be less suitable for hepatic and muscle tissue.

Keywords: deoxycholic acid; hydrogel; polysaccharide; cellulose; pancreatic beta cells

Graphical Abstract

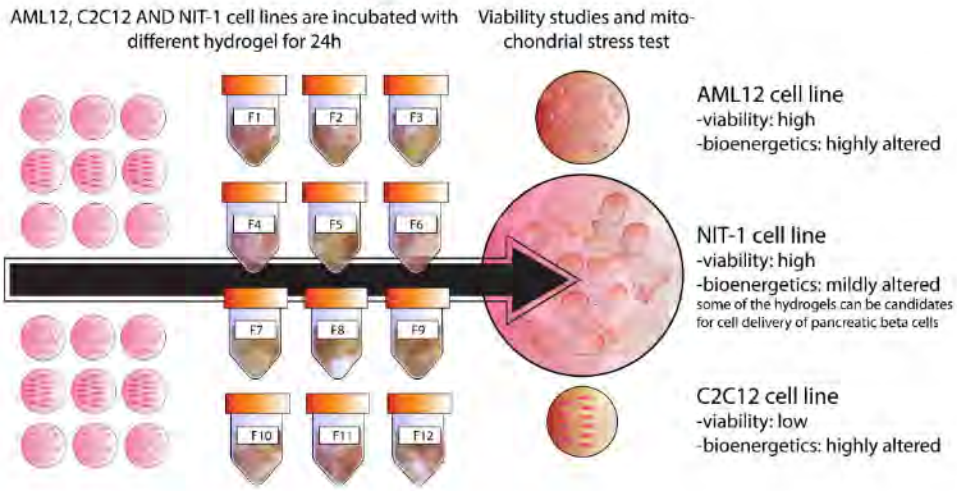

Introduction

Hydrogels are hydrophilic polymeric networks capable of containing water without disintegrating. Based on their specific mechanical properties that mimic soft tissue, hydrogels are used in diverse applications, from tissue engineering and cell and drug delivery to soft robots and electronics (1-4). One of the most promising hydrogel-producing polymers is Poloxamer 407 (Pluronic F127). Poloxamers are non-ionic hydrophilic surfactants capable of self-assembling into micelles and transitioning into a gel state above a specific temperature and concentration. Being thermo-responsive and non-toxic, different poloxamers were widely applied as a surfactant in nanoemulsions (5), dispersant for novel materials (6), successful wound dressing material (7), and bio printable hydrogel for tissue engineering (8), among others. However, as highlighted by Bonacucina et al., poloxamers are not without significant shortcomings; they are non-biodegradable, prone to rapid degradation, and have low mechanical strength (9). Combining poloxamers with known biocompatible polymers, such as polysaccharides, could improve poloxamers' rheological profile and biological performance, expanding the potential applications in medicine and beyond.

Biomedical hydrogels based on polysaccharides have significant biocompatible and biomimetic properties. Numerous polysaccharides, including pectin, acacia, starch, and carboxymethyl cellulose, are used for biomedical purposes. Pectin is an affordable, non-immunogenic, anionic, mucoadhesive polysaccharide that can be easily modified due to abundant functional hydroxyl groups. Pectin has been used as part of injectable hydrogels for tissue engineering, drug-releasing wound dressings, and drug delivery matrices (10-12). Acacia, or gum Arabic, is a non-digestible, water-soluble polysaccharide capable of forming highly viscous solutions. Furthermore, it is a biologically active polysaccharide, with reported antioxidant, antibacterial, with non-haemolytic and haemostatic properties (13, 14). Acacia, combined with alginate, was also found to promote wound healing (15). Raguvaran et al. used an acacia-alginate mix to combat the haemolytic and oxidative effect of ZnO nanoparticles on erythrocytes (16). Starch one of the primary plant polysaccharides, and is accordingly widely available and affordable. Due to its biocompatible and biodegradable properties, it has been used as a base for a novel, multi-responsive hydrogels and nanoparticles, capable of responding to pH, temperature, and light stimuli (17-19). Carboxymethyl cellulose (CMC) is a water-soluble polysaccharide and viscosity modifier. CMC is biocompatible; it readily binds with extracellular proteins (notably fibronectin and collagen) and promotes cell adhesion, migration, and tissue reepithelisation (20). CMC has previously been used as a base for electro-spun nanofibers for bone regeneration (21), novel anticancer drug carriers (22), self-healing photo-responsive hydrogels (23) and novel double-layer hydrogels for sustained drug release (24).

Adding amphiphilic compounds to hydrogels may increase interaction with proteins, lipids, and enzymes, improving biological compatibility. Bile acids (BAs) are naturally occurring amphiphilic compounds with a specific steroid structure that deviates from the standard surfactant structure. They have been found to interact with polysaccharides by adsorption and/or entrapment within polysaccharides' viscous polymeric network (25). BAs are highly biologically active molecules in addition to their dietary role in facilitating lipid metabolism. BAs have also been implicated in metabolic disorders, Mooranian et al. for example highlighted a connection between BA profile and type 1 and 2 diabetes (26). The same group demonstrated secondary BAs have both anti-inflammatory, and hypoglycaemic effects (27).

Furthermore, BAs have a beneficial impact on drug delivery formulations with polysaccharides by increasing the mechanical strength of hydrogels and increasing biocompatibility (2, 4, 28).

To examine the overall impact of hydrogels made from poloxamer 407, different polysaccharides and deoxycholic acid (DCA), we conducted in vitro studies on hepatic, muscle, and pancreatic beta-cell cell lines. We examined the viability of cells in the presence of hydrogels in normal and different hypoxic conditions and investigated the energetic profile of cells.

Methods and materials

Materials were purchased from the following vendors: deoxycholic acid, poloxamer 407, pectin (from citrus fruit), carboxymethylcellulose sodium salt (CM) and methyl 2-hydroxyethyl cellulose (ME) from Sigma Chemical Co (St. Louis, MO, USA); potato starch from PharmAust (Malaga, WA, Australia); acacia BP (spray dried gum arabic) from PCCA (Matraville, NSW, Australia). Dulbecco's modified Eagle's medium (DMEM), foetal bovine serum (FBS) and other supplements involved in tissue culture were purchased from Sigma Chemical Co (St. Louis, MO, USA).

Cell culture

AML12 hepatic cell line (CRL-2254™) and C2C12 muscle cell line (CRL-1772™) were purchased from ATCC (Manassas, VA, USA). The NIT-1 pancreatic cell line was a generous gift from Professor Grant Morahan (University of Western Australia). All three cell lines were grown in DMEM with 10% FBS and appropriate supplements included in previous protocols (29-31). Cells were incubated in a humidified atmosphere of 5% CO2 at 37°C, with media change every day for C2C12 and every other day for AML12 and NIT-1 cell lines.

Hydrogel preparation

Hydrogels were prepared by mixing poloxamer 407, polysaccharides and DCA with cold deionised water under sterile conditions. The resulting hydrogels were left at 4°C overnight. Hydrogels were tempered to room temperature before being used for rheological examinations and biological assays. All hydrogels (F1-F12) were made from Poloxamer 407 (15% w/w), hydrogels F2, F4, F6, F8, F10 and F12 had DCA (0.2% w/w), hydrogels F3 and F4 had starch (1.2% w/w), F5 and F6 had pectin (1.2% w/w), F7 and F8 acacia (1.2% w/w), F9 and F10 CM cellulose (1.2% w/w) and F11 and F12 had ME cellulose (1.2% w/w). Hydrogels were left for 30 min under UV light in sterile conditions before being used in biological assays.

Rheological analysis

Viscosity values were obtained via a Visco-88 viscometer (Malvern Instruments, Malvern, UK). The surface tension values were obtained by placing 10 ml of hydrogels in a tensiometer (Sigma 703, Ata Scientific Instruments, Caringbah NSW Australia), utilising the du Noüy ring method. Zeta potential was measured using 3000HS Zetasizer (Malvern Panalytical Ltd, Malvern, UK), with a standard operating procedure designed to measure 25 runs per measurement. All rheological analyses were done at room temperature. All obtained data were in triplicates ($n = 3$).

Cell viability

Cell viability for all three lines was measured utilising an MTT (2,5-diphenyl-2,4,5-trimethylthiazol-2-yl) (Sigma Chemical Co, St. Louis, MO, USA). To 20 µL of hydrogels was added 180 µL of media containing cells (2×10^5 cells/ml) and incubated for 24 hours. After incubation, media was discarded, cells were washed with phosphate buffer saline (PBS) (Sigma Chemical Co, St. Louis, MO, USA) and the manufacturers protocol for MTT was followed to obtain results (32). Data was normalised as a percentage of control cells' viability

(no hydrogel added), with control cells being 100%. All obtained data was in triplicates (n = 3).

Cell viability under hypoxia

Freshly detached cells were mixed with a cell-free $CoCl_2$ solution in media to achieve 50 µM (lower hypoxia) or 100 µM (higher hypoxia) solutions in wells (33). Cells were exposed to $CoCl_2$ for 20 minutes before 180 µL media with cells was added to 20 µL of hydrogels. Cells were incubated for 24 h. After incubation, media was discarded, cells were washed with PBS, and an MTT assay protocol was followed to assess viability in different hypoxic conditions. All obtained data was in triplicates (n = 3). Data is presented as a percentage based on control cells viability in normoxia.

Cellular bioenergetics

Cellular bioenergetics was assessed by Seahorse XF Cell Mito Stress Test using Seahorse Flux Analyser XF 96 (Agilent Technologies, Santa Clara, CA, USA), per established protocol (30, 32, 34, 35). Cells were incubated with hydrogels for 24 h in the same manner as for cellular viability assay. After incubation, media was discarded, cells washed with PBS, and appropriate media was added, according to Seahorse Mito stress test protocol, before running the assay. All obtained data was in triplicates (n = 3).

Statistical analysis

Statistical analysis was done by GraphPad Prism version 9.5 (Graphpad, Inc., USA). One-way ANOVA and Tukey HSD were utilised appropriate of data. All data is shown as mean ± standard errors of mean (SEM), with statistical significance defined as $p < 0.01$ (*) and $p < 0.05$ (**).

Results and discussion

Biological activity of hydrogels – Exposure to polysaccharides and DCA-enhanced poloxamer did not significantly affect the survival of AML12 cells. The addition of starch (F3), pectin (F5) and acacia (F7) benefited cell survival compared to poloxamer alone (F1). In the presence of F3, F5 and F12, there is a tentative increase compared to cells incubated without hydrogel (C) (Figure 1.a).

Muscle cells (C2C12) showed different behaviour compared with AML12 cells, as hydrogel exposure significantly decreased cell viability across all formulations (Figure 1.b). Adding pectin (F5 and F6) showed the least detrimental effect. Furthermore, adding DCA significantly decreased survival in the absence of polysaccharides (F2). Abrigo et al. observed muscle atrophy in the presence of DCA, which complies with our findings (36). Therefore, DCA's toxic effect on muscle cells may be mitigated with polysaccharides.

Pancreatic beta cells showed the most cell viability variations in hydrogels (Figure 1.c). Pectin-based hydrogels (F5 and F6) significantly decreased viability compared to the control (C). In contrast, all other formulations increased cell viability compared to the control, while the addition of starch (F3) increased survival compared to poloxamer alone (F1). Unlike muscle cells, the addition of DCA to poloxamer did not affect the survival of NIT-1 cells, as F1 and F2 show no significant difference. However, DCA addition did lower the viability of NIT-1 cells in the presence of starch (F4), acacia (F8) and ME cellulose (F12).

Rheological properties – The addition of CM and ME cellulose significantly increased the zeta potential of poloxamer (Figure 1.e). DCA addition significantly affected only the pectin-poloxamer mixture, decreasing the zeta potential. The only polysaccharide to significantly change the surface tension of poloxamer was MEC cellulose, leading to a modest increase (F11) (Figure 1.d). CM and ME cellulose-added hydrogel (F9 and F11) also had increased surface tension compared to pectin and acacia-containing hydrogels (F5 and F7). This may suggest stronger CM and MEC cellulose interactions with poloxamer than pectin and acacia. The viscosity of all hydrogels shows non-Newtonian fluid characteristics (Figure 1.f).

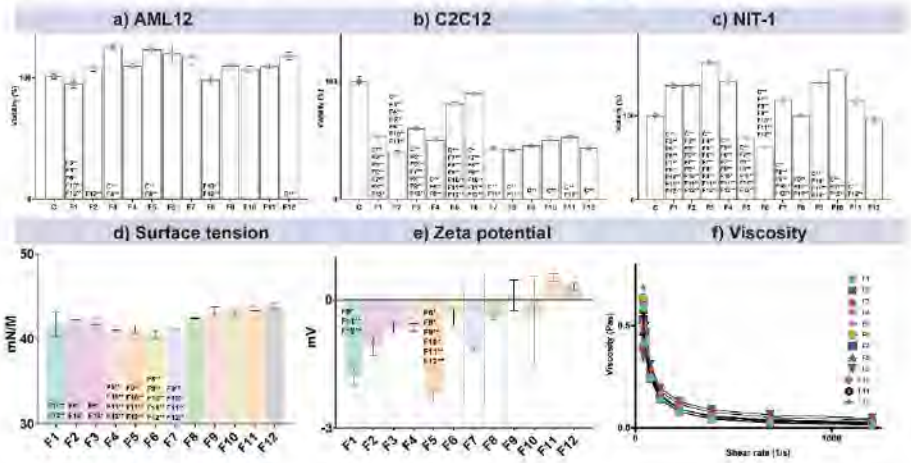

Figure 1. Viability of a) AML 12, b) C2C12, c) NIT-1 cell lines after 24 h incubation in the presence of polymers; rheology analysis showing d) surface tension, e) zeta potential, and f) viscosity of hydrogels at room temperature. Data ± SEM, *$p < 0.05$ and **$p < 0.01$.

Energetic profile of hepatic cells – Figure 2 shows the energetic profile of the hepatic AML12 cell line in hydrogels based on oxygen consumption rate (OCR) and extracellular acidification rate (ECAR). Cells in F1, F3, F4 and F10 had the highest bioenergetic profile, consistent with very energetic cells, while cells in the presence of F2, F8 and F12 had quiescent metabolism (Figure 2.a). The bioenergetic profile, in this case, is not consistent with viability, suggesting that quiescent metabolism may not affect survival, nor does high metabolism induce survival. The presence of hydrogels elevated the non-mitochondrial oxygen consumption (NMOC) of AML12 cells (Figure 2.b). Elevated non-mitochondrial consumption is linked with inflammation and the presence of stressors such as reactive oxygen species (ROS), and it is a negative marker of bioenergetic health (37). The presence of acacia, CM and ME cellulose mitigated some of the poloxamer oxidative effects. However, the lowest NMOC was achieved in the presence of DCA, which can be attributed to their quiescent metabolism rather than increased antioxidant potential in cells (F2, F8, and F12) (Figure 2.b). Furthermore, NMOC seems to be the most significant part of basal respiration in cells in the presence of all hydrogels (Figure 2.f), suggesting pro-oxidative effects of hydrogels and altered cellular respiration. While DCA is an agonist of the TGR5 receptor, known to decrease inflammation (38), and BAs are significant antioxidants as they raise glutathione levels (39), this study does not observe similar beneficial effects on the metabolism of hepatic cells. ATP production seems to utilise a smaller percentage of basal oxygen production in cells in the presence of hydrogels (Figure 2.f), with minimal percentage of detected ATP production in F2 and F11. Although, most of the APR production OCR values are not significantly different compared to control (Figure 2.e). The decrease in the share of ATP production in basal respiration seems to be negatively correlated with cell viability, while actual OCR values seem not to have as significant impact (40).

ECAR is derived mainly from glycolysis and is a parameter of anaerobic metabolism (41). The presence of poloxamer hydrogel significantly increased ECAR compared to hydrogel-free control, showing that cells within hydrogel experience a shift to anaerobic metabolism. Formulation with polysaccharides (F3, F5, F7, F9, F11) and DCA (F2, F6, F8, F10, F12) lowered ECAR compared to poloxamer-only formulation (Figure 2.h). However, ECAR decrease with F2, F8, and F12 may not be due to the beneficial anti-hypoxic impact of hydrogels, as cells were shown to have dormant metabolism in their presence.

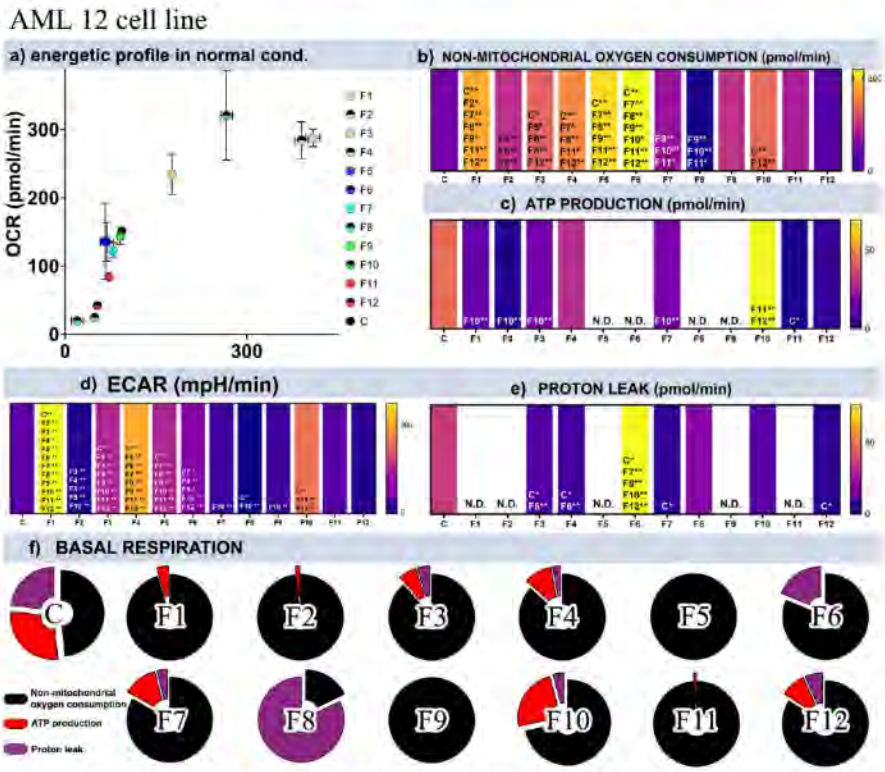

Figure 2. Bioenergetic profile of AML12 cells, after 24 h incubation, showing a) energetic profile in normal conditions, b) non-mitochondrial oxygen consumption, c) ATP production, d) ECAR, e) proton leak and f) basal respiration showed as the sum of means of non-mitochondrial oxygen consumption, ATP production and proton leak, with their sum being 100%. Data ± SEM, *$p < 0.05$ and **$p < 0.01$.

Energetic profile of muscle cells – myoblasts show decreased energy consumption in most hydrogels than hydrogel-free control (Figure 3.a). Their metabolism is not quiescent, suggesting that even with lowered viability (Figure 1.b), remaining cells are metabolically active and may combat further worsening of environmental conditions. Poloxamer (F1) did not significantly increase NMOC in C2C12 cells. Similar to AML12, F2 decreased NMOC compared to F1, suggesting an antioxidant effect of DCA (Figure 3.b). The presence of polysaccharides did not lower NMOC compared to F1. The presence of polysaccharides and DCA mixed with poloxamer did not significantly impact the ATP production of C2C12 cells (Figure 3.c). DCA addition (F2) decreased the proton leak of poloxamer (F1) (Figure 3.e). Increased proton leak is associated with increased uncoupling protein (UCP) activity, inner membrane damage, proton slippage and damage to the electron transport chain. UCP activity is increased in the presence of ROS. Thus leads to a negative feedback loop for ROS production by the mitochondria (42, 43). This contrasts with the study done by Huo et al., who reported DCA as a ROS generator in endothelial cells (44), and previous findings in AML12 cells, which suggests a selective impact of DCA on different tissues. Unlike AML12

cells, C2C12 cells retained ATP production in the presence of all hydrogels (Figure 3.c), but the share of ATP production in basal respiration decreased (Figure 3.f), suggesting altered cellular respiration and a decrease in cellular viability.

Based on ECAR values for C2C12 (Figure 3.d), F9 significantly lowered ECAR compared to the control. This may suggest shifting cell metabolism to more aerobic, but it is probably not the case considering the decreased share of ATP production in basal OCAR compared to the control (Figure 2.f).

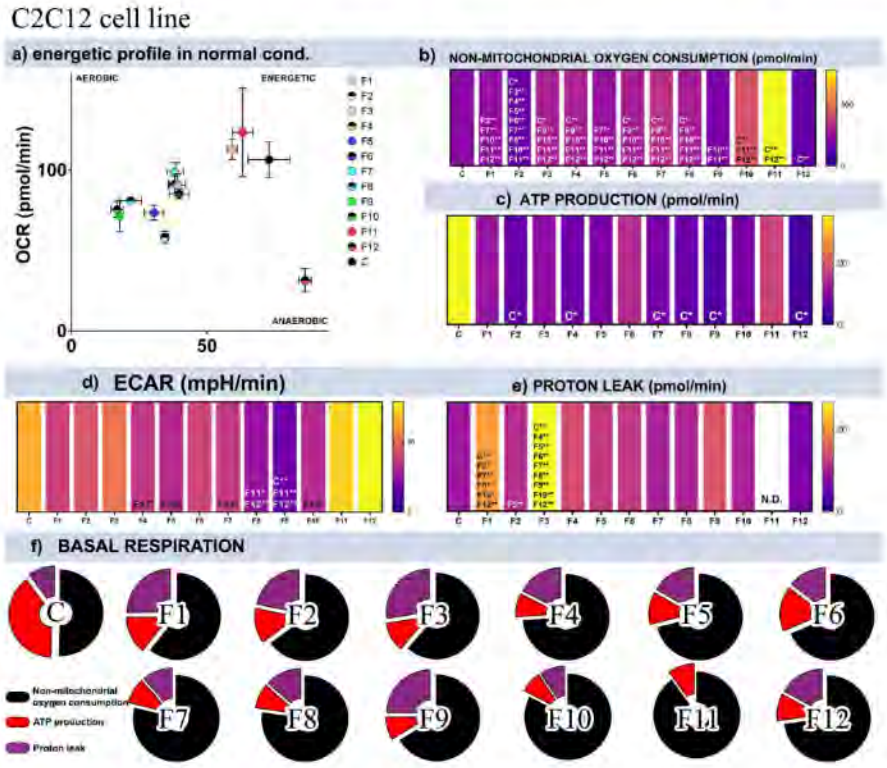

Figure 3. Bioenergetic profile of C2C12 cells, after 24 h incubation, showing a) energetic profile in normal conditions, b) non-mitochondrial oxygen consumption, c) ATP production, d) ECAR, e) proton leak and f) basal respiration showed as the sum of means of non-mitochondrial oxygen consumption, ATP production and proton leak, with their sum being 100%. Data ± SEM, *$p < 0.05$ and **$p < 0.01$.

Energetic profile of pancreatic beta cells – Figure 4.a shows increased metabolism of NIT-1 cells in hydrogels, except for F5 and F6. Viability findings (Figure 1.c) also report F5 and F6 as the only groups with significantly decreased viability. This contrasts C2C12 and AML12 findings, suggesting that NIT-1 cells may benefit more from a hydrogel environment. A soft hydrogel environment may influence this behaviour, as muscle cells need specific mechanical cues from extracellular topography to increase viability (45). On the

contrary, NIT-1 cells were found to adapt to a soft hydrogel environment (46, 47). Hydrogels increased non-mitochondrial oxygen consumption of NIT-1 cells, except for F5 and F6, which may contribute to these groups' low overall metabolism (Figure 4.b). The addition of DCA seems to lower this parameter (F2, F4, F10, F12), with the exception of acacia-based hydrogel (F8). DCA's decreasing NMOC (F2) from poloxamer's (F1) affects all cell lines. DCA addition in F2, F4, F8, F10 and F12 lowered ATP production compared to DCA-free hydrogels. F1 showed increased ATP production compared to C (Figure 4.c), while DCA addition (F2) decreased it. The addition of hydrogels did not affect the proton leak of NIT-1 cells (Figure 4.e). The distribution of ATP production and NMOC in basal respiration (Figure 4.f) shows somewhat preserved cellular respiration compared to control (C), especially in groups without DCA (F1, F3, F5, F7, F9, and F11). The addition of DCA seems to decrease the percentage of ATP production in basal OCR, especially in the presence of pectin (F6), acacia (F8) and ME cellulose (F12). Most hydrogels increased the ECAR of NIT-1 cells, while DCA addition had various effects (Figure 4.d).

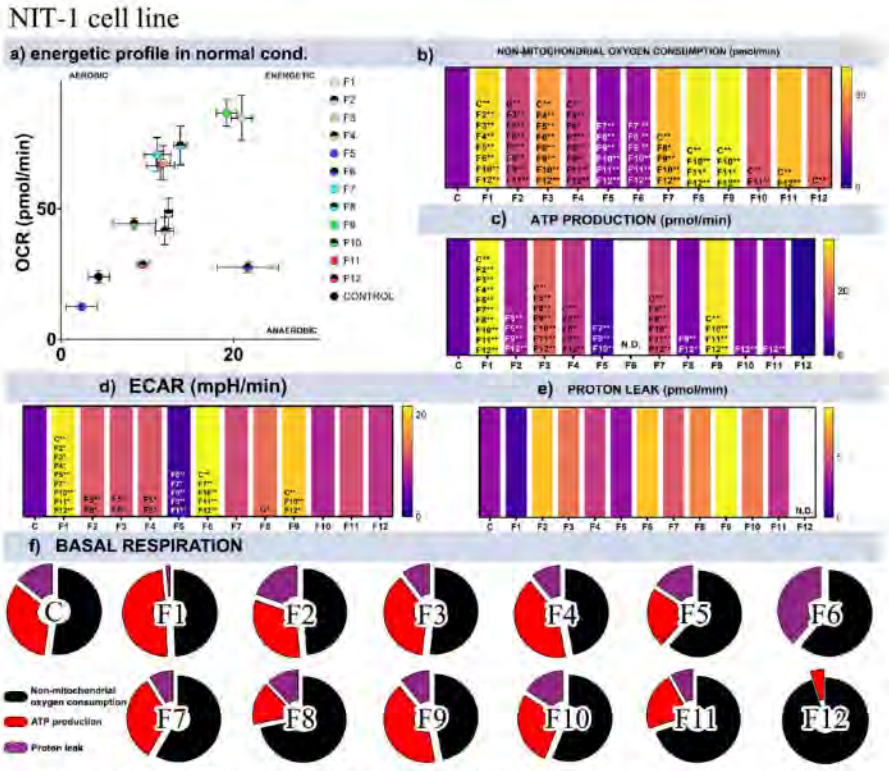

Figure 4. Bioenergetic profile of NIT-1 cells, after 24 h incubation, showing a) energetic profile in normal conditions, b) non-mitochondrial oxygen consumption, c) ATP production, d) ECAR, e) proton leak and f) basal respiration showed as the sum of means of non-mitochondrial oxygen consumption, ATP production and proton leak, with their sum being 100%. Data ± SEM ,*$p < 0.05$ and **$p < 0.01$.. Error bars ± SEM

Viability of cells in the presence of hydrogels in different hypoxic conditions – since most of the cells in the presence of hydrogel had altered anaerobic metabolism, we wanted to test how they would behave in further worsening micro-environments. Similar to the viability findings above (Figure 1.a), adding hydrogels did not significantly affect the viability of AML 12 cells in normal and low hypoxic conditions (Figure 5.a and 5.b). Hydrogels may have a protective effect on AML12 cells in high hypoxic conditions, as F1, F3, F4, F5, F7, F8, F9, F10, F11 and F12 showed a significant increase in viability (Figure 5.c). This may be very beneficial for tissue engineering and cell delivery, where hypoxic conditions are prevalent. Hydrogels decreased the viability of muscle cells (Figure 5.d, 5.e and 5.f). However, the decrease does not seem dependent on hypoxia conditions, as viability in hydrogels stays constant, while the viability of control changes based on conditions. This suggests that hydrogels may accustom C2C12 to hypoxia. For NIT-1 cells with increased hypoxia, F1, F2, F3, and F4 had significantly higher viability than control in both hypoxia environments. CM cellulose-based hydrogels lost their beneficial effect with increased hypoxia (Figure 5.h and 5.i). A decrease in viability connected with DCA in normal conditions was lost in increased hypoxia conditions (Figure 5.g, 5.h and 5.i), suggesting that DCA may have less of an effect on anaerobic NIT-1 cells. Similar findings were present in studies by Kovacevic *et al.* (41-43).

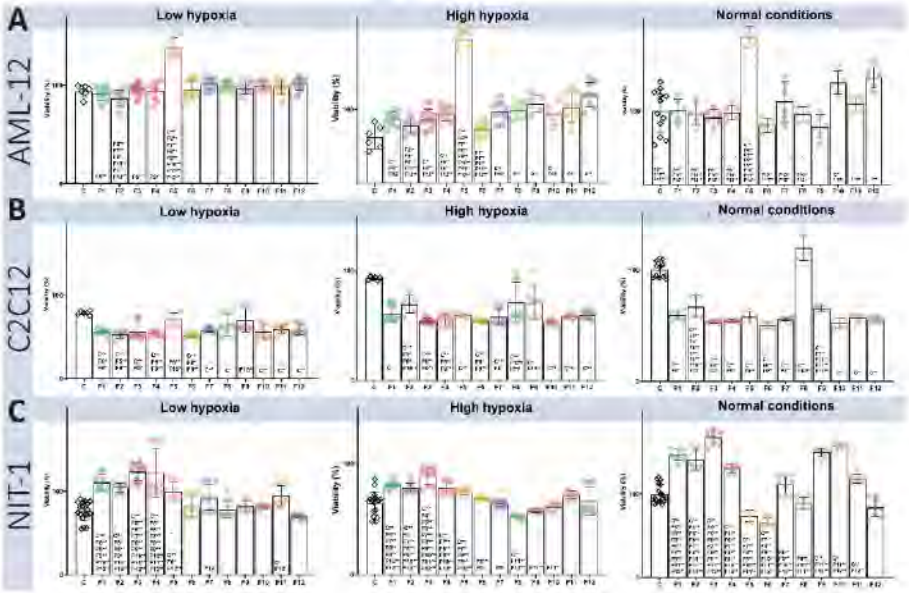

Figure 5. Viability of different cell lines under different hypoxic conditions; viability of AML12 cells in a) normoxic, b) low hypoxic, and c) high hypoxic conditions; viability of C2C12 cells in d) normoxic, e) low hypoxic, and f) high hypoxic conditions; and viability of NIT-1 cells in g) normoxic, h) low hypoxic, and i) high hypoxic conditions. Data ± SEM, *$p < 0.05$ and **$p < 0.01$.

Conclusion

Based on our findings, different tissues have unique responses to the same hydrogels. Hepatic cells show preserved viability after 24 hours, but their cellular respiration is reduced, with a substantial decrease in ATP production linked OCR in basal respiration. Conversely, muscle cells have low viability in the presence of hydrogels, but surviving cells still have detectable ATP production linked OCR. The pancreatic beta cells respond best to hydrogels, with the most negligible impact on cellular viability and respiration. Adding DCA to most hydrogels decreases the percentage of ATP production in basal respiration in hepatic and pancreatic beta cells. Due to this decrease in aerobic metabolism, DCA does not have as significant an impact on cellular viability in hypoxia as in normoxia. Among selected hydrogels, for NIT-1 cells, pectin and CM cellulose are the best-performing hydrogels when combined with DCA, and require further research on how the best to utilise hydrogels in pancreatic cell delivery.

Disclaimer

Funding: The work is partially supported by the European Union Horizon 2020 research project and innovation program under the Marie Skłodowska-Curie Grant Agreement No 872370. Curtin Faculty ORS-WAHAI Consortium and the Australian National Health and Medical Research (APP9000597).

Data Availability Statement: The data presented in this study are available on request from the corresponding author.

Acknowledgments: The authors would like to acknowledge the Australian Postgraduate Award (APA) and Curtin Research Scholarship (CRS).

Conflicts of Interest: The authors declare no conflict of interest.

Reference

1. Baumgartner M, Hartmann F, Drack M, Preninger D, Wirthl D, Gerstmayr R, et al. Resilient yet entirely degradable gelatin-based biogels for soft robots and electronics. Nature Materials. 2020;19(10):1102-9.
2. Wagle SR, Kovacevic B, Walker D, Ionescu CM, Jones M, Stojanovic G, et al. Pharmacological and Advanced Cell Respiration Effects, Enhanced by Toxic Human-Bile Nano-Pharmaceuticals of Probucol Cell-Targeting Formulations. Pharmaceutics. 2020;12(8):708.
3. Mooranian A, Raj Wagle S, Kovacevic B, Takechi R, Mamo J, Lam V, et al. Bile acid bio-nanoencapsulation improved drug targeted-delivery and pharmacological effects via cellular flux: 6-months diabetes preclinical study. Scientific Reports. 2020;10(1):106.
4. Wagle SR, Walker D, Kovacevic B, Gedawy A, Mikov M, Golocorbin-Kon S, et al. Micro-Nano formulation of bile-gut delivery: rheological, stability and cell survival, basal and maximum respiration studies. Scientific Reports. 2020;10(1):7715.
5. Pratap-Singh A, Guo Y, Lara Ochoa S, Fathordoobady F, Singh A. Optimal ultrasonication process time remains constant for a specific nanoemulsion size reduction system. Scientific Reports. 2021;11(1):9241.
6. Chae S, Oh S, Choi KH, Lee JW, Jeon J, Liu Z, et al. A study on the bio-applicability of aqueous-dispersed van der Waals 1-D material Nb2Se9 using poloxamer. Scientific Reports. 2021;11(1):176.
7. Khandelwal P, Das A, Sen CK, Srinivas SP, Roy S, Khanna S. A surfactant polymer wound dressing protects human keratinocytes from inducible necroptosis. Scientific Reports. 2021;11(1):4357.
8. Suntornnond R, Tan EYS, An J, Chua CK. A highly printable and biocompatible hydrogel composite for direct printing of soft and perfusable vasculature-like structures. Scientific Reports. 2017;7(1):16902.
9. Bonacucina G, Cespi M, Mencarelli G, Giorgioni G, Palmieri GF. Thermosensitive Self-Assembling Block Copolymers as Drug Delivery Systems. Polymers. 2011;3(2):779-811.
10. Ghorbani M, Roshangar L, Soleimani Rad J. Development of reinforced chitosan/pectin scaffold by using the cellulose nanocrystals as nanofillers: An injectable hydrogel for tissue engineering. European Polymer Journal. 2020;130:109697.
11. Long J, Etxeberria AE, Nand AV, Bunt CR, Ray S, Seyfoddin A. A 3D printed chitosan-pectin hydrogel wound dressing for lidocaine hydrochloride delivery. Materials Science and Engineering: C. 2019;104:109873.

12. Neufeld L, Bianco-Peled H. Pectin-chitosan physical hydrogels as potential drug delivery vehicles. Int J Biol Macromol. 2017;101:852-61.
13. Singh B, Sharma S, Dhiman A. Acacia gum polysaccharide based hydrogel wound dressings: Synthesis, characterization, drug delivery and biomedical properties. Carbohydrate Polymers. 2017;165:294-303.
14. Bhatnagar M, Parwani L, Sharma V, Ganguli J, Bhatnagar A. Hemostatic, antibacterial biopolymers from Acacia arabica (Lam.) Willd. and Moringa oleifera (Lam.) as potential wound dressing materials. Indian J Exp Biol. 2013;51(10):804-10.
15. Rezvanian M, Ahmad N, Mohd Amin MCI, Ng S-F. Optimization, characterization, and in vitro assessment of alginate-pectin ionic cross-linked hydrogel film for wound dressing applications. International Journal of Biological Macromolecules. 2017;97:131-40.
16. Raguvaran R, Manuja A, Manuja BK, Riyesh T, Singh S, Kesavan M, et al. Sodium alginate and gum acacia hydrogels of zinc oxide nanoparticles reduce hemolytic and oxidative stress inflicted by zinc oxide nanoparticles on mammalian cells. Int J Biol Macromol. 2017;101:967-72.
17. Su X, Xiao C, Hu C. Facile preparation and dual responsive behaviors of starch-based hydrogel containing azo and carboxylic groups. International Journal of Biological Macromolecules. 2018;115:1189-93.
18. Yuan X, Ju B, Zhang S. Novel pH- and temperature-responsive polymer: Tertiary amine starch ether. Carbohydrate Polymers. 2014;114:530-6.
19. Nain V, Kaur M, Sandhu KS, Thory R, Sinhmar A. Development, characterization, and biocompatibility of zinc oxide coupled starch nanocomposites from different botanical sources. International Journal of Biological Macromolecules. 2020;162:24-30.
20. Garrett Q, Simmons PA, Xu S, Vehige J, Zhao Z, Ehrmann K, et al. Carboxymethylcellulose binds to human corneal epithelial cells and is a modulator of corneal epithelial wound healing. Invest Ophthalmol Vis Sci. 2007;48(4):1559-67.
21. Gašparič P, Kurecic M, Kargl R, Maver U, Gradisnik L, Hribernik S, et al. Nanofibrous polysaccharide hydroxyapatite composites with biocompatibility against human osteoblasts. Carbohydrate Polymers. 2017;177.
22. Rasoulzadeh M, Namazi H. Carboxymethyl cellulose/graphene oxide bio-nanocomposite hydrogel beads as anticancer drug carrier agent. Carbohydr Polym. 2017;168:320-6.
23. Wang C, Fadeev M, Zhang J, Vázquez-González M, Davidson-Rozenfeld G, Tian H, et al. Shape-memory and self-healing functions of DNA-based carboxymethyl cellulose hydrogels driven by chemical or light triggers. Chemical Science. 2018;9(35):7145-52.
24. Hu Y, Hu S, Zhang S, Dong S, Hu J, Kang L, et al. A double-layer hydrogel based on alginate-carboxymethyl cellulose and synthetic polymer as sustained drug delivery system. Scientific Reports. 2021;11(1):9142.
25. Naumann S, Schweiggert-Weisz U, Bader-Mittermaier S, Haller D, Eisner P. Differentiation of Adsorptive and Viscous Effects of Dietary Fibres on Bile Acid Release by Means of In Vitro Digestion and Dialysis. International Journal of Molecular Sciences. 2018;19(8):2193.
26. Armin M, Nassim Z, Ryu T, Giuseppe L, Momir M, Svetlana G-K, et al. Modulatory Nano/Micro Effects of Diabetes Development on Pharmacology of Primary and Secondary Bile Acids Concentrations. Current Diabetes Reviews. 2020;16(8):900-9.
27. Mooranian A, Zamani N, Ionescu CM, Takechi R, Luna G, Mikov M, et al. Oral gavage of nano-encapsulated conjugated acrylic acid-bile acid formulation in type 1 diabetes altered pharmacological profile of bile acids, and improved glycaemia and suppressed inflammation. Pharmacological Reports. 2020;72(2):368-78.

28. Wagle SR, Kovacevic B, Walker D, Ionescu CM, Shah U, Stojanovic G, et al. Alginate-based drug oral targeting using bio-micro/nano encapsulation technologies. Expert Opinion on Drug Delivery. 2020;17(10):1361-76.
29. Kovacevic B, Ionescu CM, Wagle SR, Jones M, Lewkowicz M, Wong EYM, et al. Impact of Novel Teflon-DCA Nanogel Matrix on Cellular Bioactivity. Journal of Pharmaceutical Sciences. 2022.
30. Mooranian A, Ionescu CM, Walker D, Jones M, Wagle SR, Kovacevic B, et al. Single-Cellular Biological Effects of Cholesterol-Catabolic Bile Acid-Based Nano/Micro Capsules as Anti-Inflammatory Cell Protective Systems. Biomolecules. 2022;12(1):73.
31. Kovacevic B, Wagle SR, Ionescu CM, Jones M, Lewkowicz M, Wong EYM, et al. Novel hydrogel comprising non-ionic copolymer with various concentrations of pharmacologically active bile acids for cellular injectable gel. Colloids and Surfaces B: Biointerfaces. 2023;222:113014.
32. Mooranian A, Foster T, Ionescu CM, Walker D, Jones M, Wagle SR, et al. Enhanced Bilosomal Properties Resulted in Optimum Pharmacological Effects by Increased Acidification Pathways. Pharmaceutics. 2021;13(8):1184.
33. Li Q, Ma R, Zhang M. CoCl2 increases the expression of hypoxic markers HIF-1α, VEGF and CXCR4 in breast cancer MCF-7 cells. Oncol Lett. 2018;15(1):1119-24.
34. Mooranian A, Jones M, Ionescu CM, Walker D, Wagle SR, Kovacevic B, et al. Advancements in Assessments of Bio-Tissue Engineering and Viable Cell Delivery Matrices Using Bile Acid-Based Pharmacological Biotechnologies. Nanomaterials. 2021;11(7):1861.
35. Mooranian A, Jones M, Walker D, Ionescu CM, Wagle SR, Kovacevic B, et al. Pharmacological Dose-Effect Profiles of Various Concentrations of Humanised Primary Bile Acid in Encapsulated Cells. Nanomaterials. 2022;12(4):647.
36. Abrigo J, Gonzalez F, Aguirre F, Tacchi F, Gonzalez A, Meza MP, et al. Cholic acid and deoxycholic acid induce skeletal muscle atrophy through a mechanism dependent on TGR5 receptor. Journal of Cellular Physiology. 2021;236(1):260-72.
37. Chacko Balu K, Kramer Philip A, Ravi S, Benavides Gloria A, Mitchell T, Dranka Brian P, et al. The Bioenergetic Health Index: a new concept in mitochondrial translational research. Clinical Science. 2014;127(6):367-73.
38. Kuipers F, Bloks VW, Groen AK. Beyond intestinal soap—bile acids in metabolic control. Nature Reviews Endocrinology. 2014;10:488.
39. Kovacevic B, Jones M, Ionescu C, Walker D, Wagle S, Chester J, et al. The emerging role of bile acids as critical components in nanotechnology and bioengineering: Pharmacology, formulation optimizers and hydrogel-biomaterial applications. Biomaterials. 2022;283:121459.
40. Kovacevic B, Ionescu CM, Jones M, Wagle SR, Lewkowicz M, Đanić M, et al. The Effect of Deoxycholic Acid on Chitosan-Enabled Matrices for Tissue Scaffolding and Injectable Nanogels. Gels [Internet]. 2022; 8(6).
41. Mookerjee SA, Goncalves RLS, Gerencser AA, Nicholls DG, Brand MD. The contributions of respiration and glycolysis to extracellular acid production. Biochimica et Biophysica Acta (BBA) - Bioenergetics. 2015;1847(2):171-81.
42. Mailloux RJ, Harper M-E. Uncoupling proteins and the control of mitochondrial reactive oxygen species production. Free Radical Biology and Medicine. 2011;51(6):1106-15.
43. Nanayakkara GK, Wang H, Yang X. Proton leak regulates mitochondrial reactive oxygen species generation in endothelial cell activation and inflammation - A novel concept. Archives of Biochemistry and Biophysics. 2019;662:68-74.
44. Huo X, Juergens S, Zhang X, Rezaei D, Yu C, Strauch ED, et al. Deoxycholic acid causes DNA damage while inducing apoptotic resistance through NF-κB activation in benign

Barrett's epithelial cells. American Journal of Physiology-Gastrointestinal and Liver Physiology. 2011;301(2):G278-G86.
45. Alarcin E, Bal-Öztürk A, Avci H, Ghorbanpoor H, Dogan Guzel F, Akpek A, et al. Current Strategies for the Regeneration of Skeletal Muscle Tissue. International Journal of Molecular Sciences. 2021;22(11):5929.
46. Mooranian A, Negrulj R, Al-Salami H. The incorporation of water-soluble gel matrix into bile acid-based microcapsules for the delivery of viable β-cells of the pancreas, in diabetes treatment: biocompatibility and functionality studies. Drug Delivery and Translational Research. 2016;6(1):17-23.
47. Mooranian A, Negrulj R, Jamieson E, Morahan G, Al-Salami H. Biological Assessments of Encapsulated Pancreatic β-Cells: Their Potential Transplantation in Diabetes. Cellular and Molecular Bioengineering. 2016;9(4):530-7.

Chapter 4

Poloxamer 407 And Bile Acid-Based Nanogels For Inner Ear Delivery: Rheological Properties And Biocompatibility

Chapter 4

Poloxamer 407 And Bile Acid-Based Nanogels For Inner Ear Delivery: Rheological Properties And Biocompatibility

The contents of this chapter are covered by publication 8 (pages 142-151), publication 9 (pages 153-169) and publication 10 (pages 171-181).

Publication 8 (pages 142-151):

Kovacevic B, Wagle SR, Ionescu CM, Foster T, Đanić M, Mikov M, Mooranian A, Al-Salami H. The biocompatibility and the metabolic impact of thermoresponsive, bile acid-based nanogels on auditory and macrophage cell lines. European Journal of Pharmaceutics and Biopharmaceutics. 2023;190:248-57.

Sub-objective (7): to design and create nanogels utilising poloxamer 407, polyvinyl alcohol, deoxycholic acid, lithocholic acid and ursodeoxycholic acid and to examine the shear stress, viscosity, surface tension, torque, microstructure, and zeta potential of nanogels. Additionally, the nanogels were incubated with 2 different cell lines (HEI-OC1 and RAW264.7) and their impact on viability, total intracellular reactive oxygen species, as well as their impact on bioenergetic parameters, was investigated.

European Journal of Pharmaceutics and Biopharmaceutics 190 (2023) 248–257

Contents lists available at ScienceDirect

European Journal of Pharmaceutics and Biopharmaceutics

journal homepage: www.elsevier.com/locate/ejpb

Research paper

The biocompatibility and the metabolic impact of thermoresponsive, bile acid-based nanogels on auditory and macrophage cell lines

Bozica Kovacevic [a], Susbin Raj Wagle [a], Corina Mihaela Ionescu [a], Thomas Foster [a], Maja Đanić [b], Momir Mikov [b], Armin Mooranian [a,c,1,*], Hani Al-Salami [a,d,1,*]

[a] The Biotechnology and Drug Development Research Laboratory, Curtin Medical School & Curtin Health Innovation Research Institute, Curtin University, Bentley, Perth, WA 6102, Australia
[b] Department of Pharmacology, Toxicology and Clinical Pharmacology, Faculty of Medicine, University of Novi Sad, Novi Sad 21101, Serbia
[c] School of Pharmacy, University of Otago, Dunedin, Otago, New Zealand
[d] Medical School, University of Western Australia, Perth, Australia

ARTICLE INFO

Keywords:
Thermoresponsive hydrogel
Nanogel
Biocompatibility
RAW264.7
HEI OC1
Bioenergetics
Poloxamer 407
Bile acid

ABSTRACT

Deoxycholic acid (DCA), lithocholic acid (LCA), and ursodeoxycholic acid (UDCA) are bile acids that may serve as permeation enhancers when incorporated within the nanogel matrix for drug delivery in the inner ear. In this study, thermoresponsive nanogels were formulated with DCA, LCA and UDCA and their rheological properties and biocompatibility were assessed. The impact of nanogel on cellular viability was evaluated via cell viability assay, the impact of nanogels on cellular bioenergetic parameters was estimated by Seahorse mito-stress test and glycolysis-stress test, while the presence of intracellular free radicals was assessed by reactive oxygen species assay. Nanogels showed a high level of biocompatibility after 24-hour exposure to auditory and macrophage cell lines, with minimal cytotoxicity compared to untreated control. Incubation with nanogels did not alter cellular respiration and glycolysis of the auditory cell line but showed possible mitochondrial dysfunction in macrophages, suggesting tissue-dependent effects of bile acids. Bile acid-nanogels had minimal impact on intracellular reactive oxygen species, with LCA demonstrating the most pro-oxidative behaviour. This study suggests that thermoresponsive nanogels with bile acid, particularly DCA and UDCA, may be promising candidates for inner ear drug delivery.

1. Introductions

Drug delivery systems are conventionally used to solubilise drugs of interest, and/or improve their bioavailability, and subsequently modulate the drug's pharmacokinetics and pharmacodynamics [1]. Nanogels are multifunctional drug delivery systems that can be modified to serve different delivery models, including active targeting by nanogels' surface modification, passive targeting through enhanced permeability and retention effect, as well as time- and location-controlled drug delivery strategies mediated by stimuli-responsive properties [2,3]. Nanogels are a subclassification of hydrogels with particle sizes in the submicron range, with tuneable biocompatibility, water content, size, surface area, and three-dimensional structure, that are essential in facilitating drug delivery [4].

The customisable nature of nanogels is beneficial in challenging drug delivery sites, such as the inner ear. Drug delivery to the inner ear is especially problematic due to anatomical and biological barriers. Currently, most treatments are limited to systemic drug delivery, intratympanic injections and surgery, each possessing certain risks and side effects [5]. Systemic drug delivery often relies on high drug concentrations due to the inner ear's limited blood supply and the drug's low penetration through the blood–labyrinth barrier, leading to adverse side effects and increasing focus on targeted, local drug delivery [6,7]. Hydrogels are desirable for inner ear delivery as they can prolong drug contact with targeted tissue and decrease drug clearance through the eustachian tube. Increased permeability of round window membrane is required, to increase drug uptake to the inner ear and reduce the effects of round window membrane inter variability [8]. Combining different

* Corresponding authors at: The Biotechnology and Drug Development Research Laboratory, Curtin Medical School & Curtin Health Innovation Research Institute, Curtin University, Bentley, Perth, WA 6102, Australia.
E-mail addresses: a.mooranian@curtin.edu.au (A. Mooranian), al-salami@curtin.edu.au (H. Al-Salami).
[1] Authors contributed equally.

https://doi.org/10.1016/j.ejpb.2023.08.003
Received 29 June 2023; Received in revised form 2 August 2023; Accepted 8 August 2023
Available online 9 August 2023
0939-6411/© 2023 Published by Elsevier B.V.

strategies in one therapeutic delivery matrix may be the most useful strategy to overcome multiple barriers within the inner ear drug delivery route.

One of the polymers capable of forming nanogels is Poloxamer 407. Poloxamer 407 is a triblock amphiphilic copolymer that responds to temperature stimuli [9]. Fabrice et al. achieved prolonged dexamethasone release in the inner ear fluids via *trans*-tympanic injection of drug-poloxamer nanogel [10]. More recently, Liao et al. facilitated inner ear delivery of the same drug in a poloxamer vehicle utilising ultrasound and microbubbles [11]. Zhu et al. found otoprotective effects of dexamethasone and other steroids in poloxamer hydrogel on a hearing loss guinea pig model [12]. To aid drug delivery to the inner ear, permeation agents are likely necessary, and bile acids (BA)s may be a novel solution.

BAs are amphipathic surfactants with steroid nuclei, with the ability to self-assemble to micelles, and more complex secondary polymolecular aggregates [13]. They are endogenously produced in humans to facilitate lipid adsorption, with increasing numbers of other physiologic and pathophysiologic roles [14,15]. BAs and their derivatives may be permeation enhancers as they widen tight junctions between cells, increasing paracellular and transcellular drug absorption. Furthermore, BAs enhance membrane permeability via cell swelling. However, this effect can be membranolytic at high concentrations [16]. BAs are reported to be promising transdermal absorption enhancers [17], as well as valuable permeation enhancers for ocular delivery [18]. With a hearing loss being a worldwide epidemic, BAs can be useful in mitigating challenges in delivery of therapeutic agents to inner ear as permeation enhancers [19].

Deoxycholic acid (DCA), lithocholic acid (LCA) and ursodeoxycholic acid (UDCA) may be potential candidates for permeation enhancers in nanogel drug delivery in the inner ear. All three BAs have established pharmacology in the literature. DCA has been investigated as part of ligand-PEG-lipid conjugates in targeted cancer treatment [20] and as the permeation enhancer for oral medication in chemotherapy [21]. LCA provides bio-based polyesters' solubility and thermal stability [22]. Yadav et al. investigated the benefits of LCA in lipid drug conjugates for effective breast cancer therapy [23]. Matsusaki et al. showed that incorporating LCA into biopolymers affects the hydrophobicity and cell adhesion of these structures [24]. UDCA has shown promising anti-cancer effects as a prodrug conjugate [25], and part of prodrug nanoparticles for bone regeneration [26]. Nanoencapsulated geraniol/UDCA conjugate has been found to penetrate nasal mucosa and suggest direct nose to brain delivery of the prodrug without damaging the structural integrity of nasal mucosa [27]. BAs are also thought to improve the delivery of genes in nanotechnology to the inner ear [28].

Therefore, this study will investigate the rheological properties of poloxamer 407-based nanogels with the addition of BAs. Furthermore, this study reports the biocompatibility of novel nanogels, investigating their impact on the viability and metabolism of auditory and macrophage cell lines.

2. Methods and materials

The Poloxamer 407, polyvinyl alcohol (PVA), DCA, LCA and UDCA were bought from Sigma Chemical Co (St. Louis, MO, USA). Foetal bovine serum (FBS) and Dulbecco's modified Eagle's medium (DMEM) were bought from Sigma Chemical Co (St. Louis, MO, USA). RAW 264.7 (ATCC®, TIB-71™) cell line was purchased from a commercial vendor, American Type Culture Collection (ATCC). HEI-OC1 (House Ear Institute-Organ of Corti 1) cell line was kindly provided by Prof Federico Kalinec (University of California, CA, USA). Both cell lines were cultured in high glucose DMEM with 10 % FBS without antibiotics. RAW264.7 were incubated at 37 °C and 10 % CO_2 with media change every 48 h. HEI-OC1 were cultured at a permissive temperature (33 °C), and 10 % CO_2 with media change every 48 h.

BAs (DCA, LCA and UDCA) were prepared in a 3 % poloxamer solution with deionised water for BA viability studies. BAs concentrations were 0.02 %, 0.06 %, 0.1 %, 0.2 %, 0.5 %, 1 %, 1.5 %, 2 % and 3 %. Prepared formulations were treated under UV light for 30 min and used in cell viability tests. HEI-OC1 cells were seeded 180 μl (1.5×10^5/ml) per well in 96-well plates, left overnight and then treated with 20 μl of BA formulations. Cells were left to incubate for 24 h at a permissive condition, and cellular viability was assessed with Water Soluble Tetrazolium Salts-1 (WST-1) assay. The 10 % v/v of WST-1 was added to each well and incubated for 3 h. Per the manufacturer's protocol, the resulting absorbance was measured on a PerkinElmer Multimode Plate Reader (Waltham, MA, USA). The data were normalised against the background and presented as a percentage of cells treated with 0 % BA. All obtained data were in triplicates (n = 3).

The nanogels were made using 18 % Poloxamer 407 for all groups, 0.06 % PVA for groups G2, G3, G4 and G5, 0.02 % DCA for G3, 0.02 % LCA for G4 and 0.02 % UDCA for G5. PVA was first dissolved in deionised water at 60 °C under constant stirring. The PVA solution was allowed to cool to room temperature, after which BAs and Poloxamer were added. Nanogels were stirred at 4 °C overnight until a clear, transparent nanogel solution was obtained. The nanogels were treated under UV light for 30 min before usage in any tissue culture assays. All obtained data were in triplicates (n = 3).

The gelation time was assessed via the vial tilting method. Briefly, 500 μl of nanogels were added at room temperature to vials, and placed in a water bath to set at 37 °C. The tubes were tilted regularly, and the gelation time was recorded when the nanogels lost their fluidity upon tilting [29].

The mean particle size and zeta potential of nanogels were measured using 3000HS Zetasizer (Malvern Instruments, Malvern, UK) by placing samples in a glass cuvette with a square aperture. The adjacent software's standard operating procedure was designed with 25 runs per measurement [30]. Surface tension values were obtained by a tensiometer (Sigma 703, ATA Scientific, Caringbah, Australia), utilising the du Noüy ring method. The rheological parameters were obtained from freshly made formulations using a Visco 88 viscometer (Malvern Instruments, Malvern, UK) for viscosity, shear stress and shear rate. Aliquots of samples were placed in the instrument cup, and results were obtained at six different rotational speeds. All measuring processes were done at room temperature, following established protocols [31–37]. All obtained data were in triplicates (n = 3) using our established methods.

Nanogels were freeze-dried for 48 h using Dynavac FD3 Freeze Dryer (Dynapumps, Seven Hills, Australia). The samples were platinum-coated, and scanning electron microscope (SEM) micrographs were obtained using Clara (Tescan, Brno, CZ) at 10 mm working distance, 2 kV, and 100 Å beam current.

Curve fitting for the Power law model (Eq.1) was performed using the solver function in Microsoft Excel, adopting the nonlinear optimisation code. The best fit of the minimum sum of square errors (SSE) was used as the criteria for curve fitting. The R^2 (the goodness of the fit) was calculated as $R^2 = 1 - (SSE/SST)$, with SST being the total corrected sum of squares [38].

The power Law equation:

$$\tau = K\dot{\gamma}^n \tag{1}$$

where τ is the shear stress (Pa), K is the consistency coefficient, $\dot{\gamma}$ is the shear rate (s^{-1}), and n is the flow behaviour index.

For the cell viability assay, for each cell line HEI-OC1 and RAW264.7, cells in the 1.5×10^5/ml concentration were seeded 180 μl per well and left overnight in growth media. Afterwards, 20 μl of nanogels was added per well and left to incubate for 24 h, followed by WST-1 assay. The data were normalised against the background and presented as a percentage of untreated cells (C). All obtained data were in triplicates (n = 3).

The cell viability was further confirmed with an ALIVE/DEAD assay. Cells were seeded in 96-well plates in concentration 1.5×10^5/ml, 180 μl per well. 20 μl of nanogels was added per well and left to incubate for 24 h, followed by staining with Carboxyfluorescein Diacetate

Succinimidyl Ester (CFSE) (CellTrace™ CFSE Cell Proliferation Kit, Thermo Fisher Scientific Inc., MA, USA) and Propidium Iodide (PI) (Thermo Fisher Scientific Inc., MA, USA) as per established protocols [38]. Fluorescent images were obtained by Olympus IX51 inverted microscope (Olympus, Tokyo, Japan). The cells were considered dead if they emitted a PI fluorescence signal (red) and alive if they emitted a green fluorescence signal. All obtained data were in triplicates (n = 3).

For bioenergetics parameters, cells were treated the same as for viability assays. After 24 h incubation, the Seahorse XF Cell Mito Stress Test and the Seahorse XF Glycolysis Stress Test were performed using Seahorse Flux Analyser XF 96 (Agilent Technologies, Santa Clara, CA, USA). Tests were performed on both cell lines using in-house developed methods and manufacturer protocols [31]. Control cells were untreated cells. All obtained data were in triplicates (n = 3).

For the reactive oxygen species (ROS) assay, cells were seeded overnight at 0.5–1 × 10^5/ml in a 96-well plate, 180 µl per well. Cells were stained per the manufacturer's protocol Cellular ROS Assay Kit (Deep Red, Abcam, Cambridge, UK) and treated with 20 µl of nanogels. The fluorescence excitation of 650 nm and emission of 675 nm signal was monitored using the PerkinElmer Multimode Plate Readers after 30 min. The same protocol was followed for visualisation, and the signal was obtained using Operetta CLS (PerkinElmer, Mulgrave, VIC, Australia) high throughput microplate imager. Control cells were untreated cells. All obtained data were in triplicates n = 3.

Part of the referenced literature has been added by searching for key words: bile acid, nanogel, deoxycholic acid, ursodeoxycholic acid and lithocholic acid on ProQuest and Scopus databases.

Statistical analysis was done by GraphPad Prism version 9.3 (Graphpad, Inc. San Diego, CA, USA). One-way ANOVA, regression analysis, and Tukey HSD were utilised appropriate of data. All data is shown as mean ± SEM, with statistical significance defined as $p < 0.05$ (*) and $p < 0.01$ (**).

3. Results

To better assess the impact of BA concentrations on the viability of the HEI-OC1 cell line, we conducted WST-1 test after 24 h incubation with the addition of different concentrations of either DCA, UDCA or LCA, solubilised in 4 % poloxamer 407. The viability results are presented in Fig. 1, with the HEI-OC1 cell line showing a sigmoidal dose response to all three BAs. DCA and UDCA show stark cytotoxic effects above 1 % (Fig. 1a and 1b), with the highest viability at the lowest concentrations. HEI-OC1 show a different response to LCA, with preserved relatively high viability even at higher concentrations (Fig. 1c). Other studies reported a similar, complex relationship between BAs and cellular viability. Sharma et al. found a direct linear relationship between BAs toxicity and their hydrophobicity in an esophagus cell line. In contrast, this relationship was not confirmed in the hepatic carcinoma cell line [39]. As LCA is the most hydrophobic BA of examined BAs, followed by DCA and UDCA, there is not direct relationship between hydrophobicity and cytotoxicity for the HEI-OC1 cell line. LCA has been found to have a detrimental effect on osteocytes, with effects that can be neutralised by UDCA [40]. This does not seem to be the case in this auditory cell line. Based on this data, it was decided to add the same low concentration (0.02 %) of BA to poloxamer 407-PVA nanogel.

The gelation times for all five nanogels formulations are less than ten seconds when moving 0.5 mL of nanogel from room temperature to 37 °C (Fig. 2a). The addition of LCA (G4) has a slightly shortened gelation time, especially compared to nanogel with DCA (G3). This may be related to the higher viscosity of G4 compared to the other hydrogels in this study (Fig. 2f). The mean particle size at room temperature is <200 nm for all nanogels (Fig. 2b). The nanogel with LCA (G4) has a smaller particle size compared to the nanogels with DCA (G3) and UDCA (G5) (Fig. 2b). The nanoscale of hydrogel is beneficial, as drug delivery involving nanomaterials has been shown to have improved biocompatibility, safety, and specificity [41]. The surface tension of poloxamer 407 (G1) increases with the addition of PVA (G2) (Fig. 2c). DCA (G3) and LCA (G4) slightly lower the surface tension compared to poloxamer-PVA control (G2), with LCA lowering surface tension more than DCA. BAs are amphiphilic surfactants shown to decrease surface tension [42], with their hydrophobicity influencing the level of interaction [43]. UDCA (G5) did not alter surface tension compared to G2 (Fig. 2e). The zeta potential of all nanogels is close to zero (Fig. 2d). Neutral surface charge of the hydrogel may be important as previous studies have found that hydrogels may resist albumin adsorption, delaying foreign body reaction [44]. Shear stress and viscosity rheograms (Fig. 2e and 2f) suggest non-Newtonian shear thinning flow behaviour. This is further confirmed with values of flow behaviour index n (Table 1), where $n < 1$ indicted pseudoplastic (shear-thinning) fluid behaviour [30]. The presence of PVA and BAs in nanogels (G2, G3, G4, and G5) seems to increase the pseudoplastic behaviour of poloxamer 407 (G1). Upon application of shear force, the viscosity of the nanogel is lowered, creating a fluid-like flow that allows for easy injection and less additional stress on therapeutic cargo [45]. The consistency coefficient (K) represents the viscosity level, with higher K values suggesting higher viscosity [46]. The addition of LCA (G4), and UDCA (G5), seems to have the highest viscosity at room temperature (Table 1). A high coefficient of determination (R^2) suggests good accuracy of the experimental data (Table 1). The SEM micrographs show complex, porous microstructure consistent with freeze dried hydrogels [47]. Porous structure may be beneficial for drug loading within nanogels, and well as during drug release. Different nanogels do not show significant difference in morphology between different formulations (Fig. 2g). Nanogels G4 and G5 show striping line pattern on the surface, which may be result of freeze drying process.

The viability of HEI-OC1 cells seems to be preserved in the presence of nanogels, without a significant decrease in viability in the presence of any nanogel (Fig. 3a). The presence of G1, G2 and G3 seems to impact inner ear cell viability slightly. At the same time, the incubation with G4 and G5 does not alter viability compared to the untreated cells (C). Similarly, 24 h incubation with nanogels does not significantly alter the viability of the RAW 264.7 cell line compared to the control (Fig. 3b). The presence of DCA (G3) seems to increase viability slightly compared to gel without BAs (G1 and G2).

Incubation with nanogels does not significantly alter the mitochondrial metabolism of the HEI-OC1 cell line (Fig. 4). There is no significant difference between values for basal respiration-linked oxygen consumption (OCR) (Fig. 4a), ATP production-linked OCR (Fig. 4b), coupling efficiency (Fig. 4c), proton leak-linked OCR (Fig. 4d) and non-

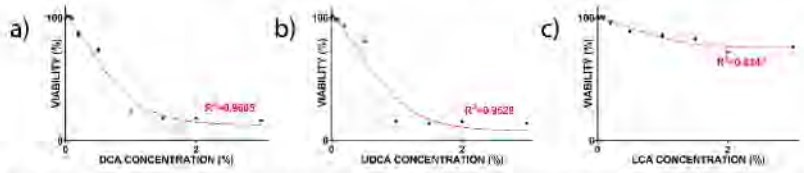

Fig. 1. Shows the viability of HEI-OC1 when exposed to a) DCA, b) UDCA and c) LCA concentration gradient. The viability of control cells is 100 %.

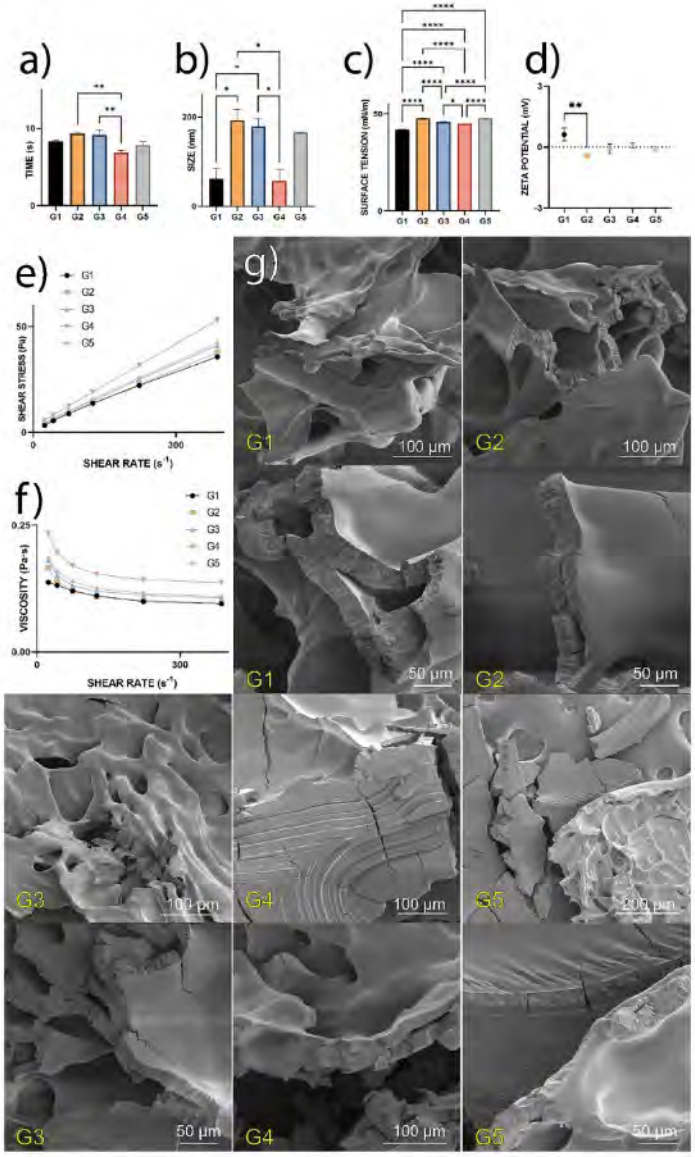

Fig. 2. Shows nanogels' a) gelation times, b) average particle size, c) surface tension, d) zeta potential, e) shear stress, f) viscosity, and g) SEM micrographs of freeze-dried nanogels. Data are shown as mean ± SEM, n = 3. $p < 0.05$ (*) and $p < 0.01$ (**).

Table 1
Parameters from power law fitting $\sigma = K\dot{\gamma}^n$ of rheological properties of different nanogels.

	Temperature (°C)	Consistency coefficient, K	Flow behaviour index, n	Coefficient of determination, R^2
G1	22 ± 0.5	0.21814 ± 0.00794	0.85992 ± 0.00710	0.99966 ± 0.00014
G2	22 ± 0.5	0.28863 ± 0.01599	0.80698 ± 0.01144	0.99741 ± 0.00088
G3	22 ± 0.5	0.28881 ± 0.01993	0.82543 ± 0.01381	0.99653 ± 0.00117
G4	22 ± 0.5	0.42846 ± 0.00416	0.79598 ± 0.00202	0.99849 ± 0.00013
G5	22 ± 0.5	0.34347 ± 0.00455	0.79821 ± 0.00199	0.99907 ± 0.00003

mitochondrial oxygen consumption linked OCR (Fig. 4e). Non-significant differences in ATP production and proton leak suggest good integrity of the electron transport chain and mitochondrial membrane [48]. As previous studies found significant disruption in ATP production in the presence of higher concentrations of BAs [42,49,50], it seems that current formulations may be better optimised for biocompatibility. The mitochondrial stress test shows an increase in extracellular acidification rate (ECAR) during basal metabolism (Fig. 4f). The increased ECAR may suggest intensified glycolysis with amplified lactate production [51]. However, the following glycolysis stress test reported a slight increase in glycolysis in cells exposed to nanogels. Still, these findings are not statistically significant (Fig. 4g). There is an increase in non-glycolytic acidification linked to ECAR in the presence of LCA (G4) compared to control nanogel (G2) (Fig. 4h). Significant contributors to non-glycolytic acidification linked ECAR are TCA cycle linked CO_2 production and breakdown of intracellular glycogen [52], but as G4 non-glycolytic acidification is not different to untreated control, it may not be physiologically relevant. There are no statistically significant differences in other observed glycolysis parameters, including glycolytic capacity, glycolytic reserve, and glycolytic reserve as a percentage of glycolysis, when comparing untreated cells (C) with treated ones (G1-G5) (Fig. 4i, 4j and 4k).

Incubation with nanogels altered the metabolic profile of the macrophage cell line (Fig. 5). There is a significant increase in basal respiration-linked OCR of cells exposed to control nanogels (G1 and G2) compared to untreated cells (C) (Fig. 5a). The presence of BAs,

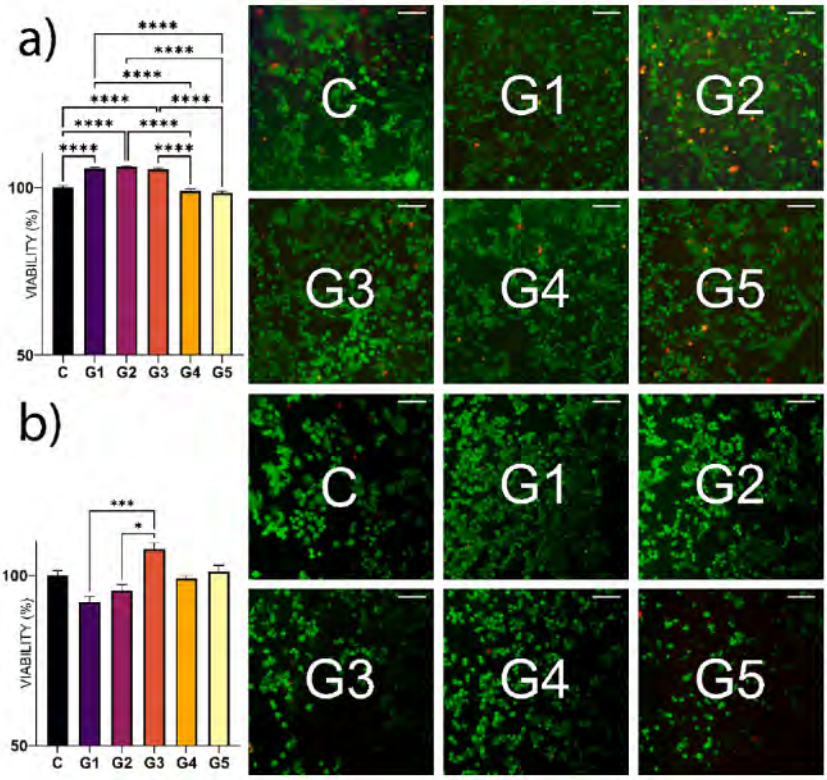

Fig. 3. Shows the viability of a) HEI-OC1 cells, and b) RAW264.7 cells after 24 h incubation with different nanogels. The viability of untreated control is used as 100 %. The green indicates the cytoplasm of cells stained by CFSE and red indicates dead cells stained by PI. The scale bar is 100 μm. Data are shown as mean ± SEM, n 3. $p < 0.05$ (*) and $p < 0.01$ (**). (For interpretation of the references to colour in this figure legend, the reader is referred to the web version of this article.)

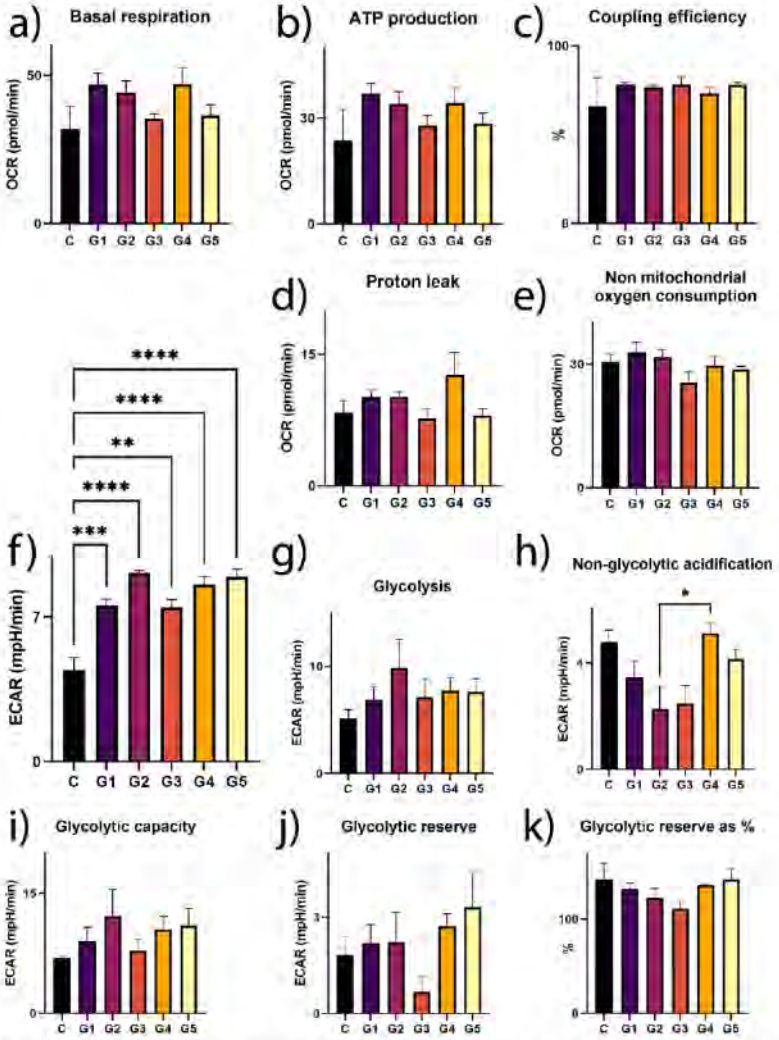

Fig. 4. Metabolic profile of HEL-OC1 cell line after 24 h incubation with different nanogels showing: a) basal respiration linked OCR, b) ATP production linked OCR, c) coupling efficiency, d) proton leak linked OCR, e) non-mitochondrial oxygen consumption linked OCR, f) ECAR, g) glycolysis linked ECAR, h) non-glycolytic acidification linked ECAR, i) glycolytic capacity linked ECAR, j) glycolytic reserve linked ECAR and k) glycolytic reserve as % of glycolysis. C are untreated control cells. Data are shown as mean ± SEM, n = 3, $p < 0.05$ (*) and $p < 0.01$ (**).

specifically DCA (G3) and UDCA (G4), seem to decrease basal respiration compared to the control gel (G1). Nanogels with BAs (G3-G5) did not alter basal respiration compared to the untreated cells (C) (Fig. 5a). The presence of BAs in nanogels (G3, G4 and G5) decreased ATP-production linked OCR compared to both untreated cells (C) and control nanogel (G1) (Fig. 5b). All groups exposed to nanogels (G1-G5) have significantly lowered coupling efficiency, using only 20–30 % of basal respiration-linked OCR for ATP production, compared to 80 % usage in untreated cells (Fig. 5c). The increase in basal respiration (Fig. 5a) is reflected in an increase in proton leak-linked OCR (Fig. 5d) and non-mitochondrial oxygen consumption-linked OCR among a majority of nanogel groups (Fig. 5e). The G3 group showed only an insignificant

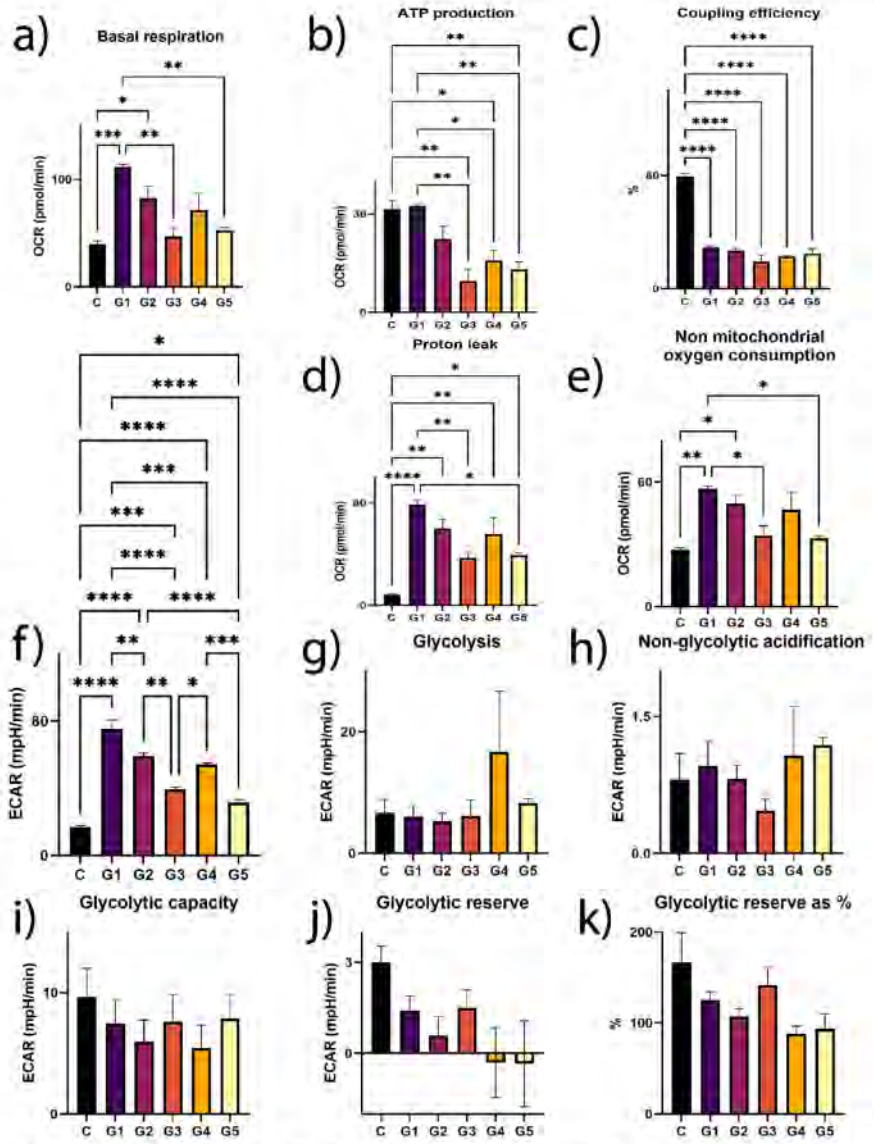

Fig. 5. Metabolic profile of RAW264.7 cell line after 24 h incubation with different nanogels showing: a) basal respiration linked OCR, b) ATP production linked OCR, c) coupling efficiency, d) proton leak linked OCR, e) non-mitochondrial oxygen consumption linked OCR, f) ECAR, g) glycolysis linked ECAR, h) non-glycolytic acidification linked ECAR, i) glycolytic capacity linked ECAR, j) glycolytic reserve linked ECAR and k) glycolytic reserve as % of glycolysis. C are untreated control cells. Data are shown as mean ± SEM; n = 3; $p < 0.05$ (*) and $p < 0.01$ (**).

proton leak increase (Fig. 4d). In contrast, BAs nanogels (G3-G5) did not significantly increase non-mitochondrial oxygen consumption linked OCR compared to untreated cells (C), unlike control nanogels G1 and G2 (Fig. 5e). The increase in proton leak and non-mitochondrial oxygen consumption may be connected with increased cytosolic ROS, electron slippage, damage to the inner mitochondrial membrane and electron transport chain, and increased uncoupling protein (UCP) activity [48]. The ECAR rate shows a significant increase in the presence of all nanogels (Fig. 5f). However, other glycolysis parameters, including glycolysis (Fig. 5g), non-glycolytic acidification rate (Fig. 5h), glycolytic capacity (Fig. 5i), glycolytic reserve (Fig. 5j) and glycolytic reserve as the percentage of glycolysis (Fig. 5k), do not show any significant differences between observed groups. The glycolytic reserve (Fig. 5j) is calculated as the difference between glycolytic reserve and glycolysis. It can be close to zero or in negative values when investigated cells do not have a significant response to oligomycin injection, making glycolytic reserve smaller than glycolysis. Damage to the inner mitochondrial membrane and/or electron transport chain may allow protons to leak into the cytosol, adding to increased ECAR without changes in glycolytic metabolism [53].

The intracellular ROS are present in the HEI-OC1 cell line, and their amount is increased after 30 min of incubation with certain nanogels (Fig. 6a). G1, G4 and G3 increase the ROS concentration compared to the untreated cells (C), with LCA (G4) showing the highest response (Fig. 6a). DCA (G3) and UDCA (G5) nanogels have a smaller amount of intracellular ROS compared to LCA nanogel (G4) (Fig. 6a). In RAW264.7 cells, the incubation with nanogels shows less diverse ROS concentrations (Fig. 6b). Control nanogel (G2) and LCA nanogel (G4) show a significant increase in intracellular ROS compared to untreated cells (C). UDCA nanogel (G5) appears less pro-oxidative compared to LCA nanogel (G4) (Fig. 6b) in the RAW264.7 cell line. In this study, nanogels with UDCA (G5) has been found to be less oxidative than LCA (G4) in both cell lines. This is in accordance with previous studies which found UDCA to be less oxidative and pro-inflammatory than LCA. UDCA has been found to have antioxidative effects in mice and rat hepatocytes [54,55], and exert protective effects on the mitochondrial metabolism of stressed neurones [56] and renal tissue [57]. Ko et al. found UDCA-related inhibition of inflammatory response by lipopolysaccharide-stimulated

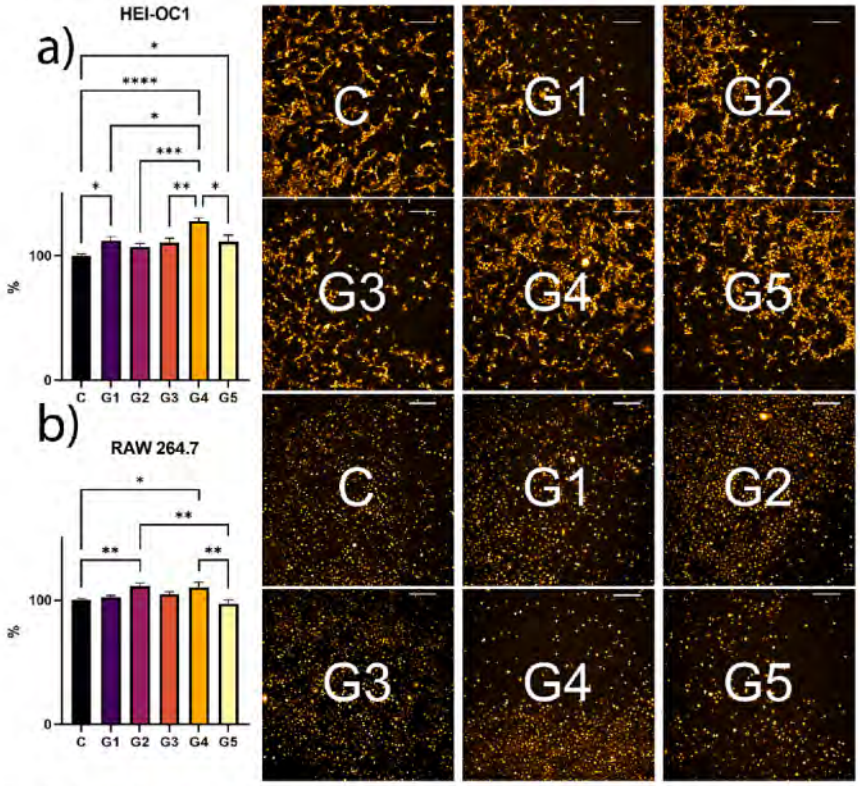

Fig. 6. ROS profile of a) HEI-OC1 cell line and b) RAW264.7 cell line after 30 min incubation with different nanogels. C are untreated control cells. The % indicates the ratio of total intracellular ROS, with total ROS of C being 100 %. The scale bar is 200 μm. The orange colour indicates the intercellular ROS stained by Cellular ROS Assay Kit. Data are shown as mean ± SEM, n = 3. $p < 0.05$ (*) and $p < 0.01$ (**). (For interpretation of the references to colour in this figure legend, the reader is referred to the web version of this article.)

RAW 264.7 macrophages [58]. LCA has been found to increase oxidative stress in breast cancer cells [59,60] and to decrease intracellular antioxidant glutathione in dendritic cells [61]. Furthermore, LCA is a tumour promoter in colorectal cancer [62]. Both LCA and DCA have been found to have progressive membranolytic effects [63], and DCA is known to induce apoptosis via oxidative stress [64]. The low impact on cellular viability and ROS generation of DCA may be related to the low concentration of DCA in G3 nanogel, making it a better candidate for biocompatible formulations when compared to LCA.

4. Conclusions

Regardless of the addition of different BAs (DCA, LCA and UDCA), all nanogels retained their nano-scale structure and non-Newtonian shear thinning fluid behaviour, desirable for injecting and extruding nanogels. The addition of amphiphilic BAs neutralised nanogels' zeta potential. Different BAs can be used to tune the gelation time, viscosity, and surface tension of nanogels. Nanogels based on Poloxamer 407 with DCA, LCA or UDCA showed a high level of biocompatibility after 24 h exposure to auditory and macrophage cell lines, with minimal cytotoxicity compared to untreated control. BAs have tissue-dependent effects, as nanogels did not alter cellular respiration and glycolysis of the auditory cell line but showed possible mitochondrial dysfunction in macrophages. BA-nanogels had minimal effect on intracellular ROS, with LCA demonstrating the most pro-oxidative behaviour. Based on this study, thermoresponsive nanogels with BA, particularly DCA and UDCA, may be promising candidates for inner ear drug delivery.

5. Disclaimer

The work is partially supported by the European Union Horizon 2020 research project and innovation programmunder the Marie Sklodowska-Curie Grant Agreement No. 872370. Curtin Faculty ORS-WAHAI Consortium and the Australian National Health and Medical Research (APP9000597).

The authors would like to acknowledge the Australian Postgraduate Award (APA) and Curtin Research Scholarship (CRS). The authors acknowledge the Microscopy and Microanalysis Facility at Curtin University. The authors acknowledge The Ian Potter Foundation for funding support for equipment.

Declaration of Competing Interest

The authors declare that they have no known competing financial interests or personal relationships that could have appeared to influence the work reported in this paper.

Data availability

The datasets generated and/or analysed during the current study are not publicly available but are available from the corresponding author on reasonable request.

References

[1] M.T. Manzari, Y. Shamay, H. Kiguchi, N. Rosen, M. Scaltriti, D.A. Heller, Targeted drug delivery strategies for precision medicines, Nat. Rev. Mater. 6 (4) (2021) 351–370.

[2] Y. Yu, B. Hu, X. Yuan, L. Cai, H. Gao, Q. Yang, Nanogel: A versatile nano delivery system for biomedical applications, Pharmaceutics 12 (3) (2020) 290.

[3] V. Ramazanli, Effect of pH and temperature on the synthesis of silver nano particles extracted from olive leaf, Adv. Biol. Earth Sci. 6 (2) (2021).

[4] Y. Jiang, J. Chen, C. Deng, E.J. Suuronen, Z. Zhong, Click hydrogels, microgels and nanogels: emerging platforms for drug delivery and tissue engineering, Biomaterials 35 (18) (2014) 4969–4985.

[5] K. Mooiz, R. Mittal, A. Eshraghi, Y. Omidi, H. Omidian, Improved inner ear drug delivery using hydrogel carriers, J. Drug Delivery Sci. Technol. 79 (2023), 104086.

[6] R. Mittal, S.A. Pena, A. Zhu, R. Eshraghi, A. Eshraghi, K.J. Horesh, et al., Nanoparticle based drug delivery in the inner ear: current challenges, limitations and opportunities, Artif. Cells Nanomed. Biotechnol. 47 (1) (2019) 1312–1320.

[7] J. Hao, S.K. Li, Inner ear drug delivery: recent advances, challenges, and perspective, Eur. J. Pharm. Sci. 126 (2019) 82–92.

[8] B. Szeto, H. Chiang, C. Valentini, M. Yu, J.W. Kysar, A.K. Lalwani, Inner ear delivery: challenges and opportunities, Laryngosc. Invest. Otolaryngol. 5 (1) (2020) 122–131.

[9] K. Mooiz, Y. Kwon, Y. Omidi, H. Omidian, Contemporary applications of thermogelling PEO-PPO-PEO triblock copolymers, J. Drug Delivery Sci. Technol. 70 (2022), 103182.

[10] F. Piu, X. Wang, R. Fernandez, L. Dellamary, A. Harrop, Q. Ye, et al., OTO-104: a sustained release dexamethasone hydrogel for the treatment of otic disorders, Otol. Neurotol. 32 (1) (2011).

[11] A.-H. Liao, C.-F. Shih, M.-W. Li, Y.-C. Lin, H.-C. Chuang, C.-H. Wang, Development of thermosensitive poloxamer 407-based microbubble gel with ultrasound mediation for inner ear drug delivery, Drug Deliv. 28 (1) (2021) 1256–1271.

[12] C. Zhu, C. Gausterer Julia, H. Schöppel, M. Mierzejewska, N. Saidov, N. Almuaili, et al., Evaluation of sustained release steroid hydrogels in a guinea pig model for noise-induced hearing loss, Audiol. Neurotol. 23 (2) (2018) 73–81.

[13] M. Zhang, C. Rives, K.C. Waldron, X.X. Zhu, Self-assembly of a bile acid dimer in aqueous solutions: from nanofibers to nematic hydrogels, Langmuir 33 (4) (2017) 1084–1089.

[14] A. Perino, K. Schoonjans, Metabolic messengers: bile acids, Nat. Metabol. 4 (4) (2022) 416–423.

[15] T. Rézen, D. Rozman, T. Kovács, P. Kovács, A. Sipos, P. Bai, et al., The role of bile acids in carcinogenesis, Cell. Mol. Life Sci. 79 (5) (2022) 243.

[16] B. Kovacevic, M. Jones, C. Ionescu, D. Walker, S. Wegle, J. Chester, et al., The emerging role of bile acids as critical components in nanotechnology and bioengineering: pharmacology, formulation optimizers and hydrogel-biomaterial applications, Biomaterials 283 (2022), 121459.

[17] M.J. Alvarez-Figueroa, C. Muggli-Cañez, P.M. González, Effect of the aggregation state of bile salts on their transdermal absorption enhancing properties, J. Drug Delivery Sci. Technol. 54 (2019), 101333.

[18] Y. Dai, R. Zhou, L. Liu, Y. Lu, J. Qi, W. Wu, Liposomes containing bile salts as novel ocular delivery systems for tacrolimus (FK506): in vitro characterization and improved corneal permeation, Int. J. Nanomed. 8 (2013) 1921–1933.

[19] M. Lewkowicz, M. Jones, B. Kovacevic, C.M. Ionescu, S.R. Wegle, T. Foster, et al., Potentials and limitations of pharmaceutical and pharmacological applications of bile acids in hearing loss treatment, Ther. Deliv. 13 (10) (2022) 477–488.

[20] M. Huo, A. Zou, C. Yao, Y. Zhang, J. Zhou, J. Wang, et al., Somatostatin receptor mediated tumor-targeting drug delivery using octreotide-PEG-deoxycholic acid conjugate-modified N-deoxycholic acid-O, N-hydroxyethylation chitosan micelles, Biomaterials 33 (27) (2012) 6393–6407.

[21] R. Pangeni, S.K. Jha, R. Maharjan, J.U. Choi, K.-Y. Chang, Y.K. Choi, et al., Intestinal transport mechanism and in vivo anticancer efficacy of a solid oral formulation incorporating an ion pairing complex of pemetrexed with deoxycholic acid derivative, Int. J. Nanomed. 14 (2019) 6339–6356.

[22] W. Dong, H. Li, M. Chen, Z. Ni, J. Zhao, H. Yang, et al., Biodegradable bio-based polyesters with controllable photo crosslinkability, thermal and hydrolytic stability, J. Polym. Res. 18 (6) (2011) 1239–1247.

[23] K. Yadav, P. Bhargava, S. Bansal, M. Singh, S. Gupta, G. Sandhu, et al., Nature of the charged head group dictates the anticancer potential of lithocholic acid-tamoxifen conjugates for breast cancer therapy, MedChemComm 6 (5) (2015) 778–787.

[24] M. Matsusaki, T. Hang Thi, T. Kaneko, M. Akashi, Enhanced effects of lithocholic acid incorporation into liquid-crystalline biopolymer poly(coumaric acid) on structural ordering and cell adhesion, Biomaterials 26 (32) (2005) 6263–6270.

[25] D. Zhang, D. Li, L. Shang, Z. He, J. Sun, Transporter targeted cholic acid cytarabine conjugates for improved oral absorption, Int. J. Pharm. 511 (1) (2016) 161–169.

[26] Y. Arai, H. Park, S. Park, D. Kim, I. Baek, L. Jeong, et al., Bile acid-based dual-functional prodrug nanoparticles for bone regeneration through hydrogen peroxide scavenging and osteogenic differentiation of mesenchymal stem cells, J. Control. Release 328 (2020) 596–607.

[27] E.R. de Oliveira Junior, E. Truzzi, L. Ferraro, M. Fogagnolo, B. Pavan, S. Beggiato, et al., Nasal administration of nanoencapsulated geranoil/ursodeoxycholic acid conjugate: towards a new approach for the management of Parkinson's disease, J. Control. Release 321 (2020) 540–552.

[28] T. Foster, M. Lewkowicz, C. Quintas, C.M. Ionescu, M. Jones, S.R. Wegle, et al., Novel nanoencapsulation technology and its potential role in bile acid-based targeted gene delivery to the inner ear, Small 19 (8) (2023) 2204986.

[29] M.M. Carleton, M.V. Sefton, Injectable and degradable methacrylic acid hydrogel alters macrophage response in skeletal muscle, Biomaterials 229 (2019), 119477.

[30] A. Buran, M.B. Buran, C. Keskin, S.I. Kanderemir, M. Valiyeva, S. Mehraliyeva, et al., Ecofriendly/rapid synthesis of silver nanoparticles using extract of waste parts of artichoke (Cynara scolymus L.) and evaluation of their cytotoxic and antibacterial activities, J. Nanomater. 2021 (2021), 2270472.

[31] A. Mooranian, T. Foster, C.M. Ionescu, D. Walker, M. Jones, S.R. Wegle, et al., Enhanced bilosomal properties resulted in optimum pharmacological effects by increased acidification pathways, Pharmaceutics 13 (8) (2021), 1184.

[32] A. Mooranian, C.M. Ionescu, D. Walker, M. Jones, S.R. Wegle, B. Kovacevic, et al., Single-cellular biological effects of cholesterol-catabolic bile acid-based nano/micro capsules as anti-inflammatory cell protective systems, Biomolecules 12 (1) (2022) 73.

[33] A. Mooranian, M. Jones, C.M. Ionescu, D. Walker, S.R. Wegle, B. Kovacevic, et al., Advancements in assessments of bio-tissue engineering and viable cell delivery

manifacts using bile acid-based pharmacological biotechnologies, Nanomaterials 11 (7) (2021), 1861.
[34] A. Mootanian, M. Jones, D. Walker, C.M. Ionescu, S.R. Wagle, B. Kovacevic, et al., Pharmacological dose-effect profiles of various concentrations of humanised primary bile acid in encapsulated cells, Nanomaterials 12 (4) (2022), 647.
[35] A. Mootanian, S. Raj Wagle, B. Kovacevic, R. Takechi, J. Mamo, V. Lam, et al., Bile acid bio-nanoencapsulation improved drug targeted-delivery and pharmacological effects via cellular flux: 6-months diabetes preclinical study, Sci. Rep. 10 (1) (2020), 106.
[36] S.R. Wagle, B. Kovacevic, D. Walker, C.M. Ionescu, M. Jones, G. Stojanovic, et al., Pharmacological and advanced cell respiration effects, enhanced by toxic human bile nano-pharmaceuticals of probucol cell-targeting formulations, Pharmaceutics. 12 (8) (2020), 706.
[37] S.R. Wagle, D. Walker, B. Kovacevic, A. Gedawy, M. Mikov, S. Golocorbin-Kon, et al., Micro nano formulation of bile gut delivery: rheological, stability and cell survival, basal and maximum respiration studies, Sci. Rep. 10 (1) (2020), 7715.
[38] N.L. Chin, S.M. Chan, Y.A. Yusof, T.G. Chuah, R.A. Talib, Modelling of rheological behaviour of pummelo juice concentrates using master curve, J. Food Eng. 93 (2) (2009) 134–140.
[39] R. Sharma, F. Majer, V.K. Peta, J. Wang, R. Keaveney, D. Kelleher, et al., Bile acid toxicity structure–activity relationships: correlations between cell viability and lipophilicity in a panel of new and known bile acids using an oesophageal cell line (HET-1A), Bioorg. Med. Chem. 18 (18) (2010) 6886–6895.
[40] S. Ruiz Gaspà, N. Gualdoni, S. Jurado, A. Gombalis, P. Peris, A. Monegal, et al., Bilirubin and bile acids in osteocytes and bone tissue. Potential role in the cholestatic-induced osteoporosis, Liver Int. 40 (11) (2020) 2767–2775.
[41] R. Khalilov, A comprehensive review of advanced nano-biomaterials in regenerative medicine and drug delivery, Adv. Biol. Earth Sci. 8 (1) (2023).
[42] B. Kovacevic, S.R. Wagle, C.M. Ionescu, M. Jones, M. Lewkowicz, E.Y.M. Wong, et al., Novel hydrogel comprising non-ionic copolymer with various concentrations of pharmacologically active bile acids for cellular injectable gel, Colloids Surf. B Biointerfaces 222 (2023), 113014.
[43] M.H. Hojjat, O.A. Chat, P.A. Bhat, M.A. Bilt, G.M. Rather, A.A. Dar, Structural changes in trypsin induced by the bile salts: an effect of amphiphile hydrophobicity, Int. J. Biol. Macromol. 180 (2021) 121–128.
[44] J. Zhang, Y. Zhu, J. Song, J. Yang, C. Pan, L. Xu, et al., Novel balanced charged alginate/PPI polyelectrolyte hydrogel that resists foreign body reaction, ACS Appl. Mater. Interfaces 10 (8) (2018) 6879–6886.
[45] C.B. Rodell, A.L. Kaminski, J.A. Burdick, Rational design of network properties in guest-host assembled and shear-thinning hyaluronic acid hydrogels, Biomacromolecules 14 (2013), 4125.
[46] N. Abdullah, N.L. Chin, Y.A. Yusof, R.A. Talib, Modelling of rheological behaviour of guava, pomelo and soursop juice concentrates via shear rate-temperature-concentration superpositioning, J. Food Sci. Technol. 55 (3) (2018) 1207–1213.
[47] C.-C. Kuo, H. Qin, Y. Cheng, X. Jiang, X. Shi, An integrated manufacturing strategy to fabricate delivery system using gelatin/alginate hybrid hydrogels: 3D printing and freeze drying, Food Hydrocoll. 111 (2021), 106263.
[48] B.G. Hill, G.A. Benavides, J.R. Lancaster, S. Ballinger, L. Dell'Italia, J. Zhang, et al., Integration of cellular bioenergetics with mitochondrial quality control and autophagy, Biol. Chem. 393 (12) (2012) 1485–1512.
[49] B. Kovacevic, C.M. Ionescu, S.R. Wagle, M. Jones, M. Lewkowicz, E.Y.M. Wong, et al., Impact of novel Teflon DCA ionoged matrix on cellular bioactivity, J. Pharm. Sci. (2022).
[50] B. Kovacevic, C.M. Ionescu, M. Jones, S.R. Wagle, M. Lewkowicz, M. Ennié, et al., The effect of deoxycholic acid on chitosan-enabled matrices for tissue scaffolding and injectable nanogels, Gels 8 (6) (2022), 358.
[51] H.-T. Lee, C.-S. Lin, S.-C. Pan, T.-H. Wu, C.-S. Lee, D.-M. Chang, et al., Alterations of oxygen consumption and extracellular acidification rates by glutamine in PBMCs of SLE patients, Mitochondrion 44 (2019) 65–74.
[52] L.S. Pike Winer, M. Wu, Rapid analysis of glycolytic and oxidative substrate flux of cancer cells in a microplate, PLoS ONE 9 (10) (2014), e109916.
[53] A.S. Divakaruni, M.D. Brand, The regulation and physiology of mitochondrial proton leak, Physiology 26 (3) (2011) 192–205.
[54] K. Okada, J. Shoda, K. Taguchi, J.M. Maher, K. Ishizaki, Y. Inoue, et al., Ursodeoxycholic acid stimulates Nrf2-mediated hepatocellular transport, detoxification, and antioxidative stress systems in mice, Am. J. Physiol.-Gastrointestinal Liver Physiol. 295 (4) (2008) G735–G747.
[55] H. Mitsuyoshi, T. Nakashima, Y. Sumida, T. Yoh, Y. Nakajima, H. Ishikawa, et al., Ursodeoxycholic acid protects hepatocytes against oxidative injury via induction of antioxidants, Biochem. Biophys. Res. Commun. 263 (2) (1999) 537–542.
[56] H. Qi, D. Shen, C. Jiang, H. Wang, M. Chang, Ursodeoxycholic acid protects dopaminergic neurons from oxidative stress via regulating mitochondrial function, autophagy, and apoptosis in MPTP/MPP+-induced Parkinson's disease, Neurosci. Lett. 741 (2021), 135493.
[57] Y. Yang, S. Liu, H. Gao, P. Wang, Y. Zhang, A. Zhang, et al., Ursodeoxycholic acid protects against cisplatin-induced acute kidney injury and mitochondrial dysfunction through acting on ALDH1L2, Free Radic. Biol. Med. 152 (2020) 821–837.
[58] W.-K. Ko, S.-H. Lee, S.J. Kim, M.-J. Jo, N. Kumar, I.-B. Han, et al., Anti-inflammatory effects of ursodeoxycholic acid by lipopolysaccharide-stimulated inflammatory responses in RAW 264.7 macrophages, PLoS ONE 12 (6) (2017), e0180673.
[59] P. Kovács, T. Csonka, T. Kovács, Z. Sári, G. Ujlaki, A. Sipos, et al., Lithocholic acid, a metabolite of the microbiome, increases oxidative stress in breast cancer, Cancers 11 (9) (2019), 1255.
[60] K. Mikó, A. Vida, T. Kovács, G. Ujlaki, G. Trencsényi, J. Márton, et al., Lithocholic acid, a bacterial metabolite reduces breast cancer cell proliferation and aggressiveness, Biochimica et Biophysica Acta (BBA) - Bioenergetics 1859 (9) (2018) 958–974.
[61] J. Hu, Y. Zhang, S. Xi, C. Wang, X. Huang, S. Pan, et al., Lithocholic acid inhibits dendritic cell activation by reducing intracellular glutathione via TGR5 signaling, Int. J. Biol. Sci. 18 (11) (2022) 4545–4559.
[62] T.T. Nguyen, S. Lian, T.T. Ung, Y. Xia, J.Y. Han, Y.D. Jung, Lithocholic acid stimulates IL-8 expression in human colorectal cancer cells via activation of Erk1/2 MAPK and suppression of STAT3 activity, J. Cell. Biochem. 118 (9) (2017) 2958–2967.
[63] M.M. Delzenne, P.B. Calderon, H.S. Taper, M.B. Roberfroid, Comparative hepatotoxicity of cholic acid, deoxycholic acid and lithocholic acid in the rat: in vivo and in vitro studies, Toxicol. Lett. 61 (2) (1992) 291–304.
[64] J.I. Barrasa, N. Olmo, P. Pérez-Ramos, A. Santiago-Gómez, E. Lecona, J. Turnay, et al., Deoxycholic and chenodeoxycholic bile acids induce apoptosis via oxidative stress in human colon adenocarcinoma cells, Apoptosis 16 (10) (2011) 1054–1067.

Publication 9 (pages 153-169):

Pharmacological and bioenergetic effects of smart thermoresponsive polymer-bile acid enhanced nanogel on hearing cells

Kovacevic B, Wagle S, Ionescu C, Foster T, Đanić M, Mikov M, Mooranian A, Al-Salami H. Reactive and Functional Polymers

Sub-objective (8): to design and create nanogels utilising poloxamer 407, Tyloxapol, and deoxycholic acid and to examine the shear stress, viscosity, surface tension, torque, and zeta potential of nanogels. Additionally, the nanogels were incubated with 2 different cell lines (HEI-OC1 and RAW264.7), and their impact on viability and bioenergetic parameters was investigated.

Reactive and Functional Polymers

Pharmacological and bioenergetic effects of smart thermoresponsive polymer-bile acid enhanced nanogel on hearing cells

--Manuscript Draft--

Manuscript Number:	
Article Type:	Research Paper
Keywords:	Tyloxapol; bile acid; bioenergetics; poloxamer; nanogel
Corresponding Author:	Hani Al-Salami Curtin University AUSTRALIA
First Author:	Bozica Kovacevic
Order of Authors:	Bozica Kovacevic
	Susbin Raj Wagle
	Corina Mihaela Ionescu
	Thomas Foster
	Maja Đanić
	Momir Mikov
	Armin Mooranian
	Hani Al-Salami
Abstract:	This study presents novel thermoresponsive nanogels composed of chenodeoxycholic acid and Tyloxapol for potential inner ear drug delivery. The nanogels exhibit non-Newtonian, shear-thinning fluid behaviour and rapid gelation at body temperature. Biocompatibility studies were conducted on auditory and macrophage cell lines. Nanogels had a minimal impact on cellular viability, glycolysis, and mitochondrial respiration of auditory cells after 24 hours of exposure. However, exposure to macrophage cells leads to decreased viability and mitochondrial dysfunction. These findings suggest that thermoresponsive bile acid and Tyloxapol nanogels have the potential to be safe and effective drug delivery vehicles for inner ear applications.
Suggested Reviewers:	Olavi Pelkonen olavi.pelkonen@oulu.fi
	Allan Gamble allan.gamble@otago.ac.nz
Opposed Reviewers:	

- Nanogel characteristics: small particle size, average neutral charge, and shear-thinning properties.
- Cell-specific responses: The study shows varied cellular viability responses, with auditory cell lines unaffected and macrophages experiencing slightly reduced viability, mitigated by Tyloxapol.
- Metabolic changes in macrophages: Indicates decreased coupling efficiency and increased proton leak, suggesting impaired oxidative phosphorylation upon nanogel exposure.
- Importance of tailored formulations: The study underscores the need to customise nanogel formulations for specific cell types and consider matrix components to optimise drug delivery systems for biomedical applications.

Graphical Abstract

Click here to access/download;Graphical Abstract;Graphical abstract B16.tif

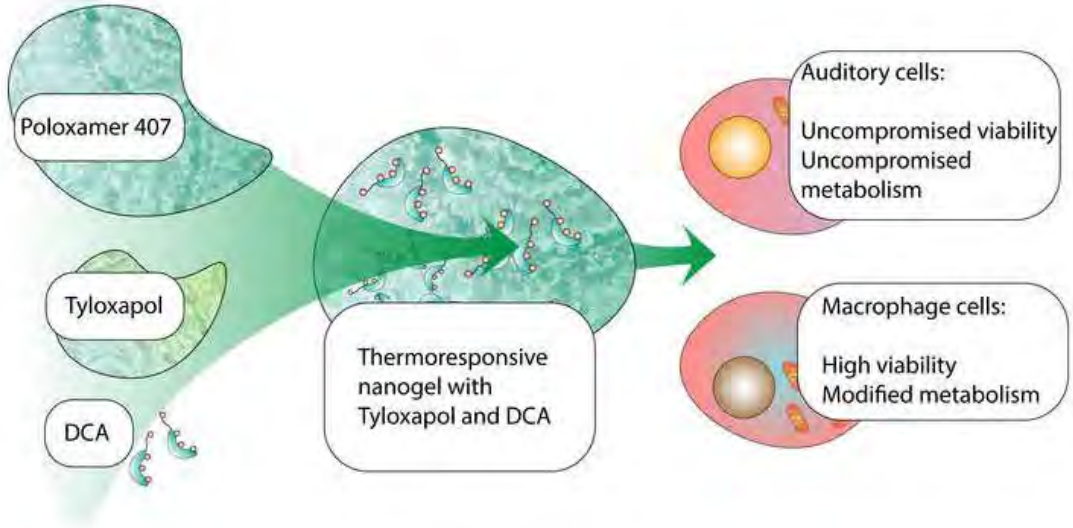

Pharmacological and bioenergetic effects of smart thermoresponsive polymer-bile acid enhanced nanogel on hearing cells

Bozica Kovacevic[1], Susbin Raj Wagle[1], Corina Mihaela Ionescu[1], Thomas Foster[1], Maja Đanić[2], Momir Mikov[2], Armin Mooranian[1,3*], Hani Al-Salami[1,4*]

[1] The Biotechnology and Drug Development Research Laboratory, Curtin Medical School & Curtin Health Innovation Research Institute, Curtin University, Bentley, Perth, WA 6102, Australia

[2] Department of Pharmacology, Toxicology and Clinical Pharmacology, Faculty of Medicine, University of Novi Sad, Novi Sad, 21101, Serbia

[3] School of Pharmacy, University of Otago, Dunedin, Otago, New Zealand

[4] UWA Medical School, University of Western Australia, Perth, Australia

* Authors Contributed Equally

* Correspondence: HAS hani.al-salami@curtin.edu.au; AM a.mooranian@curtin.edu.au

Abstract

This study presents novel thermoresponsive nanogels composed of chenodeoxycholic acid and Tyloxapol for potential inner ear drug delivery. The nanogels exhibit non-Newtonian, shear-thinning fluid behaviour and rapid gelation at body temperature. Biocompatibility studies were conducted on auditory and macrophage cell lines. Nanogels had a minimal impact on cellular viability, glycolysis, and mitochondrial respiration of auditory cells after 24 hours of exposure. However, exposure to macrophage cells leads to decreased viability and mitochondrial dysfunction. These findings suggest that thermoresponsive bile acid and Tyloxapol nanogels have the potential to be safe and effective drug delivery vehicles for inner ear applications.

Introduction

Recent research is focused on polymeric surfactants, with poloxamer block copolymers being extensively studied. Dimeric/oligomeric surfactants, some characterised by a smaller number of monomers, are emerging as promising biomaterial compounds (1, 2). Despite the focus on polymeric surfactants, oligomeric surfactants may be suitable biomaterials as they seem to exhibit low critical micelle concentration (CMC) and high viscosity at low concentrations in water solutions due to potentially large aggregates and superior surface activity (3).

The utilisation of surfactant micelles as carriers for drug delivery offers several advantages. Many of these amphiphilic aggregates have played a significant role in enhancing the solubility of hydrophobic drugs. The remarkable improvement in drug solubility is attributed to the hydrophobic interior of the micelle, fostering hydrophobic–hydrophobic interactions. However, conventional surfactant-based micellar systems seem to exhibit a high critical micelle concentration and tend to disassemble upon dilution, leading to poor in vivo performance (4).

One avenue for enhancing micelle-based delivery systems' efficiency is combining different surfactants to create mixed micelles. These mixed micelles emerge as a promising choice for drug delivery due to their thermodynamic stability and superior solubilisation capacity compared to micelles derived from individual components (5, 6).

This study examines a nanogel-based delivery system made of three surfactants: polymeric surfactant poloxamer 407, oligomeric surfactant Tyloxapol, and a bile acid, chenodeoxycholic acid (CDCA).

Poloxamers are synthetic polymers consisting of tri-block copolymers composed of two hydrophilic chains (poly(ethylene oxide)) around hydrophobic chains (poly(propylene oxide)) (7). The bioactivity, microstructure, and gel-sol temperature transition of poloxamers can be adjusted to replicate the behaviour of diverse tissue types. Additionally, their amphiphilic nature and capacity for self-assembly into micelles make them potential candidates for drug delivery systems (8).

Tyloxapol, a 4-isooctylpolyoxyethylene phenol-formaldehyde polymer, comprises an average of seven conjoined molecules of Triton X-100. Its remarkable physical and biological properties render Tyloxapol suitable for biomedical applications (9-11). It is a suitable excipient for nanotechnology-based ocular delivery systems (12, 13) and hepatic delivery systems (14).

CDCA and other bile acids show significant pharmacological and biological effects and a potential for biomaterial design (15). CDCA has shown an excipient stabilising effect on tissue-loaded microcapsules, resulting in improved graft function and survival post-transplantation (16).

Rheological properties of nanogels were assessed, including fluid behaviour, gelation time, surface tension and zeta potential. Furthermore, the biological impact on nanogels has been evaluated on two cell lines, auditory HEI-OC1 and macrophage RAW267.4, via cellular viability and bioenergetics.

Materials and Methods

Materials for the synthesis of nanogels (Tyloxapol, Poloxamer 407 and polyvinyl alcohol (PVA)) were procured from Sigma Chemical Co (St. Louis, MO, USA). CDCA was obtained from Qingdao Yuanrun Chemical Co., Ltd (Qingdao, Shandong, China). Unless otherwise specified, materials used in tissue culture were also obtained from Sigma Chemical Co (St. Louis, MO, USA). The HEI-OC1 auditory cell line (House Ear Institute-Organ of Corti 1) was obtained from Prof. Federico Kalinec (University of California, CA, USA), while the RAW 264.7 macrophage cell line (ATCC®, TIB-71™) was sourced from the American Type Culture Collection (ATCC, Manassas, VA, USA). Cell lines were cultured in high-glucose DMEM supplemented with 10% FBS without antibiotics, with media replacement every 48 hours. HEI-OC1 cells were cultured at 33°C with 10% CO2, whereas RAW 264.7 cells were cultured at 37°C with 10% CO2.

All five groups of nanogels had the same Poloxamer 407 concentration (18%) (D1-D5). PVA (0.5%) was added to D2, D3, D4 and D5 nanogels. Tyloxapol (0.5%) was added to D4 and D5. CDCA (0.04%) was added to D3 and D5 nanogels. The deionised water was used as a solvent. The first step in nanogel manufacture was a PVA dissolution at 60°C under constant stirring. The solution was then slowly cooled to room temperature. Tyloxapol, CDCA and Poloxamer 407 were added to the PVA solution, with Poloxamer at the end. Nanogels were left overnight at four °C under constant stirring. Nanogels were sterilised with UV light in aseptic conditions for 30 minutes prior to use in tissue culture.

Zeta potential measurements were performed using the same instrument, employing a customised SOP for zeta potential assessment and executing 25 runs for each measurement. Surface tension analysis was conducted using a tensiometer (Sigma 703, ATA Scientific, Caringbah, Australia). The average particle size of nanogels was determined utilising a 3000HS Zetasizer (Malvern Instruments, Malvern, UK) per the standard operating procedure (SOP) of the accompanying software (25 runs per measurement). The shear rate, shear stress and viscosity values of freshly prepared nanogels were measured using a Visco-88 viscometer (Malvern Instruments, Malvern, UK). All measurements were carried out at room temperature (17-23). All obtained data were in triplicates (n = 3).

The gelation time assessment was conducted using the vial tilting methodology, wherein a vial containing 500 µl of nanogels at ambient temperature was submerged in a 37°C water bath. Gelation time was recorded at the loss of fluidity during vial tilting. (24).

The rheological evaluation of the fluid was conducted by determining the Consistency coefficient (K) and the flow behaviour index (n) through the application of curve fitting of rheological data using the Power Law model (Eq. 1). The curve fitting procedure employed the solver function (Microsoft Excel), utilising a nonlinear optimisation algorithm (25).

The power Law equation:

$$\sigma = K \dot{\gamma}^n \quad (1)$$

Where σ is the shear stress (Pa), K is the consistency coefficient, $\dot{\gamma}$ is the shear rate (s^{-1}), and n is the flow behaviour index.

The cell viability assay employed a standardised protocol utilising Water Soluble Tetrazolium Salts-1 (WST-1) assay (Cell Proliferation Reagent WST-1, Sigma Chemical Co, St. Louis, MO, USA). The

identical procedure was applied to both cellular strains. Cells were seeded at a concentration of 1-1.5 x 10^5 cells/ml, with 180 µl per well, and allowed to incubate overnight to facilitate cell adhesion. Subsequently, nanogels were introduced (20 µl per well) and co-incubated with the cells for 24 hours. Following incubation, the cell media containing nanogels was aspirated, and cells were rinsed thrice with phosphate-buffered saline (PBS) prior to the WST-1 assay. The resulting absorbance was quantified using a PerkinElmer Multimode Plate Reader (Waltham, MA, USA) at a wavelength of 450 nm. The data were normalised against the background signal and expressed as a percentage relative to untreated cells (C). All experimental data were performed in triplicates.

Bioenergetics analysis was executed after coincubation with 20 µl of nanogels for 24 hours preceding assays, adhering to the identical protocol employed for viability assessments. After 24h, cells were washed three times with PBS. The Seahorse XF Cell Mito Stress Test and the Seahorse XF Glycolysis Stress Test were conducted utilising the Seahorse Flux Analyser XF 96 (Agilent Technologies, Santa Clara, CA, USA). Protocol optimisation was implemented for each specific cell line studied, following internally developed methodologies and manufacturer guidelines (17, 26-28). Untreated cells served as the control group (C). Data collection was conducted in triplicate (n = 3).

Statistical analysis was conducted using GraphPad Prism 9.5 (Graphpad, Inc. San Diego, CA, USA). One-way ANOVA, regression analysis, and Tukey HSD tests were employed as appropriate. Data are presented as mean ± SEM, with statistical significance presented as * ($p < 0.01$) and ** ($p < 0.05$).

Results

All examined groups of nanogels have rapid gelation time at 37°C, transitioning from sol to gel state in under 10 seconds (Figure 1a). Formulation with all three surfactants (D5) showed a decrease in gelation time compared to poloxamer-only control (D1), with the addition of PVA and Tyloxapol slightly prolonging gelation time (Figure 1a). The average particle size is below 200nm, classifying these formulations as nanogels (Figure 1b) (29). Adding PVA and Tyloxapol results in the smallest particle size (Figure 1b). For all groups of investigated nanogels, the zeta potential is close to neutral (0 mV), without significant differences between different nanogels (Figure 1c). The surface tension seems to be the highest in D5 nanogels, followed by nanogels with only CDCA (D3) and only Tyloxapol (D4) added (Figure 1d). Shear stress and viscosity graphs (Figures 1e and 1f) suggest shear thinning non-Newtonian fluid behaviour. Shear thinning non-Newtonian fluid behaviour is further confirmed by parameters from power law fitting (Table 1), as every nanogel has a flow behaviour index (n) less than 1.

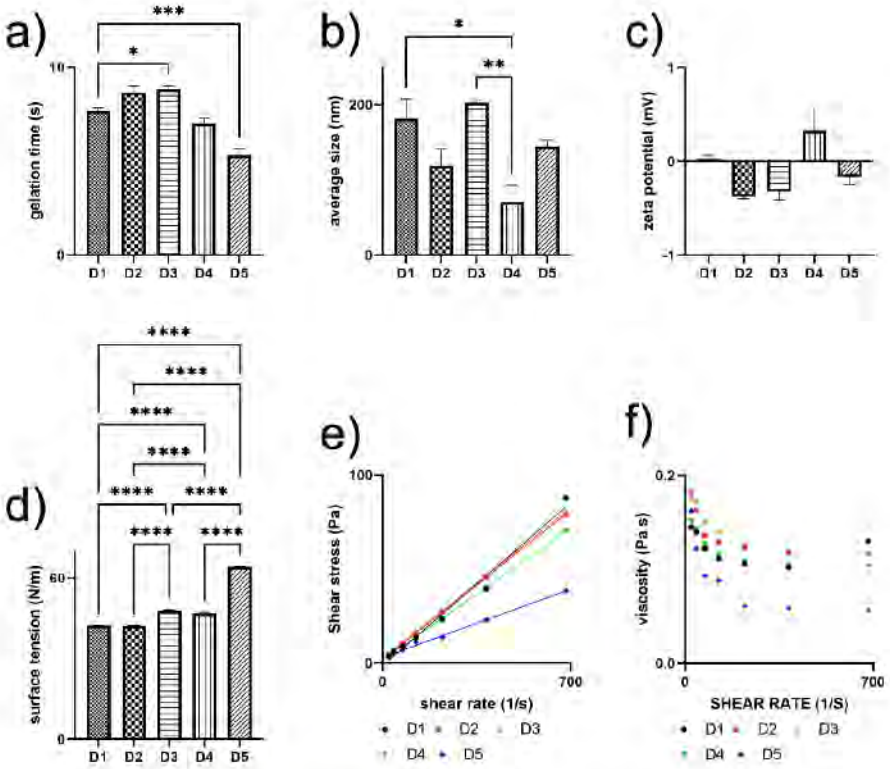

Figure 1. Rheological properties of nanogels are shown as: a) gelation time, b) average particle size, c) zeta potential, d) surface tension, e) shear stress and f) viscosity of nanogels.

	TEMPERATURE (°C)	CONSISTENCY COEFFICIENT, K	FLOW BEHAVIOUR INDEX, N	COEFFICIENT OF DETERMINATION, R^2
D1	22 ± 0.5	0.185541 ± 0.004743	0.899066 ± 0.003928	0.999678 ± 0.000227
D2	22 ± 0.5	0.178896 ± 0.001020	0.933201 ± 0.000793	0.999908 ± 0.000023
D3	22 ± 0.5	0.208492 ± 0.005197	0.911649 ± 0.004312	0.999848 ± 0.000015
D4	22 ± 0.5	0.152004 ± 0.004638	0.939099 ± 0.005569	0.999841 ± 0.000022
D5	22 ± 0.5	0.220275 ± 0.002927	0.788141 ± 0.002600	0.998295 ± 0.000054

Table 1. Parameters from power law fitting $\sigma=K\dot{\gamma}^n$ of rheological properties of investigated nanogels

The cellular viability of the auditory cell line (Figure 2a) stays high after 24h incubation with 20 µl of nanogels. CDCA and Tyloxapol nanogel (D5) may have a positive effect on cellular viability compared to control cells, which had no nanogel exposure (Figure 2a). Macrophage cell line retained high viability in the presence of nanogels (Figure 2b). Nanogels with PVA (D2) and PVA/CDCA (D3) significantly lowered cellular viability. However, the most complex nanogels (D5) did not adversely affect the viability of RAW 264.7 cells.

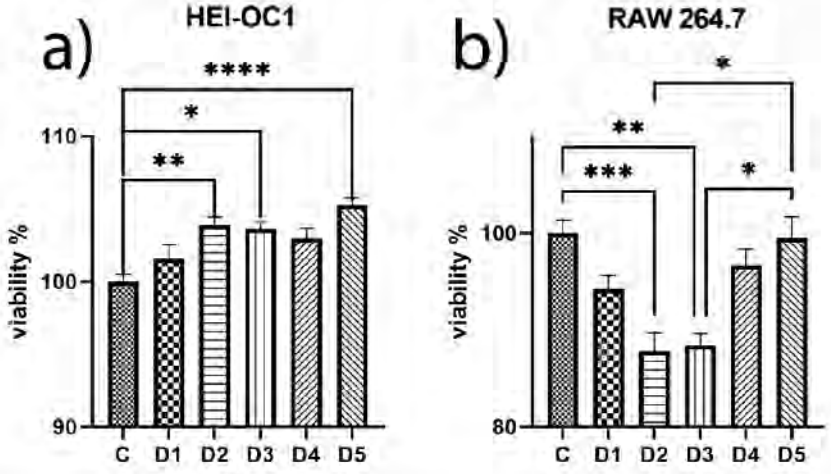

Figure 2. Cellular viability after 24h exposure to nanogels of a) HEI-OC1 cell line and b) RAW 264.7 cell line.

The mitochondrial metabolism of HEI-OC1 cells is minimally impacted by nanogels (Figure 3). Most parameters (metabolic profile, non-mitochondrial oxygen consumption, basal respiration, maximal respiration and ATP production) show no significant difference between groups (Figures 3a-3e). A slight increase in proton leak is present in D5 compared to nanogel-free control (C) but not compared to other nanogel-treated cells (Figure 3f). The coupling efficiency of D5 is mildly decreased compared to nanogel-free control (C) but not compared to other groups (Figure 3g). Dominant usage of basal respiration allocated oxygen consumption in all groups are non-mitochondrial oxygen consumption and ATP production, which is consistent with C (Figure 3h), suggesting that mitochondrial respiration was not majorly altered. Similarly, cellular glycolysis was minimally impacted by nanogels in HEI-OC1 cells. There are no significant differences in glycolysis and non-glycolytic acidification among nanogel-treated groups and nanogel-free control (Figures 3i and 3j). There is an increase in glycolytic capacity in group D1 (Figure 3k), which is further reflected in increased glycolytic reserve for D1 (Figure 3l). There are no significant changes in the ratio of glycolytic capacity and glycolysis between different groups (Figure 3m).

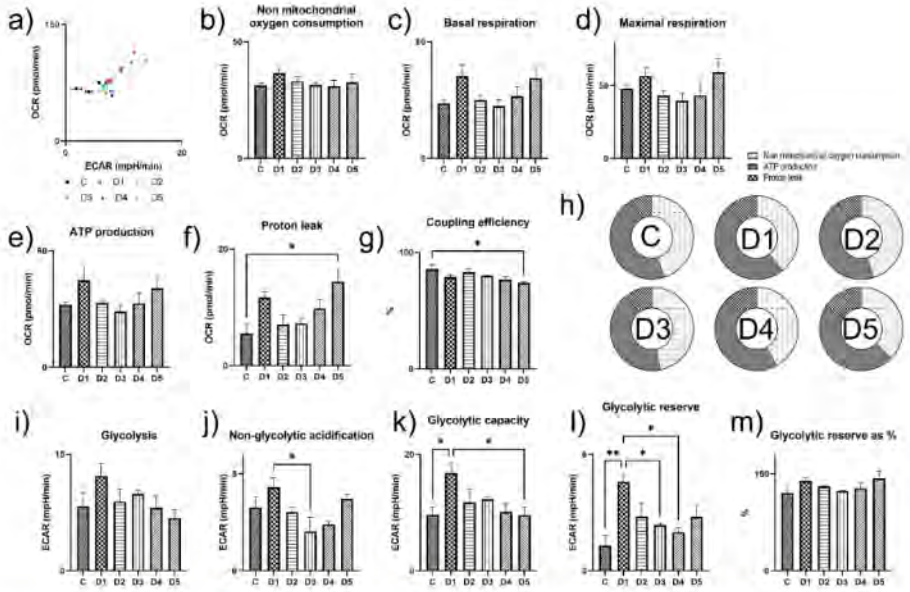

Figure 3. Cellular bioenergetics of HEI-OC1 cells after 24h incubation with nanogels. Mitochondrial stress test parameters were shown as a) metabolic profile, b) non-mitochondrial oxygen consumption, c) basal respiration, d) maximal respiration, e) ATP production, f) proton leak, g) coupling efficiency and g) overview of segments of respiration before the mitochondrial stress test. Glycolysis stress test parameters were shown as i) glycolysis, j) non-glycolytic acidification, k) glycolytic capacity, l) glycolytic reserve and m) the ratio of glycolytic capacity and glycolysis in percentage.

In RAW264.7 cells, groups D1, D2 and D3 seem to have increased mitochondrial metabolism (Figure 4a) and increased basal respiration (Figure 4c). However, this increase may be due to an increase in non-mitochondrial oxygen consumption (Figure 4b) and proton leak (Figure 4f) rather than an increase in ATP production (Figure 4e). In all groups, aside from control (C), non-mitochondrial oxygen consumption and proton leak are dominant oxygen consumption routes within basal respiration (Figure 4h), which leads to decreased coupling efficiency in all groups compared to the control (Figure 4g). No significant changes were observed in glycolytic metabolism for the RAW264.7 cell line treated with nanogels compared to the control (C) (Figure 4i-4m).

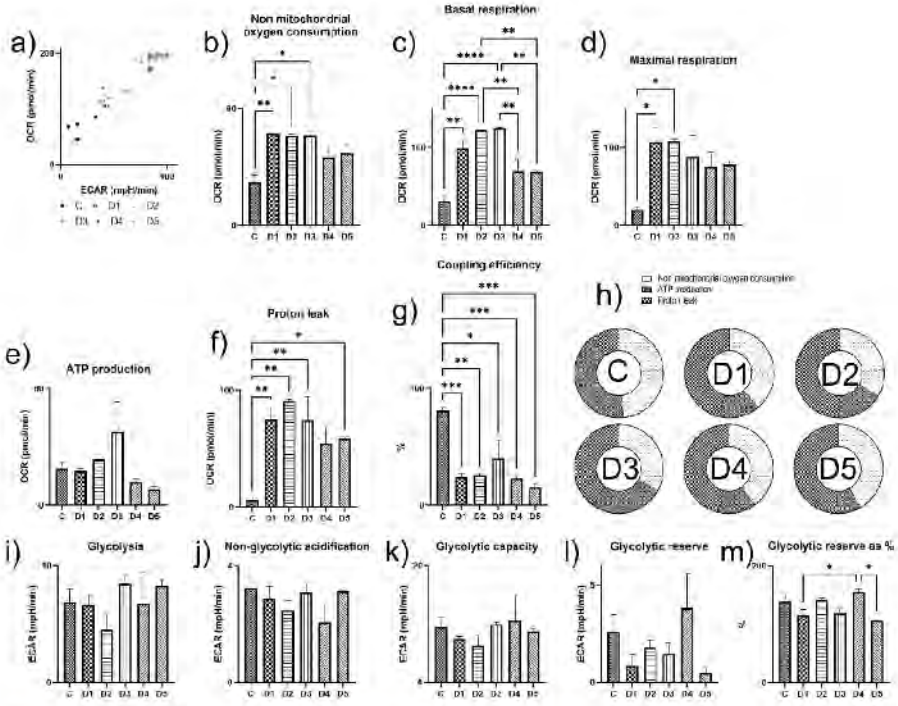

Figure 4. Cellular bioenergetics of RAW 264.7 cells after 24h incubation with nanogels. Mitochondrial stress test parameters were shown as a) metabolic profile, b) non-mitochondrial oxygen consumption, c) basal respiration, d) maximal respiration, e) ATP production, f) proton leak, g) coupling efficiency and g) overview of segments of respiration before the mitochondrial stress test. Glycolysis stress test parameters were shown as i) glycolysis, j) non-glycolytic acidification, k) glycolytic capacity, l) glycolytic reserve and m) the ratio of glycolytic capacity and glycolysis in percentage.

Discussion

The mean particle size below 1000 nm benefits nanogels, contributing to an increased drug-loading capacity and a controlled release (30). The neutral charge of investigated nanogels may delay foreign-body reaction and improve nanogel's biocompatibility and function, as the neutral charge seems to be the least suitable for albumin adsorption and cell attachment (31, 32). One of the main characteristics of nanogel is its injectability. Encapsulated cargo embedded within the nanogel encounters shear forces during injection, primarily induced by Newtonian fluids, particularly evident with low-viscosity solutions such as saline and culture medium. A flow resistance is established at the interface of the syringe and the fluid, resulting in extensional forces. This resistance causes a variation in flow velocity, with the centre of the pass-through exhibiting different velocities compared to the fluid adjacent to the internal surface of the syringe. As the disparity in diameters between the syringe and the needle increases, the magnitude of shear forces exerted on encapsulated cargo during injection proportionally escalates. Shear-thinning nanogels are preferable to facilitate such forces and protect the encapsulated material during injection (33, 34). Adding bile acids to nanogels did not change the fluid behaviour of the Poloxamer matrix, which is beneficial and concurrent with previous studies (28, 35).

Bile acids in biomaterials can have a detrimental impact on cellular viability, depending on the concentration, formulation, and tissue type (27, 36). To ensure high viability of the auditory cell line after nanogel exposure, formulations in this study based on bile acid concentration on a study by *Kovacevic et al.* (35), which showed higher viability at low bile acid concentrations. The auditory cell line showed no decrease in viability in the presence of nanogels (Figure 2a). However, the macrophage cell line did experience a reduction in viability after exposure to CDCA-enriched nanogel (Figure 2b). Interestingly, adding Tyloxapol ameliorated the negative impact of PVA and CDCA. Tyloxapol have been found to mitigate the pathological consequences of endotoxins in vivo and desensitise endotoxin-sensitive receptors on macrophages (37), with that effect being dependent on the Tyloxapol dose and the time of exposure (38).

Basal respiration shows the cellular energetic requirements before the start of the assay. ATP-linked respiration is calculated through the decline in OCR after introducing oligomycin, which acts as the ATP synthase inhibitor. The residual OCR, which is not linked to ATP synthesis, signifies proton leakage, indicating potential mitochondrial impairment. Non-mitochondrial respiration is OCR attributable to cellular enzymes, excluding mitochondria, measured after administering rotenone and antimycin A (39).

The conversion of reducing equivalents, derived from acetyl-CoA oxidation, to ATP through oxidative phosphorylation defines coupling efficiency. Mitochondrial coupling is imperfect, leading to the dissipation of redox energy as heat during normal oxidative phosphorylation. This incomplete coupling primarily results from the natural proton leak across the mitochondrial inner membrane (40). Here, coupling efficiency is calculated as ATP production linked to OCR shown as a percentage of basal respiration (41). A reduction in coupling efficiency may lead to lower energetic yield and low ATP production (42). A decrease in coupling efficiency is significant in macrophage lines exposed to all nanogels (Figure 4g), suggesting impaired oxidative phosphorylation. Furthermore, a decrease in coupling efficiency is linked with increased proton leak in the same cells (Figure 4f), further confirming metabolic dysfunction. An increase in OCR linked to proton leak may occur due to damage to the inner mitochondrial membrane, damage to the electron transport chain, increased activity of the uncoupling protein and electron slippage (43). The metabolic response of RAW 264.7 is similar across all groups of exposed nanogels, suggesting that the Poloxamer matrix may be responsible, irrelevant to added tyloxapol and CDCA (Figure 4). This is concurrent with previous studies showing that pro-inflammatory stimuli may induce a metabolic shift in macrophages from oxidative phosphorylation to glycolysis (44). Interestingly, impaired mitochondrial respiration in RAW 264.7 did not lead to changes in glycolysis (Figure 4).

Conclusion

In summary, this study highlights key innovations in nanogel technology, emphasising the significance of particle size, neutral charge, and shear-thinning properties. The investigation of nanogel impact on cellular viability reveals cell type-specific responses. While auditory cell lines remain unaffected, the macrophage cell line experiences viability reduction, mitigated by Tyloxapol. Metabolic analyses demonstrate decreased coupling efficiency and increased proton leak in macrophages exposed to nanogels, indicative of impaired oxidative phosphorylation. Notably, the Poloxamer matrix appears to influence the metabolic response across all groups, suggesting a potential role in inducing a pro-inflammatory shift in macrophage metabolism. The findings underscore the importance of tailoring nanogel formulations to specific cell types and considering the influence of matrix components on cellular responses to optimise drug delivery systems and enhance their biomedical applications.

Disclaimer

The authors want to acknowledge the Australian Postgraduate Award (APA) and Curtin Research Scholarship (CRS).

Conflicts of Interest: The authors declare no conflict of interest.

Availability of data and materials

The datasets generated and/or analysed during the current study are not publicly available but are available from the corresponding author at reasonable request.

References

1. Russo E, Villa C. Poloxamer Hydrogels for Biomedical Applications. Pharmaceutics [Internet]. 2019; 11(12).
2. Chen Y, Lee J-H, Meng M, Cui N, Dai C-Y, Jia Q, et al. An Overview on Thermosensitive Oral Gel Based on Poloxamer 407. Materials. 2021;14(16):4522.
3. Zana R. Dimeric and oligomeric surfactants. Behavior at interfaces and in aqueous solution: a review. Advances in Colloid and Interface Science. 2002;97(1):205-53.
4. Dharaiya N, Aswal VK, Bahadur P. Characterization of Triton X-100 and its oligomer (Tyloxapol) micelles vis-à-vis solubilization of bisphenol A by spectral and scattering techniques. Colloids and Surfaces A: Physicochemical and Engineering Aspects. 2015;470:230-9.
5. Gao Y, Li LB, Zhai G. Preparation and characterization of Pluronic/TPGS mixed micelles for solubilization of camptothecin. Colloids and Surfaces B: Biointerfaces. 2008;64(2):194-9.
6. Li L, Tan YB. Preparation and properties of mixed micelles made of Pluronic polymer and PEG-PE. Journal of Colloid and Interface Science. 2008;317(1):326-31.
7. Abdeltawab H, Svirskis D, Sharma M. Formulation strategies to modulate drug release from poloxamer based in situ gelling systems. Expert Opinion on Drug Delivery. 2020;17(4):495-509.
8. Zarrintaj P, Ramsey JD, Samadi A, Atoufi Z, Yazdi MK, Ganjali MR, et al. Poloxamer: A versatile tri-block copolymer for biomedical applications. Acta Biomaterialia. 2020;110:37-67.
9. Mehta SK, Jindal N. Mixed micelles of Lecithin–Tyloxapol as pharmaceutical nanocarriers for anti-tubercular drug delivery. Colloids and Surfaces B: Biointerfaces. 2013;110:419-25.
10. Jiao J. Polyoxyethylated nonionic surfactants and their applications in topical ocular drug delivery. Advanced Drug Delivery Reviews. 2008;60(15):1663-73.
11. Mehta SK, Jindal N. Tyloxapol Niosomes as Prospective Drug Delivery Module for Antiretroviral Drug Nevirapine. AAPS PharmSciTech. 2015;16(1):67-75.
12. Onugwu AL, Nwagwu CS, Onugwu OS, Echezona AC, Agbo CP, Ihim SA, et al. Nanotechnology based drug delivery systems for the treatment of anterior segment eye diseases. Journal of Controlled Release. 2023;354:465-88.
13. González-Fernández FM, Delledonne A, Nicoli S, Gasco P, Padula C, Santi P, et al. Nanostructured Lipid Carriers for Enhanced Transscleral Delivery of Dexamethasone Acetate: Development, Ex Vivo Characterization and Multiphoton Microscopy Studies. Pharmaceutics. 2023;15(2):407.
14. Harisa GI, Alanazi SA, Badran MM, Sherif AY, AlQahtani SA, Alanazi FK. Tyloxapol and nanoliposomes induce selective delivery of 5-fluorouracil into hepatic tissues via VLDL/LDL-mediated pathway. European Journal of Lipid Science and Technology. 2024;126(1):2300039.
15. Kovacevic B, Jones M, Ionescu C, Walker D, Wagle S, Chester J, et al. The emerging role of bile acids as critical components in nanotechnology and bioengineering: Pharmacology, formulation optimizers and hydrogel-biomaterial applications. Biomaterials. 2022;283:121459.
16. Mooranian A, Ionescu CM, Wagle SR, Kovacevic B, Walker D, Jones M, et al. Chenodeoxycholic Acid Pharmacology in Biotechnology and Transplantable Pharmaceutical Applications for Tissue Delivery: An Acute Preclinical Study. Cells. 2021;10(9):2437.
17. Mooranian A, Foster T, Ionescu CM, Walker D, Jones M, Wagle SR, et al. Enhanced Bilosomal Properties Resulted in Optimum Pharmacological Effects by Increased Acidification Pathways. Pharmaceutics. 2021;13(8):1184.

18. Mooranian A, Ionescu CM, Walker D, Jones M, Wagle SR, Kovacevic B, et al. Single-Cellular Biological Effects of Cholesterol-Catabolic Bile Acid-Based Nano/Micro Capsules as Anti-Inflammatory Cell Protective Systems. Biomolecules. 2022;12(1):73.
19. Mooranian A, Jones M, Ionescu CM, Walker D, Wagle SR, Kovacevic B, et al. Advancements in Assessments of Bio-Tissue Engineering and Viable Cell Delivery Matrices Using Bile Acid-Based Pharmacological Biotechnologies. Nanomaterials. 2021;11(7):1861.
20. Mooranian A, Jones M, Walker D, Ionescu CM, Wagle SR, Kovacevic B, et al. Pharmacological Dose-Effect Profiles of Various Concentrations of Humanised Primary Bile Acid in Encapsulated Cells. Nanomaterials. 2022;12(4):647.
21. Mooranian A, Raj Wagle S, Kovacevic B, Takechi R, Mamo J, Lam V, et al. Bile acid bio-nanoencapsulation improved drug targeted-delivery and pharmacological effects via cellular flux: 6-months diabetes preclinical study. Scientific Reports. 2020;10(1):106.
22. Wagle SR, Kovacevic B, Walker D, Ionescu CM, Jones M, Stojanovic G, et al. Pharmacological and Advanced Cell Respiration Effects, Enhanced by Toxic Human-Bile Nano-Pharmaceuticals of Probucol Cell-Targeting Formulations. Pharmaceutics. 2020;12(8):708.
23. Wagle SR, Walker D, Kovacevic B, Gedawy A, Mikov M, Golocorbin-Kon S, et al. Micro-Nano formulation of bile-gut delivery: rheological, stability and cell survival, basal and maximum respiration studies. Sci Rep. 2020;10(1):7715.
24. Carleton MM, Sefton MV. Injectable and degradable methacrylic acid hydrogel alters macrophage response in skeletal muscle. Biomaterials. 2019;223:119477.
25. Chin NL, Chan SM, Yusof YA, Chuah TG, Talib RA. Modelling of rheological behaviour of pummelo juice concentrates using master-curve. Journal of Food Engineering. 2009;93(2):134-40.
26. Kovacevic B, Ionescu CM, Wagle SR, Jones M, Lewkowicz M, Wong EYM, et al. Impact of Novel Teflon-DCA Nanogel Matrix on Cellular Bioactivity. Journal of Pharmaceutical Sciences. 2023;112(3):700-7.
27. Kovacevic B, Jones M, Wagle SR, Ionescu CM, Foster T, Đanić M, et al. Influence of poly-L-ornithine-bile acid nano hydrogels on cellular bioactivity and potential pharmacological applications. Therapeutic Delivery. 2023;14(8):499-510.
28. Kovacevic B, Jones M, Wagle SR, Ionescu CM, Foster T, Đanić M, et al. The effect of deoxycholic acid-based hydrogels on hepatic, muscle and pancreatic beta cells. Therapeutic Delivery. 2024;15(1):41-54.
29. Akiyama E, Morimoto N, Kujawa P, Ozawa Y, Winnik FM, Akiyoshi K. Self-Assembled Nanogels of Cholesteryl-Modified Polysaccharides: Effect of the Polysaccharide Structure on Their Association Characteristics in the Dilute and Semidilute Regimes. Biomacromolecules. 2007;8(8):2366-73.
30. Neamtu I, Rusu AG, Diaconu A, Nita LE, Chiriac AP. Basic concepts and recent advances in nanogels as carriers for medical applications. Drug Delivery. 2017;24(1):539-57.
31. Schneider GB, English A, Abraham M, Zaharias R, Stanford C, Keller J. The effect of hydrogel charge density on cell attachment. Biomaterials. 2004;25(15):3023-8.
32. Zhang J, Zhu Y, Song J, Yang J, Pan C, Xu T, et al. Novel Balanced Charged Alginate/PEI Polyelectrolyte Hydrogel that Resists Foreign-Body Reaction. ACS Applied Materials & Interfaces. 2018;10(8):6879-86.
33. Samadi A, Moammeri A, Azimi S, Bustillo-Perez BM, Mohammadi MR. Biomaterial engineering for cell transplantation. Biomaterials Advances. 2024;158:213775.
34. Bertsch P, Diba M, Mooney DJ, Leeuwenburgh SCG. Self-Healing Injectable Hydrogels for Tissue Regeneration. Chemical Reviews. 2023;123(2):834-73.
35. Kovacevic B, Raj Wagle S, Mihaela Ionescu C, Foster T, Đanić M, Mikov M, et al. The biocompatibility and the metabolic impact of thermoresponsive, bile acid-based nanogels on auditory and macrophage cell lines. European Journal of Pharmaceutics and Biopharmaceutics. 2023;190:248-57.
36. Kovacevic B, Ionescu CM, Jones M, Wagle SR, Foster T, Lewkowicz M, et al. Novel polysaccharides–bile acid–cyclodextrin gel systems and effects on cellular viability and bioenergetic parameters. Therapeutic Delivery. 2024.

37. Serikov VB, Glazanova TV, Jerome EH, Fleming NW, Higashimori H, Staub Sr NC. Tyloxapol attenuates the pathologic effects of endotoxin in rabbits and mortality following cecal ligation and puncture in rats by blockade of endotoxin receptor-ligand interactions. Inflammation. 2003;27(4):175-90.
38. Kuo J-hS, Lin Y-L, Tseng J-w. Interactions between U-937 human macrophages and tyloxapol. Colloids and Surfaces B: Biointerfaces. 2008;64(2):208-15.
39. Gu X, Ma Y, Liu Y, Wan Q. Measurement of mitochondrial respiration in adherent cells by Seahorse XF96 Cell Mito Stress Test. STAR Protocols. 2021;2(1):100245.
40. Johannsen DL, Ravussin E. The role of mitochondria in health and disease. Current Opinion in Pharmacology. 2009;9(6):780-6.
41. Iuso A, Repp B, Biagosch C, Terrile C, Prokisch H. Assessing Mitochondrial Bioenergetics in Isolated Mitochondria from Various Mouse Tissues Using Seahorse XF96 Analyzer. In: Mokranjac D, Perocchi F, editors. Mitochondria: Practical Protocols. New York, NY: Springer New York; 2017. p. 217-30.
42. Prola A, Blondelle J, Vandestienne A, Piquereau J, Denis RGP, Guyot S, et al. Cardiolipin content controls mitochondrial coupling and energetic efficiency in muscle. Science Advances. 2021;7(1):eabd6322.
43. Hill BG, Benavides GA, Lancaster JR, Ballinger S, Dell'Italia L, Zhang J, et al. Integration of cellular bioenergetics with mitochondrial quality control and autophagy. Biological Chemistry. 2012;393(12):1485-512.
44. Kelly B, O'Neill LAJ. Metabolic reprogramming in macrophages and dendritic cells in innate immunity. Cell Research. 2015;25(7):771-84.

Publication 10 (pages 171-181):

Advanced smart-polymers-bile acid chemical nano-biotechnological effects on cyclodextrin-based nanogels for ear delivery and treatment of hearing loss

Kovacevic B, Wagle S, Ionescu C, Foster T, Đanić M, Mikov M, Mooranian A, Al-Salami H.

Journal: Nano Today

Sub-objective (9): to design and create nanogels utilising poloxamer 407, polyvinyl alcohol and deoxycholic acid, and to examine the shear stress, viscosity, surface tension, torque, microstructure, and zeta potential of nanogels. Additionally, the nanogels were incubated with 2 different cell lines (HEI-OC1 and RAW264.7) and their impact on viability, total intracellular reactive oxygen species, inflammatory profile, macrophage polarisation as well as nanogel impact on bioenergetic parameters was investigated.

RESEARCH ARTICLE

ADVANCED HEALTHCARE MATERIALS
www.advhealthmat.de

Biotechnological Effects of Advanced Smart-Bile Acid Cyclodextrin-Based Nanogels for Ear Delivery and Treatment of Hearing Loss

Bozica Kovacevic, Susbin Raj Wagle, Corina Mihaela Ionescu, Thomas Foster, Maja Đanić, Momir Mikov, Armin Mooranian, and Hani Al-Salami**

Inner ear delivery requires safe and effective drug delivery vehicles incorporating high-viscosity formulations with permeation enhancers. This study designs novel thermoresponsive-smart polymer-bile acid and cyclodextrin-based nanogels for inner ear delivery. Nanogels are examined for their rheological and physical properties. The biocompatibility studies will be assessed on auditory and macrophage cell lines by investigating the impact of nanogels on cellular viability, mitochondrial respiration, glycolysis, intracellular oxidative stress, inflammatory profile, and macrophage polarization. Novel ther nanogels based on bile acid and beta-cyclodextrin show preserved porous nanogels' inner structure, exhibit non-Newtonian, shear-thinning fluid behavior, have fast gelation at 37 °C and minimal albumin adsorption on the surface. The nanogels have minimal impact on cellular viability, mitochondrial respiration, glycolysis, intracellular oxidative stress, and inflammatory profile of the auditory cell line House Ear Institute-Organ of Corti 1 after 24 h incubation. Nanogel exposure of 24 h to macrophage cell line RAW264.7 leads to decreased viability, mitochondrial dysfunction, and increased intracellular ROS and inflammatory cytokines. However, polarization changes from M2 anti-inflammatory to M1 pro-inflammatory macrophages are minimal, and inflammatory products of RAW264.7 macrophages do not overly disrupt the survivability of HEI-OC1 cells. Based on these results, thermoresponsive bile acid and cyclodextrin nanogels can be potential drug delivery vehicles for inner ear drug delivery.

1. Introduction

Delivery to the inner ear is filled with challenges, primarily due to anatomic barriers, including the tympanic membrane between the external and middle ear and the round window membrane between the middle and inner ear. Furthermore, there is a constant clearance via the Eustachian tube, shortening the drug's duration of effect.[1] Hydrogels and high-viscosity drug-carrying formulations were proposed to combat drug clearance, allowing the drug of interest to have prolonged localization. Drug diffusion to the inner ear is inconsistent, which may be overcome by the increased permeability of barrier membranes. This can be achieved via permeation enhancers.[2] Based on these strategies, the study will aim to design nanogel formulations with permeation enhancers.

Nanogels are 3D polymeric structures with similar viscoelastic properties to hydrogels. They are characterized by internal structure in the sub-micron range (20–250 nm).[3,4] Nanogels are reported to have exceptional biocompatibility, stability, mechanical properties, and more extensive surface area with enhanced water content, making them ideal candidates for application-appropriate modifications.[5] Nanogels are capable of encapsulating different nanoparticles, including dendrimers, micelles, liposomes, and lipid nanoparticles, with the nanogel's network serving as a protection mechanism and release profile facilitator for encapsulated material.[6] Drug release can further be regulated via stimuli-responsive nanogels, usually by releasing encapsulated cargo

B. Kovacevic, S. R. Wagle, C. M. Ionescu, T. Foster, A. Mooranian, H. Al-Salami
The Biotechnology and Drug Development Research Laboratory
Curtin Medical School & Curtin Health Innovation Research Institute
Curtin University
Bentley, Perth WA 6102, Australia
E-mail: a.mooranian@curtin.edu.au; hani.al-salami@curtin.edu.au

The ORCID identification number(s) for the author(s) of this article can be found under https://doi.org/10.1002/adhm.202303149

DOI: 10.1002/adhm.202303149

M. Đanić, M. Mikov
Department of Pharmacology
Toxicology and Clinical Pharmacology
Faculty of Medicine
University of Novi Sad
Novi Sad 21101, Serbia

A. Mooranian
School of Pharmacy
University of Otago
Dunedin, Otago 9016, New Zealand

H. Al-Salami
Medical School
University of Western Australia
Perth 6009, Australia

in the presence of external stimuli. These stimuli can include changes in pH, temperature, light, and magnetic field.[7–9]

Poloxamer 407 is capable of forming thermoresponsive nanogels, and it is approved by the European Medicines Agency and the USA Food and Drug Administration as a pharmaceutical excipient in drug delivery due to its biocompatibility and weak immunogenic properties.[10] It consists of poly(ethylene oxide)-poly(propylene oxide) (PEO-PPO) block copolymers, allowing for self-assembly in aqueous solution into thermodynamically stable micelles with various structures.[11] It is a good candidate for a gelling agent in drug delivery matrices with permeation enhancers.

Poloxamer polymers have been investigated for the facilitation of inner ear delivery. Studies show that drugs (mostly corticosteroids) are incorporated within poloxamer hydrogel, usually without adding permeation enhancers.[12,13] Khoo et al. used poloxamer and a combination of permeation enhancers (sodium dodecyl sulfate, limonene, and bupivacaine) for the increased trans tympanic delivery of antibiotics,[14] while Liao et al. used microbubble Poloxamer hydrogel and ultrasound mediation to enhance the permeability of round window membrane.[15] This study would be the first to examine the effect of Poloxamer 407 nanogels with the addition of naturally produced permeation agent – deoxycholic acid (DCA), as well as beta cyclodextrin (BCD) to facilitate solubilization and controlled release of poorly bioavailable, hydrophobic drugs for inner ear delivery.

Bile acids are emerging as potent permeation enhancers and formulation stabilizers,[16–21] capable of self-assembling into complex aggregates.[22] DCA is a secondary bile acid widely used as a carrier for drugs, vaccines, and biomolecules and as a permeation enhancer.[23]

BCD is a cyclodextrin with seven glucopyranose units. BCD is an extensively used molecule in the pharmaceutical industry due to its ability to form inclusion complexes with the target molecules when dissolved in water, facilitating targeted drug delivery.[24]

We characterized the rheological and physical properties of novel thermoresponsive nanogels with bile acid and BCD. The biocompatibility studies will be assessed on auditory and macrophage cell lines, investigating the impact of nanogels on cellular viability, mitochondrial respiration, glycolysis, intracellular oxidative stress, inflammatory profile, and macrophage polarization.

2. Results and Discussion

The addition of PVA (A2), DCA (A3), BCD (A4), and DCA and BCD (A5) does not seem to significantly influence the overall porous inner structure of Poloxamer 407 (A1) (**Figure** 1a). For all nanogels, the gelation time necessary to achieve a gel state at 37 °C was below 1 min. The nanogel with BCD (A4) showed an increase in gelation time compared to Poloxamer 407 (A4), while the combination of DCA and BCD (A5) resulted in improved gelation (Figure 1b). The significant differences in Figure 1b were shown for A1 comparison with other nanogels. In aqueous solutions, poloxamer monomers exhibit amphiphilic behavior, prompting self-aggregation into micelles characterized by a hydrophobic core and a hydrophilic outer shell. These nanostructures, typically ranging from 10 to 200 nm, manifest at the critical micellization concentration (CMC) and critical micellization temperature. The CMC of poloxamer in water diminishes with rising temperature, making the gelation thermosensitive.[25] The gelation mechanism of thermoresponsive poloxamer 407 aqueous solution involves temperature-induced rearrangement of micelles to a hexagonal structure. Formulations with 15–30% concentration exhibit gelation at body temperature (37 °C). Thermosensitive poloxamer-based gels exhibit temperature-sensitive

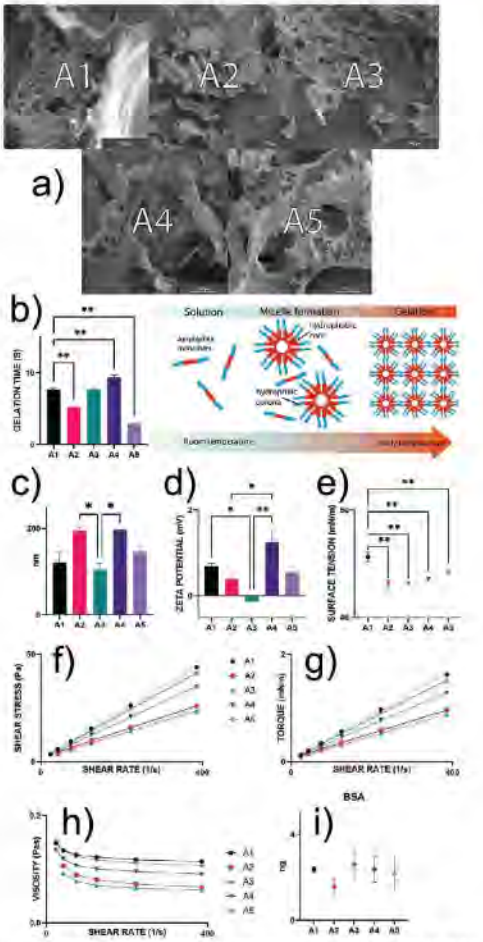

Figure 1. shows a) SEM images of freeze-dried nanogel samples; b) gelation times of nanogels, schematic of nanogel gelation mechanism; c) mean particle size; d) zeta potential of nanogels; e) surface tension of nanogels; f) the amount of adsorbed BSA on the surface of nanogels; g) shear stress as a function of shear rate; h) torque as a function of shear rate; and i) viscosity of nanogels as a function of shear rate. Data are shown as mean ± SEM, $n = 3$. $p < 0.01$ (**) and $p < 0.05$ (*).

Table 1. Power law curve fitting parameters for sample nanogels at room temperature. Data are shown as mean ± SEM, $n = 3$, $p < 0.01$ (**) and $p < 0.05$ (*).

	Temperature [°C]	Consistency coefficient, K	Flow behavior index, n	Coefficient of determination, R^2
A1	22 ± 0.5	0.16785 ± 0.00062	0.93523 ± 0.00056	0.99994 ± 0.00002
A2	22 ± 0.5	0.18014 ± 0.00322	0.83277 ± 0.00329	0.99924 ± 0.00016
A3	22 ± 0.5	0.13626 ± 0.00086	0.86438 ± 0.00066	0.99946 ± 0.00014
A4	22 ± 0.5	0.17282 ± 0.00460	0.83044 ± 0.00468	0.99966 ± 0.00010
A5	22 ± 0.5	0.18501 ± 0.00323	0.90705 ± 0.00274	0.99980 ± 0.00007

behavior, transitioning from liquid at room temperature to gel at body temperature. This characteristic makes them highly desirable drug carriers.[26]The mean particle size for all nanogel formulations was less than 1000 nm, showcasing the sub-micro range necessary for hydrogels to be categorized as nanogels.[27] The Zeta potential for all nanogels was close to zero (Figure 1d), with DCA (A3) lowering zeta potential and BDC increasing it (A4). The balanced charge of nanogels may be a beneficial property that allows for minimal protein adsorption and subsequent immune response.[28] The BSA adsorption (Figure 1i) seems to support this, as a minimal amount of BSA is detected on the surface of hydrogels after 30 min of incubation at 37 °C. However, this test is just the first step in examining protein adsorption on biomaterials as albumin is a major protein of protein corona, but not the only one.[29] Protein adsorption on biomaterials varies based on surface chemistry, topography, and competitive interactions, particularly influenced by the Vroman effect,[30] and not only on electrostatic charge. Within protein mixtures like serum, initial proteins on the surface may be displaced by subsequent proteins with lower concentration but higher surface affinity—a phenomenon termed the "Vroman effect."[31] Recent advancements in experimental and theoretical analyses provide insights into the dynamic nature of protein adsorption onto biomaterials. Despite these developments, a comprehensive understanding is hindered by the intricate dynamics of the adsorption process, including the Vroman effect, with no existing models or techniques fully elucidating the mechanism.[32]

The surface tension of nanogels seems to be lowered with the addition of polymers and bile acid (A2-A5) to the Poloxamer 407 matrix (A1) (Figure 1e). Rheological parameters (Figure 1g–i) suggest non-Newtonian, shear-thinning fluid behavior.

The Power-law curve fitting parameters further confirm that nanogels exhibit non-Newtonian, shear-thinning fluid (pseudo-plastic) behavior with a flow behavior index (n) less than 1 (**Table 1**). Flow behavior index (n) for nanogels A2-A5 is lower than Poloxamer 407 only control (A1), showing that adding proposed polymers enhances pseudo-plastic properties. The pseudo-plastic properties are the most pronounced in A2 nanogel (Table 1). There is an increase in apparent viscosity in A2, A4, and A5 compared to A1, which is evident in an increase in consistency coefficient (K).[33] The addition of DCA (A3) seems to decrease the apparent viscosity of nanogels (Table 1). The coefficient of determination (R2) close to value 1 indicates good accuracy of the experimental data.

The 24 h incubation with nanogels did not affect the viability of the HEI-OC1 cell line (**Figure 2a**). There were changes in ATP production linked to oxygen consumption rate (OCR) and subsequently in basal respiration linked OCR (Figure 2b,c). However, these differences in the amount of OCR allocated to ATP production may not be biologically significant due to similar coupling efficiency (Figure 2d). The coupling efficiency is the proportion of oxygen consumed to drive ATP production within basal respiration.[34] It is sensitive to changes in bioenergetic parameters and is likely to change in any mitochondrial dysfunction.[35] There are no significant differences in parameters for proton leak-linked OCR and non-mitochondrial oxygen consumption-linked OCR (Figure 2e,f), confirming no substantial changes in the mitochondrial function of nanogel-treated auditory cells compared to untreated control. The similarity in bioenergetic profiles is visually presented in Figure 2g, showing the fractions of non-mitochondrial oxygen consumption linked to OCR, ATP production linked OCR, and proton leak linked OCR within basal respiration. For anaerobic metabolism, there are no significant changes in glycolysis-linked extracellular acidification rate (ECAR) between treated and untreated (control) cells (Figure 2h). A glycolytic shift in metabolism has been reported previously in different cell lines exposed to bile acid-based hydrogels,[36–38] which is not the case in this study, as this effect may be concentration and tissue depended. Glycolytic capacity is energy demand after the inhibition of mitochondrial ATP production,[39] and it seems to be slightly increased with the addition of bile acid to formulation (A3), but it is not significantly different to untreated cells (Figure 2i). The non-glycolytic acidification rate, the ECAR not related to glycolytic metabolism, is the lowest in cells incubated with A5 nanogel (figure 2k). A3 has increased glycolytic reserves compared to C, A2 and A5 (Figure 2j). However, the ratio of glycolytic capacity and glycolysis (Figure 2m) remains without significant differences. This may indicate no major changes in glycolytic cellular metabolism within the HEI-OC1 cell line when exposed to nanogels.

Incubation with nanogels leads to decreased viability of the macrophage cell line (**Figure 3a**), with all groups retaining viability above 60%. The A2 group is the best-performing one, without a significant decrease compared to the control (C). Groups with BCD (A4 and A5) showed the least favorable cellular survivability (Figure 3a). The mitochondrial stress test shows increased basal respiration in cells exposed to nanogels (Figure 3b). This increase is not based on the rise in ATP production (Figure 3c) but rather on a dramatic increase in proton leak (Figure 3e) and partially on an increase in non-mitochondrial oxygen consumption (Figure 3f). Proton leak-linked OCR may be linked to damage to the inner mitochondrial membrane and electron transport chain, electron slippage, and increased activity of the uncoupling

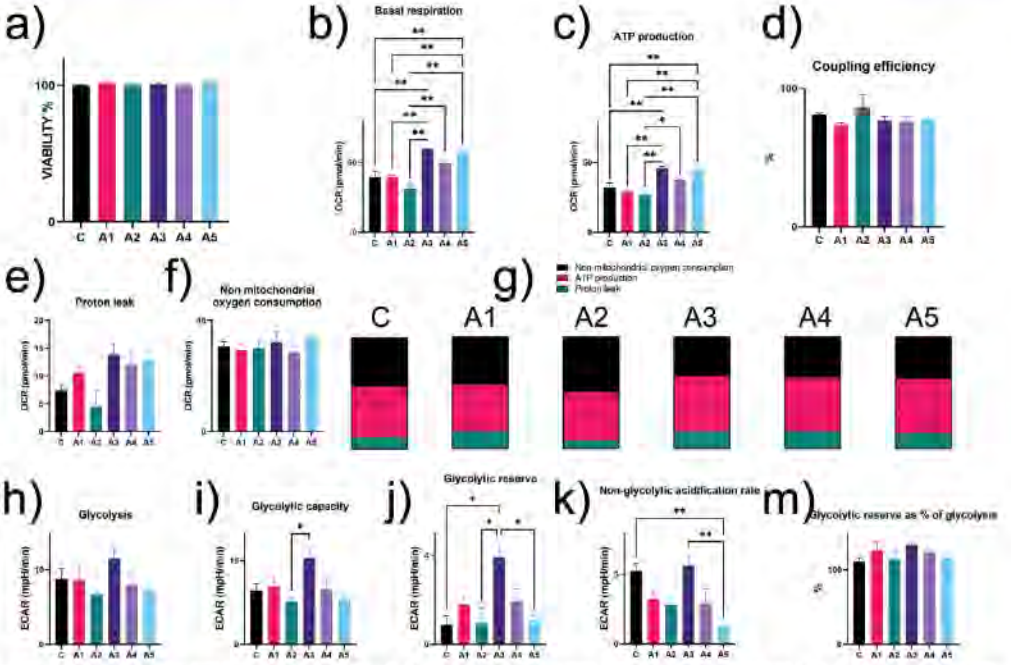

Figure 2. shows viability and metabolic parameters for HEI-OC1 cells after 24 h incubation with nanogels, a) cellular viability; b) basal respiration linked OCR; c) ATP production linked OCR; d) coupling efficiency; e) proton leak linked OCR; f) non-mitochondrial oxygen consumption linked OCR; g) visual representation of a percentage of non-mitochondrial oxygen consumption, ATP production and proton leak in respiration; h) glycolysis linked ECAR; i) glycolytic capacity linked ECAR; j) glycolytic reserve linked ECAR; k) non-glycolytic acidification rate linked ECAR; and l) glycolytic reserve expressed as a percentage of glycolysis. Data are shown as mean ± SEM, $n = 3$. $p < 0.01$ (**) and $p < 0.05$ (*).

protein.[40] Metabolic dysfunction in the presence of nanogels is further evident in lowered coupling efficiency (Figure 3d) and visual representation of metabolic fractions in basal respiration (Figure 3g). A decrease in glycolysis parameters is present in cells incubated with nanogels (Figures 3h–j); however, there are no changes in non-glycolytic acidification rate linked to ECAR (Figure 3k) and the ratio between glycolytic capacity and glycolysis (Figure 3m), suggesting that anaerobic metabolism of RAW264.7 cells is not in dysfunction.

The total amount of intracellular free radicals (ROS) is not significantly different between treated and untreated HEI-OC1 cells (**Figure 4a**). Low levels of ROS are necessary for normal cellular function, as they act as signaling molecules.[41,42] Increased levels of ROS are linked with inflammation and oxidative stress, leading to disrupted cellular homeostasis and damage to cellular organelles and molecular components.[43] There is a significant increase in intracellular ROS in RAW264.7 cells in the presence of nanogels (A1-A5) compared to untreated cells (C) (Figure 3b). As metabolic processes and mitochondrial respiration are significant sources of ROS,[44] metabolic dysfunction evident in increased proton leak and non-mitochondrial oxygen consumption linked OCR (Figure 3e,f) may be key sources of ROS in RAW264.7 cells.

Levels of granulocyte-macrophage colony stimulating factor (GM-CSF) were detected in both HEI-OC1 (**Figure 5a**) and RAW264.7 cell lines (Figure 5e) without significant differences between cells exposed to nanogels and untreated controls (C). GM-CSF is reported to be produced by cells involved in immune response, fibroblasts, and epithelial cells during inflammation to polarize myeloid cells and promote clearance of pathogens.[45–47] GM-CSF stimulates the resolution of inflammation and subsequent wound healing and tissue repair.[48] No visible and clear significant changes in levels of GM-CSF in examined cell lines may be a good prognostic indicator for inflammation caused by nanogels. Interferon-gamma (IFN gamma) was detected in both cell lines, with different expression profiles regarding treated and untreated groups (Figure 5b,f). In the case of the auditory cell line, there is a decrease of INF gamma in A2 compared to the untreated cells, no significant differences of nanogel with DCA only (A3), and an increase in INF-gamma levels in the presence of nanogels with BCA (A4 and A5) (Figure 5b). For the macrophage cell line, there is a significant increase in INF gamma levels in all groups exposed to nanogels compared to the untreated cells (C). Within treated groups, A3 had the highest expression of INF gamma (Figure 5f). INF gamma has complex pro- and anti-inflammatory effects, depending on the duration and magnitude

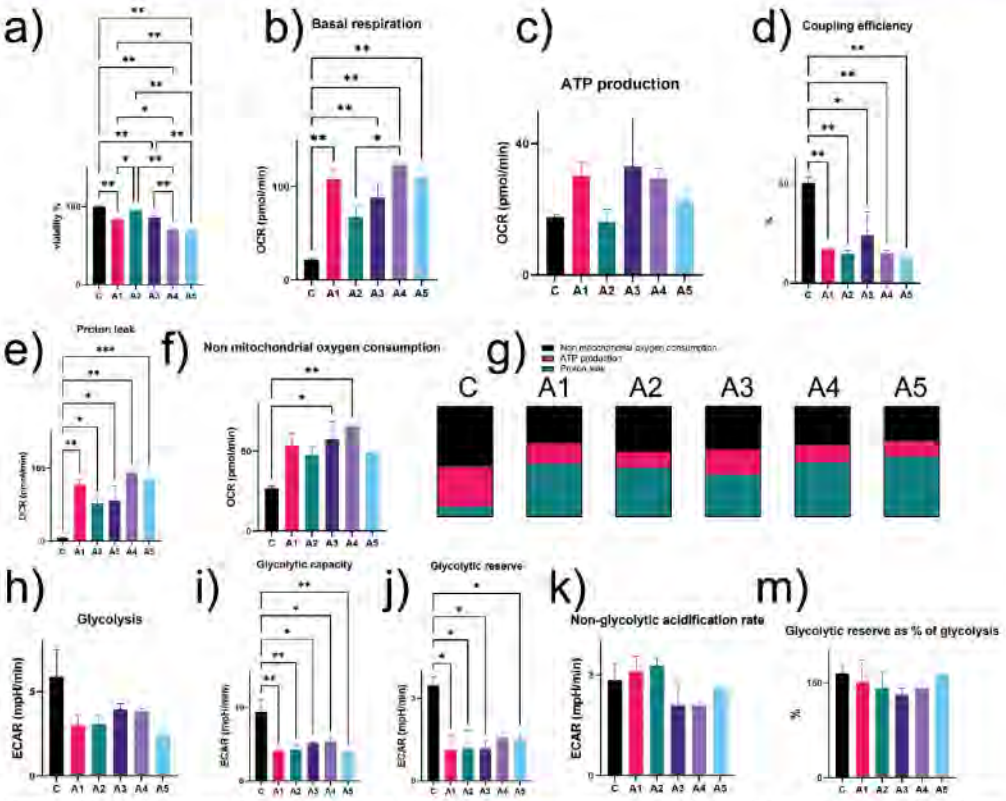

Figure 3. shows viability and metabolic parameters for RAW 264.7 cells after 24 h incubation with nanogels, a) cellular viability; b) basal respiration linked OCR; c) ATP production linked OCR; d) coupling efficiency; e) proton leak linked OCR; f) non-mitochondrial oxygen consumption linked OCR; g) visual representation of a percentage of non-mitochondrial oxygen consumption, ATP production and proton leak in respiration; h) glycolysis linked ECAR; i) glycolytic capacity linked ECAR; j) glycolytic reserve linked ECAR; k) non-glycolytic acidification rate linked ECAR; and m) glycolytic reserve expressed as a percentage of glycolysis. Data are shown as mean ± SEM, $n = 3$. $p < 0.01$(**) and $p < 0.05$ (*).

of IFN gamma signaling.[49] INF gamma is involved in promoting inflammatory and chemotactic signals, apoptosis, activation of inflammatory M1 macrophages, suppression of reparative M2 macrophages, and the regulation of ROS.[50–53] IL-3 is a colony-stimulating factor relaying on βc receptors similar to GM-CSF. IL-3 levels are increased in the presence of inflammatory stimuli, like infection or injury, and may be involved in morphological and functional programming cells to acute immune response.[54,55] There are no changes in IL-3 levels for the auditory cell line between control cells and cells exposed to nanogels (Figure 5c). Within the nanogel groups, the nanogel matrix with the addition of DCA and BCD (A5) has slightly increased IL-3 production compared to the matrix without DCA and BCD (A2). For the macrophage cell line, there is an increase in IL-3 levels in the presence of DCA nanogels (A3) and BCD (A4) compared to the control (C) (Figure 5g). However, nanogel combined with DCA and BCD (A5) does not seem to significantly increase IL-3 levels compared to the untreated control (C). IL-9 is a pleiotropic cytokine involved with allergies, autoimmune diseases, and response to parasitic infections.[56] The expression profile of IL-9 in both cell lines shows a similar pattern to the INF gamma profile (Figure 5d,b,h,f), with an increase in RAW264.7 exposed to nanogels and a modest increase in HEI-OC1 cells exposed to A5 compared to untreated cells. IL-9 and INF gamma levels in both cell lines may be related, as IL-9 may suppress INF gamma.[57]

To determine if the inflammation caused by nanogels is capable of activation of M1 macrophage phenotype, RAW234.7 cells were stained with antibodies against inducible nitric oxide synthase (iNOS), which is a marker for pro-inflammatory M1 phenotype, and arginase 1 (ARG1), a marker of reparative, anti-inflammatory M2 phenotype.[58,59] ARG1 marker is presented in purple in Figure 5j, showing that most RAW264.7 cells are in M2 polarization, regardless of exposure to nanogels. Pro-inflammatory M1 cells are presented in green (iNOS marker),

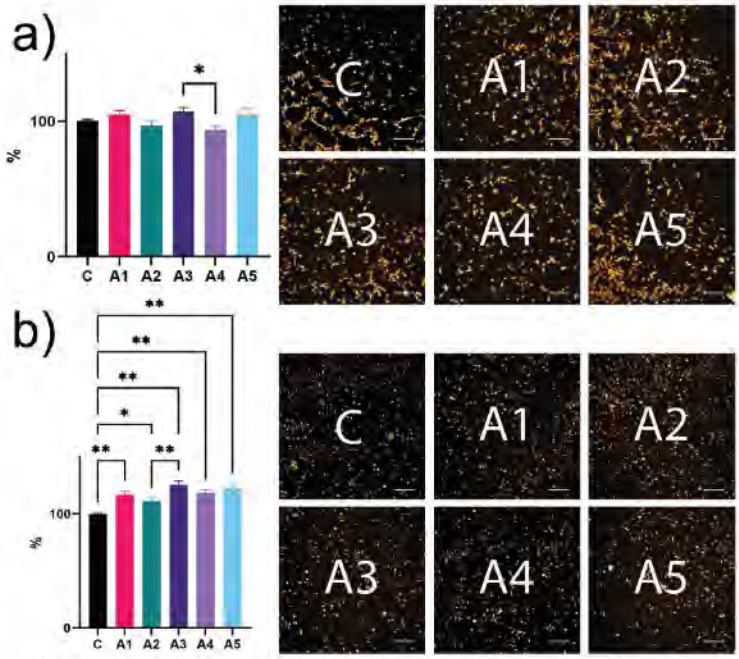

Figure 4. Total intracellular ROS profile of a) HEI-OC1 cell line and b) RAW264.7 cell line. Data is normalized based on the adsorbance intensity of untreated cells (C)(100%). The scale bar is 200 µm. The orange color indicates the intercellular ROS stained by the Cellular ROS Assay Kit. Data are shown as mean ± SEM, $n = 3$. $p < 0.01$(**) and $p < 0.05$ (*).

and they account for only several cells in groups exposed to nanogels with BCD (A4 and A5) (Figure 5j).

To assess the impact of macrophage-produced cytokines on auditory cell lines, the HEI-OC1 were incubated for 24 hours with a RAW264.7 cell media. RAW264.7 cells were incubated with nanogels for 24 h, then nanogels were removed, and the media changed. The cellular media from the following 24 h incubation with RAW264.7 cell previously exposed to nanogels was used on HEI-OC1 cells. RAW264.7 media was used as 25% of fresh media on HEI-OC1 (**Figure** 6a), 50% of fresh media (Figure 6b), and as the complete media (Figure 6c). Control cells (C) had media from untreated RAW264.7 in appropriate ratios. There is a decrease in viability among all groups exposed to RAW264.7 media, compared to the control, under all ratios (Figure 6a–c). However, this decrease in viability is minimal, as all assessed groups have viability higher than 95% of control viability (**Figure** 7).

3. Conclusion

New thermoresponsive nanogels based on bile acid and cyclodextrin show preserved porous nanogels' inner structure, exhibit non-Newtonian, shear-thinning fluid behavior, have fast gelation at 37 °C and minimal albumin adsorption on the surface. These nanogels have minimal impact on cellular viability, mitochondrial respiration, glycolysis, intracellular ROS, and inflammatory profile of auditory cell line HEI-OC1 after 24 h incubation. By combining the advantages of bile acid and cyclodextrin, these innovative nanogels offer a versatile platform for targeted drug delivery, particularly in delicate and sensitive biological environments like the inner ear. Their ability to preserve cellular integrity underscores their potential significance in revolutionizing nano-based therapies for auditory disorders and beyond.

4. Experimental Section

Materials for nanogel preparation were purchased from Sigma Chemical Co (St. Louis, MO, USA), including Poloxamer 407, polyvinyl alcohol (PVA), beta-Cyclodextrin, sulfated sodium salt (BCD), and DCA. Materials for tissue culture were acquired from Sigma Chemical Co (St. Louis, MO, USA), if not otherwise stated, including Fetal bovine serum (FBS) and Dulbecco's modified Eagle's medium (DMEM). The auditory cell line HEI-OC1 (House Ear Institute-Organ of Corti 1) was acquired from Prof. Federico Kalinec (University of California, CA, USA). The macrophage cell line RAW 264.7 (ATCC, TIB-71) was acquired from the American Type Culture Collection (ATCC, Manassas, VA, USA). Both cell lines were incubated with the same type of cell media, using high glucose DMEM with 10% FBS sans antibiotics, with media change every 48 hours. The HEI-OC1 cell line was incubated at a permissive temperature (33 °C) and 10% CO_2, while the RAW264.7 cell line was incubated at 37 °C and 10% CO_2.

All nanogels consisted of 18% Poloxamer 407 (A1-A5). PVA (0.5%) was part of four nanogels (A2-A5). DCA (0.06%) was added to A3 and A5

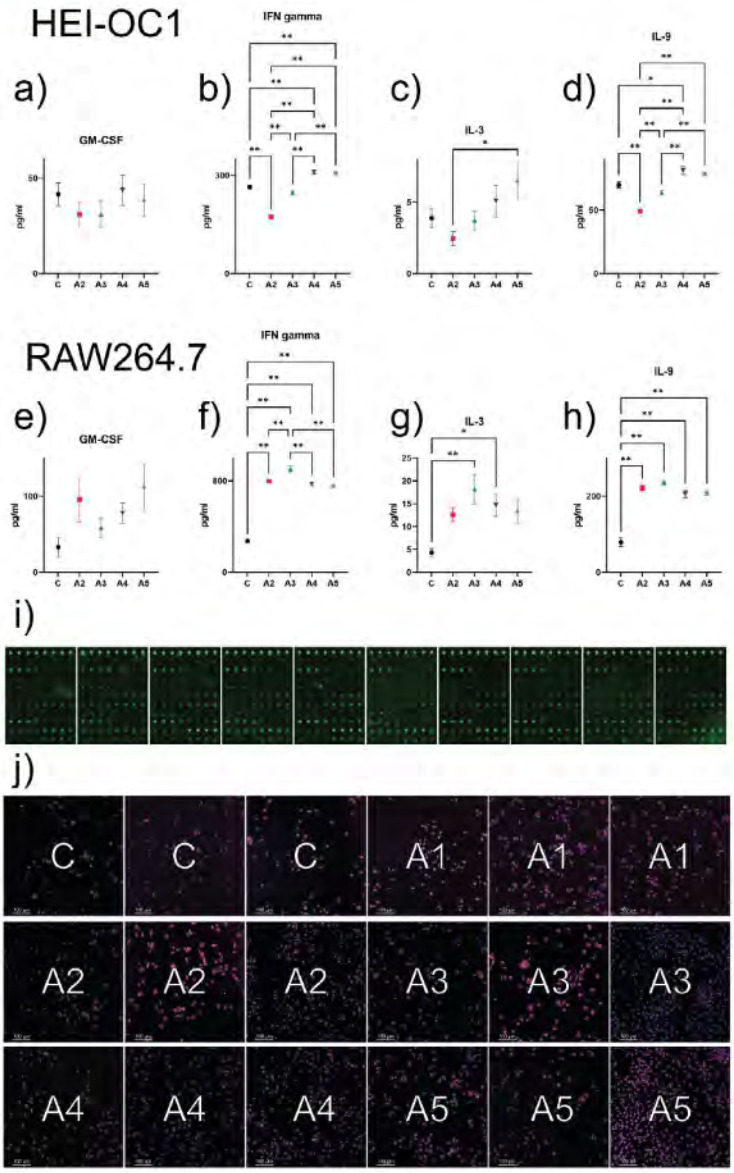

Figure 5. Levels of different cytokines in HEI-OC1 cells, including a) GM-CSF; b) INF gamma; c) IL-3; d) IL-9. Levels of different cytokines in RAW264.7 cells, including e) GM-CSF; f) INF gamma; g) IL-3; h) IL-9; i) cytokines expressed in cellular media after 24 h incubation with nanogels; j) macrophage phenotype markers for RAW264.7 cell line with purple showing ARG1, green iNOS and blue nuclei. The scale bar is 100 µm. Data are shown as mean ±SEM, $n = 3$. $p < 0.01$(**) and $p < 0.05$ (*).

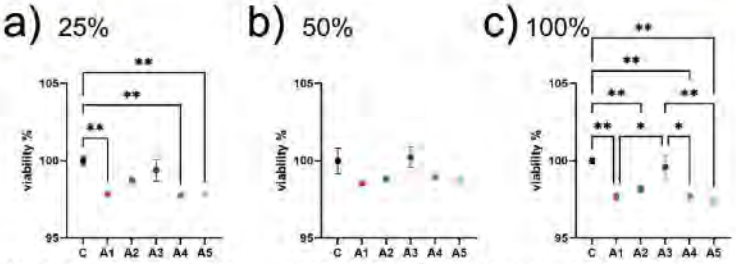

Figure 6. Cellular viability of HEI-OC1 after 24 h incubation with RAW264.7 media. The media used on HEI-OC1 cells comprised a) 25% RAW264.7 media and 75% fresh media, b) 50% RAW264.7 media and 50% fresh media, and c) 100% RAW264.7 media. Data are shown as mean ± SEM, $n = 3$. $p < 0.01$ (**) and $p < 0.05$ (*).

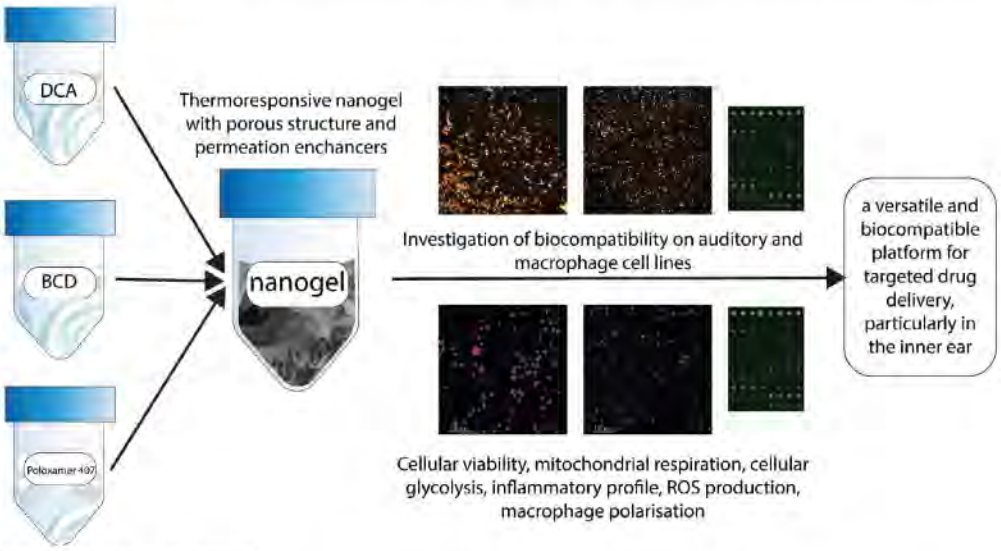

Figure 7. A summary figure of this study.

nanogels. BCD (0.5%) was part of A4 and A5. The nanogel preparation started with dissolving PVA in deionized water at 60 °C under constant stirring. The PVA solution was allowed to cool to room temperature. In cooled, PVA solution was added first DCA and then Poloxamer 407. Nanogels were stirred overnight at 4 °C until transparent, liquid nanogel was obtained. The resulting nanogels were treated with UV light in sterile conditions for 30 min before use in tissue culture assays.

To obtain scanning electron microscope (SEM) micrographs, Clara (Tescan, Brno, CZ) at 10 mm working distance, 2 kV, and 100 Å beam current was used on platinum-coated freeze-dried nanogels. Freeze drying was done by Dynavac FD3 Freeze Dryer (Dynapumps, Seven Hills, Australia) for 48 hours.

The mean particle size of nanogels was measured using 3000HS Zetasizer (Malvern Instruments, Malvern, UK), with the adjacent software's standard operating procedure (SOP) having 25 runs per measurement. The zeta potential was measured using the same machine with adjusted SOP for zeta potential measurement, again with 25 runs per measurement. Surface tension was assessed by a tensiometer (Sigma 703, ATA Scientific, Caringbah, Australia) based on the du Noüy ring method. The shear stress, shear rate, and viscosity values were measured from freshly made nanogels using a Visco-88 viscometer (Malvern Instruments, Malvern, UK). All measuring processes were done following established protocols at room temperature,[66–66] All obtained data were in triplicates ($n = 3$).

The gelation time was evaluated using the vial tilting method by placing a vial with 500 µl of room temperature nanogels in a 37 °C water bath. The gelation time was noted as soon as the nanogels lost their fluidity during vial tilting.[67] All obtained data were in triplicates ($n = 3$).

The protein adhesion test was performed as a modification of the protocol presented in.[28] Fifty microliters] of nanogel was added to 96 well plates and left on ice for 15 min to reduce bubbles on the nanogel surface. Afterward, nanogels were transferred to a 37 °C environment and left for 30 min to set completely. Bovine serum albumin (BSA) (Thermo Fisher Scientific Inc., MA, USA) was added (0.5 mg ml^{-1}, 50 µ) on solid nanogels and incubated for 30 min at 37 °C. The nanogels were washed three times

with phosphate-buffered saline (PBS) (Sigma Chemical Co, St. Louis, MO, USA) and followed by a bicinchoninic acid assay (BCA Protein Assay Kit, Abcam, Cambridge, UK) to assess the amount of BSA left on the nanogel surface using manufacturer's protocol. The resulting value was obtained by subtracting the signal of BSA-free nanogels from BSA-treated nanogels. All obtained data were in triplicates ($n = 3$).

Consistency coefficient K and flow behavior index n for rheological assessment were calculated using rheological data via curve fitting for the Power law model (Equation (1)). Curve fitting was done using the solver function in Microsoft Excel, adopting the nonlinear optimization code.[68]

The power Law equation:

$$\sigma = K\dot{\gamma}^{n} \quad (1)$$

where σ is the shear stress (Pa), K is the consistency coefficient, $\dot{\gamma}$ is the shear rate (s^{-1}), and n is the flow behavior index.

Cell viability assay utilized established protocol for water soluble tetrazolium salts-1 (WST-1) assay (Cell Proliferation Reagent WST-1, Sigma Chemical Co, St. Louis, MO, USA). The same protocol was used for both cell lines. Cells were seeded in a $1–1.5 \times 10^5$ ml^{-1} concentration, 180 µl per well and incubated overnight to promote cell adhesion. Afterward, nanogels were added (20 µl per well) and incubated with cells for 24 h. The cell media with nanogels was removed, and cells were washed three times with PBS, followed by a WST-1 assay. The resulting absorbance was determined via a PerkinElmer Multimode Plate Reader (Waltham, MA, USA) at 450 nm. The data were normalized against the background and presented as a percentage of untreated cells (C). All obtained data were in triplicates ($n = 3$).

For bioenergetics analysis, cells were treated with 20 µl of nanogels for 24 h prior to assays, following the same protocol as per viability assays. After 24 h of incubation, the cells were washed, and the Seahorse XF Cell Mito Stress Test and the Seahorse XF Glycolysis Stress Test were performed using Seahorse Flux Analyzer XF 96 (Agilent Technologies, Santa Clara, CA, USA). Protocols were optimized for each cell line performed and executed per in-house developed methods and manufacturer protocols.[60] Control cells (C) were untreated cells. All obtained data were in triplicates ($n = 3$).

Total intracellular ROS assay was done using Cellular ROS Assay Kit (Deep Red, Abcam, Cambridge, UK) following the manufacturer's protocol. Both cell lines were treated equally. Cells were seeded at $0.5–1 \times 10^5$ ml^{-1} in a 96-well plate, 180 µl per well, and left to adhere overnight. Afterward, cells were stained per the manufacturer's protocol and treated with 20 µl nanogels. After 30 min of incubation, the signal was obtained at Ex/Em = 650/675 nm using a PerkinElmer Multimode Plate Reader (Waltham, MA, USA). The same protocol was followed for ROS visualization for both cell lines. The images were acquired using Operetta CLS (PerkinElmer, Mulgrave, VIC, Australia) high throughput microplate imager. Control cells were untreated cells. All obtained data were in triplicates $n = 3$.

Mouse Cytokine Antibody Array A (20 Targets) – Quantitative (ab197465, Abcam, Cambridge, UK) was used for the inflammatory profile. The cells were seeded per the previous protocol for cellular viability and incubated with nanogels (A2-A5) for 24 h using FBS-free media. Afterward, cells were washed and incubated for 24 h in fresh FBS-free media. That media was collected, and the inflammatory profile was assessed using the manufacturer's Mouse Cytokine Antibody Array protocol. A hundred microliters of pooled cell media were used per group. The signal was obtained using InnoScan 710 (Innopsys Inc, Chicago, IL, USA) with a Cy3 filter. Data were quantified and exported using Mapix – Microarray image acquisition and analysis software (Innopsys Inc, Chicago, IL, USA). Of 20 potential targets in this microarray assay (GM-CSF, IFN gamma, IL-1α, IL-1β, IL-2, IL-3, IL-4, IL-5, IL-6, IL-9, IL-10, IL-12, IL-13, IL-17, KC, MCP-1, MCSF, RANTES, TNFα, VECF), two targets did not satisfy precise calibration curve (MCP-1 and KC) and were excluded from analysis. Of the 18 remaining targets, only four were above the detection threshold (GM-CSF, IFN gamma, IL-3, IL-9). The data were normalized based on cellular viability during media collection. All obtained data were in triplicates $n = 3$.

RAW264.7 were seeded on eight well-chamber slides (1.5×10^5 ml^{-1}) and left overnight to adhere. They were treated with nanogels in the ratio of 9:1 (cell media: nanogel) and incubated for 3 h. After incubation, cells were washed, fixed (4% paraformaldehyde), permeabilized (0.1% Triton X-100), and blocked (2% BSA), all purchased from Sigma Chemical Co, St. Louis, MO, USA. Cells were stained with Arginase 1 Polyclonal Antibody (PA5-29645, Thermo Fisher Scientific Inc., MA, USA) and iNOS Monoclonal Antibody Alexa Fluor 488 (53-5920-82, Thermo Fisher Scientific Inc., MA, USA) and incubated overnight at 4 °C. The secondary antibody Goat Anti-Rabbit IgG H&L (Alexa Fluor 647) (ab150079, Abcam, Cambridge, UK) was incubated for one hour at room temperature.[69] The counter stain for nuclei was Hoechst 33342 (ab145597, Abcam, Cambridge, UK). The slides were imaged via Andor Dragonfly Spinning Disk Confocal Microscope (Oxford Instruments plc, Abingdon, UK). All obtained data were in triplicates ($n = 3$).

The impact of macrophage cellular products on the auditory cell line was assessed based on a protocol.[70] The RAW264.7 was treated as per protocol for the inflammatory profile. Collected FBS-free media was mixed with fresh FBS-free media as 25%, 50%, or 100% resulting media. The resulting media was put on seeded HEI-OC-1 cells and incubated for 24 h. The cellular viability was assessed via WST-1 assay. The data were normalized against the background and presented as a percentage of viability of HEI-OC-1 incubated with media of untreated RAW264.7 cells (C).

Statistical analysis was conducted using GraphPad Prism 9.3 (GraphPad, Inc. San Diego, CA, USA). One-way ANOVA, regression analysis, and Tukey HSD tests were employed as appropriate. Data are presented as mean ± SEM, with statistical significance denoted as ** ($p < 0.01$) and * ($p < 0.05$).

Acknowledgements

A.M. and H.A.-S. contributed equally to this work. The authors wanted to acknowledge the Australian Postgraduate Award (APA) and Curtin Research Scholarship (CRS). The authors acknowledge the Microscopy and Microanalysis Facility at Curtin University. The authors acknowledge The Ian Potter Foundation for funding support for equipment.

Correction added on 28 March 2024 after online publication: Acknowledgment section is updated in this version.

Conflict of Interest

The authors declare no conflict of interest.

Data Availability Statement

The data that support the findings of this study are available from the corresponding author upon reasonable request.

Keywords

bioenergetics, glycolysis, HEI-OC1, mitochondrial respiration, nanogels, RAW264.7, thermoresponsive hydrogel

Received: September 21, 2023
Revised: February 26, 2024
Published online:

[1] Z. Zhang, X. Li, W. Zhang, D. S. Kohane, *Adv. Funct. Mater.* **2021**, *31*, 2008701.
[2] B. Szeto, H. Chiang, C. Valentini, M. Yu, J. W. Kysar, A. K. Lalwani, *Laryngoscope Invest. Otolaryngol.* **2020**, *5*, 122.
[3] N. K. Preman, R. R. Barki, A. Vijayan, S. G. Sanjeeva, R. P. Johnson, *Eur. J. Pharm. Biopharm.* **2020**, *157*, 121.

[4] E. Dalir Abdolahinia, G. Barati, Z. Ranjbar-Navazi, J. Kadkhoda, M. Islami, N. Hashemzadeh, S. Maleki Dizaj, S. Sharifi, *J. Drug Delivery Sci. Technol.* **2022**, *68*, 103109.
[5] H.-Q. Wu, C.-C. Wang, *Langmuir* **2016**, *32*, 6211.
[6] M. E. Napier, J. M. Desimone, *Polym. Rev.* **2007**, *47*, 321.
[7] M. Samiei, Z. Aghazadeh, E. D. Abdolahinia, A. Vahdati, S. Daneshvar, A. Noghani, *Acta Odontol. Scand.* **2020**, *78*, 494.
[8] M. Fathi, E. D. Abdolahinia, J. Barar, Y. Omidi, *Nanomedicine* **2020**, *15*, 2171.
[9] Z. Li, J. Huang, J. Wu, *Biomater. Sci.* **2021**, *9*, 574.
[10] L. Djekic, B. Čalija, Đ. Medarević, *J. Mol. Liq.* **2020**, *303*, 112639.
[11] A. M. Bodratti, P. Alexandridis, *J. Funct. Biomater.* **2018**, *9*, 11.
[12] N. El Kechai, F. Agnely, E. Mamelle, Y. Nguyen, E. Ferrary, A. Bochot, *Int. J. Pharm.* **2015**, *494*, 83.
[13] K. Mfoafo, R. Mittal, A. Eshraghi, Y. Omidi, H. Omidian, *J. Drug Delivery Sci. Technol.* **2023**, *79*, 104086.
[14] X. Khoo, E. J. Simons, H. H. Chiang, J. M. Hickey, V. Sabharwal, S. I. Pelton, J. J. Rosowski, R. Langer, D. S. Kohane, *Biomaterials* **2013**, *34*, 1281.
[15] A.-H. Liao, C.-P. Shih, M.-W. Li, Y.-C. Lin, H.-C. Chuang, C.-H. Wang, *Drug Delivery* **2021**, *28*, 1256.
[16] B. Kovacevic, M. Jones, C. Ionescu, D. Walker, S. Wagle, J. Chester, T. Foster, D. Brown, M. Mikov, A. Mooranian, H. Al-Salami, *Biomaterials* **2022**, *283*, 121459.
[17] S. Mathavan, C. M. Ionescu, B. Kovacevic, M. Mikov, S. Colocorbin-Kon, A. Mooranian, C. R. Dass, H. Al-Salami, *Ther. Delivery* **2020**, *11*, 157.
[18] A. Mooranian, N. Zamani, R. Takechi, H. Al-Sallami, M. Mikov, S. Goločorbin-Kon, B. Kovacevic, F. Arfuso, H. Al-Salami, *Ther. Delivery* **2019**, *10*, 563.
[19] A. Mooranian, N. Zamani, B. Kovacevic, M. C. Ionescu, C. Luna, M. Mikov, S. Goločorbin-Kon, G. Stojanovic, S. Kojic, H. Al-Salami, *Curr. Diabetes Rev.* **2022**, *18*, 10.
[20] M. Jones, D. Walker, C. M. Ionescu, B. Kovacevic, S. R. Wagle, A. Mooranian, D. Brown, H. Al-Salami, *Ther. Delivery* **2020**, *11*, 791.
[21] S. R. Wagle, C. M. Ionescu, B. Kovacevic, M. Jones, T. Foster, P. Lim, M. Lewkowicz, M. Đanić, M. Mikov, A. Mooranian, H. Al-Salami, *Nanomedicine* **2018**, *13*, 923.
[22] A. Jover, F. Fraga, F. Meijide, J. Vázquez Tato, J. Cautela, A. Del Giudice, M. C. Di Gregorio, *J. Colloid Interface Sci.* **2021**, *604*, 415.
[23] O. V. Salomatina, I. I. Popadyuk, A. L. Zakharenko, O. D. Zakharova, A. A. Chepanova, N. S. Dyrkheeva, N. I. Komarova, J. Reynisson, R. O. Anarbaev, N. F. Salakhutdinov, O. I. Lavrik, K. P. Volcho, *Steroids* **2021**, *165*, 108771.
[24] G. Narayanan, J. Shen, I. Matai, A. Sachdev, R. Boy, A. E. Tonelli, *Prog. Mater. Sci.* **2022**, *124*, 100869.
[25] E. Russo, C. Villa, *Pharmaceutics* **2019**, *11*, 671
[26] Y. Chen, J.-H. Lee, M. Meng, N. Cui, C.-Y. Dai, Q. Jia, E.-S. Lee, H.-B. Jiang, *Materials* **2021**, *14*, 4522.
[27] Y. Tahara, K. Akiyoshi, *Adv. Drug Delivery Rev.* **2015**, *95*, 65.
[28] J. Zhang, Y. Zhu, J. Song, J. Yang, C. Pan, T. Xu, L. Zhang, *ACS Appl. Mater. Interfaces* **2018**, *10*, 6879.
[29] R. M. Visalakshan, M. N. Macgregor, S. Sasidharan, A. Ghazaryan, A. M. Mierczynska-Vasilev, S. Morsbach, V. Mailänder, K. Landfester, J. D. Hayball, K. Vasilev, *ACS Appl. Mater. Interfaces* **2019**, *11*, 27615.
[30] R. A. Latour, *Encycl. Biomater. Biomed. Eng.* **2005**, *1*, 270.
[31] K. Nakanishi, T. Sakiyama, K. Imamura, *J. Biosci. Bioeng.* **2001**, *91*, 233.
[32] J. Kim, *Colloids Surf., B* **2020**, *188*, 110756.
[33] S. Wang, L. Zhao, Q. Li, C. Liu, J. Han, L. Zhu, D. Zhu, Y. He, H. Liu, *Food Hydrocolloids* **2019**, *91*, 34.
[34] W. Dott, P. Mistry, J. Wright, K. Cain, K. E. Herbert, *Redox Biol.* **2014**, *2*, 224.
[35] M. D. Brand, D. G. Nicholls, *Biochem. J.* **2011**, *435*, 297.
[36] B. Kovacevic, C. M. Ionescu, S. R. Wagle, M. Jones, M. Lewkowicz, E. Y. M. Wong, M. Đanić, M. Mikov, A. Mooranian, H. Al-Salami, *J. Pharm. Sci.* **2023**, *112*, 700.
[37] B. Kovacevic, S. R. Wagle, C. M. Ionescu, M. Jones, M. Lewkowicz, E. Y. M. Wong, S. Kojic, G. Stojanovic, M. Đanić, M. Mikov, A. Mooranian, H. Al-Salami, *Colloids and Surf., B* **2023**, *222*, 113014.
[38] B. Kovacevic, C. M. Ionescu, M. Jones, S. R. Wagle, M. Lewkowicz, M. Đanić, M. Mikov, A. Mooranian, H. Al-Salami, *Gels* **2022**, *8*, 358.
[39] A. Freitas-Martins, M. I. Sousa, M. I. Cristo, J. Ramalho-Santos, S. Amaral, *Andrology* **2024**, *12*, 410.
[40] B. G. Hill, C. A. Benavides, J. R. Lancaster Jr., S. Ballinger, L. Dell'Italia, Z. Jianhua, V. M. Darley-Usmar, *Biol. Chem.* **2012**, *393*, 1485.
[41] N. Diwanji, A. Bergmann, *Semin. Cell Dev. Biol.* **2018**, *80*, 74.
[42] F. Serras, *Fly* **2016**, *10*, 128.
[43] Y. Yao, H. Zhang, Z. Wang, J. Ding, S. Wang, B. Huang, S. Ke, C. Gao, *J. Mater. Chem. B* **2019**, *7*, 5019.
[44] K. Brieger, S. Schiavone, F. J. Miller, K. H. Krause, *Swiss Med. Wkly.* **2012**, *142*, w13659.
[45] A. Sheih, W. C. Parks, S. F. Ziegler, *Mucosal Immunol.* **2017**, *10*, 705.
[46] A. Arizai, J. L. Choi, S. He, A. M. Fenn, M. Nairz, S. Rattik, C. S. Mcalpine, J. E. Mindur, C. T. Chan, Y. Iwamoto, B. Tricot, G. R. Wojtkiewicz, R. Weissleder, P. Libby, M. Nahrendorf, J. R. Stone, B. Becher, F. K. Swirski, *J. Exp. Med.* **2017**, *214*, 3293.
[47] K. Hirota, M. Hashimoto, Y. Ito, M. Matsuura, H. Ito, M. Tanaka, H. Watanabe, G. Kondoh, A. Tanaka, K. Yasuda, M. Kopf, A. J. Potocnik, B. Stockinger, N. Sakaguchi, S. Sakaguchi, *Immunity* **2018**, *48*, 1220.
[48] M. Dougan, G. Dranoff, S. K. G. M.-C. S. F. Dougan, *Immunity* **2019**, *50*, 796.
[49] A. M. Gocher, C. J. Workman, V. DaA, *Nat. Rev. Immunol.* **2022**, *22*, 158.
[50] S. Spranger, R. Bao, T. F. Gajewski, *Nature* **2015**, *523*, 231.
[51] K. Kang, S. H. Park, J. Chen, Y. Qiao, E. Giannopoulou, K. Berg, A. Hanidu, J. Li, G. Nabozny, K. Kang, K.-H. Park-Min, L. B. Ivashkiv, *Immunity* **2017**, *47*, 235.
[52] D. Jorgovanovic, M. Song, L. Wang, Y. Zhang, *Biomark Res.* **2020**, *8*, 49.
[53] J. D. Burke, H. A. Young, *Semin. Immunol.* **2019**, *43*, 101280.
[54] J. E. Mindur, F. K. Swirski, *Arterioscler., Thromb., Vasc. Biol.* **2019**, *39*, 1275.
[55] C. S. Mcalpine, J. Park, A. Griciuc, E. Kim, S. H. Choi, Y. Iwamoto, M. G. Kiss, K. A. Christie, C. Vinegoni, W. C. Poller, J. E. Mindur, C. T. Chan, S. He, H. Janssen, L. P. Wong, J. Downey, S. Singh, A. Anzai, F. Kahles, M. Jorfi, P. F. Feruglio, R. I. Sadreyev, R. Weissleder, B. P. Kleinstiver, M. Nahrendorf, R. E. Tanzi, F. K. Swirski, *Nature* **2021**, *595*, 701.
[56] S. Chakraborty, K. F. Kubatzky, D. K. Mitra, *Int. J. Mol. Sci.* **2019**, *20*, 2113.
[57] H. S. Kim, D. H. Chung, *Mucosal Immunol.* **2013**, *6*, 347.
[58] M. Kieler, M. Hofmann, G. Schabbauer, *FEBS J.* **2021**, *288*, 3694.
[59] L. Zhao, W. Ye, Y. Zhu, F. Chen, Q. Wang, X. Lv, Y. Hua, Z. Du, X. Zhu, Y. Yu, H. Zou, L. Liu, Y. Xue, *Lab. Invest.* **2022**, *102*, 1054.
[60] A. Mooranian, T. Foster, C. M. Ionescu, D. Walker, M. Jones, S. R. Wagle, B. Kovacevic, J. Chester, E. Johnston, E. Wong, M. D. Atlas, M. Mikov, H. Al-Salami, *Pharmaceutics* **2021**, *13*, 1184.
[61] A. Mooranian, C. M. Ionescu, D. Walker, M. Jones, S. R. Wagle, B. Kovacevic, J. Chester, T. Foster, E. Johnston, J. Kuthubutheen, D. Brown, M. D. Atlas, M. Mikov, H. Al-Salami, *Biomolecules* **2022**, *12*, 73.
[62] A. Mooranian, M. Jones, C. M. Ionescu, D. Walker, S. R. Wagle, B. Kovacevic, J. Chester, T. Foster, E. Johnston, M. Mikov, H. Al-Salami, *Nanomaterials* **2021**, *11*, 1861.
[63] A. Mooranian, M. Jones, D. Walker, C. M. Ionescu, S. R. Wagle, B. Kovacevic, J. Chester, T. Foster, E. Johnston, J. Kuthubutheen, D.

Brown, M. D. Atlas, M. Mikov, H. Al-Salami, *Nanomaterials* **2022**, *12*, 647.
[64] A. Mooranian, S. Raj Wagle, B. Kovacevic, R. Takechi, J. Mamo, V. Lam, G. F. Watts, M. Mikov, S. Golocorbin-Kon, C. Stojanovic, H. Al-Sallami, H. Al-Salami, *Sci. Rep.* **2020**, *10*, 106.
[65] S. R. Wagle, B. Kovacevic, D. Walker, C. M. Ionescu, M. Jones, G. Stojanovic, S. Kojic, A. Mooranian, H. Al-Salami, *Pharmaceutics* **2020**, *12*, 708.
[66] S. R. Wagle, D. Walker, B. Kovacevic, A. Gedawy, M. Mikov, S. Golocorbin-Kon, A. Mooranian, H. Al-Salami, *Sci. Rep.* **2020**, *10*, 7715.
[67] M. M. Carleton, M. V. Sefton, *Biomaterials* **2019**, *223*, 119477.
[68] N. L. Chin, S. M. Chan, Y. A. Yusof, T. G. Chuah, R. A. Talib, *J. Food Eng.* **2009**, *93*, 134.
[69] H. Hirata, N. Zhang, M. Ueno, D. Barati, J. Kushioka, H. Shen, M. Tsubosaka, M. Toya, T. Lin, E. Huang, Z. Yao, J. Y. Wu, S. Zwingenberger, F. Yang, S. B. Goodman, *Immun. Ageing* **2022**, *19*, 14.
[70] Y. Zhu, Z. Ma, L. Kong, Y. He, H. F. Chan, H. Li, *Biomaterials* **2020**, *256*, 120216.

Chapter 5

General Discussion and Conclusion

General Discussion and Conclusion

This thesis examined the role of bile acids as components of biocompatible hydrogels and nanogels as potential drug delivery vehicles. Bile acids greatly impacted cellular viability and mitochondrial respiration based on the type and concentration of present bile acid. The addition of bile acids did not change the overall fluid behaviour of the polymer matrix (non-Newtonian, shear-thinning fluid behaviour for polymer matrices based on sodium alginate or Poloxamer 407). Bile acids influenced the surface tension of hydrogels and nanogels, depending on whether the concentration of bile acids was above or below the polymer saturation point of the given formulation. Bile acids mostly contributed to the more balanced zeta potential of hydrogel formulations. The addition of bile acids to the polymer matrix minimally impacted the hydrogel's microstructure.

Tissues responded differently to bile acids. Generally, in the presence of high concentrations of bile acids, bile acids disrupt mitochondrial respiration, specifically ATP production, shifting overall cellular metabolism to anaerobic metabolism. This usually leads to a decline in cell viability. Further evidence of impaired mitochondrial respiration is seen in the lack of response to hypoxia in cells exposed to high concentrations of bile acids.

Nanogels based on Poloxamer 407 with adjusted concentrations of bile acids showed substantial biocompatibility. The presence of nanogels had an insignificant impact on mitochondrial function, glycolysis, cellular viability, and intracellular reactive oxygen species in the auditory cell line. Effects on macrophage cell line were more pronounced. Nanogels with deoxycholic acid and ursodeoxycholic acid demonstrated the best biocompatibility.
Thermoresponsive nanogels created with Poloxamer 407, deoxycholic acid and beta-cyclodextrin had porous inner structures and exhibited non-Newtonian, shear-thinning fluid behaviour. The gelation at 37°C was fast, and there was minimal albumin adsorption on the nanogels surface. These nanogels slightly impacted the House Ear Institute-Organ of Corti 1

cell line. The cellular viability, mitochondrial respiration, glycolysis, intracellular oxidative stress, and inflammatory profile were not profoundly impacted by the presence of nanogels. Furthermore, nanogel exposure to macrophage cell line RAW264.7 leads to minimal polarisation changes from M2 anti-inflammatory to M1 pro-inflammatory macrophages. Inflammatory products of macrophages did not overly disrupt the survivability of auditory cells. This study suggests that thermoresponsive nanogels with bile acid can be potential inner ear drug delivery candidates.

Limitations

Firstly, natural polymers used in this study (sodium alginate, starch, acacia, pectin, carboxymethyl and methyl 2-hydroxyethyl cellulose) were purchased from appropriate commercial vendors and used without further modifying or purifying. This may affect the results obtained from subsequent, repeated experiments, as the physicochemical properties of natural polymers may vary depending on a vendor and batch. For example, the properties of sodium alginate vary depending on the ratio of L-guluronate and D-mannuronate, sodium alginates' main components, and that ratio differs depending on batch and manufacturer. In addition, only endogenous bile acids were used (DCA, UDCA, CDCA, TCA, LCA), with an accent on deoxycholic acid, which may omit beneficial properties of other bile acids, given the heterogenicity of the bile acid pool and their various physicochemical and biological effects.

Incubation with hydrogels and nanogels was limited to 24 h, and more long-term effects of hydrogels and nanogels should be explored to confirm long-term biocompatibility. Furthermore, suitable cellular and animal models need to be explored to confirm relevant drug penetration properties in the inner ear.

Future Perspective

Limitations of this thesis should be addressed in future studies arising from this work. Thus, future studies should implement longer-duration biocompatibility studies on cell models and investigate the more precise mechanisms behind the permeation enhancer effect of bile acids. Furthermore, a wider range of bile acids should be included, and the relationship between drug permeation, biocompatibility and molecular structure of bile acids should be investigated. The biocompatibility of nanogels should be investigated during longer time intervals, including daily, weekly, and monthly time periods, utilising cellular and animal models.

Thermoresponsive nanogels should be further optimised for optimal physicochemical and microbiologic stability. Nanogels should be optimised based on the application, especially in terms of viscosity and gelation speed.

As there is an increase in pro-inflammatory molecules from macrophages in the presence of nanogels, the immune response to nanogels should be more thoroughly investigated using different *in vitro* and *in vivo* models.

A drug of interest should be selected, including hydrophobic drugs with low bioavailability and tissue permeation, and drug permeation should be observed with and without nanogels to facilitate local drug permeation in cellular and animal models for inner ear delivery. Further studies should consider in vivo studies of mice and larger mammals such as cats and primates with the ultimate intention of progressing into human clinical trials.

Appendix A

Contribution of Thesis Author to Publications

I, Bozica Kovacevic, as the author of this thesis, contributed to the following publications as outlined below. As for all the co-authors, signed authorship forms approved by Curtin University and having attributed contributions of each and every co-author (including myself) are available upon request from the primary supervisor of this thesis and the corresponding author of all these publications within this thesis, Dr Hani Al-Salami (phone: +61 8 9266 9816; email: hani.al-salami@curtin.edu.)

Publication 1 (Chapter 1):
Comprehensive literature search, analysis and drafting of the review, as well as editing and reviewing the manuscript for publication.

Publication 2-5 (Chapter 2):
#1: Conception and design of the project
#2: Analysis and interpretation of research data
#3: Drafting significant parts of the work or critically revising it so as to contribute to the interpretation.
#4: Significant contribution to data interpretation and presentation resulting in significant improvement of the quality of the manuscript

Publication 6 and 7 (Chapter 3):
#1: Conception and design of the project
#2: Analysis and interpretation of research data
#3: Drafting significant parts of the work or critically revising it so as to contribute to the interpretation.

#4: Significant contribution to data interpretation and presentation, resulting in significant improvement of the quality of the manuscript

Publication 8-10 (Chapter 4):

#1: Conception and design of the project (including animal ethics application preparation)

#2: Analysis and interpretation of research data

#3: Drafting significant parts of the work or critically revising it so as to contribute to the interpretation.

#4: Significant contribution to data interpretation and presentation, resulting in significant improvement of the quality of the manuscript

Appendix B

Publisher copyright permissions

Appendix D contains all the copyright transfer permissions permitting the publications to be incorporated within this thesis and to be publicly available for viewing as part of the thesis contents.

Every reasonable effort has been made to acknowledge the owners of copyright material. I would be pleased to hear from any copyright owner who has been omitted or incorrectly acknowledged.

Publisher: Future Science

Source: Reprints, accessed 04 April 2024, https://www.future-science.com/reprints#permissions

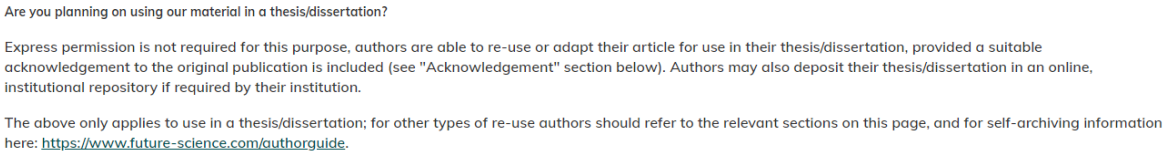

Are you planning on using our material in a thesis/dissertation?

Express permission is not required for this purpose, authors are able to re-use or adapt their article for use in their thesis/dissertation, provided a suitable acknowledgement to the original publication is included (see "Acknowledgement" section below). Authors may also deposit their thesis/dissertation in an online, institutional repository if required by their institution.

The above only applies to use in a thesis/dissertation; for other types of re-use authors should refer to the relevant sections on this page, and for self-archiving information here: https://www.future-science.com/authorguide.

Publisher: Elsevier

Re: Permission to include publication for PhD thesis [231201-010698]

Permissions Helpdesk <permissionshelpdesk@elsevier.com>
Tue 5/12/2023 2:41 PM
To:Božica Kovacevic (Student) <bozica.kovacevic@postgrad.curtin.edu.au>

Dear Bozica Kovacevic,

Thank you so much for contacting us.

Please note that, as one of the authors of these three articles, you retain the right to reuse it in your thesis/dissertation. You do not require formal permission to do so. You are permitted to post these Elsevier articles online if it is embedded within your thesis subject to proper acknowledgment;

Our preferred acknowledgement wording will be:

Example: "This article/chapter was published in Publication title, Vol number, Author(s), Title of article, Page Nos, Copyright Elsevier (or appropriate Society name) (Year)."

All the best for your thesis submission!

Kind regards,

Kaveri Thakuria

Senior Copyrights Coordinator

ELSEVIER | HCM - Health Content Management

Visit Elsevier Permissions

Publisher: MDPI

Source: MDPI Open Access Information and Policy, accessed 04 April 2024,

https://www.mdpi.com/openaccess

MDPI Open Access Information and Policy

All articles published by MDPI are made immediately available worldwide under an open access license. This means:

- everyone has free and unlimited access to the full-text of *all* articles published in MDPI journals;
- everyone is free to re-use the published material if proper accreditation/citation of the original publication is given;
- open access publication is supported by the authors' institutes or research funding agencies by payment of a comparatively low **Article Processing Charge (APC)** for accepted articles.

Permissions

No special permission is required to reuse all or part of article published by MDPI, including figures and tables. For articles published under an open access Creative Common CC BY license, any part of the article may be reused without permission provided that the original article is clearly cited. Reuse of an article does not imply endorsement by the authors or MDPI.

Publisher: Wiley

Source: How to Clear Permissions for a Thesis or Dissertation, accessed 04 April 2024, https://www.wiley.com/en-us/network/publishing/research-publishing/trending-stories/how-to-clear-permissions-for-a-thesis-or-dissertation

Do I need to request permission to use my own work as my dissertation?

If you are the author of a published Wiley article, you have the right to reuse the full text of your published article as part of your thesis or dissertation. In this situation, you do not need to request permission from Wiley for this use.